

Doutoramento
Ciências Biomédicas

Uncovering the role of beta-adrenergic signaling on breast cancer bone metastasis: a novel 3D biomodel

Francisco Pereira dos Santos Conceição

D
2022

Uncovering the role of beta-adrenergic signaling on breast cancer bone metastasis: a novel 3D biomodel
Francisco Pereira dos Santos Conceição

Uncovering the role of beta-adrenergic signaling on breast cancer bone metastasis: a novel 3D biomodel

Tese de Candidatura ao grau de Doutor em Ciências Biomédicas; Programa Doutoral do Instituto de Ciências Biomédicas Abel Salazar da Universidade do Porto.

Orientador – Doutora Meriem Lamghari

Categoria – Investigadora Principal

Afiliação – I3S: Instituto de Investigação e Inovação em Saúde, INEB: Instituto de Engenharia Biomédica & ICBAS: Instituto de Ciências Biomédicas Abel Salazar, Universidade do Porto.

Co-orientador – Doutora Joana Paredes

Categoria – Investigadora Principal

Afiliação – I3S: Instituto de Investigação e Inovação em Saúde, IPATIMUP: Instituto de Patologia e Imunologia Molecular da Universidade do Porto & FMUP: Faculdade de Medicina da Universidade do Porto.

Co-orientador – Doutora Daniela Sousa

Categoria – Investigadora Pós-Doutoral

Afiliação – I3S: Instituto de Investigação e Inovação em Saúde, INEB: Instituto de Engenharia Biomédica.

The work presented in this thesis was developed at:

Neuro & Skeletal Circuits Group

I3S – Instituto de Investigação e Inovação em Saúde

INEB – Instituto de Engenharia Biomédica

Universidade do Porto, Porto, Portugal

Rua Alfredo Allen, 208

4200-135 Porto, Portugal

www.i3s.up.pt | www.ineb.up.pt



Financial Support

Francisco Pereira dos Santos Conceição was a recipient of a PhD grant (SFRH/BD/128771/2017) from Fundação para a Ciência e Tecnologia (FCT).

This work was financed by FEDER—Fundo Europeu de Desenvolvimento Regional funds through the COMPETE 2020—Operacional Programme for Competitiveness and Internationalisation (POCI), Portugal 2020, and Portuguese funds through FCT/MCTES in the framework of the project Institute for Research and Innovation in Health (POCI-01-0145-FEDER-030158), and in the framework of the financed project PTDC/MED-PAT/30158/2017. The I3S Scientific Platforms Proteomics, BioSciences Screening and Bioimaging, were integrated in the National Roadmap of Research Infrastructures of Strategic Relevance (ROTEIRO/0028/2013; LISBOA-01-0145-FEDER-022125), the PT-OPENSREEN (NORTE-01-0145-FEDER-085468) and Portuguese Platform of Bioimaging (PPBI-POCI-01-0145-FEDER-022122).



Declaração

Declaro que a presente tese é de minha autoria e não foi utilizada previamente noutro curso ou unidade curricular, desta ou de outra instituição. As referências a outros autores (afirmações, ideias, pensamentos) respeitam escrupulosamente as regras da atribuição, e encontram-se devidamente indicadas no texto e nas referências bibliográficas, de acordo com as normas de referência. Tenho consciência de que a prática de plágio e auto-plágio constitui um ilícito académico.

Francisco Pereira dos Santos Conde

Acknowledgements

Gostava, claro, de começar por agradecer a ti, Meriem, por toda a atenção e disponibilidade que demonstraste durante estes anos todos. Obrigado por me teres guiado durante esta viagem, tanto a nível profissional como a nível pessoal. Por teres aturado as minhas manias e pela paciência e frontalidade com que lidaste comigo durante este tempo. Pela maneira como me ensinaste a vender os meus projetos. Olhando para trás consigo ver com clareza a minha evolução desde que comecei a trabalhar contigo, e também o quanto o nosso grupo cresceu durante este tempo todo. Não podia ter escolhido melhor orientadora.

Um agradecimento especial também a ti, Daniela, pelo acompanhamento constante e por toda a ajuda que me deste durante este tempo. Tornaste a minha jornada muito mais fácil. Obrigado pelo companheirismo e pela disponibilidade, mesmo com dois pequenos em casa a chagar-te o juízo! Senti que tinha sempre alguém a quem recorrer, e por isso obrigado mais uma vez.

Quero também agradecer aos membros que fazem ou fizeram parte do nosso Neuro & Skeletal Circuits group pelo que conseguimos alcançar nestes anos e pelo excelente espírito de entreajuda que encontrei aqui. Estrela, Juliana, Daniela, Ricardo, Andrea, Emine, Clive, Carolina, Marina, Filipe, Carlos, Luis, as dificuldades tornaram-se facilidades graças a vocês.

Joana, obrigado por aceites ser minha co-orientadora, por me receberes sempre de porta aberta e pela ajuda que me deste, tanto em sugestões como contribuições para os vários artigos que saíram da minha tese. Obrigado também ao Kent e à Anne, por toda a ajuda e hospitalidade durante os poucos meses que estive fora do país, a adaptação foi extremamente fácil e consegui trazer de volta imenso conhecimento e protocolos para o nosso grupo graças a vocês.

Quero agradecer também aos serviços técnicos do I3S pela ajuda e profissionalismo que demonstraram sempre que precisei. Dalila, Maria, André, Hugo, Ricardo, Manuela, Paula e Tânia, obrigado pela simpatia e disponibilidade.

Obrigado também aos membros do INEB com quem me cruzei durante a minha viagem. Um abraço em especial ao Paulo, pelas noitadas de jogatana e por explorar comigo o mundo das microfluídicas.

Não podia deixar de fora, claro, a malta dos Resquícios. Obrigado Ivo, Pedro, Ricardo, Ruben, João F., Luis, Rui, Miguel, Sofia, João G., Ana, e as mais recentes adições ao grupo Daniela, Inês, Bárbara, Cátia, Inês, Andreia e a piquena Benedita. Obrigado pela amizade,

pelas discussões e incontáveis memórias e histórias, obrigado por me mostrarem que é fácil e que parece natural manter um grupo unido por mais de 20 anos.

De igual forma, quero agradecer ao João R., Gonçalo, Clara, Ana M., Fred, Lia, Maria, Ana G. e Joana, por terem percorrido comigo este percurso. Obrigado por me mostrarem que há mais do que estudo na faculdade e pelas viagens e memórias que partilhamos desde o ano de 2010. Deixei o João T. de fora deste ilustre grupo para agradecer de forma especial pelos dois anos de convivência, pelas cervejas e cozinhados e por termos sobrevivido àqueles primeiros meses de confinamento sem grandes percalços!

Obrigado Ana, Luis, Zé, Cátia, Elsa, Patrícia, Andreia, Rita, Tiago e Cláudia por partilharem comigo todos os momentos dentro e fora do instituto nestes 5 anos. Apesar dos vossos gostos questionáveis em matéria de discotecas, não podia deixar de realçar que as nossas saídas fizeram maravilhas para me distrair e olhar para o trabalho de cabeça mais fresca. Não no dia a seguir, no entanto.

Um agradecimento especial à malta das segundas-feiras mágicas, obrigado pelas francesinhas e picanhas e por me deixarem acabar o doutoramento sem nenhuma lesão grave.

Obrigado João, Filipe e André, pelas magiczadas pela noite dentro. Obrigado pelo sal e política dos nossos jogos de commander, que além de serem um poço sem fundo para a carteira, foram também pausas semanais sagradas para limpar a cabeça de tudo o resto.

À minha família, em particular aos meus pais, à Teresa e ao pequeno Luís, obrigado pelo vosso apoio incondicional e por serem os alicerces que me suportaram neste caminho. Não precisei de me preocupar com nada durante este tempo todo, deixando-me livre para me focar no meu futuro. O meu doutoramento não teria sido possível sem vocês.

Por fim, à Isa por ter partilhado comigo as dores de cabeça de um projeto de doutoramento. Obrigado pelo carinho, pelas rants e pelas piadas secas. Por suportares as minhas excentricidades e os cliques do rato. Obrigado por me fazeres olhar para o futuro com outros olhos.

List of Publications

F. Conceição*, D. M. Sousa, S. Tojal, C. Lourenço, C. Carvalho-Maia, H. Estevão-Pereira, J. Lobo, M. Couto, M. M. Rosenkilde, C. Jerónimo, M. Lamghari (2022) The Secretome of Primary and Bone Metastatic Breast Cancer Elicits Distinct Outcomes in Human Osteoclast Activity After Activation of β 2 Adrenergic Signaling. (under revision for British Journal of Pharmacology, IF – 7.64)

F. Conceição*, D. M. Sousa, J. Loessberg-Zahl, A. R. Vollertsen, E. Neto, K. Søre, J. Paredes, A. Leferink and M. Lamghari (2022) A Metastasis-On-a-Chip Approach to Explore the Sympathetic Modulation of Breast Cancer Bone Metastasis. *Materials Today Bio.* 13, 100219 (<https://doi.org/10.1016/j.mtbio.2022.100219>) (IF – 7.44)

F. Conceição*, D.M. Sousa, J. Paredes, M. Lamghari (2021) Sympathetic activity in breast cancer and metastasis: partners in crime, *Bone Research*, 9, 9. (<https://doi.org/10.1038/s41413-021-00137-1>) (IF – 11.59)

Other Publications:

C. Lourenço, **F. Conceição**, C. Jerónimo, M. Lamghari and D. M. Sousa (2022) Stress in Metastatic Breast Cancer: to the Bone and Beyond. *Cancers* (under major revision) (IF – 6.639)

C. J. Alves, M. Couto, D. M. Sousa, A. Magalhães, E. Neto, L. Leitão, **F. Conceição**, A. C. Monteiro, M. Ribeiro-da-Silva and M. Lamghari (2020) Nociceptive mechanisms driving pain in a post-traumatic osteoarthritis mouse model. *Scientific Reports*, 10 (1), 15271. (<https://doi.org/10.1038/s41598-020-72227-9>) (IF – 4.38)

L. Leitão, E. Neto, **F. Conceição**, A. Monteiro, M. Couto, C. J. Alves, D. M. Sousa and M. Lamghari (2020) Osteoblasts are inherently programmed to repel sensory innervation. *Bone Research*, 8, 20. (<https://doi.org/10.1038/s41413-020-0096-1>) (IF – 11.59)

D. M. Sousa, P. S. Martins, L. Leitão, C. J. Alves, M. Gomez-Lazaro, E. Neto, **F. Conceição**, H. Herzog and M. Lamghari (2020) The lack of neuropeptide Y-Y₁ receptor signaling modulates the chemical and mechanical properties of bone matrix. *The FASEB Journal*, 34 (3), 4163-4177. (<https://doi.org/10.1096/fj.201902796R>) (IF – 5.19)

M. Couto, D. P. Vasconcelos, D. M. Sousa, B. Sousa, **F. Conceição**, E. Neto, M. Lamghari and C. J. Alves (2020) The Mechanisms Underlying the Biological Response to Wear Debris in Periprosthetic Inflammation. *Frontiers in Materials*, 7 (224). (<https://doi.org/10.3389/fmats.2020.00274>) (IF – 3.51)

L. Leitão, C. J. Alves, D. M. Sousa, E. Neto, **F. Conceição** and M. Lamghari (2019) The alliance between nerve fibers and stem cell populations in bone marrow: life partners in sickness and health. *The FASEB Journal*, 33 (8), 8697-8710. (<https://doi.org/10.1096/fj.201900454R>) (IF – 5.19)

L. Leitão, C. J. Alves, I. S. Alencastre, D. M. Sousa, E. Neto, **F. Conceição**, C. Leitão, P. Aguiar, G. Almeida-Porada and M. Lamghari (2019) Bone marrow cell response after injury and during early stage of regeneration is independent of the tissue-of-injury in 2 injury models. *The FASEB Journal*, 33 (1), 857-872. (<https://doi.org/10.1096/fj.201800610RR>) (IF – 5.19)

E. Neto, C. J. Alves, L. Leitão, D. M. Sousa, I. S. Alencastre, **F. Conceição** and M. Lamghari (2017) Axonal outgrowth, neuropeptides expression and receptors tyrosine kinase phosphorylation in 3D organotypic cultures of adult dorsal root ganglia. *PLoS ONE*, 12 (7), e0181612. (<https://doi.org/10.1371/journal.pone.0181612>) (IF – 3.24)

Abstract

Breast cancer (BC) remains the most common cancer diagnosed in women worldwide. Advanced BC patients often present osteolytic bone metastases, where colonizing BC cells in the bone marrow disrupt the normal bone remodeling process and drive extensive bone degradation. Several epidemiologic observations and pre-clinical studies in the past decade have highlighted an important contribution of the sympathetic nervous system (SNS) in BC patient survival and the establishment and exacerbation of bone metastatic foci, in particular through β_2 adrenergic receptor (β_2 -AR) signaling. The role of this neuro-skeletal axis on the progression of BC is further emphasized by the extensive sympathetic innervation of the periosteum and bone marrow, as well as the expression of adrenergic receptors in BC cells and bone cells.

Nonetheless, the benefits of BC therapeutic interventions targeting sympathetic effectors are still controversial. Multiple epidemiologic studies have reported no benefits of drugs targeting the β_2 -AR on patient survival. Furthermore, most pre-clinical data available is derived from *in vivo* experiments, where the identification of the soluble factors and signaling pathways involved in the sympathetic modulation of the BC bone metastatic niche is extremely challenging. Novel *in vitro* models are being proposed, in particular using microfluidic organ-on-a-chip platforms, to tackle the constraints of standard *in vivo* models in the study of BC extravasation and colonization of the bone. However, to our knowledge, no microfluidic platforms have been designed to address the sympathetic modulation of BC bone metastasis.

In this thesis, we aimed to identify soluble mediators involved in the crosstalk between BC and bone cells under sympathetic activation, in particular through β_2 -AR signaling, at different stages of disease progression.

To address this issue, we first developed a novel metastasis-on-a-chip microfluidic *in vitro* model in order to characterize the mechanisms involved in the sympathetic control of the BC bone metastatic niche. This platform is able to compartmentalize sympathetic neurons, BC cells and osteoclasts seeded on bone slices and facilitate intercellular communication through secreted factors, while preventing direct cell-cell contact between the different cell types. We provided compelling evidence that a dynamic crosstalk between sympathetic neurons, osteoclasts and metastatic BC cells is required in order to raise pro-inflammatory cytokine levels in the BC compartment. Furthermore, the added versatility provided by the inclusion of Quake valves allowed to dictate the direction of communication between compartments, and show that crosstalk between osteoclasts and sympathetic neurons is dispensable for the observed levels of pro-inflammatory cytokines.

We further characterized the SNS modulation of BC bone metastatic niche through a combination of clinical data, proteomic profiling and functional studies with primary human bone cells. We demonstrated that circulating epinephrine levels in BC patients are elevated in the earlier stages of the disease and are maintained after metastatic spread of BC. In order to mimic an exacerbation of adrenergic activity in the different stages of BC progression, we then assessed how pharmacological activation of β_2 -AR would affect the proteomic expression profile in primary or metastatic BC *in vitro*. In primary BC, β_2 -AR signaling led to an overexpression of osteoclast inhibitors, which in turn translated in a robust decrease in human osteoclast differentiation and resorption activity. In contrast, we showed that paracrine signaling from metastatic BC under β_2 -AR do not affect osteoclast resorption. Furthermore, we concluded that the addition of osteoblasts to the model rescued the osteoclast resorption activity after exposure to the secretome of β_2 -AR primed primary BC.

Overall, this thesis presented novel insights on the role of sympathetic signaling in BC bone metastasis. In particular, we highlight the adrenergic exacerbation in BC patients and the changes in the proteomic profile of BC after β_2 -AR signaling at different stages of disease progression, while using two distinct *in vitro* models: a novel metastasis-on-a-chip microfluidic model or pharmacological activation of β_2 -AR in BC. We also emphasized different outcomes in osteoclast activity after exposure to paracrine signaling from primary or metastatic BC cells. Our findings set the basis for future studies on the link between sympathetic activation and the establishment and progression of BC bone metastasis, and suggest that therapeutic interventions targeting β_2 -AR should tackle BC at earlier stages of disease progression before metastatic spread.

Resumo

O cancro da mama é atualmente o tipo de cancro mais comum diagnosticado em mulheres. Pacientes de cancro da mama avançado apresentam frequentemente metástases osteolíticas, nas quais as células do cancro da mama colonizam a medula óssea e destabilizam o processo normal de remodelação óssea, levando a uma extensa degradação do osso. Na última década, vários estudos epidemiológicos e pré-clínicos destacaram uma importante contribuição do sistema nervoso simpático na taxa de mortalidade dos pacientes de cancro da mama e no estabelecimento e exacerbação de focos metastáticos no osso, em particular pela sinalização celular do recetor adrenérgico β_2 (β_2 -AR). O papel deste eixo neuro-esquelético na progressão do cancro da mama é ainda mais sublinhado pela extensa inervação do perióstio e da medula óssea, assim como pela expressão de recetores adrenérgicos em células de cancro da mama e do osso. Não obstante, os benefícios de intervenções terapêuticas que têm como alvo efetores adrenérgicos são ainda controversos. Vários estudos epidemiológicos reportaram a inexistência de benefícios de fármacos inibidores do β_2 -AR na sobrevivência de pacientes do cancro da mama. Além disso, a maior parte dos dados pré-clínicos disponíveis de momento é proveniente de experiências *in vivo*, onde a identificação de fatores solúveis e vias de sinalização envolvidas na modulação simpática do nicho metastático ósseo do cancro da mama é extremamente complexa. Novos modelos *in vitro* estão a ser desenvolvidos para contornar as limitações dos modelos *in vivo* tradicionais para o estudo da extravasão e colonização do osso, em particular usando plataformas microfluídicas organ-on-a-chip. No entanto, no nosso conhecimento, nenhuma plataforma microfluídica foi ainda desenhada para estudar a modulação simpática da metástase óssea do cancro da mama.

Nesta tese, procurámos identificar mediadores solúveis envolvidos na comunicação celular entre o cancro da mama e as células do osso sob ativação simpática, em particular através do β_2 -AR, em diferentes estádios da progressão da doença.

Para alcançar este objetivo, desenvolvemos um novo modelo *in vitro* de metastasis-on-a-chip em plataformas microfluídicas de modo a caracterizar os mecanismos envolvidos no controlo simpático do nicho metastático ósseo do cancro da mama. Esta plataforma é capaz de compartimentalizar neurónios simpáticos, células do cancro da mama e osteoclastos cultivados em lâminas de osso, e facilita a comunicação intercelular através de fatores secretados enquanto impede o contacto direto entre os diferentes tipos celulares. Nós fornecemos provas convincentes que demonstram que uma comunicação dinâmica entre neurónios simpáticos, osteoclastos e células de cancro da mama metastáticas é necessária para aumentar os níveis de citocinas pró-inflamatórias no

compartimento do cancro da mama. Adicionalmente, a versatilidade oferecida pela inclusão de válvulas Quake permitiu controlar a direção de comunicação entre compartimentos, e mostrou que a comunicação entre osteoclastos e neurónios simpáticos é dispensável para os níveis de citocinas pró-inflamatórias observados.

Posteriormente, procedemos à caracterização da modulação do nicho metastático ósseo do cancro da mama pelo sistema nervoso simpático através de uma combinação de dados clínicos, perfil proteómico e estudos funcionais com células de osso primárias humanas. Demonstrámos que os níveis de epinefrina na circulação de pacientes de cancro da mama primário estão elevados e são mantidos após a propagação metastática da doença. De forma a mimetizar uma exacerbação de atividade adrenérgica nos diferentes estadios de progressão do cancro da mama, avaliámos de seguida o efeito da ativação farmacológica do β_2 -AR no perfil de expressão proteómica de células de cancro da mama primário ou metastático *in vitro*. Em células de cancro da mama primário, a ativação da via de sinalização β_2 -AR levou a uma sobreexpressão de inibidores de osteoclastos, que por sua vez se traduziu numa redução robusta da diferenciação e atividade de reabsorção óssea de osteoclastos. Pelo contrário, mostrámos que a comunicação parácrina de cancro da mama metastático após estimulação do β_2 -AR não afeta a atividade de reabsorção do osso. Adicionalmente, concluímos que a adição de osteoblastos ao nosso modelo reverteu os níveis de reabsorção óssea de osteoclastos expostos ao secretoma de cancro da mama primário sob influência de sinalização de β_2 -AR.

De modo geral, este trabalho trouxe novas considerações no papel da sinalização simpática na metástase óssea do cancro da mama. Em particular, identificámos uma exacerbação adrenérgica em pacientes de cancro da mama assim como mudanças no perfil proteómico do cancro da mama após sinalização β_2 -AR em diferentes estadios de progressão da doença, usando dois modelos *in vitro* distintos: ativação farmacológica do β_2 -AR no cancro da mama ou um novo modelo microfluídico de metastasis-on-a-chip. Também destacámos resultados distintos na atividade de osteoclastos após exposição a sinalização parácrina de cancro da mama primário ou metastático. Estas descobertas podem servir de base para a investigação futura dos mecanismos envolvidos no controlo do sistema nervoso simpático sobre o estabelecimento e progressão de metástases ósseas de cancro da mama, e sugerem que as estratégias terapêuticas com alvo no β_2 -AR devam focar-se na janela de tempo que precede a metástase.

Table of Contents

Acknowledgements	ix
List of Publications	xi
Abstract	xiii
Resumo	xv
List of Abbreviations	xx
Chapter I. Introduction and motivation	1
1.1. Nervous system and bone.....	2
1.2. Sympathetic nervous system and bone	4
1.2.1. <i>Anatomic and molecular characterization of the sympathetic nervous system</i>	4
1.2.2. <i>SNS control of bone metabolism</i>	4
1.3. SNS and breast cancer	7
Sympathetic Activity in Breast Cancer and Metastasis: a partner in crime.....	7
<i>Abstract</i>	8
1.3.1. <i>Introduction</i>	9
1.3.2. <i>BC and the SNS: a complex picture</i>	10
1.3.3. <i>BC Metastasis and the Bone Niche</i>	17
1.3.4. <i>BC and Beta-Blockers: Clinical Perspective</i>	21
1.3.5. <i>Conclusion and Future Perspectives</i>	26
1.4. <i>In vitro</i> microfluidic models	29
1.4.1. <i>Microfluidic models of bone metastasis</i>	29
1.4.2. <i>Microfluidic models of bone innervation</i>	32
1.5. Thesis outline and objectives	39
1.6. References	41
Chapter II. Development of an organ-on-a-chip platform to study the effect of synergistic crosstalk of osteoclasts and sympathetic neurons on the BC secretome	59
2.1. Fabrication of microfluidic templates for organ-on-a-chip models	60
2.2. Metastasis-on-a-chip microfluidic model of sympathetic modulation of breast cancer bone metastasis	62

A Metastasis-On-a-Chip Approach to Explore the Sympathetic Modulation of Breast Cancer Bone Metastasis	62
<i>Abstract</i>	63
2.2.1. <i>Introduction</i>	64
2.2.2. <i>Materials and Methods</i>	66
2.2.3. <i>Results</i>	71
2.2.4. <i>Discussion</i>	83
<i>Supplementary Data</i>	88
<i>Acknowledgements</i>	93
2.3. Chapter conclusions.....	94
2.4. References	95
Chapter III. <i>In vitro</i> pharmacological β_2-AR activation and its effect on the breast cancer modulation of the bone niche in different stages of disease progression..	102
3.1. Breast cancer regulation of the pre-metastatic bone niche.....	103
3.2. β_2 -Adrenergic modulation of the BC bone metastatic niche.....	105
The Secretome of Primary and Bone Metastatic Breast Cancer Elicits Distinct Outcomes in Human Osteoclast Activity After Activation of β_2 Adrenergic Signaling.....	105
<i>Abstract</i>	106
3.2.1. <i>Introduction</i>	107
3.2.2. <i>Materials and Methods</i>	108
3.2.3. <i>Results</i>	115
3.2.4. <i>Discussion</i>	130
3.3. Comparison of the proteomic profile of primary and metastatic BC.....	135
<i>Supplementary Data</i>	138
3.4. Chapter Conclusions	158
3.5. References	159
Chapter IV. Main Conclusions.....	168
4.1. Main Conclusions	169
4.2. References	172
Annex A.....	174
Annex B.....	187

List of Abbreviations

3D	Three-dimensional
α -AR	α -Adrenoreceptor
ATF4	Activating transcription factor 4
β -AR	β -Adrenoreceptor
BDNF	Brain derived neurotrophic factor
BMSC	Bone marrow stromal cells
cAMP	Cyclic adenosine monophosphate
CATK	Cathepsin K
CGRP	Calcitonin gene-related peptide
CNS	Central Nervous System
COMT	Catechol-O-methyltransferase
COX2	Cyclooxygenase-2
CTC	Circulating tumor cells
DBH	Dopamine β -hydroxylase
DRG	Dorsal root ganglia
ECM	Extracellular matrix
EMT	Epithelial and mesenchymal transition
EPAC	Exchange protein directly activated by cAMP
Epi	Epinephrine
ER	Estrogen receptor
GPCR	G protein-coupled receptor
HER2	Epidermal growth factor receptor 2
HPA	Hypothalamic/Pituitary Axis
HSC	Hematopoietic Stem Cell
HUVEC	Human umbilical vein endothelial cell
ICV	Intra-cerebro-ventricular
IGF	Insulin growth factor
IL	Interleukin
ISO	Isoproterenol
L-DOPA	Dihydroxyphenylalanine
LOX	Lysyl Oxidase
MAO	Monoamine oxidase
MCP1	Monocyte chemoattractant protein 1
M-CSF	Macrophage colony stimulating factor

MMP	Matrix metalloproteinase
MSC	Mesenchymal Stem Cells
NE	Norepinephrine
NET	Norepinephrine transporter
NPY	Neuropeptide Y
PD-1	Programmed death 1
PDGF	Platelet derived growth factor
PD-L1	Programmed death ligand 1
PDMS	Polydimethylsiloxane
PGE2	Prostaglandin E2
PKA	Protein kinase A
PMMA	Poly methyl methacrylate
PNMT	Phenylethanolamine N-methyltransferase
PNS	Peripheral Nervous System
PPAR γ	Peroxisome proliferator-activated receptor γ
PR	Progesterone receptor
PSNS	Parasympathetic nervous system
PTH	Parathyroid hormone
PTHr1	Parathyroid hormone receptor 1
PTHrP	Parathyroid hormone related protein
PTX3	Pentraxin 3
RANKL	Receptor activator of NF- κ B ligand
ROS	Reactive oxygen species
SHH	Sonic Hedgehog
SNS	Sympathetic Nervous System
SP	Substance P
TAM	Tumor-associated macrophages
TGF- β	Transforming growth factor β
TH	Tyrosine Hydroxylase
TNBC	Triple negative breast cancer
TNF- α	Tumor necrosis factor α
TRAcP	Tartrate Resistant Acid Phosphatase
UV	Ultra-violet
VEGF	Vascular endothelial growth factor

Chapter I. Introduction and motivation

1.1. Nervous system and bone

The nervous system is responsible for the control of all physiological functions of the body, from the regulation of heart rate, breathing, digestion and body temperature, to complex processes such as memory and cognition^[1]. The central nervous system (CNS) is able to integrate external and internal stimuli and trigger adequate neuronal or neuroendocrine responses to maintain body homeostasis, via the autonomic branch of the peripheral nervous system (PNS) or the hypothalamic/pituitary axis (HPA), respectively^[2] (Figure 1a). HPA downstream effectors target multiple tissues, including the bone^[3]. Skeletal homeostasis is important during all stages of development and is maintained through a tightly regulated bone remodeling process, where old or damaged bone matrix is resorbed and new mineralized matrix is deposited in a synchronized fashion. The first evidences of a central regulation of bone remodeling emerged from observations that transgenic mice lacking leptin (*ob/ob* mice), a hormone involved in energy metabolism and gonadal function, displayed high bone mass phenotype, and that intra-cerebro-ventricular (ICV) infusion of leptin in *ob/ob* mice reverted this outcome^[4]. Interestingly, central control of bone remodeling by leptin was later shown through parabiosis experiments to be exerted through neuronal autonomic pathways and not through hormonal release in the circulation^[5]. Other central neuroendocrine mechanisms involved in the regulation of bone remodeling have since then been described *in vivo*, highlighting the complexity of the brain-bone crosstalk. For instance, osteoanabolic stimuli through growth hormone^[6], thyroid stimulating hormone^[7] and melatonin^[8], and osteocatabolic signaling such as the Neuropeptide Y (NPY) pathway^[9-11] and the follicular stimulating hormone^[12] act to balance the bone remodeling process and maintain homeostasis.

Besides neuroendocrine regulation of bone metabolism, signals from the CNS can be relayed to the bone through nerve terminals from the PNS (Figure 1b). In fact, the bone is highly innervated with sensory and sympathetic nerve endings in the periosteum and along blood vessels in the bone marrow^[13]. In addition to their role in thermal and mechanical sensing and pain, sensory neurons are able to modulate bone metabolism through the release of several neurotransmitters directly in the bone microenvironment. The importance of sensory neurotransmitters substance P (SP) and calcitonin gene-related peptide (CGRP) was demonstrated in sensory denervation studies that show a reduction in murine bone formation and concomitant increase in bone resorption activity *in vivo*^[14, 15]. Sensory

innervation is also crucial during fracture healing, since mice with altered disrupted sensory signaling displayed impaired bone biomechanical strength and bone callus maturation^[16, 17].

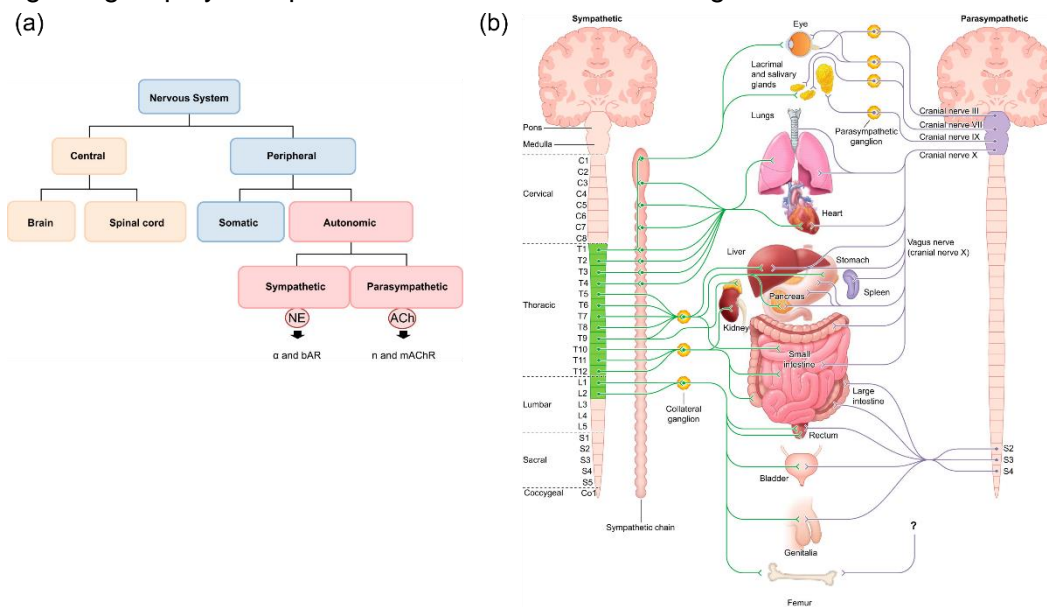


Figure 1. Anatomical representation of the nervous system. (a) Functional anatomy of the nervous system. (b) Anatomical representation of the autonomic nervous system. Sympathetic and parasympathetic nerves relay information from the central nervous system to target tissues and organs. Adapted with permission from ^[18].

Bone cells are not only capable of receiving input from nerve endings but they can also shape the pattern of innervation by guiding axonal extension and neurite growth. This is evident during embryonic development and during fracture healing, where extensive sensory sprouting towards areas of high osteogenic activity is observed^[19, 20]. In pathological settings where bone homeostasis is deregulated, such as bone cancer and osteoporosis, changes in innervation pattern of the bone are common and suggest alterations in bone neurotrophic signaling^[21-23]. Mechanistically, it is widely accepted that mesenchymal stem cells (MSC), a subpopulation of cells present in the bone marrow, promote axonal extension through expression of brain derived neurotrophic factor (BDNF) and nerve growth factor (NGF) ^[24]. Moreover, multinucleated bone resorbing osteoclasts, cells of the hematopoietic lineage that are usually overactive in osteoporosis and metastatic breast cancer (BC), are able to promote sensory axonal growth and sensitization through the expression of netrin-1^[21] and monocyte chemoattractant protein 1 (MCP1)^[25], in addition to the acidification of their extracellular environment as a result of bone resorption activity^[26]. On the other hand, differentiated bone forming osteoblasts of the mesenchymal lineage were shown to repress sensory axonal growth through sonic hedgehog (SHH)^[27], highlighting the contrasting effects of bone forming and bone degrading cells on sensory innervation during bone remodeling.

1.2. Sympathetic nervous system and bone

1.2.1. Anatomic and molecular characterization of the sympathetic nervous system

As stated above, the PNS is involved in the relay of information from the CNS to maintain homeostasis in target peripheral tissues. The PNS is divided in two opposing arms, the parasympathetic nervous system (PSNS) and the sympathetic nervous system (SNS). While the PSNS regulates digestive, excretory and reproductive body functions, the SNS is mainly involved in acute stress responses, being able to promote energy mobilization and change heart and respiratory rates after perceived external and internal stressors^[28]. Sympathetic preganglionic neurons extend from the spinal cord towards dorsal root ganglia, where they synapse with adrenergic postganglionic neurons that in turn innervate most of the tissues of the body, including the bone^[29]. Sympathetic neurons are present in the periosteum, intra-cortical pores and bone marrow, being usually associated with blood vessels and showing increased density around active bone remodeling surfaces^[13, 30]. Sympathetic neurons are characterized by the expression of tyrosine hydroxylase (TH), an enzyme involved in the production of the main sympathetic neurotransmitters, the catecholamines norepinephrine (NE) and epinephrine (Epi)^[31]. The first, rate-limiting step of catecholamine synthesis is the conversion of tyrosine to dihydroxyphenylalanine (L-DOPA) by TH. L-DOPA is then converted to dopamine through L-aromatic amino acid decarboxylase. Finally, dopamine is converted to NE by the action of dopamine β -hydroxylase (DBH) and can then be further processed into Epi through phenylethanolamine N-methyltransferase (PNMT)^[18]. NE released by sympathetic neurons or Epi released systemically by the adrenal gland bind to their endogenous receptors in target cells, the α/β -adrenoreceptors (α -ARs, β -ARs), and trigger signaling pathways that ultimately lead to the “fight or flight” response to acute stress^[32-34]. Expressed in a multitude of tissues throughout the body, ARs are a family of transmembrane receptors comprised of nine different receptors: G_q protein-coupled α_{1A} , α_{1B} and α_{1D} ARs; G_i protein-coupled α_{2A} , α_{2B} and α_{2C} ARs; G_s protein-coupled β_1 , β_2 , β_3 ARs. After signal transduction in the target cells, the remaining NE is reuptaken by neurons through the NE transporter (NET) or metabolized by monoamine oxidase (MAO) and catechol-O-methyltransferase (COMT)^[18].

1.2.2. SNS control of bone metabolism

Despite bone forming osteoblasts and bone resorbing multinucleated osteoclasts being the main players in the process of bone remodeling, they are part of a complex

microenvironment with a multitude of other cells, including neurons, that can also impact their activity. In fact, osteoblasts-lineage cells and osteoclasts are able to receive and integrate SNS input, since both cell types express ARs and are also able to uptake and catabolize NE from their extracellular surroundings^[35-38]. Although α -AR expression was detected in osteoblasts^[39], β_2 -AR is the most prevalent AR in both osteoblasts and osteoclasts^[35, 36, 38]. β_2 -AR stimulation leads to intracellular cyclic adenosine monophosphate (cAMP) and protein kinase A (PKA) activation, ultimately culminating transcription factor translocation and target gene expression.

Most of the available data on the consequences of β_2 -AR signaling on bone remodeling concerns murine pharmacological and genetic *in vitro* and *in vivo* approaches. *In vivo*, long term, daily intraperitoneal injection of the β_1/β_2 -AR agonist isoproterenol (ISO) led to a marked decrease in bone formation rates and bone mass^[5]. Similar findings were observed after subcutaneous injection of specific β_2 -AR agonists salbutamol and clenbuterol during six weeks, where bone mass, mineral density and strength was reduced after treatments^[40]. This effect was shown to be mediated in part by elevated levels of osteopontin and increased osteoclast activity after pharmacological β -AR activation *in vivo*^[41]. The opposite approach revealed consistent outcomes, since the pharmacological blockage of β -AR signaling with β_1/β_2 -AR antagonist propranolol led to increased bone mass and mineral density^[5]. This effect was also observed in ovariectomy-driven bone loss models, where propranolol together with exercise or intermittent parathyroid hormone (PTH) treatment led to improvements in bone mass and bone architecture^[42, 43].

Genetic manipulation of β -AR expression helped to elucidate the role of these receptors in bone remodeling. Mice lacking all three β -AR show an increased vertebral and cortical bone mass, but also display alterations in body weight that could impact bone mass accrual^[44]. On the other hand, previous studies showed that germline deletion of β_2 -AR led to a high bone mass phenotype and that ICV infusion of leptin did not induce bone loss in these animals, indicating that SNS signaling is required for the effect of leptin in the modulation of bone mass^[45]. Furthermore, this phenotype was mediated by a decreased osteoblast expression of receptor activator of NF- κ B ligand (RANKL), a major regulator of osteoclast differentiation and bone resorption activity, and consequent inhibition of osteoclast numbers^[45]. Furthermore, similarly to the germline deletion of β_2 -AR, the removal of β_2 -AR specifically in osteoblasts led to an increase in bone mass and decreased levels of RANKL, in an activating transcription factor 4 (ATF4) dependent fashion^[46].

Mechanistically, *in vitro* pharmacological stimulation of β_2 -AR with NE or ISO increased murine bone marrow derived osteoclast differentiation and resorption, either by direct osteoclast stimulation or indirectly through osteoblast RANKL induction in co-culture experiments^[47]. The upregulation of RANKL expression seems to be the main outcome of

β_2 -AR stimulus in osteoblast-lineage cells, evidenced in bone marrow stromal cells, calvarial osteoblasts and also in osteocytic MLO-Y4 cell lines, that eventually leads to increased osteoclastogenesis^[48-50]. On the other hand, the direct effect of ISO on osteoclasts was shown to be mediated by the generation of reactive oxygen species (ROS) in both murine bone marrow osteoclasts or RAW264.7 osteoclast-like cell lines^[35]. Reports on the effect of adrenergic stimulus on human osteoclasts are scarce, but human osteoclasts derived from bone marrow surgical waste of elderly patients were shown to display increased differentiation and resorption activity after Epi or ISO stimulation^[51]. Overall, both *in vivo* and *in vitro* studies point to an osteocatabolic effect of adrenergic signaling on physiological bone remodeling, either through central or peripheral regulation of osteoblast/osteoclast function.

1.3. SNS and breast cancer

[Review Article]

Sympathetic Activity in Breast Cancer and Metastasis: a partner in crime

This chapter was based on the following published article:

F. Conceição, D.M. Sousa, J. Paredes, M. Lamghari (2021) Sympathetic activity in breast cancer and metastasis: partners in crime, *Bone Research*, 9, 9.

(<https://doi.org/10.1038/s41413-021-00137-1>)

Abstract

The vast majority of advanced breast cancer (BC) patients present skeletal complications that severely compromise their quality of life. BC cells are characterized by a strong tropism to the bone niche. After engraftment and colonization on the bone, BC cells interact with native bone cells to hinder the normal bone remodeling process and establish an osteolytic “Metastatic Vicious Cycle”. The sympathetic nervous system has emerged in recent years as an important modulator of BC progression and metastasis, potentiating and accelerating the onset of the vicious cycle, leading to extensive bone degradation. Furthermore, sympathetic neurotransmitters and their cognate receptors have been shown to promote several hallmarks of BC such as proliferation, angiogenesis, immune escape and invasion of the extracellular matrix.

In this review, we gathered the current knowledge concerning the complex interactions that take place at the tumor microenvironment, with a special emphasis on the sympathetic modulation of BC cells and stromal cells. Of note, the differential action of epinephrine and norepinephrine, either through α/β -Adrenergic Receptors, on BC progression prompts careful consideration when designing new therapeutic options. In addition, the contribution of sympathetic innervation to the formation of bone metastatic foci is also highlighted. Particularly, the remarkable ability of the adrenergic signaling to condition the native bone remodeling process and modulate the bone vasculature driving BC cell engraftment in the bone niche. Finally, clinical perspectives and developments on the use of β -Adrenergic Receptor inhibitors for BC management and treatment are also discussed.

Keywords

Adrenergic Receptor, Beta-Blocker, Bone metastasis, Breast Cancer, Sympathetic nervous system.

1.3.1. Introduction

Under physiological conditions, the Sympathetic Nervous System (SNS) is involved in the so called “fight-or-flight” response to acute stress. Upon perceiving threats to internal homeostasis, the SNS acts on multiple molecular and cellular processes throughout the body that will ensure a coordinated adaptive response to different stressors. Physical mobility is boosted through the increase of heart and respiratory rate, as well as energy mobilization from the adipose tissue and liver^[52, 53]. On the other hand, anabolic processes such as digestion, gastrointestinal motility and reproduction are hampered^[34, 53, 54]. Sympathetic signaling is mainly achieved through the peripheral release of Norepinephrine (NE) by sympathetic nerve terminals or systemic release of Epinephrine (Epi) into the circulation by the adrenal gland. These catecholamines are the endogenous ligands of α/β Adrenoreceptors (α -AR, β -AR), with widespread expression in a multitude of cell types and tissues^[32, 33, 51, 55]. This family of receptors is composed of a total of nine G protein-coupled receptors (GPCRs): G_q -coupled α_1A , α_1B and α_1D ARs; G_i -coupled α_2A , α_2B and α_2C ARs; and finally, G_s -coupled β_1 , β_2 and β_3 ARs.

BC is still a major socioeconomic issue, being the leading cause of cancer-specific death of women in 2018 (<https://gco.iarc.fr/today/home>). It is a highly heterogeneous disease, usually being characterized by Estrogen receptor (ER), Progesterone receptor (PR) and Epidermal Growth Factor Receptor 2 (HER2) status of the primary tumor. Advances in diagnostic and adjuvant therapies have improved the life expectancy of BC patients, but this condition remains incurable in later stages of disease progression^[56]. Surgery and radiation therapy are gold standards for the treatment of early stage BC, as well as hormone therapy and HER2 targeting antibody trastuzumab for HER2 positive cancers. Systemic administration of hormone therapy, targeted therapy, chemotherapy or a combination of these is usually the preferred treatment route in late stage metastatic BC. Nonetheless, the 5-year survival rate of women diagnosed with distant metastasis is 27% (<https://www.cancer.org/cancer/breast-cancer>). These treatments are still ineffective and commonly associated to toxic side effects, and therefore there is still a need for improved therapeutic options. A better understanding of the pathological processes through which BC thrives in the host is of paramount importance to uncover new therapeutic targets.

In the past decade, the physiological mechanisms that govern the response to stress have emerged as a potential therapeutic target in BC due to several epidemiologic and pre-clinical studies^[57-59]. In particular, the action of NE and Epi on their cognate receptors has raised important considerations regarding their role on BC progression, analogously to what is observed in other bone tropic cancers such as the prostate cancer^[60-64]. However, the

adrenergic regulation of the multiple cellular processes that drive BC still remains a matter of intense debate.

In this review, we will discuss the current knowledge found in the literature concerning preclinical and clinical data on SNS modulation of BC. Most metastatic BC patients present severe skeletal complications such as hypercalcemia, pain and increased incidence of fractures^[65]. Therefore, insights on the sympathetic regulation of bone metastatic disease will be also discussed in the following sections.

1.3.2. BC and the SNS: a complex picture

Adrenoreceptors (ARs) have been reported to be expressed in a wide range of BC cell lines (Table I), as well as in tumor samples of BC patients^[66-68]. AR overexpression, particularly β_2 -AR, was correlated with poor prognosis of ER- BC patients in a recent study by Kurozumi *et al*^[68], where immune biomarkers, such as the grade of tumor-infiltrating lymphocytes and programmed death ligand 1 (PD-L1) expression, were shown to be significantly reduced in these patients. Another report by Liu *et al*^[66] demonstrated that β_2 -AR level was correlated with lower disease-free survival and higher lymph node metastasis in a small cohort of HER2⁺ BC patients. Both these studies point to a putative role of β_2 -AR in BC pathology, but scrutinizing the mechanisms by which it promotes disease progression is still a complex exercise. In this section, we will gather the available data regarding the effect of multiple ARs on BC, from primary tumor proliferation and survival to Extracellular Matrix (ECM) invasion and entrance into systemic circulation.

Table I. AR expression on human BC cell lines

Cell Line	Molecular Subtype	AR expressed	Reference
T47D	Luminal A (ER ⁺ , PR ⁺ , HER2 ⁻)	α_{2A} -AR, α_{2B} -AR, α_{2C} -AR	[69]
MCF7	Luminal A (ER ⁺ , PR ⁺ , HER2 ⁻)	α_1 -AR, α_{2B} -AR, α_{2C} -AR, β_1 -AR, β_2 -AR	[66, 70-72]
ZR-75	Luminal A (ER ⁺ , PR ⁺ , HER2 ⁻)	β_1 -AR, β_2 -AR	[70]
BT474	Luminal B (ER ⁺ , PR ⁺ , HER2 ⁺)	β_2 -AR	[66]
SKBR3	HER2 (ER ⁻ , PR ⁻ , HER2 ⁺)	β_2 -AR	[66]
MDA-MB-453	HER2 (ER ⁻ , PR ⁻ , HER2 ⁺)	β_2 -AR	[70]
MDA-MB-231	Basal (ER ⁻ , PR ⁻ , HER2 ⁻)	β_2 -AR	[58, 72-74]
MDA-MB-468	Basal (ER ⁻ , PR ⁻ , HER2 ⁻)	β_1 -AR, β_2 -AR	[70, 73]
HS578T	Basal (ER ⁻ , PR ⁻ , HER2 ⁻)	α_{2A} -AR	[72]

1.3.2.1. Proliferation and survival

Cancer cell proliferation and inhibition of apoptosis are crucial hallmarks of cancer^[75]. Adrenergic signaling has been implicated in several apoptosis pathways and it has been

previously suggested that endogenous catecholamines directly exert pro-survival effects on BC cells^[76-78] (Figure 2, 3). Epi was described as an antiapoptotic stimulus in human BC cells *in vitro*, inactivating the proapoptotic protein BAD through phosphorylation in a PKA-dependent fashion^[77]. Furthermore, another *in vitro* experiment by Reeder and colleagues have shown that NE and Epi decrease the efficacy of commonly used drugs targeting proliferating cells, such as paclitaxel, since these catecholamines arrest MDA-MB-231 BC cells in G1 phase, slowing down the cell cycle^[78]. These results are consistent with evidence from other *in vitro* studies that show that β_2 -AR agonists hamper triple-negative BC cell proliferation and DNA synthesis^[76, 79, 80]. Strikingly, low concentrations of Epi increased MCF7 and MDA-MB-231 cell proliferation, while β_2 -AR agonist ISO decreased proliferation in both cell lines^[80]. These findings could be explained by the fact that Epi was shown to differentially bind to distinct ARs depending on its concentration, with greater affinity to α_2 -AR in nM concentrations, while shifting to β_2 -AR binding at μ M concentrations^[76]. Moreover, the increase in proliferation evoked by low concentrations of Epi was abrogated by the addition of the α_2 -AR antagonist rauwolscine^[76]. Exciting questions remain, such as the impact of fluctuations in Epi or NE levels in the tumor microenvironment for BC progression, and how the translation of that knowledge to a clinical setting can be made. There are already recent *in vivo* evidence that shed some light on the impact of circulating Epi on tumor growth, where Walker and colleagues have shown that adrenal denervation and inhibition of Epi release does not impact disease progression^[81].

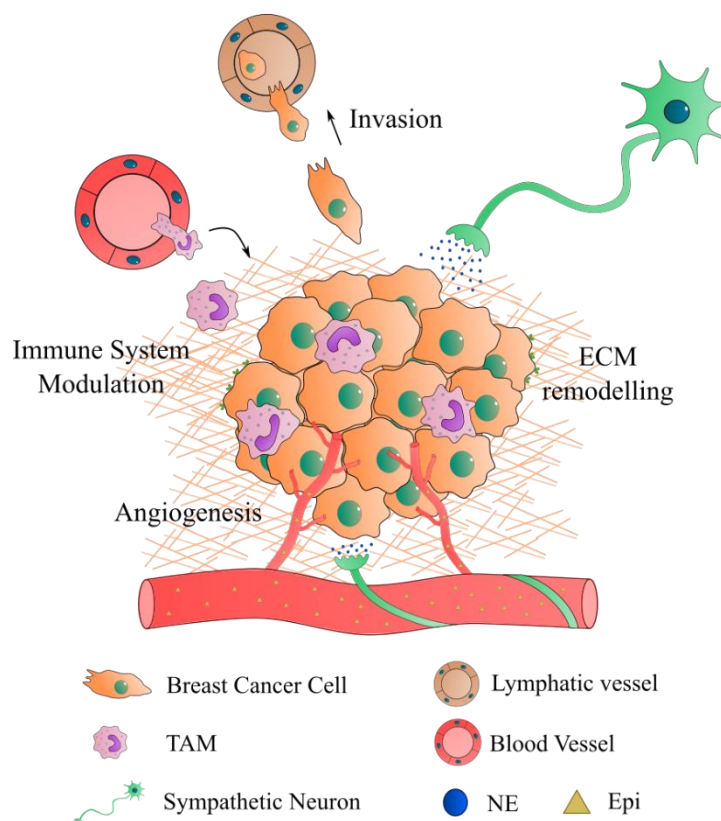
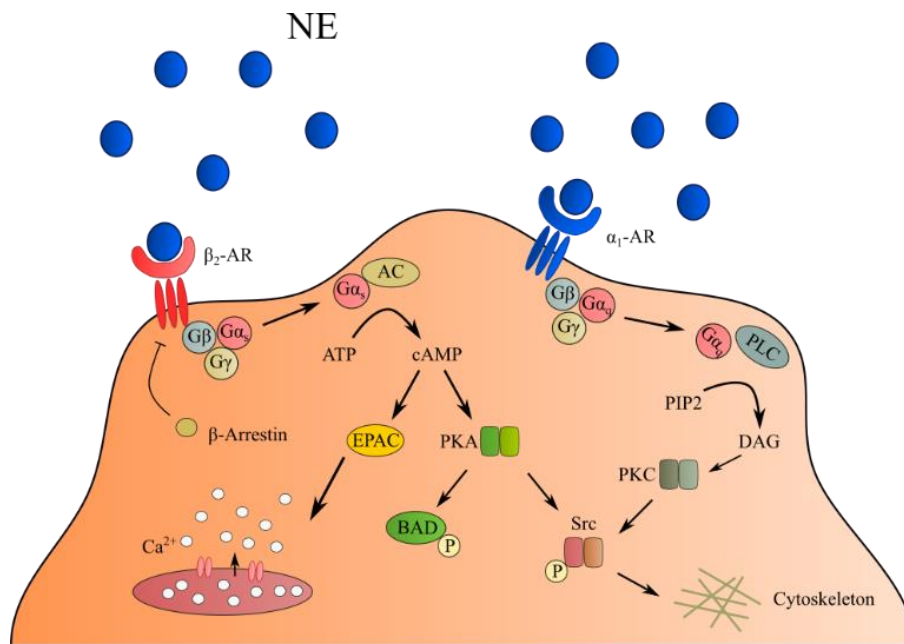


Figure 2. Sympathetic control of BC progression. NE released from sympathetic neurons closely associated with blood vessels, as well as Epi that diffuses from the circulation, modulate several important hallmarks of BC such as survival, angiogenesis, immune surveillance escape, ECM remodeling and invasion. NE, norepinephrine; Epi, epinephrine; TAM, tumor-associated macrophage; ECM, extracellular matrix.

Some observations from *in vivo* studies point to a negligible effect of β -ARs on primary tumor growth, since ISO stimulation of orthotopic BC tumors did not change primary tumor proliferation compared to vehicle controls^[58, 76, 82, 83]. It is unclear whether these results are due to the direct action of β_2 -AR on tumor cell proliferation, or if tumor growth is inhibited by other cell types in the stroma, or even by a combination of direct and indirect effects. Another study, using human xenografts in immunocompromised mice, reported an increased ER⁺/PR⁺ BC tumor growth after inoculation with α_2 -AR agonist clonidine^[84]. Tumor growth was accompanied by a similar increase in proliferation of tumor associated fibroblasts, and thus an indirect effect of α_2 -AR agonism through the tumor microenvironment cannot be ruled out^[84]. It is also intriguing that Thaker and colleagues reported an increase in MDA-MB-231 tumor growth after chronic stress induction in an orthotopic BC model^[85], contrasting with the studies previously discussed. Of note, pharmacological β -AR activation seems to inhibit primary tumor growth^[58, 76], while endogenous chronic stress either causes negligible effects or increases tumor growth^[82, 83, 85-87]. This raises important questions such as the possible existence of compensatory mechanisms exerted by other ARs when endogenous stress models are used, since Epi and NE can stimulate both α -ARs and β -ARs. In fact, α_2 -AR antagonists were shown to counteract the increase in tumor growth evoked by restraint stress^[86]. Lamkin and colleagues also showed that α_2 -AR blockade, in the absence of chronic stress, recapitulates the tumor growth observed when the SNS was endogenously activated^[86], adding another layer of complexity to the impact of the SNS signaling on BC. This observation probably stems from the fact that pre-synaptic α_2 -ARs in peripheral SNS neurons provide a negative feedback loop to control NE release from neuronal terminals^[88]. Thus, blockage of α_2 -ARs, in the absence of chronic stress, will boost the release of NE in the tumor microenvironment, mirroring the endogenous activation of the SNS.



↑ Survival, ECM remodelling, Cytoskeletal reorganization
 ↑ Angiogenesis, TAM recruitment

Figure 3. Adrenergic receptor downstream signaling. β_2 -AR activation triggers several downstream signaling pathways, mediated by an increase in intracellular cAMP, leading to Ca^{2+} release, apoptosis inhibition through phosphorylation of BAD, and cytoskeletal rearrangement. β_2 -ARs are quickly desensitized by β -arrestins after ligand binding and signal transduction. Alternatively, α_1 -AR stimulation has also been described to promote invasive phenotypes through PKC-mediated signaling pathways. NE, norepinephrine; TAM, tumor-associated macrophage; ECM, extracellular matrix

1.3.2.2. Angiogenesis

As breast tumors proliferate and grow, the need for nutrients and oxygen rises concordantly. These needs are met by the sprouting of new blood vessels that give rise to a network of often aberrant vasculature in the tumor microenvironment^[89]. The SNS has been emerging as an important player in neo-angiogenesis, since it has been already shown that sympathetic outflow can induce the secretion of proangiogenic factors by BC cells, namely the vascular endothelial growth factor (VEGF)^[82, 90-92]. In addition, direct cell-cell contact between BC cells and endothelial cells leads to increased capillary structures *in vitro*, a result markedly potentiated by the addition of NE^[91]. This effect was proven to be mediated by the β_2 -AR/PKA/mTOR pathway and by the upregulation of Notch ligand Jagged-1, directly augmenting Notch signaling in endothelial cells^[91]. Interestingly, there seems to be a cell specific response to β_2 -AR agonists in terms of VEGF expression, not entirely due to

differential β_2 -AR expression^[90]. β_2 -AR agonists increased VEGF production in a brain tropic variant of MDA-MB-231 cell line *in vitro*, but not on the parental cell line or in low β_2 -AR expressing cells, such as MCF7 cells^[90]. Distinct targets of downstream effectors of the β_2 -AR/PKA pathway in the different cell lines might explain the disparity in terms of angiogenic responses.

Other players have recently been suggested to be involved in the sympathetic regulation of tumor angiogenesis. Activation of Peroxisome proliferator-activated receptor γ (PPAR γ) markedly decreased VEGF expression from 4T1 murine BC cells *in vitro* and NE was shown to inhibit PPAR γ expression in these cells^[92]. This inhibition was abrogated by the addition of ICI118551 pointing towards a β_2 -AR mediated effect^[92].

In addition to *in vitro* data previously discussed, there is growing evidence gathered from several *in vivo* studies showing that chronic stress modulates neo-angiogenesis and BC lymph vasculature. Chronic restraint stress, as a model of endogenous SNS activation, increased VEGFC secretion from MDA-MB-231 orthotopic tumors in immunocompromised mice, as well as from 66cl4 tumors in immunocompetent mice, leading to increased tumor lymphatic vessel density^[82]. This effect was recapitulated or abrogated by ISO and propranolol treatment, respectively, hinting towards a β -AR specific signaling pathway^[82]. Stress-induced production of VEGF in 66cl4 murine BC primary tumors, and consequent increase in vascularization, was also described^[83]. Increased tumor vasculature was also suggested to be an additional route of cancer cell escape^[82, 83] (Figure 2), facilitating metastasis as will be discussed in following sections.

1.3.2.3. Immune System Modulation

The crosstalk between the SNS and the immune system in the regulation of inflammation is already recognized. Dendritic cells and monocytes express both α -AR and β -ARs subtypes, and adrenergic activation in these cells leads to the downregulation of Tumor Necrosis Factor α (TNF- α), IL-1 and IL-6, resulting in the promotion of an immunosuppressive phenotype^[93]. The effect of the SNS on the different immune cell populations in the context of inflammation and hematopoiesis has been already previously reviewed^[94].

Among the several cellular components of the tumor microenvironment that are affected by SNS catecholamines, tumor-associated macrophages (TAM) are crucial for cancer progression. SNS signaling prompts BC cells to secrete pro-inflammatory cytokines, such as IL-6^[90] and M-CSF^[83], which can enhance the recruitment and infiltration of macrophages into the primary tumor (Figure 2). On the other hand, macrophage β_2 -AR activation increases the expression of cancer progression promoting factors *in vivo*, such as Transforming Growth Factor β (TGF- β), matrix metalloproteinase (MMP) 9, VEGF and

cyclooxygenase-2 (COX2)^[83]. Macrophage expression of COX2, and consequent secretion of prostaglandin E2 (PGE2), further drives the production of VEGFC by cancer cells to induce lymphangiogenesis^[82]. In addition, peripheral sympathetic nerve ablation, using 6-Hydroxydopamine in an orthotopic BC model, led to the inhibition of TAM recruitment and to a decrease in tumor IL-6 levels^[95].

Upon chronic stress induction in syngeneic BC mouse models, TAMs are mostly primed towards an immunosuppressive M2 phenotype: genes such as Arginase-1 and IL-10 are overexpressed, while conversely M1 phenotype characteristic genes are downregulated^[83, 96]. In addition, Bucsek and colleagues reported a significant decrease of tumor infiltrating effector cytotoxic CD8⁺ T cells upon β -AR activation and a concomitant 4T1 BC tumor growth^[97]. Immunosuppressive CD4⁺ Treg cells and spleen myeloid-derived suppressor cells were also elevated in stressed mice^[97].

Furthermore, and in agreement with the reports discussed so far, Kamiya and colleagues elegantly illustrated the influence of tumor sympathetic innervation on immune checkpoint expression and cancer progression^[87]. Using a viral vector-based tool, the authors were able to specifically denervate the tumor stroma without affecting surrounding tissues^[87]. The subsequent decrease in tumor NE content abrogated tumor growth and metastatic spread. Moreover, sympathetic denervation downregulated immune checkpoint molecules, such as programmed death 1 (PD-1) from β_2 -AR expressing CD4⁺ and CD8⁺ tumor infiltrating lymphocytes. The authors have observed the same outcomes in chemically induced and spontaneous BC models, and reported a correlation between the density of sympathetic fibers, PD-1 expression and tumor recurrence in a small cohort of human BC patients^[87].

These observations reinforce the hypothesis that SNS driven immunosuppression, and subsequent evasion to the immune surveillance, play an important role in BC progression.

1.3.2.4. Extracellular Matrix Invasion

As the disease progresses, a cascade of cellular events triggers the ability of BC cells to remodel and invade adjacent tissues, eventually escaping into circulation through intravasation in blood or lymphatic vessels^[98]. Crosstalk between the tumor microenvironment and BC cells is crucial for the acquisition of invasive features, and the SNS has been directly linked to the process of epithelial and mesenchymal transition (EMT)^[99].

Adrenergic signaling, namely through β_2 -AR, was shown to directly modulate several cellular processes in BC cell lines. ISO stimulation led to an increased invasive capacity of highly metastatic MDA-MB-231 cells *in vitro*, and this effect was β_2 -AR specific ^[99].

Interestingly, overexpression of β_2 -AR in MCF7 cells resulted in augmented invadopodia number and invasive capacity after incubation with ISO^[99].

The molecular mechanisms that govern this adrenergic response have been starting to be elucidated in recent years. Stimulation of β_2 -AR *in vitro* causes the accumulation of intracellular cAMP through G_{α_s} / Adenylyl cyclase pathway and consequent dephosphorylation of ERK1/2^[74]. This increase in cAMP activates PKA and exchange protein directly activated by cAMP (EPAC) leading to increased mobilization of Ca^{2+} in a feedforward loop that will ultimately drive cell invasion mechanisms^[74] (Figure 2). In other *in vitro* studies, β_2 -AR activation led to an increased motility and invasiveness of MDA-MB-231 cells, partly through changes in actin remodeling and contractility and increased plasma membrane protrusions^[100, 101]. Interestingly, β -AR agonist ISO reduced the number of focal adhesions while increasing the number of invadopodia, favoring motility in three-dimensional spaces but not on two-dimensional surfaces^[100].

Although most of the available data in the literature concerns experiments with the β_2 -AR and MDA-MB-231 cells, other cell lines and ARs should not be overlooked. DeZong and colleagues reported that proto-oncogene tyrosine-protein kinase Src mediated invasion and migration was modulated by different ARs in MDA-MB-231 and MCF7 cell lines *in vitro*, β_2 -AR and α_1 -ARs respectively^[71]. Src was targeted for phosphorylation by different signaling pathways, i.e., PKA in MDA-MB-231 and PKC in MCF7 cells^[71]. This data might explain the seemingly contradictory results observed in previous studies, where MCF7 cells were described to decrease their migration capacity upon ISO stimulation, a β -AR agonist^[80]. The same study reported a decrease in MDA-MB-231 cell migration after ISO stimulation^[80], which could be due to the fact that a parental MDA-MB-231 cell line was used instead of the highly metastatic variants of MDA-MB-231^[74, 100, 101].

In addition to direct effects of NE on BC cells, stimulation of tumor stromal α_2 -AR was reported to promote BC progression and invasion. Pharmacological activation of α_2 -AR, but not of α_1 -AR nor β -AR, increased the rate of metastasis in a syngeneic orthotopic BC model^[102]. These changes were correlated with altered collagen structure and were cancer-cell independent, since the cell line used did not respond to NE *in vitro*^[102]. Nevertheless, no insights were provided on the stromal players targeted by α_2 -AR agonists that are involved in collagen remodeling.

As could be appreciated by the gathered information from the previous studies, the interplay between BC and the SNS is extremely complex. Therefore, it is clear that the knowledge concerning the combination of α -AR and β -AR signaling on cancer progression, as well as on the distinct cellular players of the tumor microenvironment, is still scarce. Therefore, careful consideration should be enforced when designing experiments and therapeutic interventions.

1.3.3. BC Metastasis and the Bone Niche

After escaping into the vasculature, BC cells disseminate and egress towards distant organs in a complex multistep process that is not yet fully elucidated. BC exhibits specific tropism towards organs such as lung, brain, liver and bone, and there are indications that this tropism is associated with BC receptor status^[103]. Luminal A/B tumors are the most prevalent type in BC patients and they mostly metastasize to the bone^[104, 105]. Luminal A/B bone metastases are typically indolent in the first years of follow up, and patients presenting only bone metastases have higher overall survival rates than patients presenting metastasis in other distant sites^[104, 105]. Nevertheless, around 70% of all late stage BC patients exhibit bone metastatic foci leading to severe complications such as hypercalcemia, pain and bone fractures^[103, 106]. Metastatic foci are found mostly in long bones, ribs, pelvis and vertebrae, which contain abundant marrow and provide an immune context favorable for cancer cell survival, the bone marrow microenvironment being crucial for the maintenance of the hematopoietic stem cell niche^[107]. In addition, bone stromal cells secrete a combination of cytokines and growth factors that favor BC cell homing, survival and proliferation^[108]. BC cells establish close interactions with bone cells, namely osteoclasts and osteoblast-lineage cells, and the SNS can potentiate this crosstalk.

1.3.3.1. The Metastatic Vicious Cycle

The skeletal system plays a critical role in all stages of human development. The skeleton is responsible for locomotion, it is the preferential site for hematopoiesis, regulates mineral homeostasis and protects vital organs, such as brain, heart and lungs. It is, therefore, crucial to maintain skeletal structural integrity and function throughout life. This is achieved mainly through a highly dynamic bone remodeling process, where the bone matrix is degraded and subsequently replaced by new mineralized bone in a coordinated fashion. Osteoclasts are specialized multinucleated cells of the hematopoietic lineage that are able to demineralize and resorb the bone matrix using a combination of secreted enzymes, such as Cathepsin K (CATK)^[109] and Tartrate Resistant Acid Phosphatase (TRAcP)^[110]. During resorption, factors secreted from osteoclasts and by-products of bone matrix degradation recruit precursors of bone forming cells, coupling between bone resorption and bone formation. These precursors of a mesenchymal lineage differentiate into mature osteoblasts, which are then responsible for the deposition of high amounts of ECM proteins and mineralize them^[111]. Osteoblasts can then entomb themselves in the matrix they produce and become osteocytes. These cells make up for more than 90% of the cells present on cortical bone and have long extensions, creating an interconnecting network between osteocytes

themselves and cells in the bone marrow^[112]. Osteocytes are thought to have an endocrine^[113] and mechanosensitive role^[114, 115] in the bone, participating in the complex adaptations to internal and external stimuli.

BC often leads to highly osteolytic bone metastases, where cancer cells exploit the normal bone remodeling process and shift the balance towards increased bone resorption. Parathyroid hormone related protein (PTHrP), MMPs and PGE2 are some of the factors released by tumor cells that modulate the expression of Receptor activator of NF- κ B ligand (RANKL) by osteoblasts, the latter being a master regulator of osteoclast differentiation^[116, 117]. Increased RANKL production by osteoblasts and osteocytes will in turn boost osteoclast differentiation and activity, leading to extensive bone degradation. On the other hand, bone matrix embedded factors, such as transforming growth factor- β (TGF- β), insulin growth factor (IGF) and platelet derived growth factor (PDGF) released during resorption, among others, will further stimulate tumor growth and perpetuate a “vicious cycle” of bone destruction^[118]. Biphosphonates and denosumab (a RANKL human monoclonal antibody) are commonly used as adjuvant therapy for the treatment of metastatic bone disease, in order to normalize osteoclastic activity levels^[119]. However, although these treatments alleviate skeletal related symptoms, new and more effective therapeutic targets are needed to hamper the establishment of the vicious cycle.

1.3.3.2. The SNS and bone metastatic disease

Bones are highly innervated organs, with high density of sensory and sympathetic nerve fibers in the periosteum and along blood vessels in the bone marrow^[120]. A physical and functional association of nerve fibers and bone cells is to be expected^[27], since nerve fiber density is usually higher near elevated bone turnover surfaces^[30].

Although cells of osteoblast and osteoclast lineages were reported to express α -AR mRNA, their relative expression compared to the β_2 -AR subtype is very reduced^[39, 121, 122]. β_2 -AR, but not β_1 -AR and β_3 -AR, is widely found in primary osteoclasts and osteoclastic cell lines^[35, 51], as well as in osteoblast lineage cells^[5, 36, 38]. β_2 -AR is fully functional in bone cells, since β_2 -AR agonism triggers an increase in intracellular cAMP *in vitro*^[5]. Interestingly, cells of the osteoblast lineage also express Monoamine Oxidase (MAO) α and MAO β ^[47], as well as the NE transporter (NET)^[37], thus being able to intake and catabolize NE from the external milieu.

β -AR activation in bone triggers osteoclastic differentiation, diminished bone formation and consequent bone loss (reviewed in ^[18]), mostly due to an increase in RANKL production by osteoblast lineage cells *in vivo*^[45, 49] (Figure 4). Similarly, β_2 -AR agonism was reported to increase RANKL production by osteocytic MLO-Y4 cell line *in vitro*, and consequently induce the differentiation of RAW264.7 osteoclastic cell line in co-culture experiments^[50].

Although osteocytes have received increasing attention in the past years regarding their role on the modulation of BC progression^[123-126], data on the action of adrenergic signaling pathways on osteocytes in this context is still scarce. Osteocytes express β_2 -AR and, being the most common cell type in the bone, the importance of their putative crosstalk with the SNS on BC should not be overlooked. Regardless, SNS activation of osteoblast-lineage cells seems to further potentiate the establishment of a metastatic vicious cycle upon BC bone metastatic colonization.

Campbell and colleagues have made important contributions to this field of research. Using a mouse model of bone metastasis, by intracardiac injection of bone-tropic MDA-MB-231 cells, the authors have shown that adrenergic stimulation of the bone stroma potentiated the establishment of the metastatic vicious cycle^[58]. Chronic immobilization stress, as a model of endogenous sympathetic activity, was used to demonstrate that augmented catecholamine levels led to larger osteolytic lesions, an effect mediated by β_2 -AR^[58]. Moreover, ISO inoculation, before injection of BC cells, increased tumor foci and lesion number in the bone, suggesting that sympathetic triggering at the bone microenvironment facilitated BC cell engraftment. The authors suggested that this effect was partially due to RANKL signaling and its chemotactic action on MDA-MB-231 cells^[58].

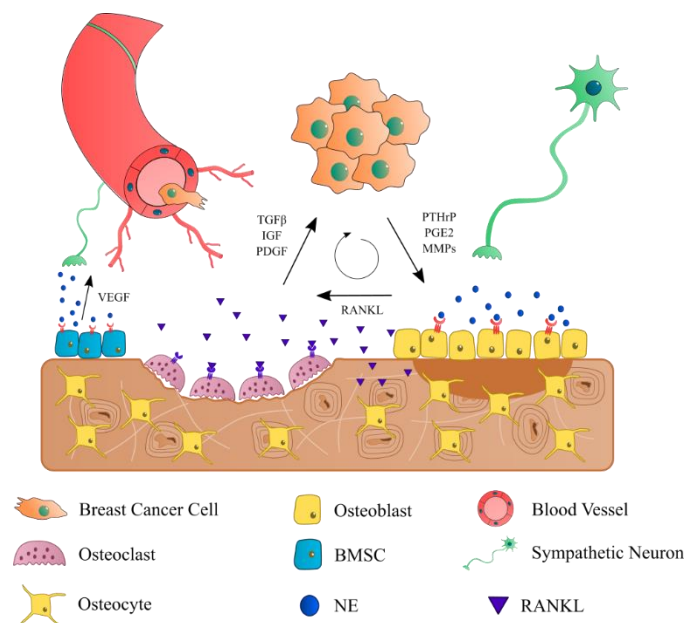


Figure 4. The bone metastatic niche and the metastatic vicious cycle. Once engrafted in the bone, BC cells secrete pro-osteoclastic factors such as PTHrP, PGE2, and MMPs, which induce the expression of RANKL by osteoblasts and osteocytes, promoting osteoclast differentiation and activity. In turn, factors released from the bone matrix enhance

the growth of cancer cells, establishing a metastatic vicious cycle that leads to extensive bone degradation. NE, norepinephrine; BMSC, bone marrow stromal cell.

In addition to augmented RANKL signaling, adrenergic stimulus promoted BC extravasation and retention in the bone through the modulation of the bone vasculature. Nude mice subjected to either chronic immobilization stress or ISO inoculation showed increased VEGF-A expression by bone marrow stromal cells (BMSCs), and consequent angiogenesis, which resulted in the promotion of BC colonization^[127]. Furthermore, incubation of BMSCs with ISO led to the release of IL-1 β , which in turn activated endothelial cell E/P-selectin expression and enabled BC adhesion and retention *in vitro*^[128] (Figure 5).

Interestingly, the interplay between the SNS and BC in the bone metastatic niche is not unidirectional. Not only is the SNS capable of inducing BC cell engraftment and proliferation through RANKL and VEGF-A signaling but, conversely, BC may also be able to regulate AR dynamics in the bone niche. BC secreted PTHrP is a well-known modulator of bone turnover in the metastatic niche (reviewed in^[129]). PTHrP binds to PTH receptor 1 (PTHR1) expressed in osteoblasts and upregulates RANKL expression to promote osteoclastogenesis, driving the metastatic vicious cycle^[130].

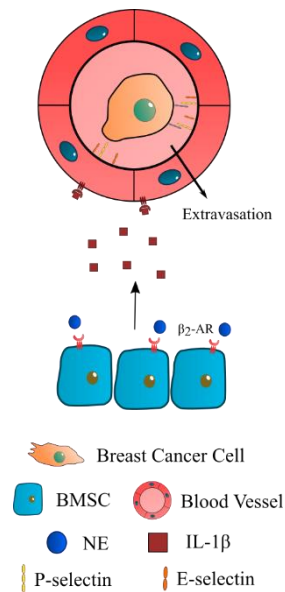


Figure 5. BC cell extravasation into the bone niche. NE stimulation of stromal β_2 -AR is associated with an increased release of VEGF and IL-1 β , which leads to augmented angiogenesis and expression of P- and E-selectins in endothelial cells. The latter event promotes BC cell extravasation from the circulation into the bone marrow.

Interestingly, PTHR1, β_2 -AR and their respective downstream pathways in osteoblastic cells seem to be intimately connected. Using germline β_2 -AR knockout mice, Hanyu *et al*

demonstrated that β_2 -AR expression is required for the osteoanabolic effect of PTH and that β_2 -AR modulates the expression of PTHR1 target genes in osteoblasts such as RANKL, alkaline phosphatase, bone sialoprotein and osteoprotegerin (a RANKL decoy receptor)^[131]. On the other hand, PTH was shown to directly downregulate β_2 -AR expression in osteoblast-like MC3T3-E1 cells *in vitro*^[132]. This interdependency might be explained by common intracellular downstream effectors that are triggered by their respective ligand binding. Both PTHR1 and β_2 -AR are GPCRs that signal through the adenylyl cyclase/PKA axis and promote the phosphorylation of cAMP-response element binding protein to induce transcription of target genes^[132]. Furthermore, after ligand binding, both receptors are rapidly desensitized through β -arrestin and β -Adrenergic Kinase 1 dependent pathways^[133-135], which can also act as protein scaffolds that subsequently lead to the activation of mitogen-activated protein kinase ERK1/2 and several other effector molecules^[136]. However, while these interactions were described to occur between PTHR1 and β_2 -AR in the context of intermittent PTH treatment, it is still unknown whether BCsecreted PTHrP can elicit the same response in the context of bone metastatic disease. While PTHrP and PTH share the same receptor, there are several described non-canonical pathways for the action of PTHrP whose importance is still poorly understood^[129]. Therefore, more data on the interplay between PTHrP and β_2 -AR in BC bone metastasis is urgently required, since it could change our understanding on the dynamics of β_2 -AR expression in bone throughout the progression of the disease and facilitate the design of new, more effective therapeutic options.

1.3.4. BC and Beta-Blockers: Clinical Perspective

Although the pre-clinical data is extremely valuable for the understanding of the several processes that rule BC progression and metastatic spread, it is crucial to translate the results into a clinical setting. In the past decade, increasing attention has been paid to the effect of sympathetic activity on BC patient survival and breast cancer recurrence^[57, 137]. In this section, we will review the published epidemiologic and clinical data on the effect of several β -AR antagonists (henceforth called Beta-Blockers) on BC and discuss the limitations associated to the interpretation of the reported results.

Epidemiologic studies have previously suggested that cancer patients subjected to high levels of psychosocial stress usually have poorer prognosis and survival^[138]. SNS targeting Beta-Blockers are thus potential therapeutic options for the treatment of cancer and are already widely used in other pathological settings, such as the treatment of asthma and hypertension^[139, 140]. The safety profile of these drugs is well described and they are not

associated with increased incidence of BC, as evidenced by previous epidemiologic studies^[141, 142].

A proof-of-principle study performed by Powe *et al* analyzed the effect of Beta-blocker prescription prior to BC diagnosis on patient survival^[57]. A reduction in tumor recurrence, incidence of metastasis and increased patient survival rates was reported in the Beta-blocker treated group, with no significant differences in tumor stage, size, grade and vascular invasion between treated and placebo groups.

Nonetheless, the population size of the study is relatively small and no distinction between the type of Beta-Blockers used was included in the analysis^[57]. Atenolol and Bisoprolol are β_1 -AR specific, while Propranolol and Timolol are non-specific $\beta_{1/2}$ -AR antagonists; therefore, the contributions of the different ARs to the reported results cannot be pinpointed. In fact, another population-based study by Barron *et al* has shown a beneficial effect of Propranolol, but not Atenolol, on BC metastasis and patient survival^[143]. Interestingly, Melhem-Bertrand *et al* reported a beneficial effect of β_1 -AR targeting drugs Metoprolol and Atenolol on Triple Negative BC (TNBC) recurrence but not on ER positive BC, highlighting the importance of BC receptor status on the response to Beta-blockers^[144]. Thus, it is still unclear which receptors are the main contributors for the reported beneficial effects of Beta-blockers on BC recurrence and a matter of intense debate. Nevertheless, we can hypothesize that a broader acting Beta-Blocker, such as Propranolol, could be even more advantageous than specific Beta-Blockers to manage BC recurrence and metastasis.

Several studies have suggested that Beta-Blocker usage could be explored as an adjuvant therapy in BC treatment^[57, 82, 143-147]. However, these have some limitations, such as the retrospective design, population size, difficulties in the assessment of Beta-blocker treatment duration and compliance, and also lack of access to comorbidity and other medication data. Other retrospective studies reported no correlation between Beta-Blocker usage and reduced breast-cancer specific mortality or recurrence^[137, 148-150], and thus the benefits of these drugs remain controversial (for more details, refer to Table II). Randomized clinical trials are warranted in order to assess the clinical relevance of Beta-Blockers for BC treatment.

To our knowledge, the only results from Phase II placebo-controlled clinical trials published to date address the effect of perioperative propranolol administration on several metastatic biomarkers in early BC patients. Zhou and colleagues reported a decreased immunosuppression after propranolol administration in BC perioperative period, when compared to placebo controls^[151]. Propranolol was also shown to block patient derived regulatory T cell proliferation^[151]. Shaashua^[152] and Haldar^[153] reported a reduction of EMT related gene expression in the resected primary tumors from patients subjected to simultaneous administration of Propranolol and the COX-2 inhibitor etodolac. The resected

tumor also showed reduced expression of pro-metastatic, anti-apoptotic and proliferation markers, as well as increased infiltration of B-cells and decreased presence of TAMs. Propranolol and COX-2 treated patients also presented reduced levels of circulating inflammatory cytokines, IFN γ and IL-6, and increased levels of NK cell activation during treatment^[152]. Another randomized clinical trial by Hiller *et al* has shown similar results with the administration of Propranolol for one week before surgical resection of the primary BC tumor^[154]. In this study, patients under Propranolol usage before surgery have shown reduced EMT gene expression and increased infiltration of dendritic cells and M1 macrophage polarization in the resected tumor, when compared to placebo-treated controls. Interestingly, patients clinically non-responsive to Propranolol (i.e. no significant reduction in blood pressure and heart rate after Beta-blockade) also showed decreased tumor EMT gene expression, although the immune cell infiltration in the primary tumor changed compared to clinically responsive patients^[154]. These clinical trials pointed to a possible beneficial effect of Propranolol on reducing the metastatic potential of BC primary tumors. Nevertheless, adequately powered clinical trials with focus on overall survival and cancer recurrence are still needed before Propranolol can be used for BC treatment.

Table II. Summary of epidemiologic studies regarding the influence of β -blockers on BC outcome

Treated Group Size / Total Size	β -Blocker Used (Population Size)	Improved patient survival (HR; CI)	Reduced Tumour Recurrence (HR; CI)	Reduced Incidence of Metastasis (HR; CI)	Reference
43 / 466	Atenolol (25) Propranolol (7) Bisoprolol (7) Timolol (4)	Yes (0.291; 0.119-0.715)	Yes (-)	Yes (0.430; 0.200-0.926)	[57]
595 / 4738	Atenolol (525) Propranolol (70)	Yes (0.19; 0.06-0.60)	N.D.	Yes (-)	[143]
204 / 1779	Atenolol (-) Metoprolol (-) Propranolol (-) Others (-)	No (0.76; 0.44-1.33)	No (0.86; 0.57-1.32)	N.D.	[155]
102 / 1413	Metoprolol (43) Atenolol (38) Others (21)	No (0.64; 0.38-1.07)	Yes (0.52; 0.31-0.88)	N.D.	[144]
74 / 800	Carvedilol (11) Sotalol (3) Atenolol (27) Betaxolol (1) Bisoprolol (11) Metoprolol (8) Nebivolol (13)	Yes (0.42; 0.18-0.97)	Yes (0.52; 0.28-0.97)	Yes (0.32; 0.12-0.90)	[146]
3660 / 18733	Metoprolol (1793) Atenolol (622) Propranolol (586) Others (659)	N.D.	No (1.3; 1.1-1.5)	N.D.	[149]

1770 / 55252	Propranolol (1770)	No (0.94; 0.77-1.16)	N.D.	N.D.	[137]
1443 / 5754	Carvedilol (22)	No (1.11; 0.94-1.32)	N.D.	N.D.	[150]
	Sotalol (84)				
	Atenolol (854)				
	Bisoprolol (189)				
	Metoprolol (45)				
Propranolol (249)					
153 / 1144	Bisoprolol (59)	No (1.05; 0.85-1.29)	Yes (0.81; 0.66-0.99)	N.D.	[147]
	Metoprolol (48)				
	Atenolol (28)				
	Propranolol (13)				
	Others (5)				
93 / 956	N.D.	Yes (0.48; 0.23-0.99)	No (0.93; 0.39-2.25)	Yes (0.40; 0.17-0.93)	[82]

HR – Hazard Ratio; CI – 95% Confidence Interval (Lower limit – Higher limit); N.D. – No data

1.3.5. Conclusion and Future Perspectives

Despite the advances made in recent years, the knowledge on the impact of endogenous stress on the complex interactions governing BC disease progression is still incomplete. This review summarizes and combines the available data regarding the SNS signaling in the orchestration of BC.

So far, the adrenergic signaling has been implicated in several steps of disease progression, promoting tumor growth, angiogenesis, immunosuppression and invasion (Figure 2). While several *in vitro* studies and animal models have illustrated the intricate control of the SNS over cancer cellular processes, the contribution of the different ARs expressed in the multiple cellular components of the tumor microenvironment remains puzzling. Furthermore, the inherent heterogeneity of BC presents an additional challenge in modelling this disease. Distinctive AR expression patterns on BC cell lines widely used in the various experimental models is certainly relevant and more information on the adrenergic control of disease progression in different cell lines is urgently needed.

The modelling of the various cellular and structural components of the cancer niche is still technically challenging. The use of immunodeficient mice is required for xenograft tumor models, but the contribution of the immune system is not taken into account in these models. Thus, current *in vitro* and *in vivo* models do not completely recapitulate the complexity of the disease but as new, more complicated models are being developed, discerning the specific contributions of each cellular type grows increasingly more difficult. Specific deletion of β_2 -AR on not only BC cells^[99], but also in osteoblasts^[127] and macrophages^[156] could be used as an important tool to elucidate the role of this receptor in various models of the disease, although no conditional β_2 -AR knockout models specifically in osteoclasts or osteocytes were described to date. Furthermore, microfluidic systems also present several advantages when compared to traditional *in vitro* models since they allow the compartmentalization of different cell types and the introduction of fluidic flow, which can be physiologically relevant. There are already microfluidic platforms developed for the study of BC metastasis to bone^[157-160], but the modelling of the SNS in these platforms is still challenging.

Metastatic tropism for bone is an evident feature of BC, being the most common site of metastasis in Luminal breast cancer patients^[103]. Although adrenergic stimulation of the bone microenvironment is thought to increase osteolysis and potentiate the metastatic vicious cycle, the interactions between BC and bone cells under sympathetic control remain mostly unexplored, apart from the contributions of Eleftheriou and his group^[58, 127, 128]. Although the use of Luminal A BC cell lines on bone metastasis models presents technical challenges due to their less invasive phenotype, it would be crucial to understand the

molecular changes that might be elicited by the SNS in these cells. Furthermore, since Luminal A tumors are the most common subtype of BC found in patients, the use of Luminal subtype BC cells in *in vitro* and *in vivo* models of the disease is certainly more clinically relevant than the current widespread use of aggressive TNBC cells.

Future developments on novel targeted therapeutic strategies, such as tumor specific denervation using viral vectors^[87], are exciting fields of research that will require input from various areas of expertise before becoming applicable in a clinical setting. It is still unclear if this technique could be applied to locally and specifically denervate the bone in pre-clinical studies. In addition, other denervation techniques such as chemical sympathectomy by local delivery of guanethidine using an osmotic mini pump in the femoral bone marrow were previously established^[161], which could help to clarify the role of sympathetic nerves on bone metastasis.

Finally, clinical observations on the usage of Beta-blockers for treatment of BC suggest that interfering with SNS signaling could have beneficial outcomes for patients, particularly in the control of metastatic spread. Nevertheless, systemic administration of beta-blockers can also have unforeseen consequences in the progression of BC, and adequately powered clinical trials are needed before therapy implementation. To circumvent the disadvantages of systemic administration of these drugs, targeted drug delivery systems could provide the answer for a currently unmet clinical challenge. The unique biochemical and biophysical characteristics of the bone microenvironment provide the means for a targeted drug delivery to bone metastatic tumors. Bisphosphonates^[162], acidic amino acid peptidic sequences^[163], liposomes^[164], organic^[165] and inorganic^[166] nanoparticles, chimeric peptides targeting CATK^[167] and also HER2 targeting nanoparticles^[168] have been previously used to achieve bone metastasis specific drug and gene delivery *in vivo*. Whether these strategies could be used to deliver SNS targeting drugs specifically to the bone microenvironment and if that would translate into a clinical benefit remains to be elucidated.

Taken together, the data summarized in this review highlight the importance of SNS activation on BC. Exciting new developments are expected in the next few years that would allow us to complement our understanding of the molecular cues that drive BC progression.

Acknowledgments

This work was financed by FEDER – Fundo Europeu de Desenvolvimento Regional funds through the COMPETE 2020 – Operacional Programme for Competitiveness and Internationalisation (POCI), Portugal 2020, and by Portuguese funds through FCT/MCTES in the framework of the project “SproutOC” (POCI-01-0145-FEDER-030158, PTDC/MED-PAT/30158/2017). F.C. is recipient of the Ph.D. fellowship SFRH/BD/128771/2017. DMS is a recipient of a Post-Doc fellowship (SFRH/BPD/115341/2016).

1.4. *In vitro* microfluidic models

Before widespread use of beta-blockers in clinical practice, clarification of the cellular and molecular mechanisms that drive BC metastasis to the bone is of crucial importance. Most studies on BC bone metastasis are performed using standard two-dimensional *in vitro* culture or employing animal models of BC. However, although they are cheap and allow high throughput procedures, conventional *in vitro* cultures do not recapitulate the complexity of the bone microenvironment^[169]. Alternatively, *in vivo* modeling of BC reflects important pathological cues such as cell-cell and cell-matrix interactions, and integrates the reaction of the whole organism to the onset of disease. Nevertheless, distinct responses in mice and human cells limits the ability of these models to predict human disease^[170]. Furthermore, the complex interpretation of specific signaling pathways together with the ethical issues associated with the use of animal experiments hampers the effective use of these models^[170].

In order to tackle some of the constraints associated to the use of animal models, microfluidic tools have emerged in the past decade as alternative platforms that are able to recapitulate characteristic features of the bone metastatic microenvironment^[158]. Microfluidics are versatile devices designed to address a specific scientific question and are usually produced by soft photolithography processes in specialized clean rooms. They take advantage of micrometric features to allow the fine control of culture parameters, the use of shear stress and fluidic flow and the promotion of physical and chemical gradients, in order to ultimately mimic the biological attributes of the metastatic niche^[171]. Examples of such attributes include the presence of suitable ECM, vascularization, innervation and also paracrine crosstalk between the different cellular players that constitute the tumor microenvironment. These features are critical for an improved modeling of the interactions taking place during bone metastasis and to help decipher the role of innervation in the onset of this disease.

1.4.1. Microfluidic models of bone metastasis

Bone metastasis is characterized by a complex sequence of events that begin with the extravasation of circulating tumor cells (CTC) from the blood stream towards the bone marrow. After a period of dormancy, cancer cells eventually escape quiescence and start bone marrow colonization and expansion, recruiting and modulating native bone-residing cell activity to favor tumor growth^[106]. Due to the intricacy of the cell-cell and cell-matrix interactions involved in bone metastasis, modeling the bone metastatic niche is difficult to achieve using standard *in vitro* and *in vivo* models. Due to the advantages mentioned

above, microfluidics can be suitable for fundamental research on the mechanisms involved in bone metastasis, and multiple microfluidic platforms have been developed to study these processes (Table III). For instance, interactions between CTC and endothelial cells, the biochemical gradients established in the bone microenvironment and their impact on tumor cell extravasation and colonization can be modelled using microfluidic tools^[157, 159, 160, 172-176]. Kong and colleagues took advantage of microfluidic compartmentalization to study BC CTCs specific migration towards different organs^[172]. First, the authors coated several microchannels with human umbilical vein endothelial cells (HUVEC) that were separated from the organ compartments by a porous membrane. Then, each compartment was seeded with murine primary cells from bone, liver, lung and muscle tissue. Finally, fluidic flow of CTCs through diffusion channels was promoted and BC preferential migration towards bone, lung and liver in opposition to muscle tissue was demonstrated (Figure 6)^[172]. Similarly, interaction and retention of lymphoma and leukemia cells in compartments containing different human bone marrow cell populations encapsulated in three dimensional (3D) matrices were previously assessed using microfluidic tools^[174]. The authors took advantage of the fact that microfluidic tools are compatible with multiple imaging techniques to monitor fluorescent tracked cancer cell homing and retention in the different compartments^[174].

In addition to compartmentalization, microfluidic tools allow the use of 3D matrices to recapitulate important cell-matrix interactions that take place at the metastatic niche. For example, collagen or fibrin hydrogels laden with differentiated MSCs were used to assess the extravasation of perfused BC cells towards the bone compartment^[159, 160]. The authors recreated the interactions that take place between blood vessels and BC cells during extravasation by including micro-channels coated with HUVEC before CTC seeding in the diffusion microchannels. In addition, to better mimic the bone ECM, hydrogels can also be modified with varying concentrations of hydroxyapatite, as Ahn and colleagues demonstrated when assessing the effect of bone ECM on human colorectal and gastric cancer cells proliferation, migration and angiogenesis^[177]. By changing the experimental setup and compartmentalization of the different cell types, the authors were able to evaluate cancer cell proliferation, migration and angiogenesis in the same platform^[177]. Besides hydrogel matrices, other sources of bone ECM can also be applied in microfluidic models: HUVECs and MSCs were previously cultured in native bone decellularized matrices to mimic the bone microenvironment and used to assess perfused BC cell retention and growth^[173]; furthermore, Hao and colleagues adapted a microfluidic chamber for long term culture of differentiated murine MC3T3-E1 osteoblastic cells, which led to the deposition of a matrix of mineralized collagen fibers that was used to study BC colonization^[158].

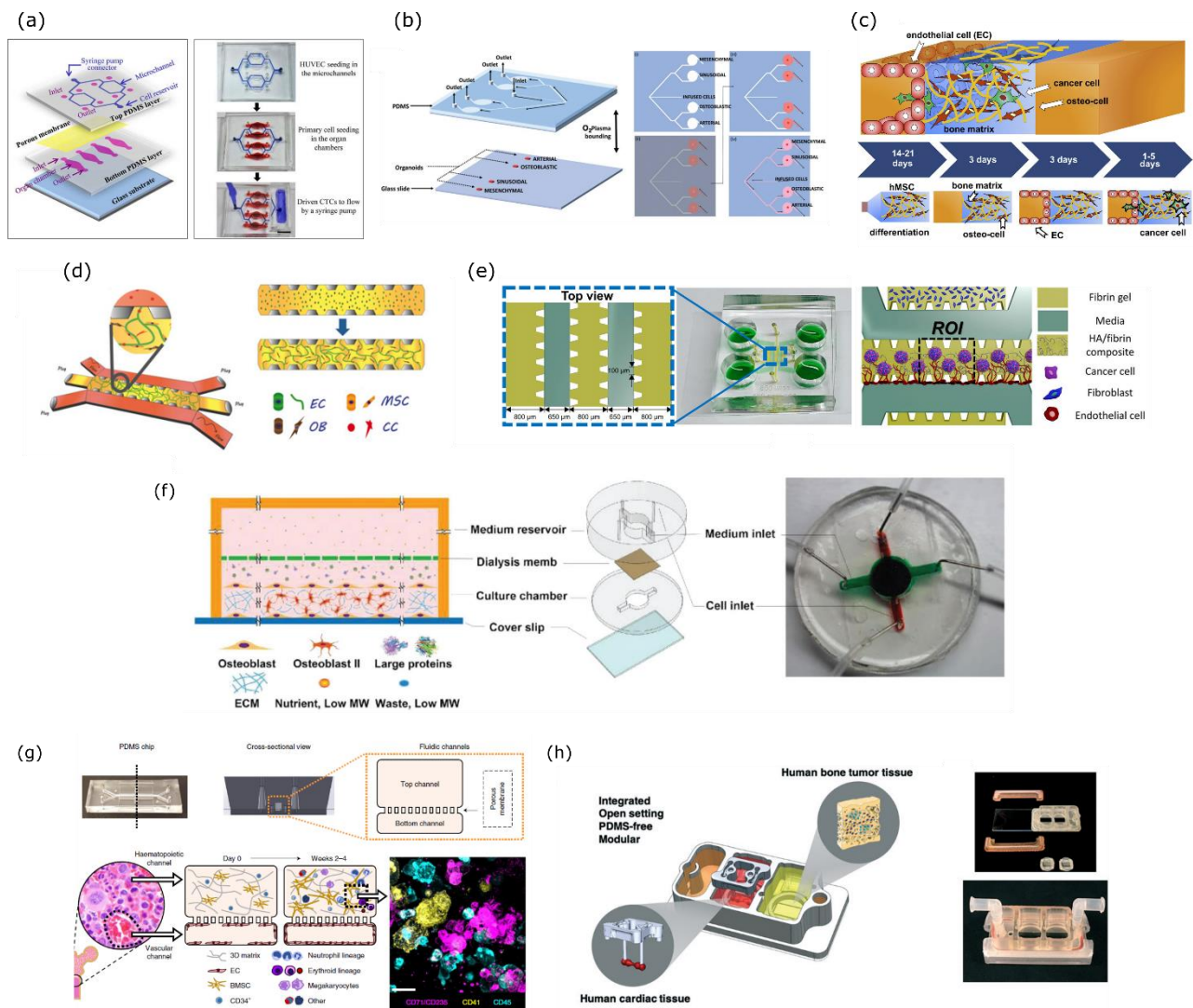


Figure 6. Microfluidic models of bone physiology and cancer metastasis. (a) Compartmentalized microfluidic to study BC CTC migration and retention towards different tissues. (b) Microfluidic model designed to study lymphoma and leukemia cell migration and retention in compartments with distinct bone marrow cell populations. (c) BC extravasation model where the migration of BC cells through an endothelial cell barrier towards a collagen hydrogel seeded with differentiated osteoblasts. (d) Microfluidic model to study BC extravasation towards a fibrin gel containing endothelial cells, osteoblasts and MSCs. (e) Schematic image of a microfluidic model used to study the effect of different hydrogel/hydroxyapatite compositions in colorectal and gastric cancer cell migration, proliferation and angiogenesis. (f) Microfluidic device designed to allow long term culture of murine osteoblasts and promote ECM deposition, and later on study BC engraftment and proliferation. (g) *In vitro* microfluidic model aimed at the replication of the bone marrow microenvironment for drug screening assays. (h) Integration of cardiac and bone compartments in the same microfluidic device for cardiotoxicity assessment of several

commonly used chemotherapeutics. Adapted under the terms of CC-BY license ^[172, 177]. Adapted with permission from ^[158-160, 174, 178, 179].

The versatility of microfluidic platforms for cancer research is further illustrated by the integration of drug screening assays for personalized medicine^[178-180]. In particular, the improved resemblance of these platforms to the *in vivo* pathological features of the tumor microenvironment translates into enhanced modeling of cellular behavior in response to particular drugs or treatment regimens^[178, 179]. For instance, Chou and his team were able to recreate the human bone marrow hematopoietic niche by using human CD34⁺ hematopoietic progenitors seeded in fibrin gels and fed exclusively through HUVEC lined diffusion channels ^[178]. Hematopoietic progenitors gave rise to myeloid and erythroid lineage cells and the authors were able to recapitulate the bone marrow toxicity of 5-Fluorouracil, a drug commonly used in chemotherapeutic regimens to treat cancer ^[178]. The ability to use patient derived samples to investigate patient-specific responses is another advantage of microfluidic platforms that cannot be easily replicated in animal models^[178, 180]. Furthermore, the modular integration of different organ models in the same platform allows the assessment of off-target drug toxicity that is not apparent in standard *in vitro* models^[179]. This was illustrated by Chramiec and his team, since they integrated cardiac tissue and decellularized bone scaffolds to study Ewing sarcoma bone tumor response to linsitinib, and were able to recapitulate mild cardiac toxicity of this drug that is also observed in the clinical practice^[179]. Thus, microfluidic models can potentially be used to improve translational research of new therapeutic strategies and help predict cell behavior in the human bone metastatic microenvironment.

1.4.2. Microfluidic models of bone innervation

Bone is highly innervated by TH⁺ SNS neurons and CGRP⁺ and SP⁺ sensory fibers^[13]. Sympathetic and sensory fibers are involved in the regulation of bone metabolism both in homeostatic and pathological conditions. In particular, the effect of the sensory innervation in bone metastasis is well documented, since an exacerbation of sensory sprouting is evident in bone metastasis of breast and prostate cancer and is linked to hypersensitivity and bone pain^[22, 23]. However, data on sensory and sympathetic innervation and their role on bone metastasis is obtained mostly from *in vivo* animal models, rendering the in depth analysis of the signaling pathways involved extremely difficult.

Microfluidic platforms can be a powerful tool to decipher the bone cell modulation of innervation patterns in both physiological context and during bone metastasis. The main advantage of these platforms is the ability to compartmentalize the neuronal cellular bodies

and axonal terminals. *In vivo*, neurons in the dorsal root ganglia (DRG) extend their nerve endings towards distant sites, including the bone. Several studies have successfully recreated this trait using microfluidics, and were able to investigate neuronal sprouting while keeping the neuronal bodies confined in distinct compartments (Figure 7) [27, 181-183]. For instance, establishment of murine osteoblast-neuron synapses were demonstrated using microfluidic platforms, similar to *in vivo* innervation of the bone [183]. These approaches have uncovered new mechanisms of neuronal regulation in physiological conditions. Compartmentalized microfluidics were successfully used to determine the mechanisms responsible for osteoblast-driven patterning of bone innervation [27]. The authors were able to show that differentiated osteoblasts provide a non-permissive environment for sensory neuron outgrowth through the secretion of SHH, in opposition to the axonal growth promoting role of undifferentiated MSCs [27].

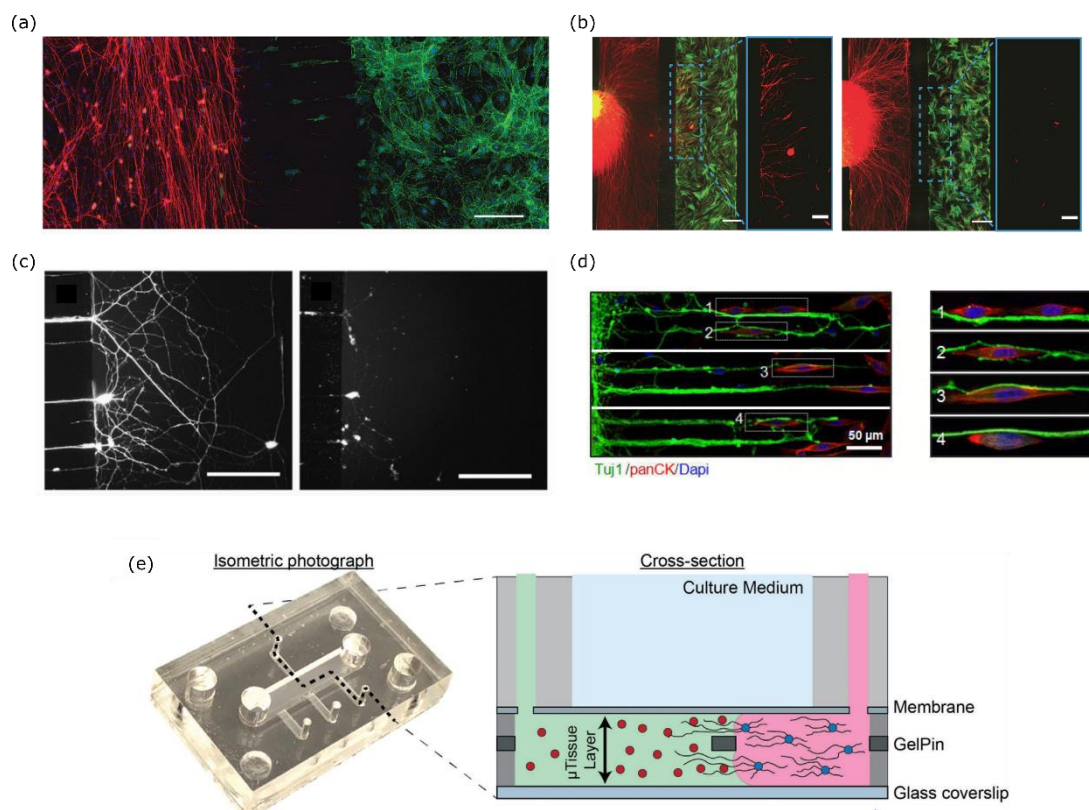


Figure 7. Microfluidic models of sensorial and sympathetic innervation. (a) Microfluidic model of bone innervation. Sensory neurons (red) are cultured in one compartment and extend their axonal terminals through microgrooves towards the opposite compartment, where they establish synapses with murine MC3T3 osteoblasts (green). Scale bar – 500 μm . (b) Microfluidic model to study bone cell driven innervation patterning. The ability of MSCs (left image) or differentiated osteoblasts (right image) to promote axonal growth is evaluated. Sensory neurons (red), MSCs/osteoblasts (green). Scale bar - 500 μm . Inset scale bar - 200 μm . (c) Microfluidic model of axonal degeneration. Axonal terminals are

seen in control conditions (left image) or after paclitaxel administration (right image). Scale bar - 100 μm . (d) Microfluidic devices were used to study prostate cancer perineural invasion. Microfluidic microgrooves facilitated imaging procedures to observe cancer cell guidance by the neuronal extensions. Scale bar - 50 μm . (e) Microfluidic device used to study murine sympathetic innervation of the cardiac tissue. The inclusion of pins allowed for the seeding of two separate hydrogels containing cardiomyocytes and adherent cardiac cells (green hydrogel) or post ganglionic SNS neurons from the superior cervical ganglion (red hydrogel). Adapted under the terms of the CC-BY license ^[27]. Adapted with permission from ^[181-184].

Furthermore, in pathological settings, microfluidic platforms were also used to study perineural invasion of prostate, pancreatic and BC cells as a mechanism for cancer cell escape and dissemination ^[181]. The importance of the physical separation of the neuronal bodies and axonal projections is further highlighted in a study by Yang and colleagues, showing that paclitaxel treatment leads to axonal degeneration but has no effect when applied to the neuronal soma ^[182]. In the same study, human erythropoietin applied to the axonal compartment showed neuroprotective effects, illustrating the suitability of compartmentalized microfluidics for drug screening assays ^[182].

Microfluidic modeling of sympathetic innervation of cardiac tissues has been previously described^[184]. A mixture of murine cardiomyocytes and adherent cardiac cells was cultured together with post ganglionic SNS neurons from the superior cervical ganglion, and both axonal extension and beating rate were quantified after adrenergic stimuli ^[184]. Nonetheless, no microfluidic platforms designed to investigate the effect of sympathetic neurons on bone metastasis have been reported so far. Microfluidic compartmentalization and the inclusion of suitable 3D microenvironment could be advantageous to the development of future models of sympathetic control of bone metastasis.

Table III. *In vitro* microfluidic platforms addressing the study of bone cancer and innervation

Objective of the study	Platform features	Cells used	Reference
Tumor cell extravasation			
Model metastatic extravasation of BC cells towards different organs.	Four different culture chambers in contact with fluidic micro-channels through a porous membrane.	MCF7 or MDA-MB-231 breast cancer cells were perfused through channels lined with HUVEC. Migration towards compartments containing primary mice lung, bone marrow, muscle and liver cells was assessed.	[172]
Study interactions of leukemia and lymphoma cells with different populations of the bone marrow.	Simple setup where an inlet is connected to four different compartments through microfluidic channels.	Normal human CD34+ bone marrow cells, U937 lymphoma cells or MOLM13 leukemia cells were perfused through compartments containing human arterial, sinusoidal, mesenchymal and osteoblastic bone marrow populations.	[174]
Study BC cell extravasation towards bone mimicking matrices.	Four independent gel chambers in contact with media channels coated with matrigel for endothelial cell seeding.	Differentiated MSCs were seeded within collagen gels. HUVEC were seeded on the media channels to mimic blood vessels and MDA-MB-231 BC cells were perfused in these channels.	[159]
Study breast cancer cell extravasation towards bone mimicking matrices.	One central channel in contact with two perfusion channels was used for hydrogel seeding.	Fibrin gels containing HUVECs and MSCs were used to mimic bone matrix deposition and vascularization. MDA-MB-231 BC cells were perfused through the media channels and extravasation towards the central compartment was assessed.	[160]
Assess breast cancer cell retention and growth on perfused decellularized bone matrices.	Three parallel chambers with decellularized bovine bone matrices were used, each connected to medium inlets and outlets.	Decellularized bone matrices were seeded with MSCs and HUVECs, and later on perfused with MDA-MB-231 BC cells.	[173]
Study prostate cancer cell extravasation through collagen ECM towards osteoblast-like cells.	Simple setup where cells are seeded on the lateral side of a cell compartment, which is later on filled with collagen and perfused with medium to create a hollow channel.	MC3T3-E1 murine osteoblastic cell lines are seeded on the lateral side of the cell compartment. After filling the compartment with collagen, LNCaP prostate cancer cells are	[176]

		seeded on the hollow collagen channel and extravasation towards osteoblasts is assessed.	
Investigate the effect of osteocytes in BC extravasation into bone.	Microfluidic platform composed of an osteocyte compartment connected to a lumen channel. Each compartment is amenable to fluid flow and shear stress stimulus.	MLO-Y4 osteocytic cell line was seeded on the bone compartment, subjected or not to fluidic flow. MDA-MB-231 BC cells were then seeded on the lumen channel coated with endothelial cells and the extravasation was assessed.	[157]
Identify genes associated with BC migration towards bone mimicking substrates.	Simple device with two medium channels and one hydrogel channel in between.	Differentiated human bone marrow MSCs were cultured in collagen hydrogels in the hydrogel channel. One of the medium channels was coated with HUVECs to mimic a blood vessel and BC MDA-MB-231 were seeded on the same channel as the HUVECs, after which invasion towards the bone mimicking hydrogel was assessed.	[175]
Bone tumor colonization			
Investigate BC colonization of bone mimicking matrices.	Cell culture chamber was adapted for long term culture. Two different compartments, one cell chamber and one medium perfusion channel, were separated by a dialysis membrane to allow nutrient and metabolite exchange without having to disturb the cell chamber.	MC3T3-E1 murine osteoblastic cell lines were cultured undisturbed for 30 days in the cell culture chamber, and deposited mineralized collagen matrices. MDA-MB-231 or its metastatic suppressed variant MDA-MB-231BRMS cells were then seeded on the mineralized matrix and proliferation was assessed.	[158]
Assess the effect of mineralized fibring hydrogels on colorectal and gastric cancer cellular processes.	The device consists of five parallel chambers with microposts to better immobilize the hydrogels without leaking.	SW620 colorectal and MKN74 gastric cancer cells were used in the study. Angiogenesis was assessed with HUVECs. Normal human lung fibroblasts were cultured in the outermost channels to promote cancer cell growth.	[177]
Study the effect of osteocyte paracrine signaling on breast and	Two channels on top of one another and separated by a microporous membrane.	BC MDA-MB-231 and MCF-7 and prostate cancer PC-3 and LNCaP cells were cultured on the top channel. Osteocyte-	[185]

<p>prostate cancer proliferation and migration after applying shear stress.</p>	<p>The bottom channel is smaller in height to increase shear stress.</p>	<p>like MLO-Y4 cells were cultured on the bottom channel and subjected to shear stress.</p>	
<p>Drug screening platforms for bone cancer</p>			
<p>Recreate the hematopoietic niche to study drug induced hematotoxicity .</p>	<p>Two different channels on top of one another and separated by a porous membrane. The top channel is the hematopoietic niche chamber and the bottom channel is the perfusion channel.</p>	<p>Human CD34+ cells and BMSC were cultured in fibrin gels in the hematopoietic chamber. These cells were perfused exclusively through the perfusion channel that was lined with HUVEC to mimic a blood vessel.</p>	[178]
<p>Study the interactions of multiple myeloma cells with the bone marrow.</p>	<p>Microfluidic platform with eight parallel culture chambers with a fiber mesh near each outlet to avoid flushing of the cells during culture.</p>	<p>Human osteoblasts were cultured together with patient derived multiple myeloma cells in each chamber, and proliferation of multiple myeloma cells was investigated.</p>	[180]
<p>Investigate anti-tumor efficacy and cardiac toxicity of drugs used in the treatment of bone tumors of Ewing Sarcoma</p>	<p>A modular device containing two culture chambers separated from one perfusion channel through a nylon mesh.</p>	<p>Differentiated human MSCs were cultured together with either metastatic (SK-N-MC) or non-metastatic (RD-ES) Ewing Sarcoma cells in decellularized bone matrix scaffolds in the bone chamber. Cardiac tissue was obtained through a mixture of normal human dermal fibroblasts and differentiated human induced pluripotent stem cells in fibrinogen hydrogels. Differentiated cardiac tissue was placed in the cardiac chamber, and both chambers were perfused, either in isolation or in co-culture of bone and cardiac tissue.</p>	[179]
<p>Innervation in bone and in cancer</p>			

Model the interaction between neurons and cancer cells, particularly during perineural invasion.	Simple device with two channels connected by small microgrooves to allow the passage of neuronal extensions.	Hippocampal neurons, cortical neurons or DRGs were extracted from embryonic or postnatal rats and seeded on the neuronal channel. PC-3 prostate cancer, Panc-1 pancreatic cancer and MCF-7 BC cells were cultured in the cancer channel. Migration of each cell type was quantified.	[181]
Investigate the mechanisms of paclitaxel induced axonal degeneration.	Simple device with two channels connected by small microgrooves to allow the passage of neuronal extensions.	DRGs were cultured in the neuronal channel and axonal extensions projected towards the opposite compartment. The effect of paclitaxel either on the cellular bodies or on the neuronal extensions was assessed.	[182]
Model the interactions between osteoblasts and sensory neurons.	Simple device with two channels connected by small microgrooves to allow the passage of neuronal extensions.	DRGs were cultured in the neuronal channel and axonal extensions were projected towards the bone compartment, where MC3T3-E1 osteoblasts were seeded. Neurite growth and synapses were observed and measured.	[183]
Investigate the effect of osteoblasts on different stages of differentiation on neurite growth.	Simple device with two channels connected by small microgrooves to allow the passage of neuronal extensions.	DRGs were cultured in the neuronal channel and axonal extensions were projected towards the bone compartment. Undifferentiated MSCs or osteoblasts at different stages of differentiation were cultured in the bone compartment and their effect on neuronal extension was assessed.	[27]
Study the effect of sympathetic stimulation on cardiac activity.	Device with a cell culture channel with pins in the central part to enable the crosslink of two different hydrogels in the same channel. The bottom cell culture channel is separated from the top medium channel through a porous membrane to allow exchange of nutrients.	Primary rat cardiomyocytes and adherent cardiac cells were seeded in GelMA hydrogels on the cell culture channel. Primary rat postganglionic sympathetic neurons from the superior cervical ganglion were seeded in GelMA hydrogels adjacent to the cardiac hydrogel. Axons extended towards the cardiac hydrogel while keeping the neuron soma in the neuronal hydrogel. Cardiac beat rate and innervation were quantified.	[184]

1.5. Thesis outline and objectives

Sympathetic hyperactivity has been implicated in the progression of several types of cancer, including prostate and BC^[58, 61]. These cancers mostly metastasize to bone, and SNS signaling, in particular through β_2 -AR activation, was shown to exacerbate skeletal deterioration in multiple models of BC metastasis^[58, 127, 128]. Together with clinical observations that correlate beta-blocker treatment with improved BC survival^[57, 143], these data point to a potential therapeutic benefit of SNS targeting in the treatment of BC metastasis.

Nevertheless, our understanding of the interactions governing SNS control BC bone metastasis and the bi-directional crosstalk between cancer cells and the bone niche is still incomplete. Other epidemiologic studies have shown no correlations between beta-blocker intake and BC survival and recurrence^[137, 149], and thus the benefit of beta-blockers remains controversial. *In vitro* modeling of the bone metastatic niche is particularly difficult due to the complex interactions taking place between BC cells and bone cells. Organ-on-a-chip devices have been used to study BC extravasation and proliferation in the bone, however, to our knowledge, no organ-on-a-chip model of sympathetic control of BC bone metastasis has been developed so far. In addition, several questions require clarification before translation of pre-clinical evidence into clinical benefits: how does the SNS impact BC cellular processes in the context of bone metastasis? How does the crosstalk between human bone cells and BC cells changes under sympathetic activation? Does the cellular communication under sympathetic signaling changes during BC progression? Are the factors involved in the modulation of the bone niche different in primary versus metastatic BC?

In this work, we attempted to answer some of these questions by employing different approaches ranging from microfluidic modeling, cellular and molecular biology, proteomic screening and computational algorithms. We studied the interaction between BC cells and bone cells under sympathetic activation using two different approaches:

I. Development of an organ-on-a-chip platform to study the effect of synergistic crosstalk of osteoclasts and sympathetic neurons on the BC secretome (CHAPTER II)

We designed, fabricated and validated a novel organ-on-a-chip model that aimed to investigate the mechanisms involved in the bi-directional and synergistic communication between distinct cellular players. By taking advantage of cell compartmentalization and manipulation of the direction of communication with pressure actuated Quake valves, we

facilitated the identification of secreted factors involved in intercellular crosstalk while preventing direct cell-cell interactions. In particular, our organ-on-a-chip platform was used to analyze the soluble mediators implicated in the crosstalk between human sympathetic neurons, osteoclasts and bone metastatic BC cells, mimicking the interactions that take place at the BC bone metastatic niche.

II. *In vitro* pharmacological β_2 -AR activation and its effect on the BC modulation of the bone niche in different stages of disease progression (CHAPTER III)

Through a combination of clinical data, proteomic profiling and functional studies with human primary cells, we investigated the effect of sympathetic control of BC cellular processes in the context of bone metastasis. We evaluated the status of circulating epinephrine in a cohort of primary and metastatic BC patients. In addition, we assessed how β_2 -AR signaling affects the crosstalk between BC cells and osteoclasts/osteoblasts, comparing the effect of parental and metastatic variants of BC on bone degradation.

1.6. References

- [1] A. Idelevich, R. Baron, (2018) Brain to bone: What is the contribution of the brain to skeletal homeostasis?, *Bone*, 115, 31-42
- [2] F. Elefteriou, (2008) Regulation of bone remodeling by the central and peripheral nervous system, *Archives of Biochemistry and Biophysics*, 473, 231-236
- [3] E. Otto, P.-R. Knapstein, D. Jahn, J. Appelt, K.-H. Frosch, S. Tsitsilonis, J. Keller, (2020) Crosstalk of Brain and Bone—Clinical Observations and Their Molecular Bases, *International Journal of Molecular Sciences*, 21, 4946
- [4] P. Ducy, M. Amling, S. Takeda, M. Priemel, A. F. Schilling, F. T. Beil, J. Shen, C. Vinson, J. M. Rueger, G. Karsenty, (2000) Leptin Inhibits Bone Formation through a Hypothalamic Relay: A Central Control of Bone Mass, *Cell*, 100, 197-207
- [5] S. Takeda, F. Elefteriou, R. Levasseur, X. Liu, L. Zhao, K. L. Parker, D. Armstrong, P. Ducy, G. Karsenty, (2002) Leptin Regulates Bone Formation via the Sympathetic Nervous System, *Cell*, 111, 305-317
- [6] J. C. Fritton, K. B. Emerton, H. Sun, Y. Kawashima, W. Mejia, Y. Wu, C. J. Rosen, D. Panus, M. Bouxsein, R. J. Majeska, M. B. Schaffler, S. Yakar, (2010) Growth hormone protects against ovariectomy-induced bone loss in states of low circulating insulin-like growth factor (IGF-1), *Journal of Bone and Mineral Research*, 25, 235-246
- [7] T. K. Sampath, P. Simic, R. Sendak, N. Draca, A. E. Bowe, S. O'Brien, S. C. Schiavi, J. M. McPherson, S. Vukicevic, (2007) Thyroid-Stimulating Hormone Restores Bone Volume, Microarchitecture, and Strength in Aged Ovariectomized Rats*, *Journal of Bone and Mineral Research*, 22, 849-859
- [8] A. K. Amstrup, T. Sikjaer, L. Heickendorff, L. Mosekilde, L. Rejnmark, (2015) Melatonin improves bone mineral density at the femoral neck in postmenopausal women with osteopenia: a randomized controlled trial, *Journal of Pineal Research*, 59, 221-229
- [9] P. A. Baldock, S. J. Allison, P. Lundberg, N. J. Lee, K. Slack, E.-J. D. Lin, R. F. Enriquez, M. M. McDonald, L. Zhang, M. J. During, D. G. Little, J. A. Eisman, E. M. Gardiner, E. Yulyaningsih, S. Lin, A. Sainsbury, H. Herzog, (2007) Novel Role of Y1 Receptors in the Coordinated Regulation of Bone and Energy Homeostasis *, *Journal of Biological Chemistry*, 282, 19092-19102
- [10] D. M. Sousa, P. S. Martins, L. Leitão, C. J. Alves, M. Gomez-Lazaro, E. Neto, F. Conceição, H. Herzog, M. Lamghari, (2020) The lack of neuropeptide Y-Y1 receptor signaling modulates the chemical and mechanical properties of bone matrix, *The FASEB Journal*, 34, 4163-4177

- [11] P. A. Baldock, A. Sainsbury, M. Couzens, R. F. Enriquez, G. P. Thomas, E. M. Gardiner, H. Herzog, (2002) Hypothalamic Y2 receptors regulate bone formation, *The Journal of Clinical Investigation*, 109, 915-921
- [12] Y. Ji, P. Liu, T. Yuen, S. Haider, J. He, R. Romero, H. Chen, M. Bloch, S.-M. Kim, D. Lizneva, L. Munshi, C. Zhou, P. Lu, J. Iqbal, Z. Cheng, M. I. New, A. J. Hsueh, Z. Bian, C. J. Rosen, L. Sun, M. Zaidi, (2018) Epitope-specific monoclonal antibodies to FSH β increase bone mass, *Proceedings of the National Academy of Sciences*, 115, 2192-2197
- [13] M. R. Lorenz, J. M. Brazill, A. T. Beeve, I. Shen, E. L. Scheller, (2021) A Neuroskeletal Atlas: Spatial Mapping and Contextualization of Axon Subtypes Innervating the Long Bones of C3H and B6 Mice, *Journal of Bone and Mineral Research*, 36, 1012-1025
- [14] S. C. Offley, T.-Z. Guo, T. Wei, J. D. Clark, H. Vogel, D. P. Lindsey, C. R. Jacobs, W. Yao, N. E. Lane, W. S. Kingery, (2005) Capsaicin-Sensitive Sensory Neurons Contribute to the Maintenance of Trabecular Bone Integrity, *Journal of Bone and Mineral Research*, 20, 257-267
- [15] Y. Ding, M. Arai, H. Kondo, A. Togari, (2010) Effects of capsaicin-induced sensory denervation on bone metabolism in adult rats, *Bone*, 46, 1591-1596
- [16] T. Niedermair, R. H. Straub, C. Brochhausen, S. Grässel, (2020) Impact of the Sensory and Sympathetic Nervous System on Fracture Healing in Ovariectomized Mice, *International Journal of Molecular Sciences*, 21, 405
- [17] M. Hofman, F. Rabenschlag, H. Andruszkow, J. Andruszkow, D. Möckel, T. Lammers, A. Kolejewska, P. Kobbe, J. Greven, M. Teuben, M. Poeze, F. Hildebrand, (2019) Effect of neurokinin-1-receptor blockage on fracture healing in rats, *Scientific Reports*, 9, 9744
- [18] F. Elefteriou, (2018) Impact of the Autonomic Nervous System on the Skeleton, *Physiological Reviews*, 98, 1083-1112
- [19] M. Hukkanen, Y. T. Konttinen, S. Santavirta, P. Paavolainen, X. H. Gu, G. Terenghi, J. M. Polak, (1993) Rapid proliferation of calcitonin gene-related peptide-immunoreactive nerves during healing of rat tibial fracture suggests neural involvement in bone growth and remodelling, *Neuroscience*, 54, 969-979
- [20] G. Sisask, C. J. Silfverswärd, A. Bjurholm, O. Nilsson, (2013) Ontogeny of sensory and autonomic nerves in the developing mouse skeleton, *Autonomic Neuroscience: Basic and Clinical*, 177, 237-243
- [21] S. Zhu, J. Zhu, G. Zhen, Y. Hu, S. An, Y. Li, Q. Zheng, Z. Chen, Y. Yang, M. Wan, R. L. Skolasky, Y. Cao, T. Wu, B. Gao, M. Yang, M. Gao, J. Kuliwaba, S. Ni, L. Wang, C. Wu, D. Findlay, H. K. Eltzschig, H. W. Ouyang, J. Crane, F.-Q. Zhou, Y. Guan, X.

- Dong,X. Cao, (2019) Subchondral bone osteoclasts induce sensory innervation and osteoarthritis pain, *The Journal of Clinical Investigation*, 129, 1076-1093
- [22] J. M. Jimenez-Andrade, A. P. Bloom, J. I. Stake, W. G. Mantyh, R. N. Taylor, K. T. Freeman, J. R. Ghilardi, M. A. Kuskowski,P. W. Mantyh, (2010) Pathological Sprouting of Adult Nociceptors in Chronic Prostate Cancer-Induced Bone Pain, *The Journal of Neuroscience*, 30, 14649-14656
- [23] A. P. Bloom, J. M. Jimenez-Andrade, R. N. Taylor, G. Castañeda-Corral, M. J. Kaczmarek, K. T. Freeman, K. A. Coughlin, J. R. Ghilardi, M. A. Kuskowski,P. W. Mantyh, (2011) Breast Cancer-Induced Bone Remodeling, Skeletal Pain, and Sprouting of Sensory Nerve Fibers, *The Journal of Pain*, 12, 698-711
- [24] L. Crigler, R. C. Robey, A. Asawachaicharn, D. Gaupp,D. G. Phinney, (2006) Human mesenchymal stem cell subpopulations express a variety of neuro-regulatory molecules and promote neuronal cell survival and neuritogenesis, *Experimental Neurology*, 198, 54-64
- [25] K. Wang, Y. Gu, Y. Liao, S. Bang, C. R. Donnelly, O. Chen, X. Tao, A. J. Mirando, M. J. Hilton,R.-R. Ji, (2020) PD-1 blockade inhibits osteoclast formation and murine bone cancer pain, *The Journal of Clinical Investigation*, 130, 3603-3620
- [26] J. R. Ghilardi, H. Röhrich, T. H. Lindsay, M. A. Sevcik, M. J. Schwei, K. Kubota, K. G. Halvorson, J. Poblete, S. R. Chaplan, A. E. Dubin, N. I. Carruthers, D. Swanson, M. Kuskowski, C. M. Flores, D. Julius,P. W. Mantyh, (2005) Selective Blockade of the Capsaicin Receptor TRPV1 Attenuates Bone Cancer Pain, *The Journal of Neuroscience*, 25, 3126-3131
- [27] L. Leitão, E. Neto, F. Conceição, A. Monteiro, M. Couto, C. J. Alves, D. M. Sousa,M. Lamghari, (2020) Osteoblasts are inherently programmed to repel sensory innervation, *Bone Research*, 8, 20
- [28] M. Maryanovich, S. Takeishi,P. S. Frenette, (2018) Neural Regulation of Bone and Bone Marrow, *Cold Spring Harbor Perspectives in Medicine*, 8,
- [29] Á. Dénes, Z. Boldogkoi, G. Uhereczky, Á. Hornyák, M. Rusvai, M. Palkovits,K. J. Kovács, (2005) Central autonomic control of the bone marrow: Multisynaptic tract tracing by recombinant pseudorabies virus, *Neuroscience*, 134, 947-963
- [30] M. Sayilekshmy, R. B. Hansen, J.-M. Delaissé, L. Rolighed, T. L. Andersen,A.-M. Heegaard, (2019) Innervation is higher above Bone Remodeling Surfaces and in Cortical Pores in Human Bone: Lessons from patients with primary hyperparathyroidism, *Scientific Reports*, 9, 5361
- [31] D. B. Mach, S. D. Rogers, M. C. Sabino, N. M. Luger, M. J. Schwei, J. D. Pomonis, C. P. Keyser, D. R. Clohisy, D. J. Adams, P. O'Leary,P. W. Mantyh, (2002) Origins of

skeletal pain: sensory and sympathetic innervation of the mouse femur, *Neuroscience*, 113, 155-166

[32] H. H. Huang, T. C. Brennan, M. M. Muir, R. S. Mason, (2009) Functional α 1- and β 2-adrenergic receptors in human osteoblasts, *Journal of Cellular Physiology*, 220, 267-275

[33] L. Wu, Y. Tai, S. Hu, M. Zhang, R. Wang, W. Zhou, J. Tao, Y. Han, Q. Wang, W. Wei, (2018) Bidirectional Role of β 2-Adrenergic Receptor in Autoimmune Diseases, *Frontiers in Pharmacology*, 9,

[34] Y. Katayama, M. Battista, W.-M. Kao, A. Hidalgo, A. J. Peired, S. A. Thomas, P. S. Frenette, (2006) Signals from the Sympathetic Nervous System Regulate Hematopoietic Stem Cell Egress from Bone Marrow, *Cell*, 124, 407-421

[35] H. Kondo, S. Takeuchi, A. Togari, (2013) β -Adrenergic signaling stimulates osteoclastogenesis via reactive oxygen species, *American Journal of Physiology-Endocrinology and Metabolism*, 304, E507-E515

[36] R. E. Moore, C. K. Smith, C. S. Bailey, E. F. Voelkel, A. H. Tashjian, (1993) Characterization of beta-adrenergic receptors on rat and human osteoblast-like cells and demonstration that beta-receptor agonists can stimulate bone resorption in organ culture, *Bone and Mineral*, 23, 301-315

[37] Y. Ma, J. J. Krueger, S. N. Redmon, S. Uppuganti, J. S. Nyman, M. K. Hahn, F. Elefteriou, (2013) Extracellular Norepinephrine Clearance by the Norepinephrine Transporter Is Required for Skeletal Homeostasis, *Journal of Biological Chemistry*, 288, 30105-30113

[38] A. Togari, M. Arai, S. Mizutani, S. Mizutani, Y. Koshihara, T. Nagatsu, (1997) Expression of mRNAs for neuropeptide receptors and β -adrenergic receptors in human osteoblasts and human osteogenic sarcoma cells, *Neuroscience Letters*, 233, 125-128

[39] T. Nishiura, K. Abe, (2007) α 1-Adrenergic receptor stimulation induces the expression of receptor activator of nuclear factor κ B ligand gene via protein kinase C and extracellular signal-regulated kinase pathways in MC3T3-E1 osteoblast-like cells, *Archives of Oral Biology*, 52, 778-785

[40] N. Bonnet, C. L. Benhamou, B. Brunet-Imbault, A. Arlettaz, M. N. Horcajada, O. Richard, L. Vico, K. Collomp, D. Courteix, (2005) Severe bone alterations under β 2 agonist treatments: Bone mass, microarchitecture and strength analyses in female rats, *Bone*, 37, 622-633

[41] M. Nagao, T. N. Feinstein, Y. Ezura, T. Hayata, T. Notomi, Y. Saita, R. Hanyu, H. Hemmi, Y. Izu, S. Takeda, K. Wang, S. Rittling, T. Nakamoto, K. Kaneko, H. Kurosawa, G. Karsenty, D. T. Denhardt, J.-P. Vilaradaga, M. Noda, (2011) Sympathetic control of bone mass regulated by osteopontin, *Proceedings of the National Academy of Sciences*, 108, 17767-17772

- [42] N. Bonnet, H. Beaupied, L. Vico, E. Dolleans, N. Laroche, D. Courteix, C.-L. Benhamou, (2007) Combined Effects of Exercise and Propranolol on Bone Tissue in Ovariectomized Rats, *Journal of Bone and Mineral Research*, 22, 578-588
- [43] D. D. Pierroz, M. L. Bouxsein, R. Rizzoli, S. L. Ferrari, (2006) Combined treatment with a β -blocker and intermittent PTH improves bone mass and microarchitecture in ovariectomized mice, *Bone*, 39, 260-267
- [44] M. L. Bouxsein, M. J. Devlin, V. Glatt, H. Dhillon, D. D. Pierroz, S. L. Ferrari, (2009) Mice Lacking β -Adrenergic Receptors Have Increased Bone Mass but Are Not Protected from Deleterious Skeletal Effects of Ovariectomy, *Endocrinology*, 150, 144-152
- [45] F. Eleftheriou, J. D. Ahn, S. Takeda, M. Starbuck, X. Yang, X. Liu, H. Kondo, W. G. Richards, T. W. Bannon, M. Noda, K. Clement, C. Vaisse, G. Karsenty, (2005) Leptin regulation of bone resorption by the sympathetic nervous system and CART, *Nature*, 434, 514-520
- [46] D. Kajimura, E. Hinoi, M. Ferron, A. Kode, K. J. Riley, B. Zhou, X. E. Guo, G. Karsenty, (2011) Genetic determination of the cellular basis of the sympathetic regulation of bone mass accrual, *Journal of Experimental Medicine*, 208, 841-851
- [47] S. J. Aitken, E. Landao-Bassonga, S. H. Ralston, A. I. Idris, (2009) β -Adrenoreceptor ligands regulate osteoclast differentiation in vitro by direct and indirect mechanisms, *Archives of Biochemistry and Biophysics*, 482, 96-103
- [48] K. Baek, H.-J. Park, J.-H. Baek, H.-R. Kim, (2017) Isoproterenol Increases RANKL Expression in a ATF4/NFATc1-Dependent Manner in Mouse Osteoblastic Cells, *International Journal of Molecular Sciences*, 18, 2204
- [49] H. Liang, Y. Zeng, Y. Feng, H. Wu, P. Gong, Q. Yao, (2019) Selective β 2-adrenoreceptor signaling regulates osteoclastogenesis via modulating RANKL production and neuropeptides expression in osteocytic MLO-Y4 cells, *Journal of Cellular Biochemistry*, 120, 7238-7247
- [50] Q. Yao, H. Liang, B. Huang, L. Xiang, T. Wang, Y. Xiong, B. Yang, Y. Guo, P. Gong, (2017) Beta-adrenergic signaling affect osteoclastogenesis via osteocytic MLO-Y4 cells' RANKL production, *Biochemical and Biophysical Research Communications*, 488, 634-640
- [51] M. Arai, T. Nagasawa, Y. Koshihara, S. Yamamoto, A. Togari, (2003) Effects of β -adrenergic agonists on bone-resorbing activity in human osteoclast-like cells, *Biochimica et Biophysica Acta (BBA) - Molecular Cell Research*, 1640, 137-142
- [52] C. E. Lyons, M. Razzoli, E. Larson, D. Svedberg, A. Frontini, S. Cinti, L. Vulchanova, M. Sanders, M. Thomas, A. Bartolomucci, (2020) Optogenetic-induced sympathetic neuromodulation of brown adipose tissue thermogenesis, *The FASEB Journal*, 34, 2765-2773

- [53] S. W. Cole, A. S. Nagaraja, S. K. Lutgendorf, P. A. Green, A. K. Sood, (2015) Sympathetic nervous system regulation of the tumour microenvironment, *Nature Reviews Cancer*, 15, 563-572
- [54] B. K. Mani, S. Osborne-Lawrence, P. Vijayaraghavan, C. Hepler, J. M. Zigman, (2016) β 1-Adrenergic receptor deficiency in ghrelin-expressing cells causes hypoglycemia in susceptible individuals, *The Journal of Clinical Investigation*, 126, 3467-3478
- [55] D. C. Ali, M. Naveed, A. Gordon, F. Majeed, M. Saeed, M. I. Ogbuke, M. Atif, H. M. Zubair, L. Changxing, (2020) β -Adrenergic receptor, an essential target in cardiovascular diseases, *Heart Failure Reviews*, 25, 343-354
- [56] A. Galvano, D. Scaturro, G. Badalamenti, L. Incorvaia, S. Rizzo, L. Castellana, S. Cusenza, S. Cutaia, D. Santini, F. Guadagni, M. Roselli, S. Gori, M. A. Latteri, V. Bazan, L. M. Giulia, A. Russo, (2019) Denosumab for bone health in prostate and breast cancer patients receiving endocrine therapy? A systematic review and a meta-analysis of randomized trials, *Journal of Bone Oncology*, 18, 100252
- [57] D. G. Powe, M. J. Voss, K. S. Zänker, H. O. Habashy, A. R. Green, I. O. Ellis, F. Entschladen, (2010) Beta-Blocker Drug Therapy Reduces Secondary Cancer Formation in Breast Cancer and Improves Cancer Specific Survival, *Oncotarget*, 1,
- [58] J. P. Campbell, M. R. Karolak, Y. Ma, D. S. Perrien, S. K. Masood-Campbell, N. L. Penner, S. A. Munoz, A. Zijlstra, X. Yang, J. A. Sterling, F. Elefteriou, (2012) Stimulation of Host Bone Marrow Stromal Cells by Sympathetic Nerves Promotes Breast Cancer Bone Metastasis in Mice, *PLOS Biology*, 10, e1001363
- [59] M. M. S. Obradović, B. Hamelin, N. Manevski, J. P. Couto, A. Sethi, M.-M. Coissieux, S. Müntz, R. Okamoto, H. Kohler, A. Schmidt, M. Bentires-Alj, (2019) Glucocorticoids promote breast cancer metastasis, *Nature*, 567, 540-544
- [60] L. Perron, I. Bairati, F. Harel, F. Meyer, (2004) Antihypertensive drug use and the risk of prostate cancer (Canada), *Cancer causes & control : CCC*, 15, 535-541
- [61] S. Hassan, Y. Karpova, D. Baiz, D. Yancey, A. Pullikuth, A. Flores, T. Register, J. M. Cline, R. D'Agostino, Jr., N. Danial, S. R. Datta, G. Kulik, (2013) Behavioral stress accelerates prostate cancer development in mice, *The Journal of Clinical Investigation*, 123, 874-886
- [62] C. Magnon, S. J. Hall, J. Lin, X. Xue, L. Gerber, S. J. Freedland, P. S. Frenette, (2013) Autonomic Nerve Development Contributes to Prostate Cancer Progression, *Science (New York, N. Y.)*, 341, 1236361
- [63] A. M. Decker, Y. Jung, F. C. Cackowski, K. Yumoto, J. Wang, R. S. Taichman, (2017) Sympathetic Signaling Reactivates Quiescent Disseminated Prostate Cancer Cells in the Bone Marrow, *Molecular Cancer Research*, 15, 1644-1655

- [64] C. Coarfa, D. Florentin, N. Putluri, Y. Ding, J. Au, D. He, A. Ragheb, A. Frolov, G. Michailidis, M. Lee, D. Kadmon, B. Miles, C. Smith, M. Ittmann, D. Rowley, A. Sreekumar, C. J. Creighton, G. Ayala, (2018) Influence of the neural microenvironment on prostate cancer, *The Prostate*, 78, 128-139
- [65] J. M. Jimenez-Andrade, W. G. Mantyh, A. P. Bloom, A. S. Ferng, C. P. Geffre, P. W. Mantyh, (2010) Bone cancer pain, *Annals of the New York Academy of Sciences*, 1198, 173-181
- [66] D. Liu, Q. Deng, L. Sun, T. Wang, Z. Yang, H. Chen, L. Guo, Y. Liu, Y. Ma, N. Guo, M. Shi, (2015) A Her2-let-7- β 2-AR circuit affects prognosis in patients with Her2-positive breast cancer, *BMC Cancer*, 15, 832
- [67] E. M. Rivero, L. M. Martinez, C. D. Bruque, L. Gargiulo, A. Bruzzone, I. A. Lüthy, (2019) Prognostic significance of α - and β 2-adrenoceptor gene expression in breast cancer patients, *British Journal of Clinical Pharmacology*, 85, 2143-2154
- [68] S. Kurozumi, K. Kaira, H. Matsumoto, T. Hirakata, T. Yokobori, K. Inoue, J. Horiguchi, A. Katayama, H. Koshi, A. Shimizu, T. Oyama, E. K. Sloan, M. Kurosumi, T. Fujii, K. Shirabe, (2019) β 2-Adrenergic receptor expression is associated with biomarkers of tumor immunity and predicts poor prognosis in estrogen receptor-negative breast cancer, *Breast Cancer Research and Treatment*, 177, 603-610
- [69] L. F. Castillo, E. M. Rivero, V. Goffin, I. A. Lüthy, (2017) Alpha2-adrenoceptor agonists trigger prolactin signaling in breast cancer cells, *Cellular Signalling*, 34, 76-85
- [70] Y. Cakir, Plummer, H.K., Tithof, P.K., & Schuller, H.M., (2002) Beta-adrenergic and arachidonic acid-mediated growth regulation of human breast cancer cell lines, *International Journal of Oncology*, 21, 153-157
- [71] G. Dezhong, M. Zhongbing, F. Qinye, Y. Zhigang, (2014) Carvedilol suppresses migration and invasion of malignant breast cells by inactivating Src involving cAMP/PKA and PKC signaling pathway, *Journal of Cancer Research and Therapeutics*, 10, 991-997
- [72] S. M. Vázquez, A. G. Mladovan, C. Pérez, A. Bruzzone, A. Baldi, I. A. Lüthy, (2005) Human breast cell lines exhibit functional α 2-adrenoceptors, *Cancer Chemotherapy and Pharmacology*, 58, 50
- [73] C. Strell, B. Niggemann, M. J. Voss, D. G. Powe, K. S. Zänker, F. Entschladen, (2012) Norepinephrine Promotes the β 1-Integrin-Mediated Adhesion of MDA-MB-231 Cells to Vascular Endothelium by the Induction of a GRO α Release, *Molecular Cancer Research*, 10, 197-207
- [74] C. K. Pon, J. R. Lane, E. K. Sloan, M. L. Halls, (2016) The β 2-adrenoceptor activates a positive cAMP-calcium feedforward loop to drive breast cancer cell invasion, *The FASEB Journal*, 30, 1144-1154

- [75] D. Hanahan, Robert A. Weinberg, (2011) Hallmarks of Cancer: The Next Generation, *Cell*, 144, 646-674
- [76] C. Pérez Piñero, A. Bruzzone, M. Sarappa, L. Castillo, I. Lüthy, (2012) Involvement of α 2- and β 2-adrenoceptors on breast cancer cell proliferation and tumour growth regulation, *British Journal of Pharmacology*, 166, 721-736
- [77] K. S. R. Sastry, Y. Karpova, S. Prokopovich, A. J. Smith, B. Essau, A. Gersappe, J. P. Carson, M. J. Weber, T. C. Register, Y. Q. Chen, R. B. Penn, G. Kulik, (2007) Epinephrine Protects Cancer Cells from Apoptosis via Activation of cAMP-dependent Protein Kinase and BAD Phosphorylation, *Journal of Biological Chemistry*, 282, 14094-14100
- [78] A. Reeder, M. Attar, L. Nazario, C. Bathula, A. Zhang, D. Hochbaum, E. Roy, K. L. Cooper, S. Oesterreich, N. E. Davidson, C. A. Neumann, M. S. Flint, (2015) Stress hormones reduce the efficacy of paclitaxel in triple negative breast cancer through induction of DNA damage, *British Journal of Cancer*, 112, 1461-1470
- [79] T. A. Slotkin, J. Zhang, R. Dancel, S. J. Garcia, C. Willis, F. J. Seidler, (2000) β -adrenoceptor signaling and its control of cell replication in MDA-MB-231 human breast cancer cells, *Breast Cancer Research and Treatment*, 60, 153-166
- [80] L. Gargiulo, S. Copsel, E. M. Rivero, C. Galés, J.-M. Sénard, I. A. Lüthy, C. Davio, A. Bruzzone, (2014) Differential β 2-adrenergic receptor expression defines the phenotype of non-tumorigenic and malignant human breast cell lines, *Oncotarget*, 5,
- [81] A. K. Walker, D. Martelli, A. I. Ziegler, G. W. Lambert, S. E. Phillips, S. J. Hill, R. M. McAllen, E. K. Sloan, (2019) Circulating epinephrine is not required for chronic stress to enhance metastasis, *Psychoneuroendocrinology*, 99, 191-195
- [82] C. P. Le, C. J. Nowell, C. Kim-Fuchs, E. Botteri, J. G. Hiller, H. Ismail, M. A. Pimentel, M. G. Chai, T. Karnezis, N. Rotmensch, G. Renne, S. Gandini, C. W. Pouton, D. Ferrari, A. Möller, S. A. Stacker, E. K. Sloan, (2016) Chronic stress in mice remodels lymph vasculature to promote tumour cell dissemination, *Nature Communications*, 7, 10634
- [83] E. K. Sloan, S. J. Priceman, B. F. Cox, S. Yu, M. A. Pimentel, V. Tangkanangnukul, J. M. G. Arevalo, K. Morizono, B. D. W. Karanikolas, L. Wu, A. K. Sood, S. W. Cole, (2010) The Sympathetic Nervous System Induces a Metastatic Switch in Primary Breast Cancer, *Cancer Research*, 70, 7042-7052
- [84] A. Bruzzone, C. P. Pinero, P. Rojas, M. Romanato, H. Gass, C. Lanari, I. A. Lüthy, (2011) β 2-Adrenoceptors Enhance Cell Proliferation and Mammary Tumor Growth Acting Through both the Stroma and the Tumor Cells, *Current Cancer Drug Targets*, 11, 763-774
- [85] P. H. Thaker, L. Y. Han, A. A. Kamat, J. M. Arevalo, R. Takahashi, C. Lu, N. B. Jennings, G. Armaiz-Pena, J. A. Bankson, M. Ravoori, W. M. Merritt, Y. G. Lin, L. S.

- Mangala, T. J. Kim, R. L. Coleman, C. N. Landen, Y. Li, E. Felix, A. M. Sanguino, R. A. Newman, M. Lloyd, D. M. Gershenson, V. Kundra, G. Lopez-Berestein, S. K. Lutgendorf, S. W. Cole, A. K. Sood, (2006) Chronic stress promotes tumor growth and angiogenesis in a mouse model of ovarian carcinoma, *Nature Medicine*, 12, 939-944
- [86] D. M. Lamkin, H. Y. Sung, G. S. Yang, J. M. David, J. C. Y. Ma, S. W. Cole, E. K. Sloan, (2015) α 2-Adrenergic blockade mimics the enhancing effect of chronic stress on breast cancer progression, *Psychoneuroendocrinology*, 51, 262-270
- [87] A. Kamiya, Y. Hayama, S. Kato, A. Shimomura, T. Shimomura, K. Irie, R. Kaneko, Y. Yanagawa, K. Kobayashi, T. Ochiya, (2019) Genetic manipulation of autonomic nerve fiber innervation and activity and its effect on breast cancer progression, *Nature Neuroscience*, 22, 1289-1305
- [88] L. Hein, J. D. Altman, B. K. Kobilka, (1999) Two functionally distinct α 2-adrenergic receptors regulate sympathetic neurotransmission, *Nature*, 402, 181-184
- [89] J. A. Nagy, S.-H. Chang, S.-C. Shih, A. M. Dvorak, H. F. Dvorak, (2010) Heterogeneity of the Tumor Vasculature, *Semin Thromb Hemost*, 36, 321-331
- [90] K. S. Madden, M. J. Szpunar, E. B. Brown, (2011) β -Adrenergic receptors (β -AR) regulate VEGF and IL-6 production by divergent pathways in high β -AR-expressing breast cancer cell lines, *Breast Cancer Research and Treatment*, 130, 747-758
- [91] H. Chen, D. Liu, Z. Yang, L. Sun, Q. Deng, S. Yang, L. Qian, L. Guo, M. Yu, M. Hu, M. Shi, N. Guo, (2014) Adrenergic signaling promotes angiogenesis through endothelial cell–tumor cell crosstalk, 21, 783
- [92] J. Zhou, Z. Liu, L. Zhang, X. Hu, Z. Wang, H. Ni, Y. Wang, J. Qin, (2020) Activation of β 2-Adrenergic Receptor Promotes Growth and Angiogenesis in Breast Cancer by Down-regulating PPAR γ , *J Korean Cancer Assoc*, 0, 0-0
- [93] E. M. Sternberg, (2006) Neural regulation of innate immunity: a coordinated nonspecific host response to pathogens, *Nature Reviews Immunology*, 6, 318-328
- [94] M. Hanoun, M. Maryanovich, A. Arnal-Estapé, P. S. Frenette, (2015) Neural regulation of hematopoiesis, inflammation, and cancer, *Neuron*, 86, 360-373
- [95] M. J. Szpunar, E. K. Belcher, R. P. Dawes, K. S. Madden, (2016) Sympathetic innervation, norepinephrine content, and norepinephrine turnover in orthotopic and spontaneous models of breast cancer, *Brain Behav Immun*, 53, 223-233
- [96] D. M. Lamkin, H.-Y. Ho, T. H. Ong, C. K. Kawanishi, V. L. Stoffers, N. Ahlawat, J. C. Y. Ma, J. M. G. Arevalo, S. W. Cole, E. K. Sloan, (2016) β -Adrenergic-stimulated macrophages: Comprehensive localization in the M1-M2 spectrum, *Brain, Behavior, and Immunity*, 57, 338-346
- [97] M. J. Bucsek, G. Qiao, C. R. MacDonald, T. Giridharan, L. Evans, B. Niedzwecki, H. Liu, K. M. Kokolus, J. W.-L. Eng, M. N. Messmer, K. Attwood, S. I. Abrams, B. L.

- Hylander, E. A. Repasky, (2017) β -Adrenergic Signaling in Mice Housed at Standard Temperatures Suppresses an Effector Phenotype in CD8⁺ T Cells and Undermines Checkpoint Inhibitor Therapy, *Cancer Research*, 77, 5639-5651
- [98] R. Bill, G. Christofori, (2015) The relevance of EMT in breast cancer metastasis: Correlation or causality?, *FEBS Letters*, 589, 1577-1587
- [99] A. Chang, C. P. Le, A. K. Walker, S. J. Creed, C. K. Pon, S. Albold, D. Carroll, M. L. Halls, J. R. Lane, B. Riedel, D. Ferrari, E. K. Sloan, (2016) β 2-Adrenoceptors on tumor cells play a critical role in stress-enhanced metastasis in a mouse model of breast cancer, *Brain, Behavior, and Immunity*, 57, 106-115
- [100] S. J. Creed, C. P. Le, M. Hassan, C. K. Pon, S. Albold, K. T. Chan, M. E. Berginski, Z. Huang, J. E. Bear, J. R. Lane, M. L. Halls, D. Ferrari, C. J. Nowell, E. K. Sloan, (2015) β 2-adrenoceptor signaling regulates invadopodia formation to enhance tumor cell invasion, *Breast Cancer Research*, 17, 145
- [101] T.-H. Kim, N. K. Gill, K. D. Nyberg, A. V. Nguyen, S. V. Hohlbauch, N. A. Geisse, C. J. Nowell, E. K. Sloan, A. C. Rowat, (2016) Cancer cells become less deformable and more invasive with activation of β -adrenergic signaling, *Journal of Cell Science*, 129, 4563-4575
- [102] M. J. Szpunar, K. A. Burke, R. P. Dawes, E. B. Brown, K. S. Madden, (2013) The antidepressant desipramine and α 2-adrenergic receptor activation promote breast tumor progression in association with altered collagen structure, *Cancer prevention research (Philadelphia, Pa.)*, 6, 1262-1272
- [103] A. Soni, Z. Ren, O. Hameed, D. Chanda, C. J. Morgan, G. P. Siegal, S. Wei, (2015) Breast Cancer Subtypes Predispose the Site of Distant Metastases, *American Journal of Clinical Pathology*, 143, 471-478
- [104] A. Ignatov, H. Eggemann, E. Burger, T. Ignatov, (2018) Patterns of breast cancer relapse in accordance to biological subtype, *Journal of Cancer Research and Clinical Oncology*, 144, 1347-1355
- [105] H. Yang, R. Wang, F. Zeng, J. Zhao, S. Peng, Y. Ma, S. Chen, S. Ding, L. Zhong, W. Guo, W. Wang, (2020) Impact of molecular subtypes on metastatic behavior and overall survival in patients with metastatic breast cancer: A single-center study combined with a large cohort study based on the Surveillance, Epidemiology and End Results database, *Oncology letters*, 20, 87
- [106] K. N. Weilbaecher, T. A. Guise, L. K. McCauley, (2011) Cancer to bone: a fatal attraction, *Nature Reviews Cancer*, 11, 411-425
- [107] J. Fornetti, A. L. Welm, S. A. Stewart, (2018) Understanding the Bone in Cancer Metastasis, *Journal of Bone and Mineral Research*, 33, 2099-2113

- [108] Y. Kang, (2016) Dissecting Tumor-Stromal Interactions in Breast Cancer Bone Metastasis, *Endocrinol Metab*, 31, 206-212
- [109] F. H. Drake, R. A. Dodds, I. E. James, J. R. Connor, C. Debouck, S. Richardson, E. Lee-Rykaczewski, L. Coleman, D. Rieman, R. Barthlow, G. Hastings, M. Gowen, (1996) Cathepsin K, but Not Cathepsins B, L, or S, Is Abundantly Expressed in Human Osteoclasts, *Journal of Biological Chemistry*, 271, 12511-12516
- [110] J. M. Halleen, S. L. Alatalo, H. Suominen, S. Cheng, A. J. Janckila, H. K. Väänänen, (2000) Tartrate-Resistant Acid Phosphatase 5b: A Novel Serum Marker of Bone Resorption, *Journal of Bone and Mineral Research*, 15, 1337-1345
- [111] B. Ecarot-Charrier, F. H. Glorieux, M. van der Rest, G. Pereira, (1983) Osteoblasts isolated from mouse calvaria initiate matrix mineralization in culture, *The Journal of Cell Biology*, 96, 639-643
- [112] H. Kamioka, T. Honjo, T. Takano-Yamamoto, (2001) A three-dimensional distribution of osteocyte processes revealed by the combination of confocal laser scanning microscopy and differential interference contrast microscopy, *Bone*, 28, 145-149
- [113] J. Q. Feng, L. M. Ward, S. Liu, Y. Lu, Y. Xie, B. Yuan, X. Yu, F. Rauch, S. I. Davis, S. Zhang, H. Rios, M. K. Drezner, L. D. Quarles, L. F. Bonewald, K. E. White, (2006) Loss of DMP1 causes rickets and osteomalacia and identifies a role for osteocytes in mineral metabolism, *Nature Genetics*, 38, 1310-1315
- [114] A. G. Robling, P. J. Niziolek, L. A. Baldrige, K. W. Condon, M. R. Allen, I. Alam, S. M. Mantila, J. Gluhak-Heinrich, T. M. Bellido, S. E. Harris, C. H. Turner, (2008) Mechanical Stimulation of Bone in Vivo Reduces Osteocyte Expression of Sost/Sclerostin, *Journal of Biological Chemistry*, 283, 5866-5875
- [115] M. A. Kamel, J. L. Picconi, N. Lara-Castillo, M. L. Johnson, (2010) Activation of β -catenin signaling in MLO-Y4 osteocytic cells versus 2T3 osteoblastic cells by fluid flow shear stress and PGE₂: Implications for the study of mechanosensation in bone, *Bone*, 47, 872-881
- [116] J. J. Yin, K. Selander, J. M. Chirgwin, M. Dallas, B. G. Grubbs, R. Wieser, J. Massagué, G. R. Mundy, T. A. Guise, (1999) TGF- β signaling blockade inhibits PTHrP secretion by breast cancer cells and bone metastases development, *The Journal of Clinical Investigation*, 103, 197-206
- [117] F. Le Pape, G. Vargas, P. Clézardin, (2016) The role of osteoclasts in breast cancer bone metastasis, *Journal of Bone Oncology*, 5, 93-95
- [118] G. R. Mundy, (2002) Metastasis to bone: causes, consequences and therapeutic opportunities, *Nature Reviews Cancer*, 2, 584-593

- [119] K. Fizazi, A. Lipton, X. Mariette, J.-J. Body, Y. Rahim, J. R. Gralow, G. Gao, L. Wu, W. Sohn, S. Jun, (2009) Randomized Phase II Trial of Denosumab in Patients With Bone Metastases From Prostate Cancer, Breast Cancer, or Other Neoplasms After Intravenous Bisphosphonates, *Journal of Clinical Oncology*, 27, 1564-1571
- [120] S. R. Chartier, S. A. T. Mitchell, L. A. Majuta, P. W. Mantyh, (2018) The Changing Sensory and Sympathetic Innervation of the Young, Adult and Aging Mouse Femur, *Neuroscience*, 387, 178-190
- [121] T. L. Fonseca, V. Jorgetti, C. C. Costa, L. P. Capelo, A. E. Covarrubias, A. C. Moulatlet, M. B. Teixeira, E. Hesse, P. Morethson, E. H. Beber, F. R. Freitas, C. C. Wang, K. O. Nonaka, R. Oliveira, D. E. Casarini, T. M. Zorn, P. C. Brum, C. H. Gouveia, (2011) Double disruption of $\alpha 2A$ - and $\alpha 2C$ -adrenoceptors results in sympathetic hyperactivity and high-bone-mass phenotype, *Journal of Bone and Mineral Research*, 26, 591-603
- [122] T. Hirai, K. Tanaka, A. Togari, (2014) $\alpha 1$ -Adrenergic Receptor Signaling in Osteoblasts Regulates Clock Genes and Bone Morphogenetic Protein 4 Expression through Up-regulation of the Transcriptional Factor Nuclear Factor IL-3 (Nfil3)/E4 Promoter-binding Protein 4 (E4BP4), *Journal of Biological Chemistry*, 289, 17174-17183
- [123] A. Chen, L. Wang, S. Liu, Y. Wang, Y. Liu, M. Wang, H. Nakshatri, B.-Y. Li, H. Yokota, (2018) Attraction and Compaction of Migratory Breast Cancer Cells by Bone Matrix Proteins through Tumor-Osteocyte Interactions, *Scientific Reports*, 8, 5420
- [124] S. Liu, Y. Fan, A. Chen, A. Jalali, K. Minami, K. Ogawa, H. Nakshatri, B.-Y. Li, H. Yokota, (2018) Osteocyte-Driven Downregulation of Snail Restrains Effects of *Drd2* Inhibitors on Mammary Tumor Cells, *Cancer Research*, 78, 3865-3876
- [125] Y. Fan, A. Jalali, A. Chen, X. Zhao, S. Liu, M. Teli, Y. Guo, F. Li, J. Li, A. Siegel, L. Yang, J. Liu, S. Na, M. Agarwal, A. G. Robling, H. Nakshatri, B.-Y. Li, H. Yokota, (2020) Skeletal loading regulates breast cancer-associated osteolysis in a loading intensity-dependent fashion, *Bone Research*, 8, 9
- [126] P. Maroni, P. Bendinelli, (2020) Bone, a Secondary Growth Site of Breast and Prostate Carcinomas: Role of Osteocytes, *Cancers*, 12, 1812
- [127] P. L. Mulcrone, J. P. Campbell, L. Clément-Demange, A. L. Anbinder, A. R. Merkel, R. A. Brekken, J. A. Sterling, F. Elefteriou, (2017) Skeletal Colonization by Breast Cancer Cells Is Stimulated by an Osteoblast and $\beta 2AR$ -Dependent Neo-Angiogenic Switch, *Journal of Bone and Mineral Research*, 32, 1442-1454
- [128] L. Clément-Demange, P. L. Mulcrone, T. Q. Tabarestani, J. A. Sterling, F. Elefteriou, (2018) $\beta 2ARs$ stimulation in osteoblasts promotes breast cancer cell adhesion to bone marrow endothelial cells in an IL-1 β and selectin-dependent manner, *Journal of Bone Oncology*, 13, 1-10

- [129] T. J. Martin, R. W. Johnson, Multiple actions of parathyroid hormone-related protein in breast cancer bone metastasis, *British Journal of Pharmacology*, n/a,
- [130] R. J. Thomas, T. A. Guise, J. J. Yin, J. Elliott, N. J. Horwood, T. J. Martin, M. T. Gillespie, (1999) Breast Cancer Cells Interact with Osteoblasts to Support Osteoclast Formation, *Endocrinology*, 140, 4451-4458
- [131] R. Hanyu, V. L. Wehbi, T. Hayata, S. Moriya, T. N. Feinstein, Y. Ezura, M. Nagao, Y. Saita, H. Hemmi, T. Notomi, T. Nakamoto, E. Schipani, S. Takeda, K. Kaneko, H. Kurosawa, G. Karsenty, H. M. Kronenberg, J.-P. Vilardaga, M. Noda, (2012) Anabolic action of parathyroid hormone regulated by the β -adrenergic receptor, *Proceedings of the National Academy of Sciences*, 109, 7433-7438
- [132] S. Moriya, T. Hayata, T. Notomi, S. Aryal, T. Nakamoto, Y. Izu, M. Kawasaki, T. Yamada, J. Shirakawa, K. Kaneko, Y. Ezura, M. Noda, (2015) PTH Regulates β -Adrenergic Receptor Expression in Osteoblast-Like MC3T3-E1 Cells, *Journal of Cellular Biochemistry*, 116, 142-148
- [133] E. N. Bianchi, S. L. Ferrari, (2009) β -arrestin2 regulates parathyroid hormone effects on a p38 MAPK and NF κ B gene expression network in osteoblasts, *Bone*, 45, 716-725
- [134] R. F. Spurney, (2003) Regulated Expression of G Protein-Coupled Receptor Kinases (GRK's) and β -Arrestins in Osteoblasts, *Calcified Tissue International*, 73, 153-160
- [135] S. Fukayama, G. Kong, J. L. Benovic, E. Meurer, A. H. T. Jr, (1997) β -Adrenergic Receptor Kinase-1 Acutely Regulates PTH/PTHrP Receptor Signalling in Human Osteoblastlike Cells, *Cellular Signalling*, 9, 469-474
- [136] D. Gesty-Palmer, M. Chen, E. Reiter, S. Ahn, C. D. Nelson, S. Wang, A. E. Eckhardt, C. L. Cowan, R. F. Spurney, L. M. Luttrell, R. J. Lefkowitz, (2006) Distinct β -Arrestin- and G Protein-dependent Pathways for Parathyroid Hormone Receptor-stimulated ERK1/2 Activation, *Journal of Biological Chemistry*, 281, 10856-10864
- [137] C. R. Cardwell, A. Pottegård, E. Vaes, H. Garmo, L. J. Murray, C. Brown, P. A. J. Vissers, M. O'Rourke, K. Visvanathan, D. Cronin-Fenton, H. De Schutter, M. Lambe, D. G. Powe, M. P. P. van Herk-Sukel, A. Gavin, S. Friis, L. Sharp, K. Bennett, (2016) Propranolol and survival from breast cancer: a pooled analysis of European breast cancer cohorts, *Breast Cancer Research*, 18, 119
- [138] Y. Chida, M. Hamer, J. Wardle, A. Steptoe, (2008) Do stress-related psychosocial factors contribute to cancer incidence and survival?, *Nature Clinical Practice Oncology*, 5, 466-475
- [139] D. S. Lawrence, J. N. Sahay, S. S. Chatterjee, J. M. Cruickshank, (1982) Asthma and beta-blockers, *European journal of clinical pharmacology*, 22, 501-509

- [140] J. W. Paterson, C. T. Dollery, (1966) EFFECT OF PROPRANOLOL IN MILD HYPERTENSION, *The Lancet*, 288, 1148-1150
- [141] J. P. Fryzek, A. H. Poulsen, L. Lipworth, L. Pedersen, M. Nørgaard, J. K. McLaughlin, S. Friis, (2006) A Cohort Study of Antihypertensive Medication Use and Breast Cancer Among Danish Women, *Breast Cancer Research and Treatment*, 97, 231-236
- [142] C. I. Li, K. E. Malone, N. S. Weiss, D. M. Boudreau, K. L. Cushing-Haugen, J. R. Daling, (2003) Relation between use of antihypertensive medications and risk of breast carcinoma among women ages 65–79 years, *Cancer*, 98, 1504-1513
- [143] T. I. Barron, R. M. Connolly, L. Sharp, K. Bennett, K. Visvanathan, (2011) Beta Blockers and Breast Cancer Mortality: A Population- Based Study, *Journal of Clinical Oncology*, 29, 2635-2644
- [144] A. Melhem-Bertrandt, M. Chavez-MacGregor, X. Lei, E. N. Brown, R. T. Lee, F. Meric-Bernstam, A. K. Sood, S. D. Conzen, G. N. Hortobagyi, A.-M. Gonzalez-Angulo, (2011) Beta-Blocker Use Is Associated With Improved Relapse-Free Survival in Patients With Triple-Negative Breast Cancer, *Journal of Clinical Oncology*, 29, 2645-2652
- [145] A. Montoya, C. N. Amaya, A. Belmont, N. Diab, R. Trevino, G. Villanueva, S. Rains, L. A. Sanchez, N. Badri, S. Otoukesh, A. Khammanivong, D. Liss, S. T. Baca, R. J. Aguilera, E. B. Dickerson, A. Torabi, A. K. Dwivedi, A. Abbas, K. Chambers, B. A. Bryan, Z. Nahleh, (2016) Use of non-selective β -blockers is associated with decreased tumor proliferative indices in early stage breast cancer, *Oncotarget*, 8,
- [146] E. Botteri, E. Munzone, N. Rotmensz, C. Cipolla, V. De Giorgi, B. Santillo, A. Zanelotti, L. Adamoli, M. Colleoni, G. Viale, A. Goldhirsch, S. Gandini, (2013) Therapeutic effect of β -blockers in triple-negative breast cancer postmenopausal women, *Breast Cancer Research and Treatment*, 140, 567-575
- [147] G. Spera, R. Fresco, H. Fung, J. R. B. Dyck, E. Pituskin, I. Paterson, J. R. Mackey, (2017) Beta blockers and improved progression-free survival in patients with advanced HER2 negative breast cancer: a retrospective analysis of the ROSE/TRIO-012 study, *Annals of Oncology*, 28, 1836-1841
- [148] S. M. Shah, I. M. Carey, C. G. Owen, T. Harris, S. DeWilde, D. G. Cook, (2011) Does β -adrenoceptor blocker therapy improve cancer survival? Findings from a population-based retrospective cohort study, *British Journal of Clinical Pharmacology*, 72, 157-161
- [149] G. V. Sørensen, P. A. Ganz, S. W. Cole, L. A. Pedersen, H. T. Sørensen, D. P. Cronin-Fenton, J. P. Garne, P. M. Christiansen, T. L. Lash, T. P. Ahern, (2013) Use of β -Blockers, Angiotensin-Converting Enzyme Inhibitors, Angiotensin II Receptor Blockers,

- and Risk of Breast Cancer Recurrence: A Danish Nationwide Prospective Cohort Study, *Journal of Clinical Oncology*, 31, 2265-2272
- [150] C. R. Cardwell, H. G. Coleman, L. J. Murray, F. Entschladen, D. G. Powe, (2014) Beta-blocker usage and breast cancer survival: a nested case-control study within a UK Clinical Practice Research Datalink cohort, *International Journal of Epidemiology*, 42, 1852-1861
- [151] L. Zhou, Y. Li, X. Li, G. Chen, H. Liang, Y. Wu, J. Tong, W. Ouyang, (2016) Propranolol Attenuates Surgical Stress-Induced Elevation of the Regulatory T Cell Response in Patients Undergoing Radical Mastectomy, *The Journal of Immunology*, 196, 3460-3469
- [152] L. Shaashua, M. Shabat-Simon, R. Haldar, P. Matzner, O. Zmora, M. Shabtai, E. Sharon, T. Allweis, I. Barshack, L. Hayman, J. Arevalo, J. Ma, M. Horowitz, S. Cole, S. Ben-Eliyahu, (2017) Perioperative COX-2 and β -Adrenergic Blockade Improves Metastatic Biomarkers in Breast Cancer Patients in a Phase-II Randomized Trial, *Clinical Cancer Research*, 23, 4651-4661
- [153] R. Haldar, L. Shaashua, H. Lavon, Y. A. Lyons, O. Zmora, E. Sharon, Y. Birnbaum, T. Allweis, A. K. Sood, I. Barshack, S. Cole, S. Ben-Eliyahu, (2018) Perioperative inhibition of β -adrenergic and COX2 signaling in a clinical trial in breast cancer patients improves tumor Ki-67 expression, serum cytokine levels, and PBMCs transcriptome, *Brain, Behavior, and Immunity*, 73, 294-309
- [154] J. G. Hiller, S. W. Cole, E. M. Crone, D. J. Byrne, D. M. Shackelford, J.-M. B. Pang, M. A. Henderson, S. S. Nightingale, K. M. Ho, P. S. Myles, S. Fox, B. Riedel, E. K. Sloan, (2019) Pre-operative β -blockade with propranolol reduces biomarkers of metastasis in breast cancer: a Phase II randomized trial, *Clinical Cancer Research*, clincanres.2641.2019
- [155] P. A. Ganz, L. A. Habel, E. K. Weltzien, B. J. Caan, S. W. Cole, (2011) Examining the influence of beta blockers and ACE inhibitors on the risk for breast cancer recurrence: results from the LACE cohort, *Breast Cancer Research and Treatment*, 129, 549
- [156] K. J. Lechtenberg, S. T. Meyer, J. B. Doyle, T. C. Peterson, M. S. Buckwalter, (2019) Augmented β 2-adrenergic signaling dampens the neuroinflammatory response following ischemic stroke and increases stroke size, *Journal of Neuroinflammation*, 16, 112
- [157] X. Mei, K. Middleton, D. Shim, Q. Wan, L. Xu, Y.-H. V. Ma, D. Devadas, N. Walji, L. Wang, E. W. K. Young, L. You, (2019) Microfluidic platform for studying osteocyte mechanoregulation of breast cancer bone metastasis, *Integrative Biology*, 11, 119-129
- [158] S. Hao, L. Ha, G. Cheng, Y. Wan, Y. Xia, D. M. Sosnoski, A. M. Mastro, S.-Y. Zheng, (2018) A Spontaneous 3D Bone-On-a-Chip for Bone Metastasis Study of Breast Cancer Cells, *Small*, 14, 1702787

- [159] S. Bersini, J. S. Jeon, G. Dubini, C. Arrigoni, S. Chung, J. L. Charest, M. Moretti, R. D. Kamm, (2014) A microfluidic 3D in vitro model for specificity of breast cancer metastasis to bone, *Biomaterials*, 35, 2454-2461
- [160] J. S. Jeon, S. Bersini, M. Gilardi, G. Dubini, J. L. Charest, M. Moretti, R. D. Kamm, (2015) Human 3D vascularized organotypic microfluidic assays to study breast cancer cell extravasation, *Proceedings of the National Academy of Sciences*, 112, 214-219
- [161] P. Dubový, I. Klusáková, L. Kučera, J. Osičková, J. Chovancová, T. Loja, J. Mayer, M. Doubek, M. Joukal, (2017) Local chemical sympathectomy of rat bone marrow and its effect on marrow cell composition, *Autonomic neuroscience : basic & clinical*, 206, 19-27
- [162] H. Wu, Y. Luo, D. Xu, X. Ke, T. Ci, (2020) Low molecular weight heparin modified bone targeting liposomes for orthotopic osteosarcoma and breast cancer bone metastatic tumors, *International Journal of Biological Macromolecules*, 164, 2583-2597
- [163] B. Jiang, J. Cao, J. Zhao, D. He, J. Pan, Y. Li, L. Guo, (2012) Dual-targeting delivery system for bone cancer: synthesis and preliminary biological evaluation, *Drug Delivery*, 19, 317-326
- [164] G. Zhang, B. Guo, H. Wu, T. Tang, B.-T. Zhang, L. Zheng, Y. He, Z. Yang, X. Pan, H. Chow, K. To, Y. Li, D. Li, X. Wang, Y. Wang, K. Lee, Z. Hou, N. Dong, G. Li, K. Leung, L. Hung, F. He, L. Zhang, L. Qin, (2012) A delivery system targeting bone formation surfaces to facilitate RNAi-based anabolic therapy, *Nature Medicine*, 18, 307-314
- [165] M. Salerno, E. Cenni, C. Fotia, S. Avnet, D. Granchi, F. Castelli, D. Micieli, R. Pignatello, M. Capulli, N. Rucci, A. Angelucci, A. Del Fattore, A. Teti, N. Zini, A. Giunti, N. Baldini, (2010) Bone-targeted doxorubicin-loaded nanoparticles as a tool for the treatment of skeletal metastases, *Curr Cancer Drug Targets*, 10, 649-659
- [166] C. Wang, X. Cai, J. Zhang, X. Wang, Y. Wang, H. Ge, W. Yan, Q. Huang, J. Xiao, Q. Zhang, Y. Cheng, (2015) Trifolium-like Platinum Nanoparticle-Mediated Photothermal Therapy Inhibits Tumor Growth and Osteolysis in a Bone Metastasis Model, *Small*, 11, 2080-2086
- [167] X. Wang, Y. Yang, H. Jia, W. Jia, S. Miller, B. Bowman, J. Feng, F. Zhan, (2014) Peptide decoration of nanovehicles to achieve active targeting and pathology-responsive cellular uptake for bone metastasis chemotherapy, *Biomaterials Science*, 2, 961-971
- [168] F. M. Kievit, Z. R. Stephen, O. Veisheh, H. Arami, T. Wang, V. P. Lai, J. O. Park, R. G. Ellenbogen, M. L. Disis, M. Zhang, (2012) Targeting of Primary Breast Cancers and Metastases in a Transgenic Mouse Model Using Rationally Designed Multifunctional SPIONs, *ACS Nano*, 6, 2591-2601

- [169] M. E. Katt, A. L. Placone, A. D. Wong, Z. S. Xu, P. C. Searson, (2016) In Vitro Tumor Models: Advantages, Disadvantages, Variables, and Selecting the Right Platform, *Frontiers in Bioengineering and Biotechnology*, 4,
- [170] P. McGonigle, B. Ruggeri, (2014) Animal models of human disease: Challenges in enabling translation, *Biochemical Pharmacology*, 87, 162-171
- [171] P. Ribeiro, L. Leitão, A. C. Monteiro, A. Bortolin, B. Moura, M. Lamghari, E. Neto, (2021) Microfluidic-based models to address the bone marrow metastatic niche complexity, *Seminars in Cell & Developmental Biology*, 112, 27-36
- [172] J. Kong, Y. Luo, D. Jin, F. An, W. Zhang, L. Liu, J. Li, S. Fang, X. Li, X. Yang, B. Lin, T. Liu, (2016) A novel microfluidic model can mimic organ-specific metastasis of circulating tumor cells, *Oncotarget*, 7,
- [173] A. Marturano-Kruik, M. M. Nava, K. Yeager, A. Chramiec, L. Hao, S. Robinson, E. Guo, M. T. Raimondi, G. Vunjak-Novakovic, (2018) Human bone perivascular niche-on-a-chip for studying metastatic colonization, *Proceedings of the National Academy of Sciences*, 115, 1256-1261
- [174] J. Aleman, S. K. George, S. Herberg, M. Devarasetty, C. D. Porada, A. Skardal, G. Almeida-Porada, (2019) Deconstructed Microfluidic Bone Marrow On-A-Chip to Study Normal and Malignant Hemopoietic Cell–Niche Interactions, *Small*, 15, 1902971
- [175] S. Bersini, A. Miermont, A. Pavesi, R. D. Kamm, J. P. Thiery, M. Moretti, G. Adriani, (2018) A combined microfluidic-transcriptomic approach to characterize the extravasation potential of cancer cells, *Oncotarget*, 9,
- [176] L. L. Bischel, B. P. Casavant, P. A. Young, K. W. Eliceiri, H. S. Basu, D. J. Beebe, (2014) A microfluidic coculture and multiphoton FAD analysis assay provides insight into the influence of the bone microenvironment on prostate cancer cells, *Integrative Biology*, 6, 627-635
- [177] J. Ahn, J. Lim, N. Jusoh, J. Lee, T.-E. Park, Y. Kim, J. Kim, N. L. Jeon, (2019) 3D Microfluidic Bone Tumor Microenvironment Comprised of Hydroxyapatite/Fibrin Composite, *Frontiers in Bioengineering and Biotechnology*, 7,
- [178] D. B. Chou, V. Frisimantas, Y. Milton, R. David, P. Pop-Damkov, D. Ferguson, A. MacDonald, Ö. Vargel Bölükbaşı, C. E. Joyce, L. S. Moreira Teixeira, A. Rech, A. Jiang, E. Calamari, S. Jalili-Firoozinezhad, B. A. Furlong, L. R. O'Sullivan, C. F. Ng, Y. Choe, S. Marquez, K. C. Myers, O. K. Weinberg, R. P. Hasserjian, R. Novak, O. Levy, R. Prantil-Baun, C. D. Novina, A. Shimamura, L. Ewart, D. E. Ingber, (2020) On-chip recapitulation of clinical bone marrow toxicities and patient-specific pathophysiology, *Nature Biomedical Engineering*, 4, 394-406
- [179] A. Chramiec, D. Teles, K. Yeager, A. Marturano-Kruik, J. Pak, T. Chen, L. Hao, M. Wang, R. Lock, D. N. Tavakol, M. B. Lee, J. Kim, K. Ronaldson-Bouchard, G. Vunjak-

- Novakovic, (2020) Integrated human organ-on-a-chip model for predictive studies of anti-tumor drug efficacy and cardiac safety, *Lab on a Chip*, 20, 4357-4372
- [180] W. Zhang, W. Y. Lee, D. S. Siegel, P. Toliás, J. Zilberberg, (2013) Patient-Specific 3D Microfluidic Tissue Model for Multiple Myeloma, *Tissue Engineering Part C: Methods*, 20, 663-670
- [181] Y. Lei, J. Li, N. Wang, X. Yang, Y. Hamada, Q. Li, W. Zheng, X. Jiang, (2016) An on-chip model for investigating the interaction between neurons and cancer cells, *Integrative Biology*, 8, 359-367
- [182] I. H. Yang, R. Siddique, S. Hosmane, N. Thakor, A. Höke, (2009) Compartmentalized microfluidic culture platform to study mechanism of paclitaxel-induced axonal degeneration, *Experimental Neurology*, 218, 124-128
- [183] E. Neto, C. J. Alves, D. M. Sousa, I. S. Alencastre, A. H. Lourenço, L. Leitão, H. R. Ryu, N. L. Jeon, R. Fernandes, P. Aguiar, R. D. Almeida, M. Lamghari, (2014) Sensory neurons and osteoblasts: close partners in a microfluidic platform, *Integrative Biology*, 6, 586-595
- [184] J. R. Soucy, A. J. Bindas, R. Brady, T. Torregrosa, C. M. Denoncourt, S. Husic, G. Dai, A. N. Koppes, R. A. Koppes, (2020) Reconfigurable Microphysiological Systems for Modeling Innervation and Multitissue Interactions, *Advanced Biosystems*, 4, 2000133
- [185] S. W. Verbruggen, C. L. Thompson, M. P. Duffy, S. Lunetto, J. Nolan, O. M. T. Pearce, C. R. Jacobs, M. M. Knight, (2021) Mechanical Stimulation Modulates Osteocyte Regulation of Cancer Cell Phenotype, *Cancers*, 13, 2906

**Chapter II. Development of an organ-on-a-chip platform
to study the effect of synergistic crosstalk of
osteoclasts and sympathetic neurons on the BC
secretome**

2.1. Fabrication of microfluidic templates for organ-on-a-chip models

Microfluidic platforms have emerged as alternative tools for standard *in vitro* modeling of physiological or pathological conditions, being able to more accurately mimic characteristic features of the *in vivo* microenvironment. Most microfluidic models are produced by casting polydimethylsiloxane (PDMS), a transparent and biocompatible polymer, on templates with a wide range of configurations and functions. Templates for PDMS casting are usually manufactured by photolithography processes where a photoresist is irradiated with ultra-violet (UV) light through a specially designed mask. The non-irradiated sections of the photoresist are subsequently etched out, resulting in a master mold that retains the desired features and is suitable for PDMS casting. However, although standard photolithography methods allow for high resolution features at the low micrometer range, they are expensive and time-consuming and require access to clean room facilities and highly skilled personnel.

Alternatives to photolithography have been proposed to counteract some of these limitations. Subtractive methods such as micromilling of poly methyl methacrylate (PMMA) and aluminum templates ^[1, 2] or laser-writing of glass surfaces ^[3] generate prototype molds in a fast and cost-effective fashion. Similarly, additive manufacturing processes such as thermoplastic extrusion ^[4] and stereolithography printing ^[5] are able to quickly produce prototype molds using cheap materials, and generate complex structures with varying height profiles in a single printing step. However, these methodologies display lower resolution than photolithography and generate rougher surfaces that could affect PDMS casting and binding. Furthermore, photo-initiators used for cross-linking of stereolithography resins can interfere with the curing process of PDMS ^[6].

Although all mold manufacturing methods for PDMS casting present advantages and limitations, the potential of stereolithography 3D printing to generate prototypes with adequate resolution for *in vitro* microfluidic models is appealing. The high design freedom characteristic of 3D printing applications coupled with the low cost and expertise required to operate these tools facilitates the implementation of new microfluidic platforms. Thus, by taking advantage of the versatility of stereolithography tools, developed a new microfluidic platform that aimed to:

- Study the dynamic interplay between bone tropic breast cancer cells, sympathetic neurons and osteoclasts seeded on bone matrices, while compartmentalizing each different cell type and focusing on communication by secreted paracrine factors.

- Proactively modulate the communication routes between the different cell compartments to explore indirect mechanisms of intercellular crosstalk.

2.2. Metastasis-on-a-chip microfluidic model of sympathetic modulation of breast cancer bone metastasis

[Research Paper]

A Metastasis-On-a-Chip Approach to Explore the Sympathetic Modulation of Breast Cancer Bone Metastasis

This chapter was based on the following published paper:

F. Conceição, D. M. Sousa, J. Loessberg-Zahl, A. R. Vollertsen, E. Neto, K. Søre, J. Paredes, A. Leferink and M. Lamghari (2022) A Metastasis-On-a-Chip Approach to Explore the Sympathetic Modulation of Breast Cancer Bone Metastasis. *Materials Today Bio.* 13, 100219

Abstract

Organ-on-a-chip models have emerged as a powerful tool to model cancer metastasis and to decipher specific crosstalk between cancer cells and relevant regulators of this particular niche. Recently, the sympathetic nervous system (SNS) was proposed as an important modulator of breast cancer bone metastasis. However, epidemiological studies concerning the benefits of the SNS targeting drugs on breast cancer survival and recurrence remain controversial. Thus, the role of SNS signaling over bone metastatic cancer cellular processes still requires further clarification. Herein, we present a novel humanized organ-on-a-chip model recapitulating neuro-breast cancer crosstalk in a bone metastatic context. We developed and validated an innovative three-dimensional printing based multi-compartment microfluidic platform, allowing both selective and dynamic multicellular paracrine signaling between sympathetic neurons, bone tropic breast cancer cells and osteoclasts. The selective multicellular crosstalk in combination with biochemical, microscopic and proteomic profiling show that synergistic paracrine signaling from sympathetic neurons and osteoclasts increase breast cancer aggressiveness demonstrated by augmented levels of pro-inflammatory cytokines (e.g. interleukin-6 and macrophage inflammatory protein 1 α). Overall, this work introduced a novel and versatile platform that could potentially be used to unravel new mechanisms involved in intracellular communication at the bone metastatic niche.

Keywords: Metastasis-on-a-chip, Breast Cancer, Bone Metastasis, Sympathetic Nervous System, Paracrine

2.2.1. Introduction

Breast cancer bone metastasis is a complex process that encompasses cell extravasation from the circulatory system into the bone, engraftment on a suitable niche, escape from dormancy, proliferation and uncoupling of the bone remodeling to fuel tumor growth [7]. Bone is the most common site of metastasis in breast cancer. Within the bone, breast cancer cells over-activate bone resorbing osteoclasts and shift the physiological balance in bone remodeling towards increased bone destruction. This leads to severe skeletal complications, such as bone pain, hypercalcemia and bone fractures [7]. The elucidation of the cellular and molecular mechanisms by which breast cancer cells engraft and proliferate in the bone niche is, therefore, of crucial importance to improve the available therapeutic options. However, several barriers still hamper the study of the metastatic bone niche. In vivo models, which are able to recapitulate the complexity of the human disease, are limited and of difficult execution, whereas the dissection of specific signaling pathways involved in bone metastasis progression is extremely complex. Furthermore, high mortality rates and pain associated with the in vivo modelling of this specific disease inherently raises ethical constraints that limit the use of animal models. On the other hand, classical in vitro models are simplistic and do not replicate the native features of the bone microenvironment.

Microfluidic tools have emerged in the past decade as an alternative to conventional in vitro and in vivo models, since these combine three dimensional (3D) matrices with human cells while allowing a fine control over spatial and temporal parameters of culture [8]. In addition, fluidic connection of different cell compartments as well as the control of flow and shear facilitates more physiologically relevant modelling [9]. Microfluidic platforms have in the past been already used as models for bone cancer processes including: i) selective tropism of myeloma and breast cancer cells towards bone cells [8, 10]; ii) extravasation of breast cancer cells from circulation into extracellular matrix (ECM) structures based on collagen or fibrin [11-14]; iii) colorectal, myeloma and breast cancer cell engraftment and proliferation in mineralized matrices [15-18]; iv) cancer drug screening and toxicity assessment [9, 19]. Thus, microfluidic technology can tackle constraints associated to standard in vitro tools in the study of the crosstalk occurring during breast cancer bone metastasis, and thus improve our knowledge on the signaling pathways governing the metastatic process.

Despite the numerous advantages of metastasis-on-a-chip in vitro tools, the typical photolithography processes used in their fabrication require expensive infrastructure and highly skilled personnel. 3D printing is becoming a viable alternative for microfluidic fabrication since it combines accessibility of standard benchtop 3D printers and a high

degree of design freedom which is not trivial to achieve via photolithography [20]. Furthermore, advances in printer technology have improved surface roughness of 3D printed template molds, to the point that the resulting prototypes become compatible with plasma sealing procedures [5]. 3D printing is also suited for valve fabrication, which allows the control of flow resistance and diffusion through the different fluidic compartments [21]. The sympathetic nervous system (SNS) was brought to light as a potential therapeutic target for the treatment of breast cancer due to several findings in pre-clinical and epidemiologic studies [22-24], which correlated sympathetic hyperactivity and poor patient prognosis. However, the beneficial effect of SNS targeting drugs on the treatment of breast cancer remains controversial, since other reports failed to replicate such correlations [25, 26]. It is well established that the SNS acts on multiple cellular targets throughout the body, mainly via the release of norepinephrine (NE) by sympathetic nerve endings and through systemic release of epinephrine into circulation. Functional studies demonstrated that the sympathetic stimulus is able to increase breast cancer circulating tumor cell retention and extravasation to the bone [27]. Nonetheless, dissection of sympathetic signaling in the context of human breast cancer bone metastasis was not yet reported and the mechanisms governing breast cancer cell response to sympathetic input within the bone microenvironment are still poorly understood.

As stated above, microfluidic tools offer multiple advantages regarding standard in vitro models such as compartmentalization and fine tuning of culture parameters. We have previously established models of neuronal/non-neuronal cellular communication in compartmentalized microfluidic devices to address sensory innervation in the bone microenvironment [28, 29]. However, to date there are no microfluidic models described for the study of sympathetic stimuli on the breast cancer bone metastatic niche.

In this study, we have designed and prototyped a new 3D printing based metastasis-on-a-chip platform to reproduce the effect of sympathetic activation on the dynamic crosstalk that occurs between breast cancer cells and bone cells in a fully humanized model. Our platform combines three different human cell types: 1) a bone tropic breast cancer cell variant, 2) sympathetic neurons and 3) human peripheral blood derived osteoclasts seeded on top of a bone matrix. The microfluidic platform was specially designed to physically separate the cells into different compartments to facilitate the identification of secreted factors involved in intercellular communication while preventing direct cell-cell interactions. Furthermore, inclusion of fluidic flow between different compartments allow a unidirectional communication from one compartment to the remaining ones. Our metastasis-on-a-chip platform is based on static diffusion in order to facilitate bidirectional communication between each compartment. Additionally, our platform also allows the manipulation of communication between the different compartments through

the use of incorporated pressure actuating valves. We were able to successfully optimize the culture of each cell type and demonstrated that the dynamic interaction between neurons, breast cancer cells and osteoclasts translates into an increased pro-inflammatory phenotype. In addition, manipulation of the communication between compartments allowed us to show that direct neuronal stimulation of osteoclasts is not required to observe inflammatory cytokine upregulation. Based on these results, we believe that our versatile platform can be a potential tool for fundamental research on multiple research topics. The use of widely accessible 3D printing technology further highlights the adaptability of our metastasis-on-a-chip platform.

2.2.2. Materials and Methods

2.2.2.1. Fabrication and assembly of the metastasis-on-a-chip platform

Each microfluidic component was made out of poly-dimethylsiloxane (PDMS, Sylgard 184, Dow Corning) using specially designed 3D printed molds. Molds were designed using SolidWorks (Dassault Systèmes) and 3D printed in a Form 3 printer (Formlabs) with a Grey V4 resin (Formlabs). These molds were post-processed by two rounds of immersion in isopropanol for 15 min to remove uncured resin, followed by air-drying and a heat treatment of 3 h at 60° C. PDMS was then cast into the mold with a 10:1 (w/w) ratio of base and curing agent and thermally cured for 1 h 30 min at 60°C. Each PDMS slab was separated from the mold and cleaned with residue-free tape until plasma treatment.

The microfluidic platform was designed for single use and is composed of three different structural parts bonded together: a top slab containing patterned cell compartments and diffusion channels, a bottom slab containing valve structures and a simple membrane in between. Top slabs have three equidistant compartments 6mm in diameter for cell culturing (each with two medium inlets) which are interconnected through 4.5mm long semi-circular channels 300µm wide and 150µm high. The bone and cancer compartment are 1.2mm deep to accommodate the bone slice (400µm thick) and the spheroid, while the Neuronal compartment is 600µm deep.

PDMS membranes were produced by spin coating 1.6 mL PDMS at a 10:1 (w/w) ratio of base and curing agent on top of a perfluorodecyltrichlorosilane coated silicon wafer (10 cm diameter) with an initial spinning step at 500 rpm for 15 s and 100 rpm/s acceleration, followed by a second step at 1500 rpm for 75 s and 1000 rpm/s acceleration. The membranes were then thermally cured for 1 h 30 min at 60°C.

Metastasis-on-a-chip platform assembly was achieved by covalent bonding of the different components. The membrane and cell compartment slab were first covalently bound together through oxygen plasma treatment for 1min on a Zepto Plasma Cleaner

(Diener Electronic). The membrane was then cut along the contour of the PDMS slab using a scalpel and lifted from the silicon wafer. Medium inlets and pressure inlets were then punched out of the bonded membrane and the cell compartment slab using a 1 mm biopsy puncher (Kai Medical). The resulting structures were then bonded to the valve structure slab by oxygen plasma treatment as described previously. Right after treatment and before bonding, bovine bone slices (boneslices.com, Denmark) were placed in the bone cell compartment. Both slabs were then bonded together. Each microfluidic unit was sterilized with 70% ethanol, washed thrice with phosphate buffered saline (PBS) and equilibrated in complete medium. Neuronal compartments were incubated in a solution of 5 µg/mL laminin (Sigma-Aldrich) in DMEM/F12 medium (Gibco) with 10% FBS and 1% penicillin/streptomycin (Pen/Strep, Gibco) (DMEM/F12 complete medium) for 2 h at 37°C. Compartments were washed twice with DMEM/F12 complete medium and kept at 37°C until cell seeding.

2.2.2.2. Osteoclast isolation

Human CD14⁺ monocytes were isolated from buffy coats of healthy female blood donors as previously described ^[30]. Briefly, Peripheral Blood Mononuclear Cells (PBMCs) were separated using gradient centrifugation in Ficoll-Paque Plus (GE Healthcare). PBMCs were then resuspended in 0.5% Biotin-free Bovine Serum Albumin (BSA, Sigma-Aldrich) and 2mM EDTA in PBS, incubated in BD IMag™ anti-human CD14 magnetic particles (BD-Biosciences) and magnetically separated according to manufacturer's instructions. CD14⁺ cells were seeded in T75 flasks in α-MEM (Gibco) supplemented with 10% FBS, 1% Pen/Strep and 25 ng/mL of recombinant human macrophage colony stimulating factor (rhM-CSF, R&D Systems) at 5% CO₂ at 37°C in a humidified incubator for 2 days. Cells were then differentiated into mature osteoclasts by supplementing the medium with 25ng/mL M-CSF and receptor activator of NF-κB ligand (RANKL, R&D Systems) for further 7 days of culture, changing medium twice.

2.2.2.3. Breast Cancer cell spheroids

MDA-MB-231-BoM 1833 human breast carcinoma cell line (MDA-1833 henceforth), a bone tropic variant of the MDA-MB-231 cell line, was obtained from Dr. J. Massagué (Memorial Sloan-Kettering Cancer Center, New York). MDA-1833 cells were expanded in DMEM High Glucose (Gibco) with 10% FBS and 1% Pen/Strep (DMEM complete medium) at 37°C and 5% CO₂ in a humidified incubator, changing medium twice a week until reaching 80% confluence. Cells were then trypsinized (0.25% w/v trypsin, 0.1% w/v glucose and 0.05% EDTA in PBS, Life Technologies), seeded at a density of 10 000 cells per well on round bottom ultra-low adhesion 96-well plates (Corning) and incubated

for 4 days in DMEM complete medium with 2.5% Matrigel Basement Membrane Matrix (Corning) to induce formation of cell spheroids.

2.2.2.4. Neuronal-like cell differentiation

SH-SY5Y (ATCC) cells were used as a model of human sympathetic neurons since these cells were previously reported to be able to produce NE ^[31]. SH-SY5Y cells were expanded in DMEM/F12 Complete medium at 37°C and 5% CO₂ in a humidified incubator, changing medium twice a week until reaching 80% confluence. Cells were then trypsinized and 20 000 cells were seeded in the laminin coated neuronal compartments and incubated at 37°C overnight. Differentiation was induced by Opti-MEM medium (Gibco) supplemented with 0.5% FBS, 1% Pen/Strep and 0.1 µM Retinoic Acid over the course of one week, changing medium every day.

2.2.2.5. Metastasis-on-a-chip Cell Seeding

Microfluidic experiments were set up during the course of 10 days. In order to isolate compartments before cell seeding and ensure full physical separation of the different cell types, compartments were sealed off by closing the valves with a pressure of 600 mbar using a FlowEZ 2000 mbar pressure controller module (Fluigent). SH-SY5Y cells were seeded on the neuronal compartment as previously described and differentiated for 7 days with the valves open. At day 7, medium from the bone compartment was changed for α-MEM supplemented with 0.5% FBS, 1% Pen/Strep and 25 ng/mL rhM-CSF (Osteoclast Medium) and the medium from the cancer compartment was changed for DMEM High Glucose supplemented with 0.5% FBS and 1% Pen/Strep. Differentiated osteoclasts were then detached with Accutase (Gibco) for 10 min at 37°C, centrifuged and seeded on the bone slice at a density of 75 000 cells in Osteoclast Medium, being left to adhere for 4 h. MDA-1833 individual cell spheroids were transferred to the cancer compartment, one spheroid per microfluidic device, and the platform was incubated at 37°C for 3 days to allow bone resorption to occur. When required, valves were closed with a pressure of 600 mbar throughout the experiment. The bone compartment was supplemented with fresh 50 ng/mL rhM-CSF and rh-RANKL daily. After 3 days, experiments were ended and conditioned medium was collected from each compartment while keeping the valves closed. In addition, one replicate from each condition was used for immunocytochemistry: medium was removed and the compartments were washed with PBS twice before immunocytochemistry.

2.2.2.6. Immunocytochemistry

Cells in the microfluidic platform were fixed in 4% paraformaldehyde for 10 min at RT followed by 3 steps of washing with PBS and blockage of unspecific staining in a blocking

solution of 5% FBS, 5% Horse Serum (Invitrogen) and 0,25% Triton X-100 (Sigma-Aldrich) in PBS for 1 h at 37°C. Samples were then incubated with primary antibodies overnight at 4°C (mice anti- β III Tubulin 1:2000 [Promega]; rabbit anti-TH 1:100 [Merck]; mouse anti-CATK 1:100 [Santa Cruz Biotechnology]; rabbit anti-CD49f [Sigma-Aldrich]). After incubation, samples were washed thrice with PBS and labelled with secondary antibodies accordingly (Invitrogen, 1:1000 dilution) together with Flash Phalloidin™ (Biolegend) for actin staining, for 1h at RT. Finally, cells were washed thrice with PBS and counterstained with DAPI (1:1000 dilution), washed again to remove excess DAPI and kept at 4°C until imaging. Images were acquired in a Leica SP5 confocal microscope at a resolution of 1024x1024 pixels and z-step of 5 μ m. Brightness was adjusted for better visualization and z-projections as well as artificial cell coloring were performed using ImageJ.

2.2.2.7. Flow Cytometry

MDA-1833 cell spheroids were removed from the metastasis-on-a-chip platform and dissociated with Accutase at 37°C for 20 min in a microtube, pipetting up and down every 5 min. At least 10 spheroids were pooled for each condition in one independent experiment. A commercial kit for Annexin V-APC staining (BD Pharmingen) was used according to manufacturer's instructions, but only using 1 μ L of Annexin V and 3 μ L Propidium Iodide. Immunostaining was performed in 1X Binding Buffer and quantified using a FACS CANTO II (BD Immunocytometry Systems) and FlowJo™ software (BD).

2.2.2.8. Enzyme-linked immunosorbent assays (ELISA)

Conditioned medium was collected from each compartment by closing the respective valves and aspirating the medium. Conditioned medium was centrifuged at 4°C at 400g for 5 min to remove cellular debris, transferred to a new microtube and frozen at -80°C until quantification. NE was quantified by ELISA (Abnova) from conditioned medium collected and pooled from SH-SY5Y monoculture controls from three independent experiments. Quantification was performed according to manufacturer's indications, but 300 μ L of conditioned medium was used in each replicate and a 1 ng/mL standard was added so that our samples would fit in the calibration curve. Protein levels of each sample were quantified using the DC Protein Assay (Bio-Rad) according to the manufacturer's instructions and were used to normalize differences between conditions.

The levels of interleukin 11 (IL-11) was quantified by ELISA (R&D Systems) from breast cancer and bone compartments of the metastasis-on-a-chip platform according to manufacturer's indications. Medium was diluted 10x before quantification to fit the

calibration curve and samples were normalized using the total protein levels as mentioned above.

The levels of interleukin 6 (IL-6) and macrophage inflammatory protein 1 α (MIP-1 α) were similarly quantified by ELISA (Sigma-Aldrich) from the breast cancer compartments of the microfluidics (unless otherwise stated) according to manufacturer's instructions. Medium was diluted 90x before quantification to fit the calibration curve and samples were normalized using the total protein levels.

2.2.2.9. Quantification of bone resorption

Osteoclast resorption events were stained with toluidine blue (Sigma-Aldrich). The entire bone surface was analysed using a G50 100 graticule (Pyser Optics) installed on the ocular of an BH-2 optical microscope (Olympus) as previously described ^[32]. The total number of events present throughout the bone surface were counted using the graticule as a frame (using a total of 16-17 graticules per bone slice). Individual resorption events were divided in two resorption types, pits and trenches. Pits are single, circular excavations with well-defined edges while trenches are elongated and continuous grooves with a length/width ratio equal or greater than two ^[33]. The percentage of trenches per total events was used to compare individual experiments independently of eroded surface variations. Samples were blinded before eroded surface quantification by one researcher.

2.2.2.10. Proteomic Analysis

Conditioned medium from four MDA-1833 spheroids cultured either on the metastasis-on-a-chip platform or in 96 well-plates was pooled and centrifuged at 300 g for 5 min to pellet cellular debris. Conditioned media was then transferred to micro tubes and protein concentration was measured as described above. 50 μ g of protein from each condition was processed using the solid-phase-enhanced-sample-preparation (SP3) protocol, as previously described ^[34], followed by enzymatic digestion overnight with trypsin/LysC (2 micrograms) at 37°C and 1000 rpm.

Protein identification was carried out by nano Liquid Chromatography coupled with Mass Spectrometry (LC-MS/MS) and data was analysed with Proteome Discoverer software (Thermo Scientific) as described by Osório et al ^[35]. The ratio between the protein abundances in the conditioned medium from microfluidic and well plates was used to compare between both conditions.

2.2.2.11. Protein Array

After tri-culture in the microfluidic platform, cancer compartment conditioned medium from three independent experiments was pooled and screened for proteins involved in

bone metabolism using the G-Series Human Bone Metabolism Array 1000 (RayBiotech) according to manufacturer's instructions. Briefly, the arrays were blocked for 30 min and incubated with 100 μ L of sample overnight at 4°C, followed by incubation with biotinylated antibody cocktail for 4 h at room temperature. The slides were then incubated with Cy3 conjugated streptavidin for 1 h in the dark at room temperature. After washing steps, droplets were removed using a compressed argon stream. Slides were sent to the supplier to be imaged (Tebu-Bio). Array data was analysed using the Spotxel® software (Version 2.2.2, SICASYS Software GmbH) and the GAL file supplied by the manufacturer. After alignment with the GAL file, data was extracted using the original image without changes in intensity values. Quantification of the intensity values was performed by Flex-Spot Detection method and with noise filtering and local background correction method. Extracted intensity values were then analyzed using the Excel analysis tool supplied by the manufacturer. After intra-assay normalization, intensity values were normalized for protein content, values for the culture medium alone were subtracted to each sample and fold-changes relative to controls were calculated.

2.2.2.12. Statistics

All experiments were performed at least three times. One-way ANOVA test followed by Holm-Sidák's multiple comparison test was used to assess statistical significance between conditions. When two conditions were being compared, nonparametric Mann-Whitney tests were used. Differences between groups were considered significant when * $p < 0.05$, ** $p < 0.01$, *** $p < 0.001$. Data analysis was performed using GraphPad Prism software v.9.1.0 for Windows (GraphPad Software).

2.2.3. Results

2.2.3.1. Bone metastasis-on-a-chip design

The aim of this study was to establish a model that would allow us to clarify how breast cancer cells respond to sympathetic stimuli in a bone metastatic context, specifically focusing on the contribution of cell-secreted factors. In order to achieve this, the versatility of microfluidic platforms was appealing, since these would allow study of complex interactions between cancer cells and other significant cell components in the metastatic process, in a fully humanized system. Instead of using standard photolithography for the production of microfluidic devices, we took advantage of 3D printing to be able to quickly prototype our molds in a cost-effective fashion, while maintaining an adequate resolution (smallest feature of the mold is 150 μ m while the minimum laser spot size of the 3D printer is 85 μ m).

Our microfluidic chip was designed to compartmentalize three different cell types with no direct cell-cell contact but still allow diffusion dependent chemical communication between compartments (Figure 1a, b). Importantly, we are able to dictate the direction of communication between compartments by using Quake valves incorporated in the metastasis-on-a-chip design. This microfluidic chip is composed of three different structural parts bonded together: a top slab containing patterned cell compartments and diffusion channels, a bottom slab containing valve structures and a simple membrane in between (Figure 1c).

The ability to close the diffusion channels is an important feature both for cell seeding and to explore indirect routes of communication between different compartments. With that in mind, valve structures 500 μ m wide and 1mm long were included in the center of the diffusion channels to block the communication between compartments when desired (Figure 1d). Three Quake valves were included on our microfluidic platform, one on each diffusion channel. Pressure applied on each valve channel will push the flexible 40 μ m thick PDMS membrane located between the main PDMS slabs, closing the diffusion channels (Figure 1e, f). To test the valves, the diffusion channels were filled with Toluidine Blue dye and a pressure of 600mbar was applied to the valve channel. Micrographs of the valve section show that there was no dye in the diffusion channel when the valves were in a closed state (Figure 1f, right) while dye was observed in the diffusion channel when the valves were in an open state (Figure 1f, left). Similarly, 5kDa fluorescent-labelled Dextran was not able to diffuse through a closed valve, further validating their functionality (Figure S1). Furthermore, no diffusion was observed from one compartment to the other when all the valves were closed after three days of incubation, which was a relevant timeframe for our cell culture setup (Figure S1). The closure of the valves was reversible (Supplementary movie 1) and the valves maintained their function over 20 cycles of opening and closure without rupturing (data not shown). As already mentioned, current in vitro models fail to replicate the three-dimensional features of in vivo bone, which has profound biological and biomechanical implications in osteoclast biology. To circumvent that limitation, mineralized bone ECM preserving the structural and biological cues of in vivo bone were included in our model. Furthermore, to hamper the migration of osteoclasts and breast cancer cells from each respective compartment, a spatial offset between the bone and cancer compartment floor and the diffusion channels was incorporated in the design (Figure 1d, right panel). This was not the case for the neuronal compartment to allow neuronal cells to elongate their axonal extensions into the diffusion channels and maximize the dissemination of neuronal factors to the other compartments.

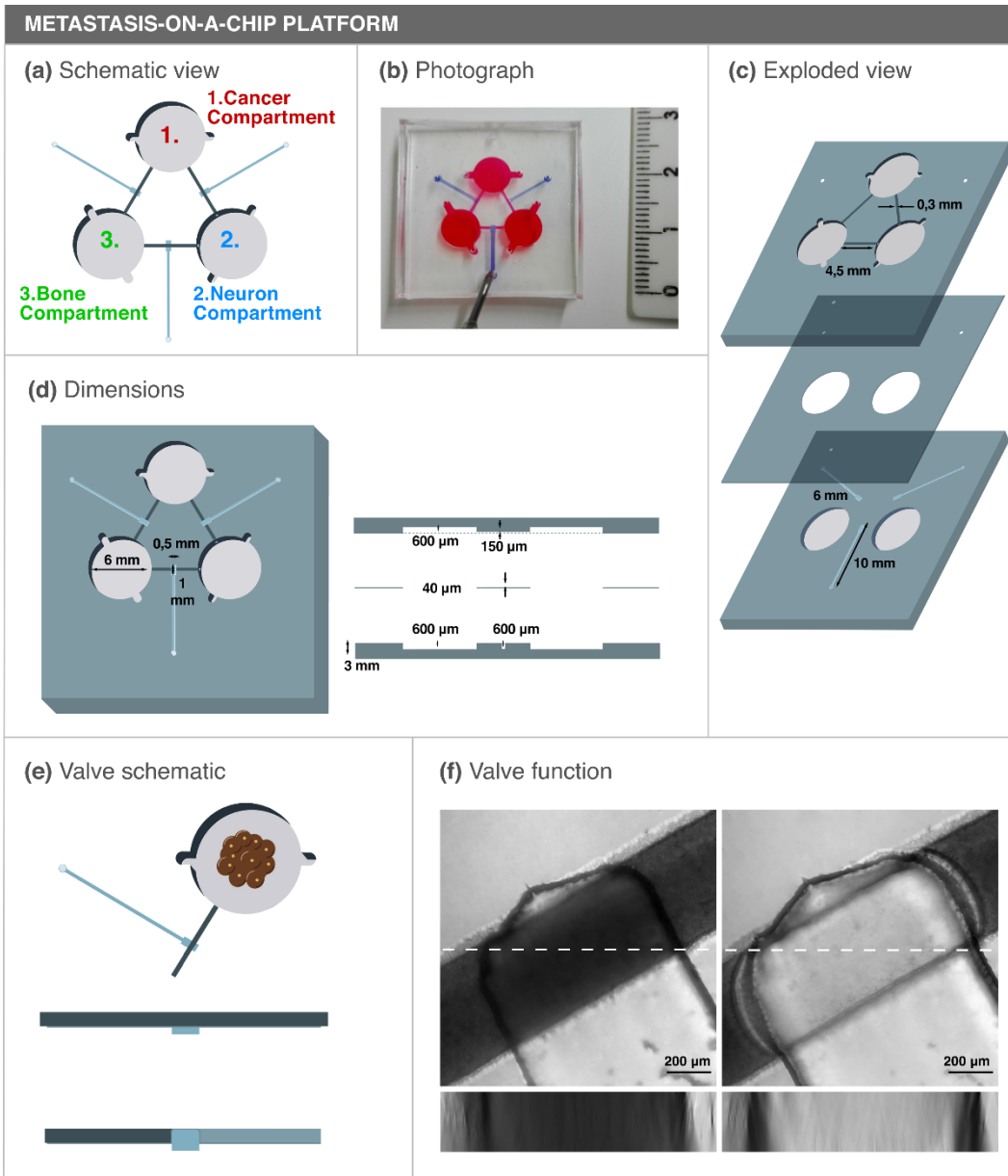


Figure 1. Concept and design of a novel microfluidic platform with three interconnected culture chambers. (a) Schematic representation of the microfluidic platform and (b) photograph of an assembled microfluidic colored with food dyes. (c) Exploded view of the three components of the microfluidic platform. (d) Top (left) and side (right) view of the microfluidic platform. (e) Schematic view of a functioning valve. When pressure is applied in the valve channel, the flexible PDMS membrane occludes the diffusion channel, blocking the communication between compartments. (f) Valve segment z-projection of an open valve (left) or closed valve (right) after applying a 600mbar pressure on the valve channel. The microfluidic compartments were filled with toluidine blue dye and a 250μm stack was obtained on a confocal microscope. An XZ orthogonal view is

also shown below each respective image (corresponding to the dashed line). Scale bar 200 μ m.

2.2.3.2. Cancer Compartment: 3D culture and proteomic analysis

To form bone metastasis, disseminated breast cancer cells acquire a specific set of characteristics that are distinct from the primary tumor^[36]. Accordingly, bone tropic breast cancer cell (MDA-1833) spheroids were used as a model of breast cancer cells that are more prone to establish metastasis in the bone, which have been previously characterized^[36] and are shown to be biologically relevant for the study of bone metastasis. In addition, breast cancer spheroids are commonly used to replicate the 3D features of *in vivo* tumors^[37].

Spheroids were introduced in the cancer compartment and cultured for 3 days inside the platform (Figure 2a). First, cell morphology was assessed by F-actin staining of MDA-1833 spheroids inside the microfluidic compartment (Figure 2b). In addition, integrin α 6 (CD49f) was previously reported to be expressed in triple negative breast cancer cells^[38] and, concordantly, positive staining for CD49f in the surface of MDA-1833 cells was observed (Figure 2c). Therefore, surface marker expression was maintained inside our platform.

After morphological characterization of the bone tropic cells, the apoptotic profile of spheroids cultured inside the microfluidic was compared to spheroids grown in standard 96-well plates. No differences regarding spheroid size were observed (Figure S2) and Annexin V staining showed that cell apoptosis was similar between conditions (Figure 2d). We then investigated whether the environment in the microfluidic platform evoked changes in the conditioned medium of MDA-1833 cells. Breast cancer cells express a plethora of pro-inflammatory factors, of which interleukin (IL) 11 was previously implicated in breast cancer progression and bone metastasis^[39]. IL-11 was therefore quantified and we observed a clear trend towards increased IL-11 levels inside the microfluidic compartment when compared to MDA-1833 cultured in standard 96-well plates (Figure 2e). Thus, we further hypothesized that our microfluidic platform could recapitulate a more aggressive breast cancer phenotype. To confirm this, the conditioned medium from MDA-1833 spheroids cultured inside the microfluidic platform and in normal 96-well plates was collected and screened for the presence of proteins relevant for our model. The level of several matrix-associated proteins was increased in the conditioned medium from MDA-1833 spheroids cultured in our metastasis-on-a-chip platform, namely connective tissue growth factor (CTGF) and matrix metalloproteinase 1 (MMP1), which were already described to promote breast cancer progression in the bone niche

(Figure 2f) [36, 40-42]. Additionally, multiple proteins previously reported to be involved in bone metabolism were shown to be more abundant when MDA-1833 spheroids were cultured inside the microfluidic platform when compared to 96-well plates, such as latent transforming growth factor- β (TGF- β) binding protein 1 (LTBP1) and Dickkopf-1 (DKK1) (Figure 2f).

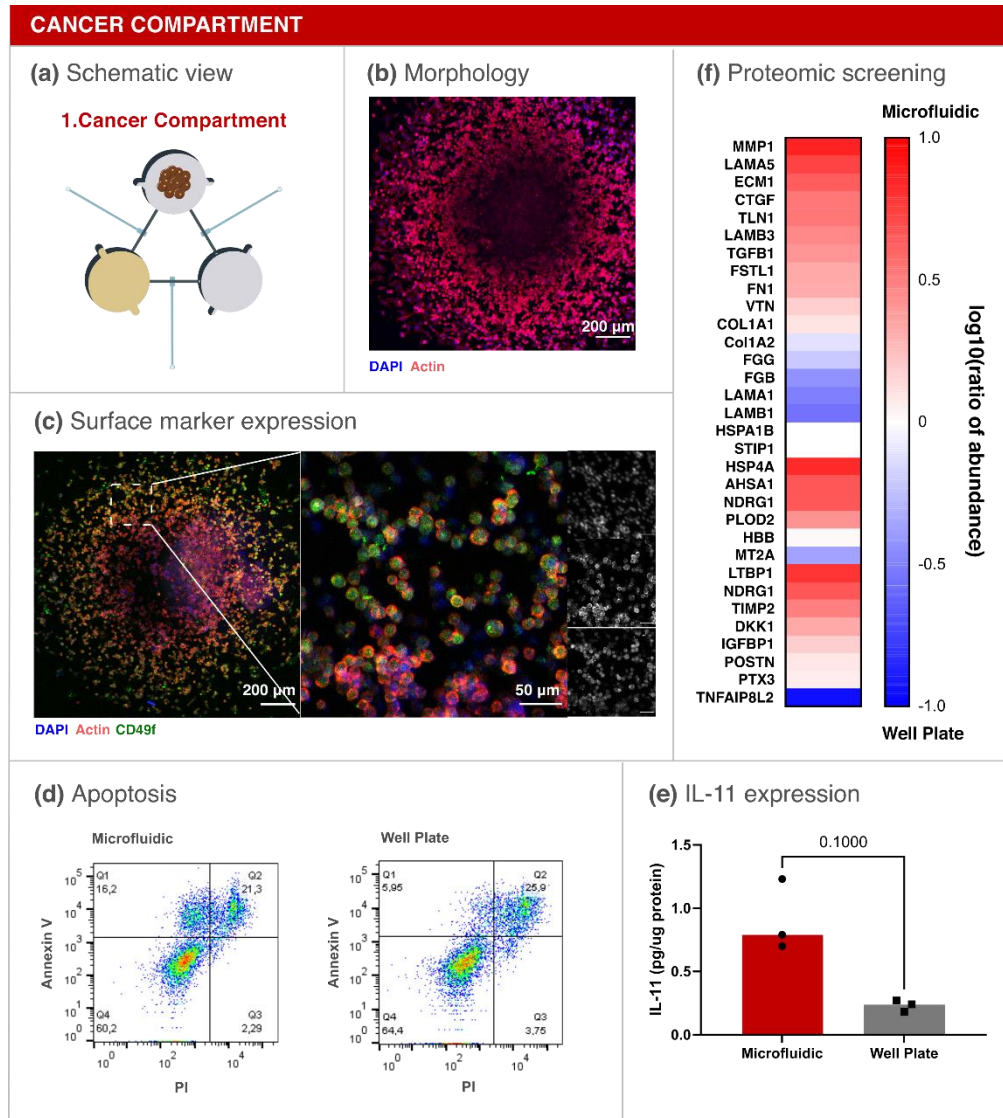


Figure 2. Breast Cancer compartment optimization. (a) Schematic representation of the breast cancer compartment. (b) Micrograph of a MDA-1833 cell spheroid cultured for 3 days on the microfluidic platform. Blue - DAPI. Red - F-actin. Scale bar - 200 μ m. (c) Expression of CD49f on MDA-1833 cells. DAPI (blue), F-Actin (red) and CD49f (green). Scale bar - 200 μ m. Inset single channel images are shown on the right DAPI (blue, top), F-Actin (red, mid) and CD49f (green, bottom). Inset scale bar - 50 μ m. (d) Annexin V quantification by flow cytometry of breast cancer spheroids cultured inside the microfluidic platform (left) or in standard well plates. Ten spheroids were pooled together

for the analysis. (e) IL-11 quantification in conditioned media from MDA-1833 spheroids cultured in the microfluidic platform or in well plates. Data is expressed as median of individual data points from 3 independent experiments and was normalized to the total protein content (Mann-Whitney test, $p=0.1000$). (f) Proteomic screening of the conditioned media from MDA-1833 spheroids cultured in the microfluidic or in standard well plates. Data is represented as the logarithm of base 10 of the ratio between the abundance of each secreted protein within the microfluidic and well plate.

2.2.3.3. Sympathetic Neuronal Compartment: Cell differentiation and catecholamine release

Sources for human sympathetic neurons for *in vitro* culture are scarce. Sympathetic neurons were previously obtained from human Pluripotent Stem Cells (hPSCs), however protocols for differentiation are inefficient and of difficult execution ^[43]. Nonetheless, neuroblastoma cell lines have been reported to produce NE ^[44], which is the main sympathetic neurotransmitter. In order to model the sympathetic nervous system contribution to bone metastasis, SH-SY5Y neuron-like cells were included in the microfluidic platform (Figure 3a). The neuronal compartment was coated with laminin and SH-SY5Y cells were allowed to differentiate for 7 days under retinoic acid stimulation, after which they presented long axonal extensions (Figure 3b). Tyrosine hydroxylase (TH) is the rate limiting enzyme in the NE synthesis cascade and commonly expressed in sympathetic neurons. TH expression was verified in SH-SY5Y cells cultured in the microfluidic platform, confirming that SH-SY5Y cells maintain a sympathetic phenotype when cultured in our metastasis-on-a-chip platform (Figure 3c). Since NE secretion would be the main contributor to our metastatic model, NE was subsequently quantified in the conditioned medium of the neuronal compartment (Figure 3d). NE was detected in a nanomolar concentration range, a concentration sufficient for adrenergic receptor stimulation ^[45]. No significant differences were observed between SH-SY5Y cells cultured in the microfluidic platform and the 96-well plate regarding NE production, validating the assumption that sympathetic input is maintained in our platform.

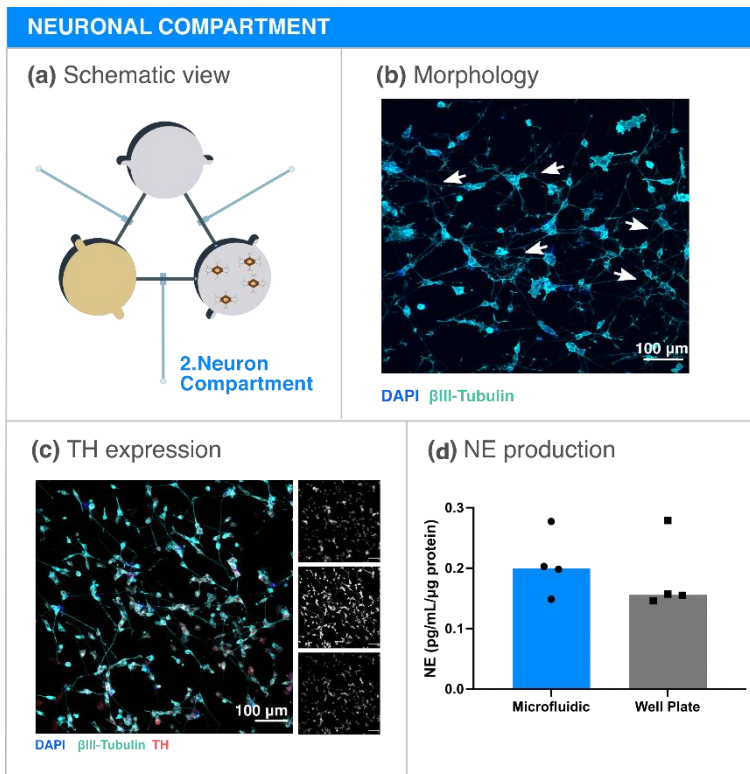


Figure 3. Neuron-like cell compartment optimization. (a) Schematic representation of the neuron-like cell compartment. (b) Micrograph of SH-SY5Y cells cultured for 7 days inside the microfluidic compartment. Several neuronal extensions are highlighted in white arrows. Blue - DAPI; Cyan - βIII Tubulin. Scale bar 100μm. (c) Expression of the sympathetic marker TH in SH-SY5Y cultured in the microfluidic platform. Single channel images are showed on the right. Blue (Top) - DAPI; Cyan (Mid) - βIII Tubulin; Red (Bottom) - TH. Scale bar - 100μm. (d) NE concentration quantification in SH-SY5Y conditioned medium from the microfluidic platform or in well plates. Data is expressed as median of individual data points from 4 independent experiments and was normalized to the total protein content (Mann-Whitney test, non-significant).

2.2.3.4. Bone Compartment: Bone resorbing osteoclasts on mineralized ECM

Breast cancer is usually of osteolytic nature, leading to extensive bone degradation. Osteoclasts, multinucleated cells that are able to resorb the bone, are therefore crucial players in the establishment of metastatic bone lesions. In fact, proteins released from the bone matrix during resorption as well as other osteoclast-secreted factors are able to modulate breast cancer cell behavior and also neuron activation in the bone microenvironment [46, 47]. Aiming to replicate these interactions, mature human osteoclasts were cultured on top of bone slices inside the microfluidic platform for three days, refreshing RANKL and M-CSF daily to ensure ample access to these cytokines

(Figure 4a). Characteristic features of mature osteoclasts were observed, namely large cytoplasm area, actin ring formation and osteoclast marker cathepsin K expression (Figure 4b, c). Of note, different morphologies were observed in various osteoclasts, namely circular actin rings (Figure 4b) or crescent-shaped actin rings (Figure 4c), which reflect the direction of resorption and are characteristic of different resorption modalities [33, 48]. Osteoclasts are inherently capable of resorbing the bone while being static or while moving across the surface of the bone, generating resorption pits or trenches, respectively (Figure 4d, e, Figure S3). Accordingly, resorption pits and trenches were visible on the surface of the bone slices, demonstrating that osteoclasts were not only morphologically differentiated but also fully functional (Figure 4d).

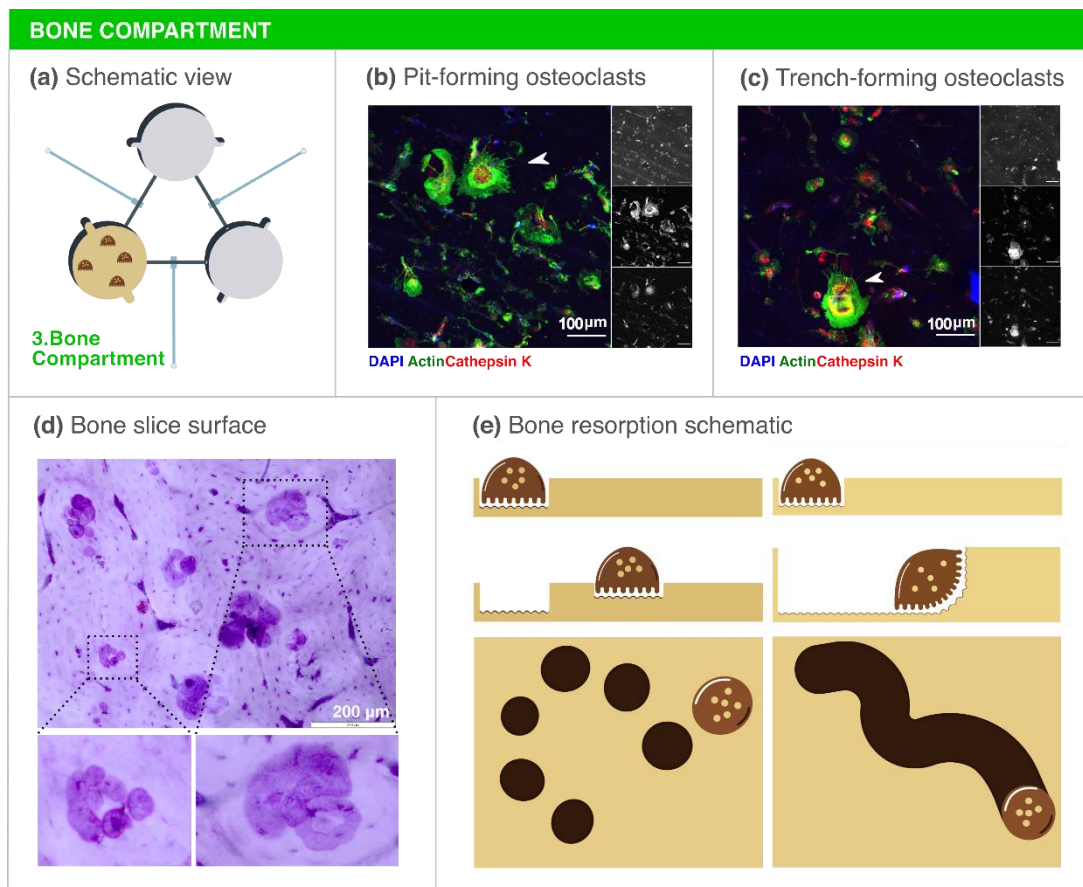


Figure 4. Bone compartment optimization. (a) Schematic representation of the bone compartment. (b) Micrograph of mature, multinucleated osteoclasts on the surface of the bone slice. The white arrow shows an osteoclast with a circular actin ring, characteristic of resorption pit formation. (c) Mature osteoclasts on top of a bone slice. The white arrow shows an osteoclast with a crescent shaped actin ring, characteristic of a resorption trench formation. Single channel images are showed on the right. Blue (Top) - DAPI; Green (Mid) - Actin; Red (Bottom) - Cathepsin K. Scale bar - 100 μ m. (d) Toluidine blue staining of the surface of the bone slice after three days of culture. Several resorption events are seen throughout the bone slice. In the left inset resorption pits are visible

while in the right inset an example of a trench is shown. Scale bar - 200 μ m. (e) Schematic representation of osteoclast resorption activity. Osteoclasts are capable of stationary resorption (left) or resorption while moving through the bone surface (right), leading to the formation of resorption pits or trenches respectively.

2.2.3.5. Non-selective crosstalk: opening communication between breast cancer-neuron-osteoclast

After individual characterization of each compartment, MDA-1833 cells, SH-SY5Y cells and osteoclasts were cultured simultaneously in the microfluidic platform (Figure 5a). To that end, SH-SY5Y were first seeded and differentiated with retinoic acid for 7 days, followed by osteoclast and MDA-1833 seeding in their respective compartments (Figure 5b). Cells were further cultured for 3 days, refreshing RANKL and M-CSF daily in the bone compartment until the end of the experiment. Cell morphology of each cell type was confirmed by immunocytochemistry in the end of the experiment (Figure 5c). This was an important validation step since we were able to show that similar morphology and differentiation status were achieved when all cells were cultured simultaneously, even though each compartment encompassed different culture media that were mixed by diffusion during the course of the experiment.

As stated above, the aim of this platform was to investigate how breast cancer cells would respond to sympathetic stimuli under osteoclast crosstalk, by focusing our study on breast cancer secreted factors. Since proteins described to modulate the bone microenvironment were detected in the conditioned media of MDA-1833 cells in the previous optimization step, we decided to restrict our search by using a bone metabolism protein array. Conditioned medium was extracted from the breast cancer compartment in the end of each experiment and screened for proteins that could be relevant for our model, e.g. IL-6 and monocyte chemoattractant protein 1 (MCP-1). After normalization for total protein content, the relative expression of each protein in the breast cancer compartment was determined (Figure 5d). Of note, when breast cancer cells were co-cultured with osteoclasts, increased levels of IL-6, IL-8, MCP-1 and macrophage inflammatory protein 1 α (MIP-1 α) were observed in the breast cancer compartment, which point to an effect of osteoclasts on MDA-1833 secretome. Interestingly, the pro-inflammatory setting was further exacerbated when SH-SY5Y cells were added to the model, where the levels of IL-6 and MIP-1 α were further augmented (Figure 5d). Indeed, sympathetic stimulus has been described to increase IL-6 levels in MDA-231 breast cancer cells with high β -adrenergic receptor (β -AR) expression^[49] and both MDA-1833 and human osteoclasts express several ARs, being therefore responsive to sympathetic

stimuli (Figure S4). Based on these results, MIP-1 α and IL-6 were then selected as potential candidate targets of sympathetic signaling in breast cancer and proceeded to validate the array by quantifying the expression of these cytokines by ELISA. Again, we observed a significant increase in MIP-1 α in the cancer compartment when all cell types were cultured together with the valves in an open state (Figure 5e). Importantly, the levels of MIP-1 α detected in the cancer compartment, when MDA-1833 cells were co-cultured with either osteoclasts or neurons, did not differ from MDA-1833 monoculture. These results highlight the potential of our microfluidic platform to capture the synergistic effect of multiple cell crosstalk and the importance of a dynamic interaction between the three cell types. On the other hand, IL-6 levels were significantly increased in the tri-culture condition when compared to MDA-1833 and osteoclast co-culture controls but were similar to MDA-1833 monoculture controls (Figure 5f). The increase in IL-6 appears to be due to neuronal inputs, since the addition of SH-SY5Y cells sharply increased IL-6 production as could be seen in MDA-11833 and neuron co-culture controls. MDA-1833 cells are the main source of IL-6 since only residual IL-6 was detected in neuronal or osteoclast mono-culture controls (Figure S5). Despite the augmented levels of MIP-1 α and IL-6 pro-inflammatory mediators in the cancer compartment, these did not affect overall osteoclast resorption activity nor resorption mode in the bone compartment (Figure 5g, h).

Taken together, our results demonstrate the importance of the dynamic communication between the different players in the metastatic niche and the ability of our microfluidic platform to capture these complex interactions.

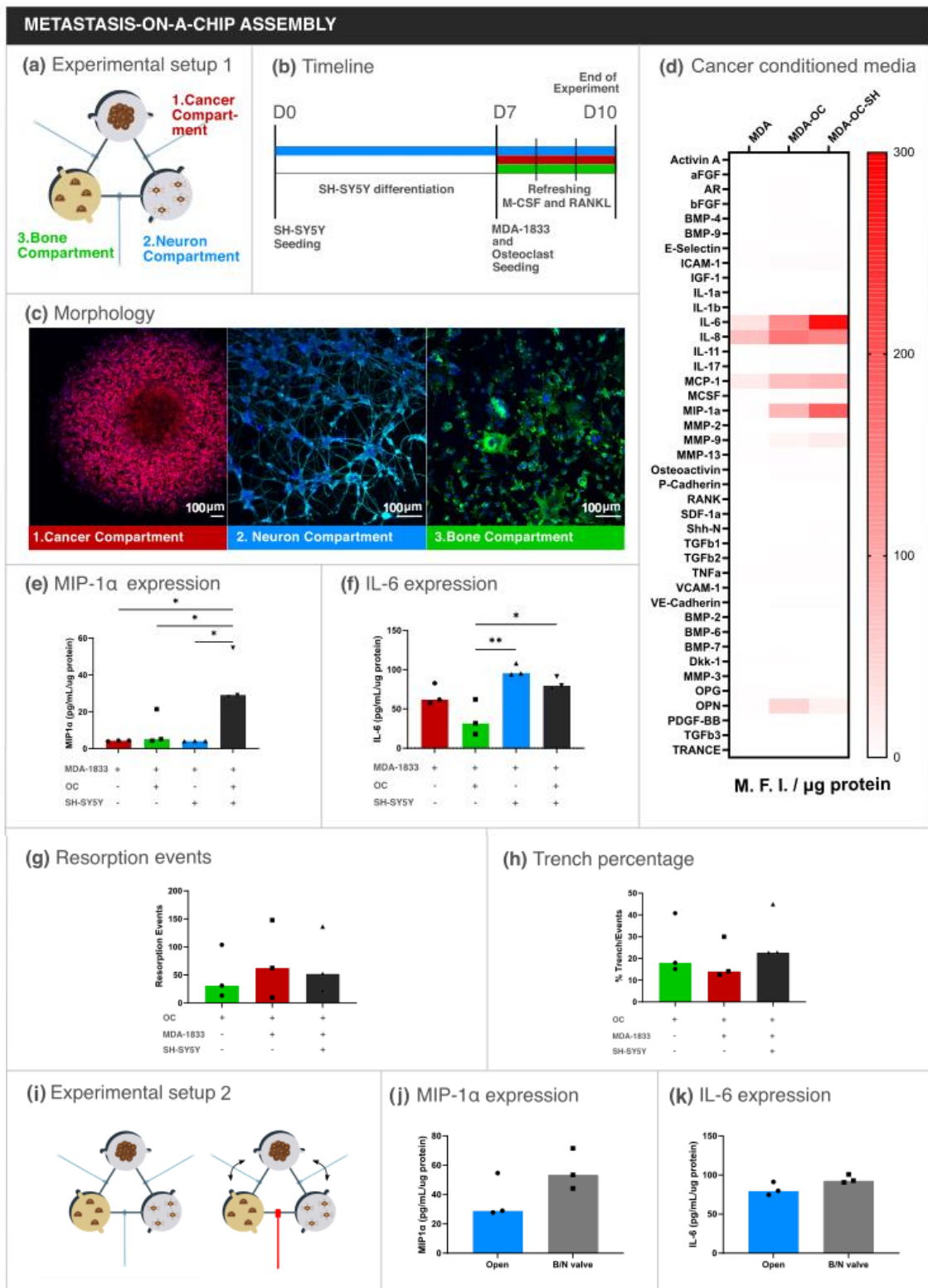


Figure 5. Tri-culture assembly on the microfluidic platform. (a) Schematic representation of the assembled microfluidic platform. (b) Timeline of the experiment. (c) Representative micrographs of (i) the bone compartment, (ii) the cancer compartment and (iii) the neuron compartment. Scale bar – 100 μ m. (d) Bone metabolism array data of conditioned medium from the cancer compartment. Data is represented as Mean Fluorescence

Intensity and normalized by total protein content. (e, f) Quantification of MIP1 α and IL-6 concentration in conditioned media from the breast cancer compartment by ELISA. Data is expressed as median of individual data points from 3 independent experiments and was normalized to the total protein content (One-way ANOVA test, * $p < 0.05$, ** $p < 0.01$). (g) Quantification of resorption event number and (h) percentage of trench number relative to total number of events. Data is expressed as median of individual data points from 3 independent experiments (One-way ANOVA test, non-significant). (i) Schematic representation of the experimental setting. Closing the valve between the neuronal and bone compartment forces communication to be preferentially through the cancer compartment. (j) Quantification of MIP1 α and (k) IL-6 concentration in conditioned media from the breast cancer compartment by ELISA. Data is expressed as median of individual data points from 3 independent experiments and was normalized to the total protein content (Mann-Whitney test, non-significant).

2.2.3.6. Selective crosstalk: Closing communication between neurons and osteoclasts

Intercellular communication on the microfluidic platform is dynamic, where each different cell type is able to shape the response of the other cells over the course of the experiment. The inclusion of valves in our platform adds an extra layer of complexity, allowing the manipulation of the communication by stopping the flow between two specific compartments. The observed increase in pro-inflammatory factors in our model supported by other previous reports have shown that direct sympathetic stimulus increases breast cancer aggressiveness^[49]. Thus, we hypothesized that the blockage of communication between the neuron and bone compartment would not affect the production of pro-inflammatory cytokines in our model. Taking advantage of the Quake valves incorporated in our metastasis-on-a-chip model, we assembled the tri-culture while keeping the valve between neuron and bone compartments closed, in order to assess the impact of different communication routes on the production of IL-6 and MIP-1 α in the cancer compartment (Figure 5i). As hypothesized, closing the valve between neuronal and bone compartment did not change the levels of MIP-1 α nor IL-6 (Figure 5 j, k). These results suggest that direct communication between SH-SY5Y cells and osteoclasts is not required for the observed levels of IL-6 and MIP-1 α levels in the breast cancer compartment, since limiting communication between neuron and osteoclasts did not change the levels of these cytokines secreted by breast cancer cells.

2.2.4. Discussion

The crosstalk between the multiple components of the breast cancer bone metastatic niche is inherently complex. Although in vitro models provide a simplistic view of these intricate interactions, microfluidic systems can be used as versatile tools that are able to recapitulate important hallmarks of disease progression. Our work describes a new metastasis-on-a-chip platform designed to dissect the interplay between different cellular players within the breast cancer bone metastatic niche. This microfluidic platform retains a high degree of complexity by allowing the culture of at least three different human cell types simultaneously, namely bone tropic breast cancer cells, neurons and osteoclasts. Moreover, the physical separation of the cellular components enables a dynamic crosstalk between the different cell types exclusively through secreted factors, which will result in a cleaner readout interpretation, since direct cell-cell interactions do not occur in our model.

The majority of the microfluidic platforms used in the literature are produced using soft lithography processes that, although allowing a high degree of spatial resolution, also require costly facilities and highly qualified personnel. Using affordable consumer grade 3D printers, we were able to produce resin molds with adequate resolution and a smooth surface compatible with plasma cleaning bonding processes. Furthermore, the combination of features of different heights in the same mold facilitates rapid prototyping and can be translated into a design freedom that is not feasible in standard photolithography. For the first time, we describe a research tool that integrates human bone tropic breast cancer, neuron cells and osteoclasts in a single PDMS platform manufactured from 3D printed molds. We believe that this methodology could be employed in other research settings, since we used widely accessible 3D printers and computer aided design tools that do not require specialized training. Our platform was designed for the analysis of secreted factors involved in the crosstalk taking place at the bone metastatic niche, but compartment dimensions, channel length and cellular types could be prototyped and adapted to fit the needs of different biological questions.

Bone tropic MDA-1833 breast cancer cell spheroids were chosen to mimic a breast cancer bone metastatic niche. Cell spheroids are widely used to model tumor niche interactions and present advantages regarding metabolic gradients, apoptosis and drug resistance profiles when compared to standard monolayer culture techniques [50, 51]. MDA-1833 cell spheroids were successfully introduced in the microfluidic platform and presented similar size and apoptosis levels as spheroids grown in normal 96 well plates. However, the environmental features inherent of the microfluidic compartment, such as lower access to nutrients and oxygen, seem to have an impact in MDA-1833 protein

expression. Normalized IL-11 levels were shown to be increased in the metastasis-on-a-chip platform when compared to 96-well plates, coherent with a more pro-inflammatory and osteolytic phenotype. In addition, MDA-1833 cells were first described by Kang *et al* and are reported to express a myriad of other osteolytic factors [36]. Of note, we showed that LTBP1 is more abundant in the conditioned medium of MDA-1833 cells cultured in the microfluidic platform when compared to normal 96-well plates. Osteoclasts are capable of cleaving LTBP1, which is subsequently involved in the release of TGF- β from the bone matrix during bone resorption [52] and will then fuel tumor growth in the bone niche. Furthermore, we showed that proteins from the matrissome [53], such as MMP1 and CTGF, were also increased in our microfluidic platform, consistent with an increased breast cancer aggressive behavior.

Since solid tumors are often of hypoxic nature due to limited or aberrant oxygen supply, hypoxia has profound implications in breast cancer progression and it has been already implicated in the establishment of bone metastasis[54]. Accordingly, the topographic features of our microfluidic platform imply a lower medium volume in the cell compartments and consequently a lower access to oxygen and nutrients environment when compared with a standard well plate. Hypoxia is described to promote the expression of CTGF in MDA-MB-231 cells [55], which might explain the observed increase in CTGF secretion.

Although we have focused on bone tropic breast cancer secreted peptides in our study, our microfluidic platform can be potentially used to analyze other secreted factors such as cancer-derived exosomes. Exosomes are extracellular vesicles that can deliver proteins, lipids and microRNAs to modulate cellular communication and have already been implicated in breast cancer bone metastasis and osteoclast differentiation [56]. In the future, this novel system can be potentially used to evaluate how sympathetic neuronal activation alters the secretion of exosomes by bone tropic breast cancer cells. In order to study breast cancer associated bone pain, the crosstalk between sensorial neurons and breast cancer cells with microfluidic platforms has been previously modelled [57]. However, to our knowledge, no previous attempts have been made to model sympathetic neuron - breast cancer cellular interactions in a bone metastatic context using microfluidic technology. The culture of murine sympathetic ganglia in microfluidic platforms was established to study cardiomyocyte stimulation, but human sources of sympathetic neurons are limited. Retinoic acid differentiated SH-SY5Y cells have been previously used as models of sympathetic neurons [44], since these cells are capable of expressing the sympathetic marker TH and produce NE. In our model, we were able to successfully cultivate NE-secreting human sympathetic neurons, which was fundamental to achieve our final goal.

Previous microfluidic models, where murine osteoclasts derived from RAW264.7 cells were co-cultured with osteocytes to unravel the effect of mechanostimulation on the crosstalk between these cellular players, have been also already described [58]. However, as far as we are aware, our work is the first to describe the culture of human osteoclasts in a microfluidic platform. One of the advantages of our proposed model is the addition of bone slices to the bone compartment. Bone slices retain important topographic and biochemical cues that are crucial for osteoclastic resorption activity, allowing for resorption activity readouts that were not yet previously seen in microfluidic devices. Importantly, in addition to the total extent of osteoclast resorption activity, it is possible to distinguish different resorption modalities in the surface of the bone slices. Variations in the trench content relative to the total number of events could be indicative of differences in collagenolysis *versus* demineralization rates and cathepsin K activity [59]. In addition, trench resorption is faster and favors bone fragility, and is associated with more aggressive bone degradation [30].

After optimization steps, microfluidic assembly of all three cell types allowed a unique glance at the intercellular crosstalk that occurs at the bone metastatic niche. In our metastasis-on-a-chip platform, we showed that bone tropic breast cancer cells received synergistic inputs from neurons and osteoclasts that resulted in increased levels of pro-inflammatory cytokines. Interestingly, IL-6 and MIP-1 α were already implicated in the progression of breast cancer bone metastasis and osteoclastogenesis [60, 61]. Furthermore, our results are consistent with previous studies where sympathetic stimulus increases IL-6 production in breast cancer [49] and melanoma cell lines in vitro [62]. On the other hand, osteoclast secreted factors or proteins released from the bone matrix during resorption were also described to promote breast cancer growth [63, 64]. As could be seen in MIP-1 α secretion levels, we showed that dynamic communication, contrarily to standard conditioned medium approaches, is of vital importance to recapitulate interactions that could take place at the bone metastatic microenvironment.

One of the main features of our platform is the inclusion of valves in each of the interconnecting channels. These valves were designed based on the Quake valve architecture, where pressure applied to a flexible membrane allows the closure of a fluidic channel [65]. Quake valves were previously used in both photolithography [66] and 3D printing applications [21] and are a valuable tool for fluidic control. In this microfluidic platform, Quake valves serve two main purposes: 1) we were able to constrain each different cell in its respective compartment during cell seeding and 2) we could alter the diffusion pattern and directionality of the stimuli from one compartment to another. We demonstrated that by closing the communication between bone and neuron compartments, cytokine levels secreted by breast cancer cells did not change

significantly, pointing towards a negligible effect of direct neuron-osteoclast communication on the changes observed in the cancer compartment. Although epinephrine was reported to increase differentiation of human osteoclast-like cells, the direct effect of NE on human osteoclast activity is still unknown [67]. Future effort should be directed towards understanding what are the osteoclast/neuron derived factors that promote a breast cancer pro-inflammatory phenotype.

Our model presents some limitations in its current form. First, we included sympathetic neurons and osteoclasts but the bone metastatic niche is extremely complex and composed of multiple cellular players [7]. We could potentially use our microfluidic platform to study how resident macrophages and lymphocytes, osteocytes, hematopoietic stem cells, fibroblasts and endothelial cells could also contribute to the establishment and progress of the metastatic disease. For instance, future improvements to this microfluidic model would include the addition of immune cells to the cancer compartment. Since macrophages are responsive to NE [68], it would be interesting to assess how they impact breast cancer bone metastasis under sympathetic stimulus. In addition, under sympathetic stimulation, osteoblast derived vascular endothelial growth factor (VEGF) and IL-1 β was able to modulate endothelial cells to facilitate breast cancer cell extravasation from circulation into the bone marrow niche, both *in vitro* and *in vivo* [23, 27]. A different platform design would be required to include endothelial cells, though, to allow hydrogel seeding, fluidic flow and self-assembly of blood vessels.

Second, several studies have shown that breast cancer cells induce osteolysis via osteoblast-lineage cells and not by direct osteoclast stimulation [69, 70]. Parathyroid hormone-related protein (PTHrP) is described to be secreted by breast cancer cells and to promote the production of RANKL by osteoblasts, subsequently resulting in osteoclast activation [70]. Furthermore, the secretome from MDA-MB-231 cells was recently described to modulate osteoblast mediated bone matrix deposition *in vivo* [71]. On the other hand, osteoblasts were observed in close contact with prostate and breast cancer cells in clinical bone metastasis biopsies, suggesting that not only secreted factors but also direct cell-cell contact between osteoblasts and cancer cells could be important for osteoclastogenesis and bone degradation [72]. The addition of primary human osteoblasts in the cancer compartment, mimicking the interactions that take place between tumor cells and cancer associated fibroblasts, could be an interesting upgrade to the microfluidic model in order to fully recapitulate the bone resorption promoting capacity of breast cancer cells.

Third, the potential of our platform to investigate the effect of different cancer cell lines on the bone niche could be further explored. We focused on metastatic MDA-1833 breast

cancer cells to mimic the local colonization of bone, nevertheless it would be interesting to assess how the parental cell line MDA-MB-231 react to osteoclast secreted factors under sympathetic activation. Furthermore, differences in the role of distinct molecular subtypes of breast cancer on the bone niche, such as luminal-like or epidermal growth factor receptor 2 (HER2) enriched breast cancer cell lines, could be investigated in future studies. Finally, prostate cancer, lung cancer and multiple myeloma also display bone tropism^[64], and thus studying the effect of sympathetic stimuli on prostate/lung or multiple myeloma bone metastatic niche would demonstrate the translational potential of our model.

Supplementary Data

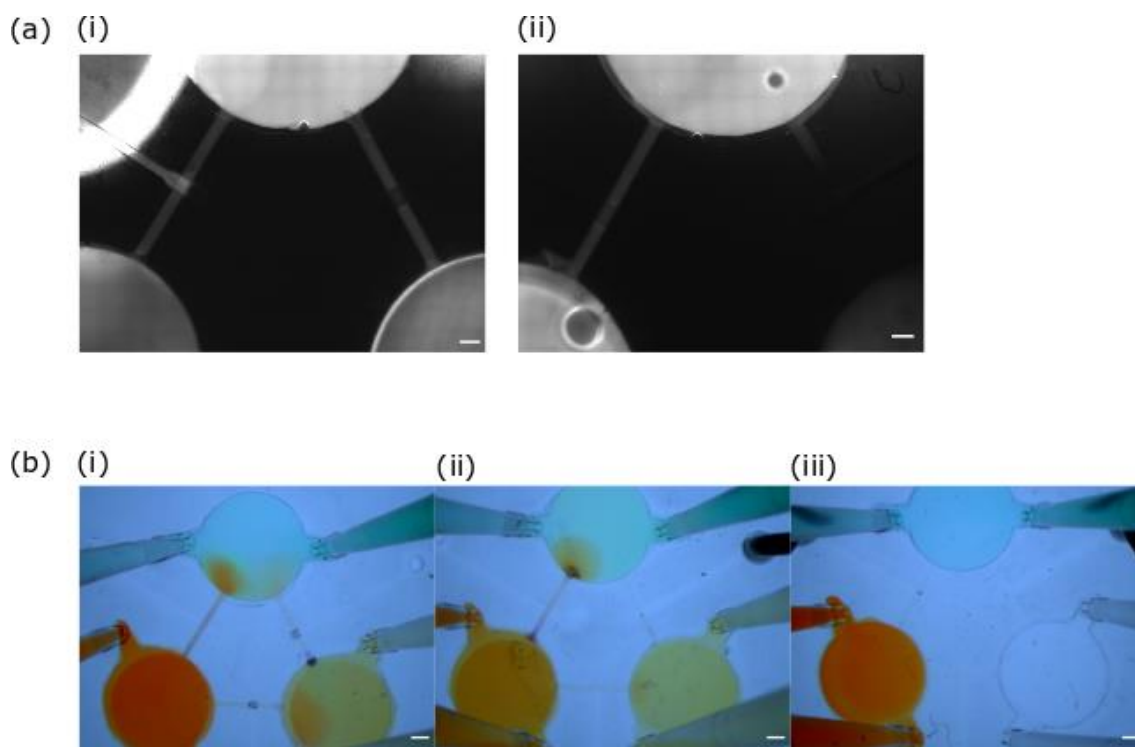


Figure S1. Demonstration of functioning valves. a) Valves prevent the diffusion of fluorescent dextran through the diffusion channels. i) Open Valves condition. FITC Dextran added to the neuronal compartment flowed to the remaining compartments when the valves were open. ii) Closed valve condition. When the valve between the neuronal and bone compartment was closed, FITC Dextran was not able to diffuse from the neuronal to the bone compartment, instead diffused only to the cancer compartment. Scale bar - 500 μ m. b) Quake valves interrupt the flow of dye between compartments. With the valves closed, the neuronal compartment was filled with green dye, the cancer compartment with orange dye and the bone compartment was filled with water. Microfluidics were left over the course of three days with (i) all the valves opened, (ii) the valve between the bone and neuronal compartments closed or (iii) all the valves closed. Scale bar - 1mm.

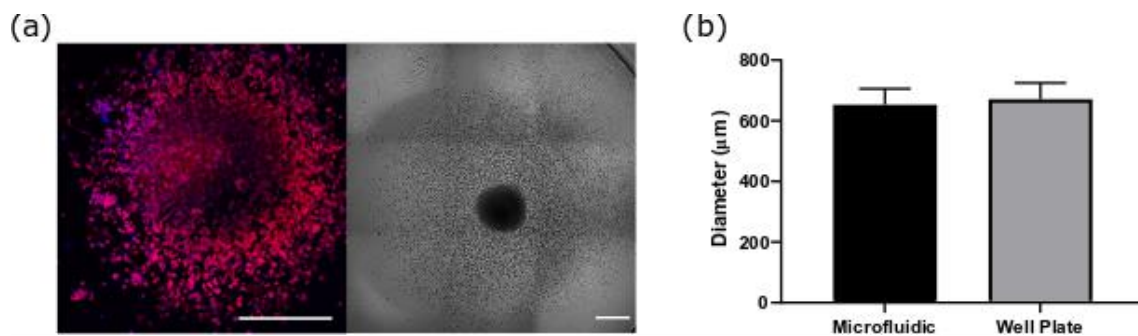


Figure S2. Comparison between MDA-1883 spheroids cultured in a standard well plate and in a microfluidic platform. (a) Immunocytochemistry micrographs of MDA-1883 spheroids cultured inside the microfluidic platform (left) and brightfield images of spheroids cultured in a well plate (right). Red - F-actin; Blue - DAPI. Scale bar - 500µm. (b) Spheroid diameter quantification. Data is expressed as mean \pm SD from 15 different spheroids.

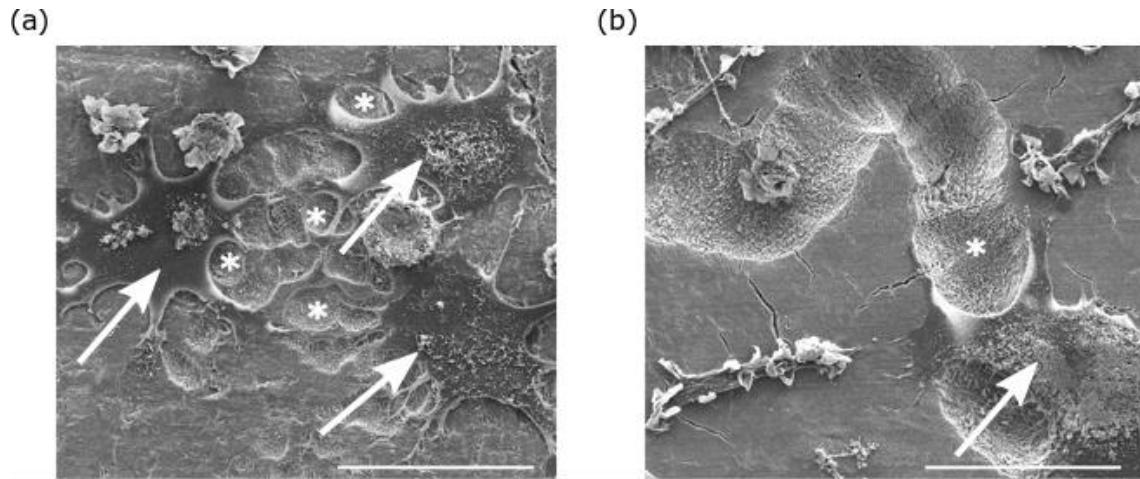


Figure S3. Scanning electron microscopy micrographs of osteoclasts cultured on top of bone slices in standard well plates. Osteoclasts (white arrows) are seen resorbing the bone surface and different resorption patterns are visible (white asterisks): (a) resorption pits and (b) trenches are characteristic modes of resorption. Scale bar - 50 μ m.

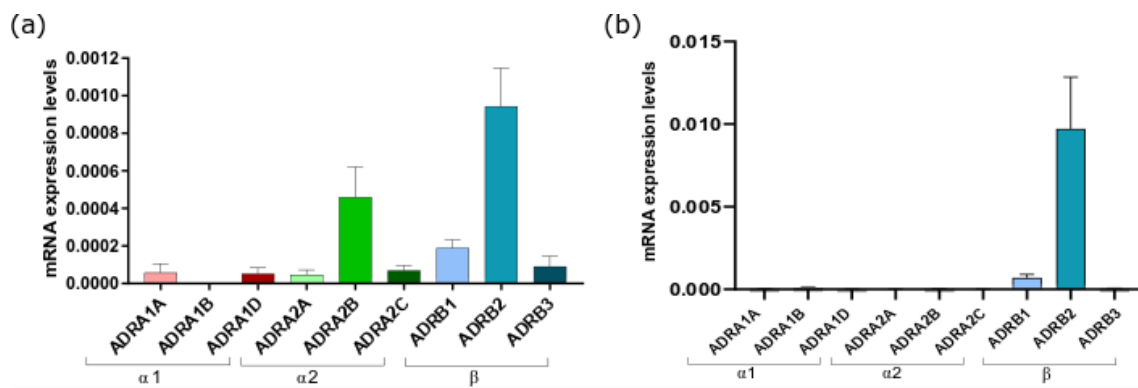


Figure S4. Quantification of AR expression. (a) Osteoclast AR expression was quantified by RT PCR. Data is expressed as mean \pm SD of the expression of the different ARs relative to the expression of beta-2 microglobulin from 6 independent experiments. (b) MDA-1833 AR expression was quantified by RT PCR. Data is expressed as mean \pm SD of the expression of the different ARs relative to the expression of beta-2 microglobulin from 6 independent experiments.

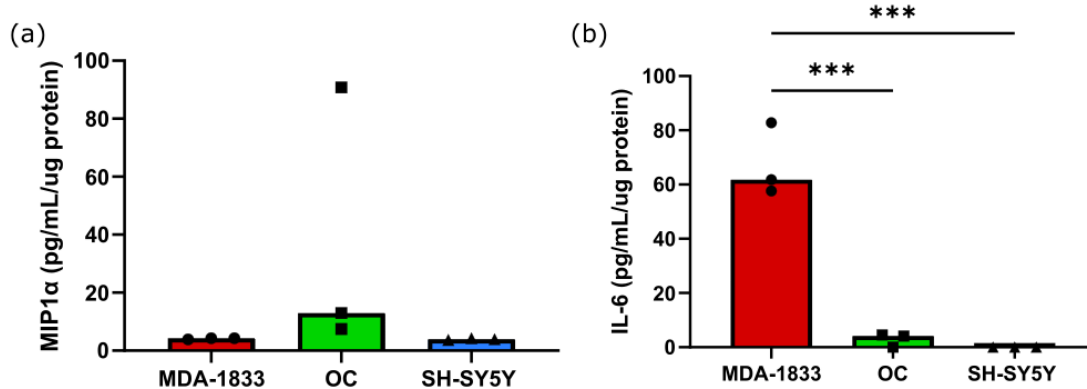


Figure S5. Cytokine quantification in mono-culture controls. Each cell type was cultured alone in their respective compartment. (a) MIP1 α and (b) IL-6 production was quantified in the conditioned medium of MDA-1833 cells, osteoclasts (OC) or SH-SY5Y cells. Data is expressed as median of individual data points from 3 independent experiments and was normalized to the total protein content (One-way ANOVA test, *** p <0.001).

Acknowledgements

The authors would like to acknowledge Inez Duursma for the first generation design of the three compartment microfluidic chip and Hugo Osório and the I3S Scientific Platform Proteomics for the help with the proteomic screening of cancer conditioned medium. The authors also thank Pedro Sousa and Anabela Nunes from the I3S Communication Unit for their help in illustration design. The authors acknowledge the support of the i3S Scientific Platform Bioimaging, member of the national infrastructure PPBI - Portuguese Platform of Bioimaging (PPBI-POCI-01-0145-FEDER-022122), for confocal imaging acquisition. This work was financed by FEDER—Fundo Europeu de Desenvolvimento Regional funds through the COMPETE 2020—Operacional Programme for Competitiveness and Internationalisation (POCI), Portugal 2020, and Portuguese funds through FCT/MCTES in the framework of the project “SproutOC” (POCI-01-0145-FEDER-030158, PTDC/MED-PAT/30158/2017). F.C. is a recipient of the Ph.D. fellowship SFRH/BD/128771/2017. D.M.S. is a recipient of Post-Doc fellowship SFRH/BPD/115341/2016. J.L. and A.R.V. were funded under the VESCEL ERC Advanced Grant to A. van der Berg (grant no. 669768).

2.3. Chapter conclusions

In summary, we have developed a new model of sympathetic regulation of breast cancer in a bone metastatic context through the integration of breast cancer cells, osteoclasts and sympathetic neuron-like SH-SY5Y cells on the same microfluidic platform. Our model displays several advantages compared to other breast cancer metastatic models: 1) manufacture is cheap and accessible without the need for specialized staff and equipment; 2) integrates a full humanized system with bone tropic breast cancer cells; 3) contains a bone matrix with intact biomechanical and biochemical cues leading to relevant bone resorption readouts; 4) includes three valve valves that allow compartment isolation during cell seeding and modulation of diffusion directionality. We successfully characterized the culture of different cell types on our platform, which led to the identification of inflammatory mediators that could be involved in the breast cancer response to sympathetic stimuli in the context of bone metastasis.

Collectively, our findings could set the basis for additional exploration of the mechanisms that govern sympathetic modulation of breast cancer bone metastasis. Further insights on the cancer-bone-neuron crosstalk could be gained by manipulating the microenvironment of each compartment by the addition of different cell players, the use of specific signaling pathway inhibitors or by including breast cancer knock-out variants. In the future, our metastasis-on-a-chip platform could also potentially be applied for drug screening assays and incorporate patient-derived tumor samples or osteoclasts for improved translational relevance. Importantly, this work presented a new platform that could be used as basis for fundamental research on various physiological and pathological settings, with the possibility of changing the different cell types to cater the needs of individual research questions.

2.4. References

- [1] A. Javidanbardan, A. M. Azevedo, V. Chu, J. P. Conde, (2022) A Systematic Approach for Developing 3D High-Quality PDMS Microfluidic Chips Based on Micromilling Technology, *Micromachines*, 13, 6
- [2] C. M. Yousuff, M. Danish, E. T. W. Ho, I. H. Kamal Basha, N. H. B. Hamid, (2017) Study on the Optimum Cutting Parameters of an Aluminum Mold for Effective Bonding Strength of a PDMS Microfluidic Device, *Micromachines*, 8, 258
- [3] Y. Liao, Y. Cheng, C. Liu, J. Song, F. He, Y. Shen, D. Chen, Z. Xu, Z. Fan, X. Wei, K. Sugioka, K. Midorikawa, (2013) Direct laser writing of sub-50 nm nanofluidic channels buried in glass for three-dimensional micro-nanofluidic integration, *Lab on a Chip*, 13, 1626-1631
- [4] J. C. McDonald, M. L. Chabiny, S. J. Metallo, J. R. Anderson, A. D. Stroock, G. M. Whitesides, (2002) Prototyping of Microfluidic Devices in Poly(dimethylsiloxane) Using Solid-Object Printing, *Anal. Chem.*, 74, 1537-1545
- [5] G. Comina, A. Suska, D. Filippini, (2014) Low cost lab-on-a-chip prototyping with a consumer grade 3D printer, *Lab on a Chip*, 14, 2978-2982
- [6] B. Venzac, S. Deng, Z. Mahmoud, A. Lenferink, A. Costa, F. Bray, C. Otto, C. Rolando, S. Le Gac, (2021) PDMS Curing Inhibition on 3D-Printed Molds: Why? Also, How to Avoid It?, *Anal. Chem.*, 93, 7180-7187
- [7] K. N. Weilbaecher, T. A. Guise, L. K. McCauley, (2011) Cancer to bone: a fatal attraction, *Nature Reviews Cancer*, 11, 411-425
- [8] J. Kong, Y. Luo, D. Jin, F. An, W. Zhang, L. Liu, J. Li, S. Fang, X. Li, X. Yang, B. Lin, T. Liu, (2016) A novel microfluidic model can mimic organ-specific metastasis of circulating tumor cells, *Oncotarget*, 7, 78421-78432
- [9] A. Chramiec, D. Teles, K. Yeager, A. Marturano-Kruik, J. Pak, T. Chen, L. Hao, M. Wang, R. Lock, D. N. Tavakol, M. B. Lee, J. Kim, K. Ronaldson-Bouchard, G. Vunjak-Novakovic, (2020) Integrated human organ-on-a-chip model for predictive studies of anti-tumor drug efficacy and cardiac safety, *Lab on a Chip*, 20, 4357-4372
- [10] J. Aleman, S. K. George, S. Herberg, M. Devarasetty, C. D. Porada, A. Skardal, G. Almeida-Porada, (2019) Deconstructed Microfluidic Bone Marrow On-A-Chip to Study Normal and Malignant Hemopoietic Cell-Niche Interactions, *Small*, 15, 1902971
- [11] S. Bersini, J. S. Jeon, G. Dubini, C. Arrigoni, S. Chung, J. L. Charest, M. Moretti, R. D. Kamm, (2014) A microfluidic 3D in vitro model for specificity of breast cancer metastasis to bone, *Biomaterials*, 35, 2454-2461

- [12] J. S. Jeon, S. Bersini, M. Gilardi, G. Dubini, J. L. Charest, M. Moretti, R. D. Kamm, (2015) Human 3D vascularized organotypic microfluidic assays to study breast cancer cell extravasation, *Proceedings of the National Academy of Sciences*, 112, 214-219
- [13] L. L. Bischel, B. P. Casavant, P. A. Young, K. W. Eliceiri, H. S. Basu, D. J. Beebe, (2014) A microfluidic coculture and multiphoton FAD analysis assay provides insight into the influence of the bone microenvironment on prostate cancer cells, *Integrative Biology*, 6, 627-635
- [14] X. Mei, K. Middleton, D. Shim, Q. Wan, L. Xu, Y.-H. V. Ma, D. Devadas, N. Walji, L. Wang, E. W. K. Young, L. You, (2019) Microfluidic platform for studying osteocyte mechanoregulation of breast cancer bone metastasis, *Integrative Biology*, 11, 119-129
- [15] J. Ahn, J. Lim, N. Jusoh, J. Lee, T.-E. Park, Y. Kim, J. Kim, N. L. Jeon, (2019) 3D Microfluidic Bone Tumor Microenvironment Comprised of Hydroxyapatite/Fibrin Composite, *Frontiers in Bioengineering and Biotechnology*, 7,
- [16] S. Hao, L. Ha, G. Cheng, Y. Wan, Y. Xia, D. M. Sosnoski, A. M. Mastro, S.-Y. Zheng, (2018) A Spontaneous 3D Bone-On-a-Chip for Bone Metastasis Study of Breast Cancer Cells, *Small*, 14, 1702787
- [17] A. Marturano-Kruik, M. M. Nava, K. Yeager, A. Chramiec, L. Hao, S. Robinson, E. Guo, M. T. Raimondi, G. Vunjak-Novakovic, (2018) Human bone perivascular niche-on-a-chip for studying metastatic colonization, *Proceedings of the National Academy of Sciences*, 115, 1256-1261
- [18] W. Zhang, W. Y. Lee, D. S. Siegel, P. Toliás, J. Zilberberg, (2013) Patient-Specific 3D Microfluidic Tissue Model for Multiple Myeloma, *Tissue Engineering Part C: Methods*, 20, 663-670
- [19] D. B. Chou, V. Frismantas, Y. Milton, R. David, P. Pop-Damkov, D. Ferguson, A. MacDonald, Ö. Vargel Bölükbaşı, C. E. Joyce, L. S. Moreira Teixeira, A. Rech, A. Jiang, E. Calamari, S. Jalili-Firoozinezhad, B. A. Furlong, L. R. O'Sullivan, C. F. Ng, Y. Choe, S. Marquez, K. C. Myers, O. K. Weinberg, R. P. Hasserjian, R. Novak, O. Levy, R. Prantil-Baun, C. D. Novina, A. Shimamura, L. Ewart, D. E. Ingber, (2020) On-chip recapitulation of clinical bone marrow toxicities and patient-specific pathophysiology, *Nature Biomedical Engineering*, 4, 394-406
- [20] P. J. Kitson, M. H. Rosnes, V. Sans, V. Dragone, L. Cronin, (2012) Configurable 3D-Printed millifluidic and microfluidic 'lab on a chip' reactionware devices, *Lab on a Chip*, 12, 3267-3271
- [21] Y.-S. Lee, N. Bhattacharjee, A. Folch, (2018) 3D-printed Quake-style microvalves and micropumps, *Lab on a Chip*, 18, 1207-1214
- [22] J. P. Campbell, M. R. Karolak, Y. Ma, D. S. Perrien, S. K. Masood-Campbell, N. L. Penner, S. A. Munoz, A. Zijlstra, X. Yang, J. A. Sterling, F. Elefteriou, (2012) Stimulation

of Host Bone Marrow Stromal Cells by Sympathetic Nerves Promotes Breast Cancer Bone Metastasis in Mice, *PLoS Biol.*, 10, e1001363

[23] L. Clément-Demange, P. L. Mulcrone, T. Q. Tabarestani, J. A. Sterling, F. Elefteriou, (2018) β 2ARs stimulation in osteoblasts promotes breast cancer cell adhesion to bone marrow endothelial cells in an IL-1 β and selectin-dependent manner, *Journal of Bone Oncology*, 13, 1-10

[24] D. G. Powe, M. J. Voss, K. S. Zänker, H. O. Habashy, A. R. Green, I. O. Ellis, F. Entschladen, (2010) Beta-Blocker Drug Therapy Reduces Secondary Cancer Formation in Breast Cancer and Improves Cancer Specific Survival, *Oncotarget*, 1,

[25] C. R. Cardwell, A. Pottegård, E. Vaes, H. Garmo, L. J. Murray, C. Brown, P. A. J. Vissers, M. O'Rorke, K. Visvanathan, D. Cronin-Fenton, H. De Schutter, M. Lambe, D. G. Powe, M. P. P. van Herk-Sukel, A. Gavin, S. Friis, L. Sharp, K. Bennett, (2016) Propranolol and survival from breast cancer: a pooled analysis of European breast cancer cohorts, *Breast Cancer Res.*, 18, 119

[26] C. R. Cardwell, H. G. Coleman, L. J. Murray, F. Entschladen, D. G. Powe, (2014) Beta-blocker usage and breast cancer survival: a nested case-control study within a UK Clinical Practice Research Datalink cohort, *Int. J. Epidemiol.*, 42, 1852-1861

[27] P. L. Mulcrone, J. P. Campbell, L. Clément-Demange, A. L. Anbinder, A. R. Merkel, R. A. Brekken, J. A. Sterling, F. Elefteriou, (2017) Skeletal Colonization by Breast Cancer Cells Is Stimulated by an Osteoblast and β 2AR-Dependent Neo-Angiogenic Switch, *J. Bone Miner. Res.*, 32, 1442-1454

[28] E. Neto, C. J. Alves, D. M. Sousa, I. S. Alencastre, A. H. Lourenço, L. Leitão, H. R. Ryu, N. L. Jeon, R. Fernandes, P. Aguiar, R. D. Almeida, M. Lamghari, (2014) Sensory neurons and osteoblasts: close partners in a microfluidic platform, *Integrative Biology*, 6, 586-595

[29] L. Leitão, E. Neto, F. Conceição, A. Monteiro, M. Couto, C. J. Alves, D. M. Sousa, M. Lamghari, (2020) Osteoblasts are inherently programmed to repel sensory innervation, *Bone Research*, 8, 20

[30] K. Søre, J.-M. Delaissé, (2010) Glucocorticoids maintain human osteoclasts in the active mode of their resorption cycle, *J. Bone Miner. Res.*, 25, 2184-2192

[31] J. M. May, Z.-c. Qu, M. E. Meredith, (2012) Mechanisms of ascorbic acid stimulation of norepinephrine synthesis in neuronal cells, *Biochem. Biophys. Res. Commun.*, 426, 148-152

[32] J. Vanderost, K. Søre, D. M. H. Merrild, J.-M. Delaissé, G. H. van Lenthe, (2013) Glucocorticoid-Induced Changes in the Geometry of Osteoclast Resorption Cavities Affect Trabecular Bone Stiffness, *Calcif. Tissue Int.*, 92, 240-250

- [33] D. M. Merrild, D. C. Pirapaharan, C. M. Andreasen, P. Kjærsgaard-Andersen, A. M. Møller, M. Ding, J.-M. Delaissé, K. Søe, (2015) Pit- and trench-forming osteoclasts: a distinction that matters, *Bone research*, 3, 15032-15032
- [34] C. S. Hughes, S. Moggridge, T. Müller, P. H. Sorensen, G. B. Morin, J. Krijgsveld, (2019) Single-pot, solid-phase-enhanced sample preparation for proteomics experiments, *Nat. Protoc.*, 14, 68-85
- [35] H. Osório, C. Silva, M. Ferreira, I. Gullo, V. Máximo, R. Barros, F. Mendonça, C. Oliveira, F. Carneiro, (2021) Proteomics Analysis of Gastric Cancer Patients with Diabetes Mellitus, *Journal of Clinical Medicine*, 10, 407
- [36] Y. Kang, P. M. Siegel, W. Shu, M. Drobnjak, S. M. Kakonen, C. Córdón-Cardo, T. A. Guise, J. Massagué, (2003) A multigenic program mediating breast cancer metastasis to bone, *Cancer Cell*, 3, 537-549
- [37] T. Ishiguro, H. Ohata, A. Sato, K. Yamawaki, T. Enomoto, K. Okamoto, (2017) Tumor-derived spheroids: Relevance to cancer stem cells and clinical applications, *Cancer Sci.*, 108, 283-289
- [38] D. L. Brooks, L. P. Schwab, R. Krutilina, D. N. Parke, A. Sethuraman, D. Hoogewijs, A. Schörg, L. Gotwald, M. Fan, R. H. Wenger, T. N. Seagroves, (2016) ITGA6 is directly regulated by hypoxia-inducible factors and enriches for cancer stem cell activity and invasion in metastatic breast cancer models, *Mol. Cancer*, 15, 26
- [39] W.-L. Cai, W.-D. Huang, B. Li, T.-R. Chen, Z.-X. Li, C.-L. Zhao, H.-Y. Li, Y.-M. Wu, W.-J. Yan, J.-R. Xiao, (2018) microRNA-124 inhibits bone metastasis of breast cancer by repressing Interleukin-11, *Mol. Cancer*, 17, 9
- [40] L. J. van 't Veer, H. Dai, M. J. van de Vijver, Y. D. He, A. A. M. Hart, M. Mao, H. L. Peterse, K. van der Kooy, M. J. Marton, A. T. Witteveen, G. J. Schreiber, R. M. Kerkhoven, C. Roberts, P. S. Linsley, R. Bernards, S. H. Friend, (2002) Gene expression profiling predicts clinical outcome of breast cancer, *Nature*, 415, 530-536
- [41] B. Kim, H. Kim, S. Jung, A. Moon, D.-Y. Noh, Z. H. Lee, H. J. Kim, H.-H. Kim, (2020) A CTGF-RUNX2-RANKL Axis in Breast and Prostate Cancer Cells Promotes Tumor Progression in Bone, *J. Bone Miner. Res.*, 35, 155-166
- [42] N. Okuyama, A. Matsumine, R. Kosugi, H. Wakabayashi, A. Uchida, (2008) Matrix metalloproteinase-1 is a crucial bone metastasis factor in a human breast cancer-derived highly invasive cell line, *Oncol. Rep.*, 20, 1497-1504
- [43] N. Zeltner, F. Fattahi, N. C. Dubois, N. Saurat, F. Lafaille, L. Shang, B. Zimmer, J. Tchieu, M. A. Soliman, G. Lee, J.-L. Casanova, L. Studer, (2016) Capturing the biology of disease severity in a PSC-based model of familial dysautonomia, *Nat. Med.*, 22, 1421-1427

- [44] J. Kovalevich, D. Langford, (2013) Considerations for the use of SH-SY5Y neuroblastoma cells in neurobiology, *Methods Mol. Biol.*, 1078, 9-21
- [45] C. Pérez Piñero, A. Bruzzone, M. Sarappa, L. Castillo, I. Lüthy, (2012) Involvement of α 2- and β 2-adrenoceptors on breast cancer cell proliferation and tumour growth regulation, *Br. J. Pharmacol.*, 166, 721-736
- [46] F. Le Pape, G. Vargas, P. Clézardin, (2016) The role of osteoclasts in breast cancer bone metastasis, *J Bone Oncol*, 5, 93-95
- [47] A. S. Andriessen, C. R. Donnelly, R. R. Ji, (2021) Reciprocal interactions between osteoclasts and nociceptive sensory neurons in bone cancer pain, *Pain Rep*, 6, e867
- [48] K. Søre, J.-M. Delaissé, (2017) Time-lapse reveals that osteoclasts can move across the bone surface while resorbing, *J. Cell Sci.*, 130, 2026-2035
- [49] K. S. Madden, M. J. Szpunar, E. B. Brown, (2011) β -Adrenergic receptors (β -AR) regulate VEGF and IL-6 production by divergent pathways in high β -AR-expressing breast cancer cell lines, *Breast Cancer Res. Treat.*, 130, 747-758
- [50] Y. Imamura, T. Mukohara, Y. Shimono, Y. Funakoshi, N. Chayahara, M. Toyoda, N. Kiyota, S. Takao, S. Kono, T. Nakatsura, H. Minami, (2015) Comparison of 2D- and 3D-culture models as drug-testing platforms in breast cancer, *Oncol. Rep.*, 33, 1837-1843
- [51] X. Jiang, L. Ren, P. Tebon, C. Wang, X. Zhou, M. Qu, J. Zhu, H. Ling, S. Zhang, Y. Xue, Q. Wu, P. Bandaru, J. Lee, H.-J. Kim, S. Ahadian, N. Ashammakhi, M. R. Dokmeci, J. Wu, Z. Gu, W. Sun, A. Khademhosseini, (2021) Cancer-on-a-Chip for Modeling Immune Checkpoint Inhibitor and Tumor Interactions, *Small*, 17, 2004282
- [52] S. L. Dallas, J. L. Rosser, G. R. Mundy, L. F. Bonewald, (2002) Proteolysis of Latent Transforming Growth Factor- β (TGF- β)-binding Protein-1 by Osteoclasts: A CELLULAR MECHANISM FOR RELEASE OF TGF- β FROM BONE MATRIX*, *J. Biol. Chem.*, 277, 21352-21360
- [53] R. O. Hynes, A. Naba, (2012) Overview of the Matrisome—An Inventory of Extracellular Matrix Constituents and Functions, *Cold Spring Harb. Perspect. Biol.*, 4,
- [54] T. Hiraga, S. Kizaka-Kondoh, K. Hirota, M. Hiraoka, T. Yoneda, (2007) Hypoxia and Hypoxia-Inducible Factor-1 Expression Enhance Osteolytic Bone Metastases of Breast Cancer, *Cancer Res.*, 67, 4157-4163
- [55] D. F. Higgins, M. P. Biju, Y. Akai, A. Wutz, R. S. Johnson, V. H. Haase, (2004) Hypoxic induction of Ctgf is directly mediated by Hif-1, *American Journal of Physiology-Renal Physiology*, 287, F1223-F1232
- [56] X. Yuan, N. Qian, S. Ling, Y. Li, W. Sun, J. Li, R. Du, G. Zhong, C. Liu, G. Yu, D. Cao, Z. Liu, Y. Wang, Z. Qi, Y. Yao, F. Wang, J. Liu, S. Hao, X. Jin, Y. Zhao, J. Xue, D. Zhao, X. Gao, S. Liang, Y. Li, J. Song, S. Yu, Y. Li, (2021) Breast cancer exosomes

contribute to pre-metastatic niche formation and promote bone metastasis of tumor cells, *Theranostics*, 11, 1429-1445

[57] T. Okui, M. Hiasa, S. Ryumon, K. Ono, Y. Kunisada, S. Ibaragi, A. Sasaki, G. D. Roodman, F. A. White, T. Yoneda, (2021) The HMGB1/RAGE axis induces bone pain associated with colonization of 4T1 mouse breast cancer in bone, *Journal of Bone Oncology*, 26, 100330

[58] K. Middleton, S. Al-Dujaili, X. Mei, A. Günther, L. You, (2017) Microfluidic co-culture platform for investigating osteocyte-osteoclast signalling during fluid shear stress mechanostimulation, *J. Biomech.*, 59, 35-42

[59] K. Søre, D. M. H. Merrild, J.-M. Delaissé, (2013) Steering the osteoclast through the demineralization–collagenolysis balance, *Bone*, 56, 191-198

[60] H. Wakabayashi, T. Hamaguchi, N. Nagao, S. Kato, T. Iino, T. Nakamura, A. Sudo, (2018) Interleukin-6 receptor inhibitor suppresses bone metastases in a breast cancer cell line, *Breast Cancer*, 25, 566-574

[61] K. L. Weber, M. Doucet, A. Shaner, N. Hsu, D. Huang, J. Fogel, S. L. Kominsky, (2012) MIP-1 δ Activates NFATc1 and Enhances Osteoclastogenesis: Involvement of Both PLC γ 2 and NF κ B Signaling, *PLoS One*, 7, e40799

[62] E. V. Yang, S.-j. Kim, E. L. Donovan, M. Chen, A. C. Gross, J. I. Webster Marketon, S. H. Barsky, R. Glaser, (2009) Norepinephrine upregulates VEGF, IL-8, and IL-6 expression in human melanoma tumor cell lines: Implications for stress-related enhancement of tumor progression, *Brain. Behav. Immun.*, 23, 267-275

[63] J. J. Yin, K. Selander, J. M. Chirgwin, M. Dallas, B. G. Grubbs, R. Wieser, J. Massagué, G. R. Mundy, T. A. Guise, (1999) TGF- β signaling blockade inhibits PTHrP secretion by breast cancer cells and bone metastases development, *The Journal of Clinical Investigation*, 103, 197-206

[64] R. E. Coleman, P. I. Croucher, A. R. Padhani, P. Clézardin, E. Chow, M. Fallon, T. Guise, S. Colangelo, R. Capanna, L. Costa, (2020) Bone metastases, *Nature Reviews Disease Primers*, 6, 83

[65] M. A. Unger, H. P. Chou, T. Thorsen, A. Scherer, S. R. Quake, (2000) Monolithic microfabricated valves and pumps by multilayer soft lithography, *Science*, 288, 113-116

[66] R. Li, X. Zhang, X. Lv, L. Geng, Y. Li, K. Qin, Y. Deng, (2017) Microvalve controlled multi-functional microfluidic chip for divisional cell co-culture, *Anal. Biochem.*, 539, 48-53

[67] M. Arai, T. Nagasawa, Y. Koshihara, S. Yamamoto, A. Togari, (2003) Effects of β -adrenergic agonists on bone-resorbing activity in human osteoclast-like cells, *Biochimica et Biophysica Acta (BBA) - Molecular Cell Research*, 1640, 137-142

[68] E. K. Sloan, S. J. Priceman, B. F. Cox, S. Yu, M. A. Pimentel, V. Tangkanangnukul, J. M. G. Arevalo, K. Morizono, B. D. W. Karanikolas, L. Wu, A. K. Sood, S. W. Cole,

(2010) The Sympathetic Nervous System Induces a Metastatic Switch in Primary Breast Cancer, *Cancer Res.*, 70, 7042-7052

[69] L. Zheng, K. Zhu, H. Jiao, Z. Zhao, L. Zhang, M. Liu, W. Deng, D. Chen, Z. Yao, G. Xiao, (2013) PTHrP Expression in Human MDA-MB-231 Breast Cancer Cells Is Critical for Tumor Growth and Survival and Osteoblast Inhibition, *Int. J. Biol. Sci.*, 9, 830-841

[70] R. J. Thomas, T. A. Guise, J. J. Yin, J. Elliott, N. J. Horwood, T. J. Martin, M. T. Gillespie, (1999) Breast Cancer Cells Interact with Osteoblasts to Support Osteoclast Formation, *Endocrinology*, 140, 4451-4458

[71] A. E. Chiou, C. Liu, I. Moreno-Jiménez, T. Tang, W. Wagermaier, M. N. Dean, C. Fischbach, P. Fratzl, (2021) Breast cancer secreted factors perturb murine bone growth in regions prone to metastasis, *Science Advances*, 7, eabf2283

[72] A. Shiirevnyamba, T. Takahashi, H. Shan, H. Ogawa, S. Yano, H. Kanayama, K. Izumi, H. Uehara, (2011) Enhancement of osteoclastogenic activity in osteolytic prostate cancer cells by physical contact with osteoblasts, *Br. J. Cancer*, 104, 505-513

Chapter III. *In vitro* pharmacological β_2 -AR activation and its effect on the breast cancer modulation of the bone niche in different stages of disease progression

3.1. Breast cancer regulation of the pre-metastatic bone niche

Advanced breast cancer patients often display metastatic foci on bone, but the causes of this specific tropism are still poorly understood. The bone niche is particularly permissive to colonization by breast cancer cells, since it is characterized by extensive vascularization with a profile of endothelial cell adhesion molecules that facilitates circulating tumor cell adhesion and extravasation. In addition, the bone marrow is hypoxic which promotes cellular dormancy and increased drug resistance. Finally, multiple cellular types in the bone marrow are responsible for the maintenance and regulation of MSCs and hematopoietic stem cells (HSC) niches, such as adipocytes, osteoclasts, osteoblasts, macrophages and T-cells, among other. Thus, the complex interplay that is established at the bone marrow leads to a microenvironment rich in growth factors and soluble mediators, such as TGF- β , IL-6, IL-8 and Ca²⁺ ions, that also promote breast cancer survival and growth.

In addition to being an intrinsic favorable environment for breast cancer colonization, the bone marrow also receives input from the primary tumor to modulate local bone metabolism and further facilitate metastasis. Primary breast cancer tumors are able to release different factors directly on the circulation, including lysyl oxidase (LOX) and PTHrP, that mobilize bone marrow stromal cells and shift the normal bone remodeling process towards increased bone resorption [1-4]. Interestingly, bone metabolism modulation by PTHrP and LOX was demonstrated in *in vivo* intracardiac injection BC models, suggesting that the augmented bone destruction occurs in later stages of BC progression when BC are already in circulation. Conversely, when mice were inoculated with the secretome from non-metastatic primary BC, an increase in mineral apposition and altered bone matrix composition was observed [5]. Notably, no changes in osteoclast gene expression were detected, pointing to an effect on osteoblast-lineage cells instead [5]. Therefore, modulation of bone metabolism by BC seems to be dynamic throughout disease progression, where the bone matrix is first altered to facilitate colonization of BC cells followed by extensive bone degradation and uncontrolled tumor growth.

Very few studies have described the interactions that take place between BC and bone cells in the context of sympathetic activation, and thus the role of the SNS in the conditioning of the bone pre-metastatic niche in BC is still poorly understood. What is known so far is that β_2 -AR activation in BMSC leads to an overexpression of RANKL, subsequently promoting the migration of RANK expressing BC cells towards the bone marrow and leading to extensive bone degradation [6]. In addition, after β_2 -AR activation, BMSC promote endothelial cell activation by secreting VEGF and IL-1 β , which facilitates BC cell adhesion and extravasation into the bone marrow [7, 8].

Most of the available data on SNS control of BC bone metastasis is derived from *in vivo* studies, where the dissection of specific signaling pathways involved in the metastatic colonization of the bone is hindered. In order to break down the role of β -adrenergic activation in the crosstalk taking place between BC cells and the bone niche at different stages of disease progression, we expanded on the knowledge generated in the previous chapters and determined:

- The changes in Epi plasma content that take place throughout BC progression in a group of primary and advanced BC patients and healthy blood donors.
- The adrenergic modulation of the secretome of BC cells, particularly through β_2 -AR, using a pharmacological approach *in vitro* with primary and metastatic bone tropic BC cell lines.
- The effect of the secretome of β_2 -AR primed primary and metastatic BC cells on human osteoclast activity, when cultured alone or in an osteoclast-osteoblast co-culture setting.

3.2. β_2 -Adrenergic modulation of the BC bone metastatic niche

[Research Paper]

The Secretome of Primary and Bone Metastatic Breast Cancer Elicits Distinct Outcomes in Human Osteoclast Activity After Activation of β_2 Adrenergic Signaling

This chapter was based on the following submitted paper:

F. Conceição, D. M. Sousa, S. Tojal, C. Lourenço, C. Carvalho-Maia, H. Estevão-Pereira, J. Lobo, M. Couto, M. M. Rosenkilde, C. Jerónimo, M. Lamghari (2022) The Secretome of Primary and Bone Metastatic Breast Cancer Elicits Distinct Outcomes in Human Osteoclast Activity After Activation of β_2 Adrenergic Signaling. (under review for British Journal of Pharmacology)

Abstract

Background and Purpose: In the past decade, the sympathetic nervous system (SNS), particularly through the β_2 adrenergic receptor (β_2 -AR), has been implicated in breast cancer (BC) metastasis, but the potential benefits of β_2 -AR antagonists in the treatment of BC remain controversial.

Experimental Approach: Plasma epinephrine levels of primary and advanced BC patients were quantified. The secretome of primary and metastatic BC cells under pharmacological activation of β -ARs was characterized by proteomic screening. Functional in vitro studies with human osteoclasts and osteoblasts were performed to assess the role of BC secreted factors on the bone metastatic niche.

Key results: In this work, we show that, when compared to healthy donors, the epinephrine levels in BC patients are augmented in the earlier stages of the disease and are maintained throughout disease progression. We demonstrate that paracrine signaling from primary BC under β_2 -AR signaling activation causes a robust decrease in human osteoclast differentiation and resorption activity, which is rescued in the presence of human osteoblasts. Conversely, metastatic bone tropic BC does not display this anti-osteoclastogenic effect.

Conclusion and Implications: In conclusion, clinical data on epinephrine levels in BC patients, together with the observed changes in the proteomic profile of BC cells under β -AR activation that take place after metastatic dissemination, provided new insights on the sympathetic control of breast cancer at different stages of disease progression. Our findings prompt careful consideration when targeting the SNS in future therapeutic interventions.

Keywords: breast cancer; beta-adrenergic; sympathetic nervous system; osteoclast; proteomic

3.2.1. Introduction

Breast cancer (BC) is the most common type of cancer diagnosed in women worldwide [9]. It is a heterogeneous disease, characterized by the primary tumor status of estrogen receptor (ER), progesterone receptor (PR) and epidermal growth factor receptor 2 (HER2). Treatment options have improved early-stage BC patient survival [10], but metastatic spread of BC cells from the primary tumor to distant organs dramatically reduces patient life expectancy. Notably, hormone receptor status of the primary tumor correlates with specific tropism towards different organs [11]. Bone is the most common site of metastasis, with around 70% of late-stage BC patients presenting bone metastatic foci that lead to skeletal complications such as increased fracture risk, hypercalcemia and severe bone pain [12].

Bone homeostasis is maintained through coupling of bone matrix deposition by osteoblasts, cells of mesenchymal origin, and bone resorption by osteoclasts, specialized multinucleated cells able to degrade old or damaged mineralized matrix [13]. Before and during colonization of bone, BC cells sequester the normal bone remodeling process and shift it towards increased bone resorption [14]. By secreting parathyroid hormone-related protein (PTHrP) and prostaglandin E2 (PGE2), among other osteolytic factors, BC cells promote osteoblast receptor activator of NF- κ B ligand (RANKL) upregulation and consequently increase osteoclast activity and bone degradation [14]. Osteoclast overactivation, on the other hand, leads to the release of embedded bone matrix proteins such as TGF- β and insulin-like growth factor (IGF) that fuel the growth of BC cells and perpetuates a “metastatic vicious cycle” of bone destruction [15].

Other players might hold an important role on BC bone metastasis. Sympathetic nervous system (SNS) activity is often exacerbated in several types of cancer [16, 17], and multiple pharmacological *in vitro* studies with human cells and murine *ex vivo* bone cultures have implicated the SNS in extravasation and colonization of the bone in prostate cancer [18, 19]. The SNS is involved in the “fight or flight” response to stress and its main effector neurotransmitters are the catecholamines norepinephrine and epinephrine, which are released in sympathetic nerve terminals in target peripheral tissues or in the circulation by the adrenal gland, respectively [20]. Epinephrine and norepinephrine bind to α and β adrenergic receptors (α/β -AR), a family of 9 receptors commonly expressed in bone cells and BC cells [21]. In particular, β_2 -AR signaling has been associated to increased BC metastatic spread, extravasation and extensive bone degradation, evidenced in pharmacological *in vitro* murine BC and endothelial cell co-culture experiments as well as in humanized bone metastatic BC models and BC xenograft denervation studies *in vivo* [6, 8, 22]. Furthermore, epidemiologic studies have shown that β_2 -AR targeting drugs

have potential benefits in BC patient survival and recurrence [23-25]. However, other retrospective studies have found no significant correlation between the use of β_2 -AR targeting drugs and improved BC survival [26-28], and thus the effect of SNS activity in BC survival and recurrence remains controversial. An improved understanding of the SNS control of the role of BC in the modulation of the bone metastatic niche, in particular through the β_2 -AR signaling, are urgently needed.

In this study, we characterized the epinephrine levels in the plasma of primary and advanced BC patients. In addition, we focused on the effect of β_2 -AR signaling on the crosstalk between BC cells and human osteoclasts/osteoblasts, mimicking interactions occurring at earlier stages of BC and during metastatic colonization. Our findings complement the current knowledge on the dynamics of adrenergic control of the metastatic bone niche, highlighting the changes in proteomic profile that take place during metastatic trait acquisition in BC. Careful consideration should be exercised before using β_2 -AR targeting drugs in the clinical setting.

3.2.2. Materials and Methods

3.2.2.1. Materials

Isoproterenol hydrochloride (ISO, Cat#I6504) and ICI 118,551 (ICI, Cat#I127) were purchased from Sigma-Aldrich. All cell culture media, penicillin/streptomycin solution (pen/strep, Cat#15140122) and trypsin (0.25% w/v trypsin, 0.1% w/v glucose and 0.05% EDTA in PBS, Cat#25200056) were purchased from Gibco, Thermo Fisher Scientific. FBS was purchased from Biowest (Cat#S181B-500). Recombinant human macrophage colony stimulating factor (rhM-CSF) and recombinant human RANKL (rhRANKL) were purchased from R&D Systems (Cat#216-MC-025 and Cat#390-TN-010, respectively). Epinephrine levels in the plasma of BC patients were quantified by ELISA (Abnova, Cat#157KA1877) according to manufacturer's instructions.

3.2.2.2. Human Patients

Peripheral blood samples from healthy donors (n=18), stage IA BC patients (n=18) and stage IV BC patients (n=18) were collected at Instituto Português de Oncologia (IPO) Porto. Briefly, peripheral blood was collected into EDTA-containing tubes and centrifuged at 2000 rpm for 10 min at 4 °C. Plasma was immediately separated, aliquoted into 1.5 mL tubes and properly stored at -80 °C until further use. All the procedures were conducted following approval by the institutional ethics committee (Comissão de Ética para a Saúde, CES-IPOFG-EPE 019/08 and CES 120/015) and sample collection was performed in accordance with the Declaration of Helsinki. Informed consent was obtained from all individual participants included in the study.

All stage IV BC patients presented distant site metastasis at diagnosis, being the bone the most common site. Detailed description of the cohort (diagnosed between October 2015 and May 2018) is available in Table S1.

3.2.2.3. Cell culture

3.2.2.3.1 Parental and bone metastatic BC cell lines

Human breast carcinoma cell line MDA-MB-231 (MDA-231 henceforth, RRID:CVCL_VR35) and its bone tropic variant MDA-MB-231-BoM 1833 cell line (MDA-1833 henceforth, RRID:CVCL_DP48) were obtained from Dr. Joan Massagué (Memorial Sloan-Kettering Cancer Center, New York). Cells were expanded in standard T75 flasks (Sarsted) in DMEM High Glucose with 10% FBS and 1% Pen/Strep at 37°C and 5% CO₂ in a humidified incubator, changing medium twice a week until reaching 80% confluence.

3.2.2.3.2 Human primary osteoblasts

Human osteoblasts were obtained from patients undergoing hip or knee replacement surgeries (following approval by the ethical committee in Hospital São João, protocol number 143/19) as previously described [29]. Informed consent was obtained from all donors before collection. Briefly, trabecular bone was washed in PBS and cut into small pieces, which were then vigorously shaken with PBS to completely remove the remaining bone marrow. Seven to eight bone pieces were then placed in each well of a 6-well plate and fixed in place with a metal grid to prevent movement during culture. Bone pieces were cultured at 37°C and 5% CO₂ in a humidified incubator for 14 days in DMEM Low Glucose (Cat#21885-108) supplemented with 10% FBS, 50 µg/mL ascorbic acid, 10 mM β-glycerophosphate and 10 nM dexamethasone (Sigma-Aldrich, Cat#49752, Cat#G-9891, Cat#D1756, respectively), changing medium at day 7. Cells began to migrate from the bone to the culture plate after 7 days, and at 14 days of culture the metal grid and bone pieces were removed. The outgrowth cells were expanded until confluence was reached, changing medium twice a week.

3.2.2.3.3. Human primary osteoclasts

Human CD14⁺ monocytes were isolated from buffy coats of healthy female blood donors as previously described [30]. Briefly, Peripheral Blood Mononuclear Cells (PBMCs) were separated using gradient centrifugation in Ficoll-Paque Plus (GE Healthcare, Cat#17-1440-03). PBMCs were then resuspended in 0.5% Biotin-free BSA (Sigma-Aldrich, Cat#A4919) and 2 mM EDTA in PBS incubated in BD IMag™ anti-human CD14 magnetic particles (BD-Biosciences, Cat#557769) and magnetically separated according to manufacturer's instructions. CD14⁺ cells were seeded in T75 flasks in α-

MEM (Cat#41061-029) supplemented with 10% FBS, 1% pen/strep (Osteoclast Medium) and 25 ng/mL of rhM-CSF at 5% CO₂ at 37 °C in a humidified incubator. After 2 days, media was changed to Osteoclast Medium supplemented with 25 ng/mL rhM-CSF and 25 ng/mL rhRANKL and cells were cultured for up to 7 days, changing media twice, until cells were morphologically differentiated.

3.2.2.4. Functional studies

3.2.2.4.1. Activation of β_2 -AR signaling in BC

MDA-231 and MDA-1833 cells were seeded at a density of 10⁴ cells/cm² and left to proliferate for 24 h. Cells were then serum-starved and stimulated with the β -AR agonist ISO (1 μ M) or with PBS as a vehicle control. To block β_2 -AR activation, the selective β_2 -AR antagonist ICI (1 μ M) was added 45 min prior and also simultaneously as ISO to ensure complete blockage of the signaling (Figure S1). These concentrations promoted cAMP accumulation in β_2 -AR expressing cancer cells, and ICI addition completely blocked β_2 -AR signal transduction (Figure S2). Cells were incubated for 24h after which conditioned media was collected, centrifuged at 4°C at 400 g to pellet cell debris and frozen at -80°C until further use.

3.2.2.4.2 Osteoclast differentiation following exposure to BC cell secretome

At day 5 of culture, pre-osteoclasts were detached with Accutase (Gibco, Cat#A11105-01) for 10 min at 37°C, centrifuged and seeded in 96-well tissue culture polystyrene (TCPS) (Orange Scientific) plates at a density of 50 000 cells/well in Osteoclast Medium with 25 ng/mL rhM-CSF and rhRANKL. Cells were left to adhere for 4h and were stimulated with BC cell secretome at a 1:1 ratio (Osteoclast Medium : BC secretome), supplemented with 25 ng/mL rhM-CSF and rhRANKL. Osteoclasts were left to differentiate until day 9. Medium/Secretome was changed on day 7 of culture.

After exposure to BC secretome, osteoclast differentiation was assessed. Cells were washed with PBS and fixed in 4% paraformaldehyde (PFA, Cat#158127) for 10 min at room temperature (RT). Following another washing step with PBS, cells were permeabilized with cold 1% (v/v) Triton X-100 (Sigma-Aldrich, Cat#X100) in PBS for 5 min. Unspecific binding was then blocked with 0.1% BSA (Sigma-Aldrich, Cat#05482) solution in PBS for 1 h at 37°C. Samples were incubated with HCS CellMask™ Deep Red Stain (Invitrogen, 1:20000 dilution, Cat#H32721) and counterstained with DAPI (Sigma-Aldrich, 1:1000 dilution, Cat#D9542) for 1 h at RT protected from light. Samples were washed twice with PBS to remove excess staining and kept at 4°C until imaging. Images were acquired using an IN Cell Analyzer 2000 (GE Healthcare) high content screening imaging system. 6 images per well were randomly acquired, on the DAPI and

Cy5 channel, with a Nikon 10X/0.45 Plan Apo objective. After image acquisition, a Pixel Classification workflow of the Ilastik toolkit (v. , RRID:SCR_015246) [31] was used for osteoclast cytoplasm and nuclei segmentation with σ values of 0.7, 1.0, 1.6 and 3.5 for the Gaussian Smoothing feature and 0.7, 1.0 and 1.6 for the remaining features: Laplacian of Gaussian, Gaussian Gradient Magnitude, Difference of Gaussian, Structure Tensor Eigenvalues and Hessian of Gaussian Eigenvalues. Up to 15 images were used in the Pixel Classification training, and batch processing of the images generated probability maps used later for segmentation. Next, both raw nuclei and cytoplasm images as well as Ilastik generated probability maps were uploaded into CellProfiler™ (v. 4.0.6., RRID:SCR_007358) [32]. A workflow was built in order to identify the nucleus and cytoplasm of all cells. Briefly, nuclei were segmented by manual thresholding applied to the previously generated probability masks. Then, the cell cytoplasm was segmented with the same method through a propagation algorithm of the cytoplasm mask starting from the segmented nuclei until the edges of the cytoplasm map. Cell cytoplasm and correspondent nuclei were matched and the analysis pipeline ended with an automatic reporting of the number of cells and nuclei per cell detected on each image (Figure S3). The number of osteoclasts with more than three nuclei was then quantified for each condition.

3.2.2.4.3. Osteoclast resorption following exposure to BC cell secretome

The effect of BC cell secretome on osteoclast resorption was performed in osteoclast monocultures or osteoclast/osteoblast co-culture experiments. After 9 days of culture, mature osteoclasts were detached with accutase for 10 min at 37°C, centrifuged and seeded on top of 0.4mm thick bone slices (boneslices.com) at a density of 50 000 cells per well in Osteoclast Medium with 0.5% FBS supplemented with 25 ng/mL rhM-CSF, being left to adhere for 4 h.

For osteoblast co-culture experiments, osteoblasts were detached with Accutase for 10 min, centrifuged and seeded on top of the bone slices with the seeded osteoclasts at a density of 12 500 cells/well in Osteoclast Medium with 0.5% FBS supplemented with 25 ng/mL rhM-CSF.

Osteoclasts mono-cultures or co-cultures with osteoblasts were then stimulated with BC secretome and Osteoclast Medium with 0.5% FBS at a 1:1 ratio, supplemented with 25 ng/mL rhM-CSF. Secretome stimulation was performed only once and culture was maintained for 3 days. In the end of culture, conditioned medium of osteoclasts was collected and centrifuged at 4°C at 400 g for 5 min, and stored immediately at -80°C.

For resorption quantification, bone slices were washed with deionized water and scrapped with cotton swabs to remove the cells from the bone surface. Osteoclast

resorption events were stained with toluidine blue (Sigma-Aldrich, Cat#89640). The entire bone surface was analysed using a G50 100 point graticule (Pyser Optics, Cat#01A20.4075) installed on the ocular of an BH-2 optical microscope (Olympus) as previously described [33]. Briefly, each intercept of a graticule point with a resorption event was counted as a hit, and the total number of hits throughout the bone surface were counted using the graticule as a frame (using a total of 16-17 graticules per bone slice). The total percentage eroded surface was estimated by dividing the total number of hits by the number of graticule grids used for the quantification. Individual resorption events were divided in two resorption types, pits and trenches. Pits are single, circular excavations with well-defined edges while trenches are elongated and continuous grooves with a length/width ratio equal or greater than two [34]. The percentage of trenches per total events was used to compare individual experiments independently of eroded surface variations. Samples were blinded before eroded surface quantification.

3.2.2.5. TRAcP activity quantification

The activity of tartrate resistant acid phosphatase (TRAcP) present in the conditioned medium of osteoclast cultures was colorimetrically quantified. *p*-nitrophenyl phosphate (Merck, Cat#4876) was added in the presence of 25 nM sodium tartrate (Merck, Cat#1066640100) to the osteoclast conditioned medium as previously described [35]. Absorbance was read at 405 nm using a Synergy Mx (BioTek) plate reader. For normalization, total protein concentration was quantified using the DC Protein Assay (Bio-Rad, Cat#5000116) according to the manufacturer's instructions.

3.2.2.6. Quantitative real-time PCR (qRT-PCR) analysis

MDA-231 and MDA-1833 cells were seeded in T75 flasks (Sarsted) and cultured as described above. When 80% confluence was reached, cells were washed with PBS and lysed with Trizol (Invitrogen, Cat#15596-018) and kept on ice. Total RNA was extracted using the Direct-zol™ RNA miniPrep according to the manufacturer's protocol (Zymo Research, USA, Cat#ZY-R2052). RNA final concentration and purity ($OD_{260/280}$) was determined using a NanoDrop 2000 instrument (NanoDrop Technologies). RNA was reverse transcribed into cDNA using the NZY First-Strand cDNA Synthesis Kit (NZYTech, Cat#MB12501), according to the manufacturer's protocol. qRT-PCR experiments were run using an iCycler iQ5 PCR thermal cycler (Bio-Rad Laboratories) and analysed with the iCycler IQ™ software (Bio-Rad). A personalized PrimePCR array (Bio-Rad Laboratories) was designed to analyze the range of adrenergic receptors. Target gene expression was quantified using the cycle threshold (Ct) values and relative mRNA expression levels were calculated as follows: $2^{-(Ct \text{ reference gene} - Ct \text{ target})}$

gene). Human β 2-microglobulin (β 2M) and glyceraldehyde 3-phosphate dehydrogenase (GAPDH) were used as reference genes. Both target and reference genes were amplified with efficiencies between $100 \pm 5\%$.

3.2.2.7. Immunocytochemistry

For β ₂-AR immunocytochemistry, MDA-231 and MDA-1833 cells were cultured in a multi-well μ Slide (Ibidi) until semi-confluence, after which they were washed twice with PBS and fixed with 4% PFA for 10 min. After another wash with PBS, cells were permeabilized with cold 1% (v/v) Triton X-100 in PBS for 5 min. Unspecific binding was then blocked with 0.1% BSA solution in PBS for 1 h at 37°C. Cells were incubated with a polyclonal rabbit anti- β ₂-AR (ProteinTech, Cat#13096-1-AP, RRID:AB_2225401) in a dilution of 1:100 in 0.1% BSA/PBS solution overnight at 4°C. Excess antibody was washed with PBS and cells were then incubated with donkey anti-rabbit AlexaFluor 568 (ThermoFisher, 1:1000 dilution, Cat#A10042, RRID:AB_2534017) for 30 min at RT. After washing excess antibody with PBS, cells were counterstained with DAPI solution in PBS (1:1000 dilution) for 5 minutes. Samples were kept in PBS at 4°C in the dark until image acquisition. Images were acquired in a SP2 confocal microscope (Leica). Representative images were taken with a 40x objective at a resolution of 2048x2048 pixels. Brightness was adjusted with ImageJ software.

3.2.2.8. Western Blot

For protein collection, BC cells were cultured seeded at a density of 10^4 cells/cm² and left to proliferate until reaching ~80% confluence. Cells were then washed in cold PBS and lysed with cold RIPA buffer together with protease and phosphatase inhibitors (Sigma-Aldrich, 1:100 dilution, Cat#P8340 and Cat#P5726) for 30 min on ice with on an orbital shaker. Lysate was collected and sonicated with three cycles of 3 s each. Samples were then centrifuged at 13 000 g for 10 min at 4°C to pellet cell debris. Protein in the supernatant was then quantified using a DC Protein Assay Kit (Bio-Rad). 15 μ g of protein from each cell lysate were prepared in non-reducing loading buffer and denatured for 5 min at 95°C. Protein lysates were then loaded and resolved in pre-cast Bolt™ 10% polyacrylamide gels (Invitrogen, Cat#NW00105BOX). Separated proteins were then dry-transferred to nitrocellulose membranes using an iBlot 2 dry blotting system (ThermoFisher). Membranes were then blocked with 5% non-fat dry milk solution for 1 h at RT, followed by incubation in primary rabbit β ₂-AR antibody (ProteinTech, Cat#13096-1-AP, RRID:AB_2225401) at 1:1000 dilution in 5% milk solution overnight at 4°C with gentle agitation. Membranes were incubated with HRP-conjugated anti-rabbit secondary antibody (Santa Cruz Biotechnology, 1:10000 dilution, Cat#sc-2030, RRID:AB_631747)

for 1h at RT under gentle agitation, followed by incubation in ECL substrate (GE Healthcare, Cat#1705061) and chemiluminescence detection for 10 s with autoradiographic films (GE Healthcare). Films were scanned on a GS-800 imaging densitometer (Bio-Rad).

3.2.2.9. Proteomic analysis

Conditioned medium from three replicate samples of MDA-231 or MDA-1833 treated with ISO as described in previous sections was collected and centrifuged at 300 g for 5 min to pellet cellular debris. Conditioned media was then transferred to micro tubes and protein concentration was measured as described above. 50 µg of protein from each condition was processed using the solid-phase-enhanced-sample-preparation (SP3) protocol, as previously described [36], followed by enzymatic digestion overnight with trypsin/LysC (2 micrograms) at 37 °C and 1000 rpm.

Protein identification was carried out by nano Liquid Chromatography coupled with Mass Spectrometry (LC-MS/MS) and data was analyzed with Proteome Discoverer software (Thermo Scientific, v2.4) as described by Osório et al [37]. Protein abundances were used to compare between conditions.

3.2.2.10. Statistics

The data and statistical analysis comply with the recommendations of the *British Journal of Pharmacology* on experimental design and analysis in pharmacology [38]. All experiments with primary human cells were performed at least five times. Five replicates were used in resorption and TRAcP activity quantification, while for differentiation quantification three replicates were used since six images were generated for each replicate. Experiments were randomized and data from resorption experiments was single blinded (blinded by D.M.S. and quantified by F.C. and S.T.), while differentiation was quantified by F.C. and S.T. in an unsupervised fashion using an algorithm described above. qRT-PCR and proteomic screening experiments were performed with three independent experiments due to the small variability inherent of the use of cell lines.

Non-parametric paired Friedman's test followed by Dunn's multiple comparisons test were used to compare between conditions unless otherwise stated. Multiple comparisons were only performed if the test was statistically significant. Differences between groups were considered significant when * $p < 0.05$, ** $p < 0.01$, *** $p < 0.001$. Data analysis was performed using GraphPad Prism software v.9.2.0. for Windows (GraphPad Software, RRID:SCR_002798). Comparison between clinical parameters of BC patients was performed using cross-tabulation analysis with the χ^2 -test for trend or

Fisher's exact test using GraphPad Prism v9.2.0. No data was excluded unless otherwise stated, and all outliers were included in the analysis.

In the proteomic screening, protein abundances were compared between conditions with t-student test using Proteome Discoverer Software (Thermo Scientific, v2.4, RRID:SCR_014477). Heat maps and volcano plots comparing protein abundance between conditions were built with GraphPad v9.2.0. Only proteins that were present in every replicate of at least one condition were considered. Networks of biological processes associated to deregulated proteins between groups were constructed using the ClueGO plugin (v2.5.8, RRID:SCR_005748) from the Cytoscape software^[39] (v3.9.0, RRID:SCR_003032) with the following parameters: GO Biological Processes ontology and "All Evidence" were selected; two sided hypergeometric test and Bonferroni step down statistical options were used and only pathways with $p < 0.05$ were shown; Minimum and maximum tree intervals were 3-6, with a minimum number of three genes; and 4% of genes selected for Gene Ontology terms, with a kappa score of 0.4. In proteomic data, P-values and abundance ratios in heat maps and volcano plots were normalized in order to properly depicted (\log_{10} for p-values and \log_2 for abundance ratios).

Principal component analysis (PCA) was performed with the Proteome Discoverer Software. Protein enrichment analysis was performed with WebGestalt toolkit (RRID:SCR_006786)^[40]. Over-Representation Analysis (ORA) was used to analyze each set of deregulated proteins with the following conditions: the minimum and maximum number of genes was 5 and 2000, respectively; significance was set to $p \leq 0.05$ with adjustments following the Benjamini-Hochberg method; Gene Ontology (Biological Process, Cellular Component, Molecular Function), Pathway (Kyoto Encyclopedia of Genes and Genomes, Panther, Reactome and Wikipathway) and disease (Disgenet, GLAD4U and OMIM) functional databases were considered for the analysis.

3.2.3. Results

3.2.3.1. Primary and advanced BC patients exhibit increased plasma epinephrine levels

We used the circulating epinephrine levels as a measure of the sympathetic tone in the plasma of primary (Stage I) and advanced (Stage IV) BC patients. We first characterized our study population according to several clinical parameters and found significant differences in tumor grade and age between primary and advanced BC patients, with no differences in menopausal status and tumor molecular subtype (Table I). Subsequently, we proceeded to compare plasma epinephrine levels of BC patients and healthy donors and found that both groups of BC patients displayed significantly increased levels of plasma epinephrine (Figure 1a). Interestingly, there is an exacerbation of circulating

epinephrine release as the disease is established but no significant differences were found between primary and advanced BC patients. Furthermore, although most of the patients were diagnosed after menopause, no apparent clusters were observed when matching epinephrine levels and menopausal state (Figure 1b). Similarly, when comparing the epinephrine levels of advanced BC patients displaying only bone metastasis with patients with multiple metastatic sites, variation in epinephrine levels was independent of the metastatic site (Figure 1c).

Table I. Clinical parameters of donors/BC patients included in our study

Variable	Healthy Donors	Stage I BC patients	Stage IV BC patients	P value
Age				
<65	16	8	15	0.0354
≥65	2	10	3	
Primary tumor grade				
T1		18		<0.0001
T2			4	
T3			5	
T4			4	
N/A			5	
Menopause				
Pre-Menopause		3	6	0.4430
Post-Menopause		15	12	
Molecular Subtype				
Luminal A		7	8	0.3416
Luminal B		8	8	
HER2			2	
N/A		3		

N/A – Not available

Since epinephrine binds to all ARs, the augmented levels of epinephrine in BC patients could affect BC cellular behavior. Thus, prior to *in vitro* functional studies, we proceeded to screen the expression of ARs in representative cell lines of primary and metastatic BC, MDA-231 and MDA-1833 respectively (Figure 1d). MDA-1833 are variants of the MDA-231 cell line that metastasize specifically to bone and were previously characterized [41]. Gene and protein expression of β_2 -AR in MDA-MB-231 and MDA-1833

cells showed that these cells predominantly express β_2 -AR and are therefore responsive to sympathetic stimuli (Figure 1e,f). Uncropped western blot can be found in Figure S4.

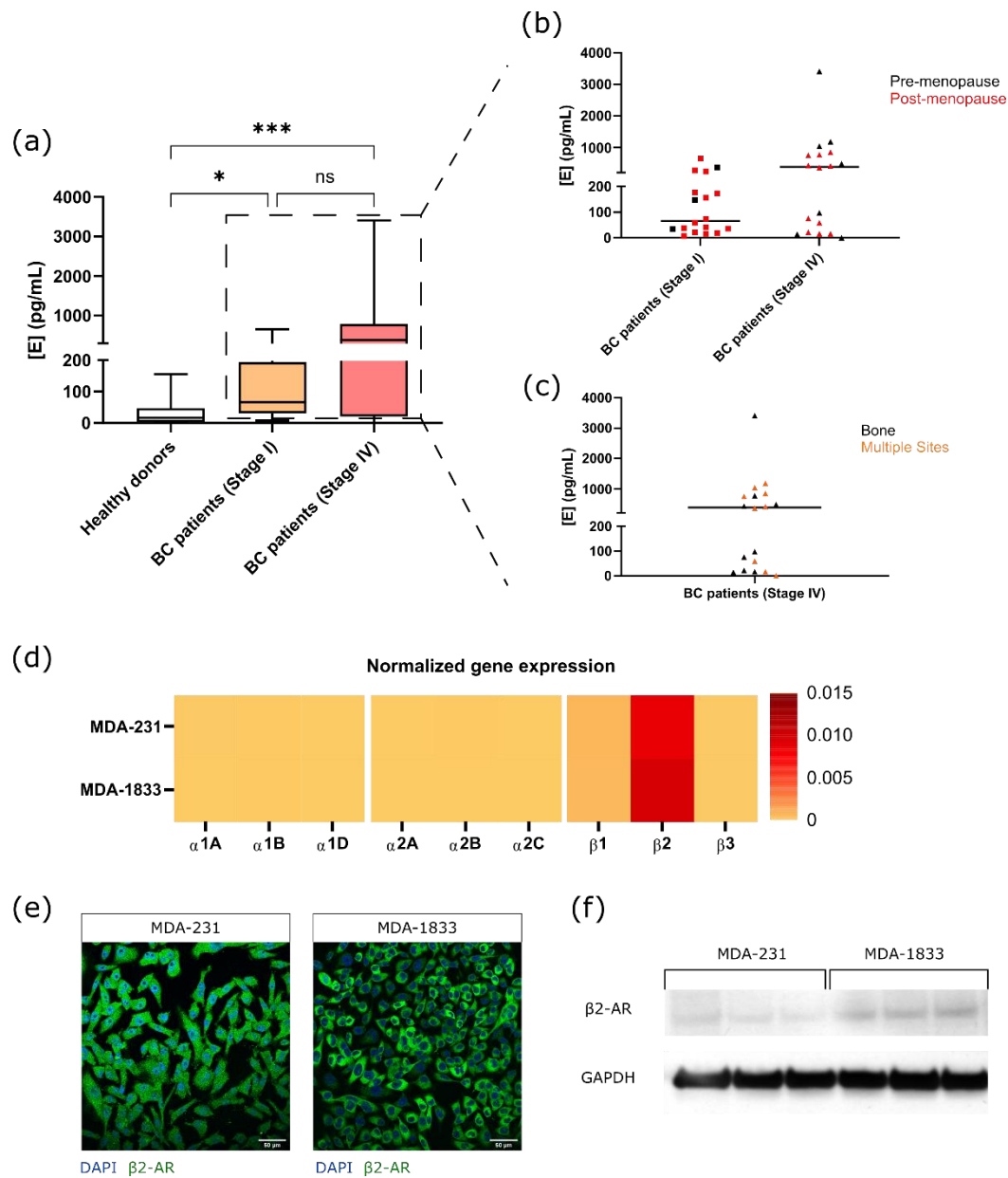


Figure 6. Adrenergic status of BC patients and cell lines. (a) Epinephrine plasma levels of BC patients. Data from 18 donors/patients for each condition is expressed as box-whiskers plot (Kruskal-Wallis test with Dunn's multiple comparison test, ns – non significant, * $p < 0.05$, *** $p < 0.001$). (b) Epinephrine plasma levels of BC patients clustered by menopausal state. Data is expressed as the median of individual data points. (c) Epinephrine plasma levels of stage IV BC patients clustered by distant metastasis sites. Data is expressed as the median of individual data points. (d) Normalized gene expression of ARs in primary MDA-231 and metastatic MDA-1833 cell lines performed

by real time PCR. (e) Representative micrograph of the expression of β_2 -AR on MDA-231 cells (left) and MDA-1833 cells (right) by immunocytochemistry. Nuclei – blue; β_2 -AR – green. Scale bar - 50 μ m. (f) Expression of β_2 -AR on MDA-231 and MDA-1833 cells by Western Blot. Original blot can be found in Figure S4.

3.2.3.2. β -AR signaling induces a shift in parental MDA-231 protein secretion towards osteoclastogenesis inhibition

BC cells were previously reported to induce changes in bone metabolism at a distance while still in the primary tumor site ^[4]. Thus, we asked whether β_2 -AR signaling could modulate BC protein expression and affect bone metabolism. Using a proteomic approach, we screened the secretome of MDA-231 treated with the β -AR agonist ISO and compared its proteomic profile with the one from MDA-231 treated with vehicle control (Figure 2a). We detected a total of 64 proteins with significant deregulated expression (28 of them were upregulated and 36 downregulated in ISO treated MDA-231 cells) (Figure 2b, Table S2). Gene ontology network analysis as well as ORA showed that deregulated proteins were significantly associated with biological processes involved in extracellular matrix remodeling (Figure 2c,d).

When analyzing the set of proteins identified, we found that known osteoclast inhibitors Stanniocalcin-1 (STC-1) ^[42] and Clusterin (Clu) ^[43] were upregulated in ISO treated MDA-231 cells. Conversely, osteoclastogenesis promoters cellular communication network 2 (CCN2) ^[44] and annexin II (ANXA2) ^[45] were downregulated with ISO treatment (Figure 2b). These results suggest that MDA-231 secretome under β -AR signaling might modulate osteoclastogenesis and could impact bone cell metabolism.

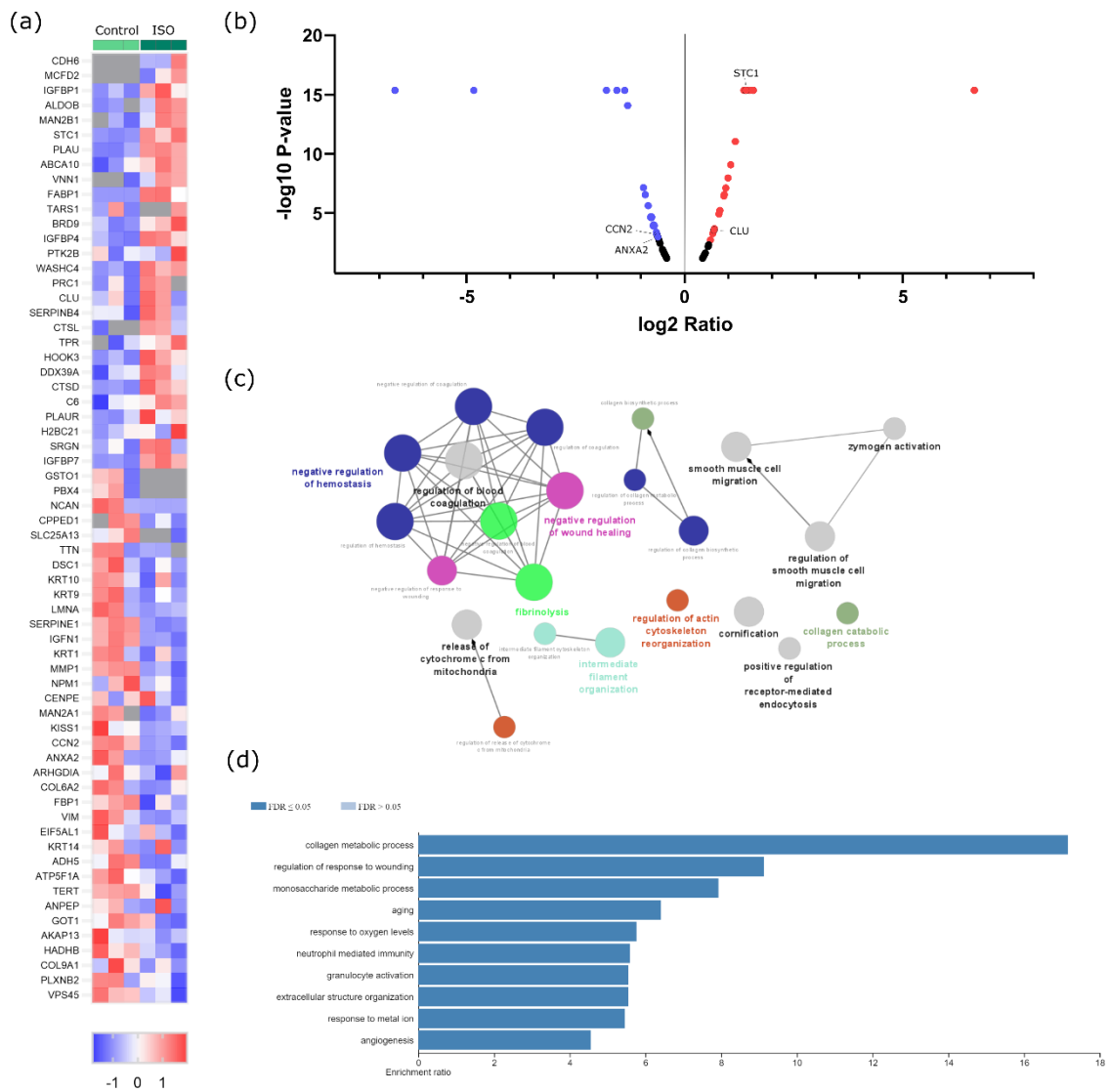


Figure 7. Proteomic screening of MDA-231 conditioned media under β_2 -AR activation. (a) Heatmap depiction of significantly deregulated proteins found in conditioned medium from control or ISO treated MDA-231 cells (Student-t test, $p \leq 0.05$). The ratio of protein abundances was color coded as shown in the legend. Data from three independent samples is shown, one sample per column. Gray cells represent proteins not detected in a particular sample. (b) Volcano plot distribution of significantly deregulated proteins. The ratio between protein abundances between MDA-231 cells treated with ISO and control samples is plotted on the X axis, and p-value is plotted on the Y axis. Red dots represent proteins with a fold change ≥ 1.5 , while purple dots represent proteins with a fold change ≤ -1.5 . (c) Gene ontology biological processes network analysis of differentially expressed proteins in ISO treated MDA-231 cells. Only networks with $p \leq 0.05$ were shown (Two sided hypergeometric test and Bonferoni step down correction). Different colors illustrate different biological processes while the size of the nodes is proportional to the statistical significance of each process. (d) Significantly

enriched biological process terms in the group of deregulated proteins in ISO treated MDA-231 cells. ORA was used and only processes with false discovery rate of ≤ 0.05 were shown.

3.2.3.3. Secretome from primary MDA-231 cells under β_2 -AR activation impairs osteoclast differentiation and resorption activity

Since the expression of proteins known to be involved in bone metabolism was modulated after β -AR activation, we next proceeded to verify if the changes in proteomic profile translated into functional significance.

3.2.3.3.1. *Osteoclast monocultures*

First, in order to ascertain the effect of MDA-231 secretome on osteoclast differentiation, human pre-osteoclasts were incubated with the secretome of MDA-231 cells. Human mature osteoclast number and area were then quantified (Figure 3a). Consistent with the proteomic screening results, the secretome of MDA-231 cells treated with ISO led to a significant decrease in osteoclast numbers (cells with more than 3 nuclei) when compared to controls (Figure 3b,c). β_2 -AR signaling was directly implicated in the observed effect since osteoclast numbers were no different from controls when ICI, a specific β_2 -AR antagonist, was added to MDA-231 together with ISO (Figure 3b,c). Coherent with the osteoclast differentiation quantification, osteoclast specific cathepsin K gene expression followed the same profile after stimulation with ISO treated MDA-231 secretome (Figure S5). On the other hand, when comparing the area of osteoclasts in the different conditions, no differences were observed (Figure 3d).

Since BC secretome could also directly affect the resorption activity of osteoclasts after they are matured and fully functional, we proceeded to incubate mature osteoclasts with MDA-231 secretome and quantified the extent of bone resorption in the absence of RANKL (Figure 3e). Similarly to the osteoclastogenesis assays, we observed a significant decrease in resorption activity when osteoclasts were incubated with the secretome from MDA-231 cells treated with ISO (Figure 3f,g). This effect was mediated by β_2 -AR since the addition of ICI abrogated this effect. Osteoclasts are able to resorb the bone surface through two characteristic modes of resorption: they resorb the bone while being static or while moving through the surface of the bone, generating resorption pits or trenches, respectively ^[46]. Resorption trench mode is inherently faster and favors bone fragility ^[30], and therefore differences in trench content could reflect changes in osteoclast aggressiveness. No significant differences were found in trench resorption content when comparing between conditions (Figure 3h). The observed decrease in total

resorption was partially due to changes in TRAcP activity, an osteoclast-specific enzyme involved in collagenolysis (Figure 3i).

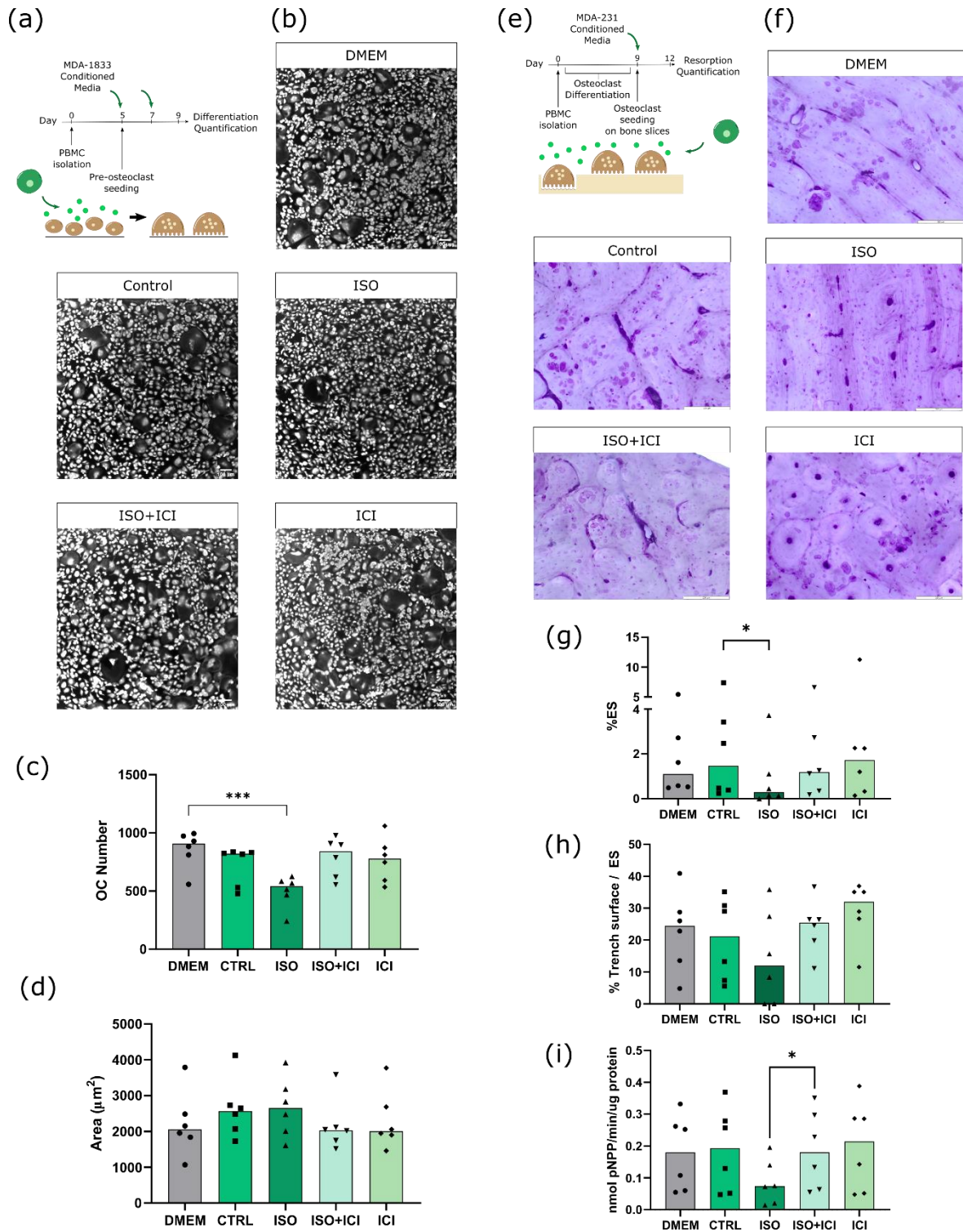


Figure 8. Effect of MDA-231 conditioned medium on osteoclast differentiation and resorption activity. (a) Timeline of the osteoclast differentiation assay. Pre-osteoclasts are seeded after five days of culture and stimulated with MDA-231 cell conditioned media for four more days, changing the media at day 7. (b) Representative micrographs of

differentiated osteoclasts stained with HCS CellMask Deep Red Stain. Scale bar – 100 μm . (c) Osteoclast number and (d) area after four days of MDA-231 conditioned media stimulation. Osteoclasts with three or more nuclei were included in the analysis. Data is expressed as median of individual data points from 6 independent experiments (Friedman's test followed by Dunn's multiple comparisons test, *** $p \leq 0.001$). (e) Timeline of the resorption assay. Osteoclasts are differentiated for nine days and seeded on top of bone slices, followed by incubation with MDA-231 cell conditioned medium for another three days. (f) Representative micrographs of the surface of bone slices after three days of resorption. Scale bar - 200 μm . (g) Estimated percentage of eroded surface, (h) trench percentage per total eroded surface and (i) TRAcP activity quantified at the end of the experiment. Data is expressed as median of individual data points from 6 independent experiments (Friedman's test followed by Dunn's multiple comparisons test, * $p \leq 0.05$).

3.2.3.3.2. *Osteoblast-osteoclast co-cultures*

In the bone microenvironment, osteoclasts receive input from neighboring osteoblasts that promote osteoclast differentiation and activation. Aiming to replicate this interaction, a co-culture of mature human osteoclasts and human osteoblasts was established. Osteoblasts were positive for the osteoblast marker alkaline phosphatase (ALP) and several calcium deposits were observed by alizarin red staining after 14 days of culture (Figure S6). We confirmed that these cells expressed RANKL and were able to increase osteoclast resorption activity in several independent experiments (Figure S6). Osteoclast and osteoblast co-cultures were exposed to the secretome from ISO treated MDA-231 cells and bone resorption activity was evaluated (Figure 4a). Contrarily to what was observed in osteoclast monocultures, no statistically significant differences were observed between conditions in total resorption activity (Figure 4b,c), trench percentage (Figure 4d) and also TRAcP activity (Figure 4e). Therefore, our results suggest that the supply of RANKL by osteoblasts in the co-culture model rescued the resorption activity of osteoclasts.

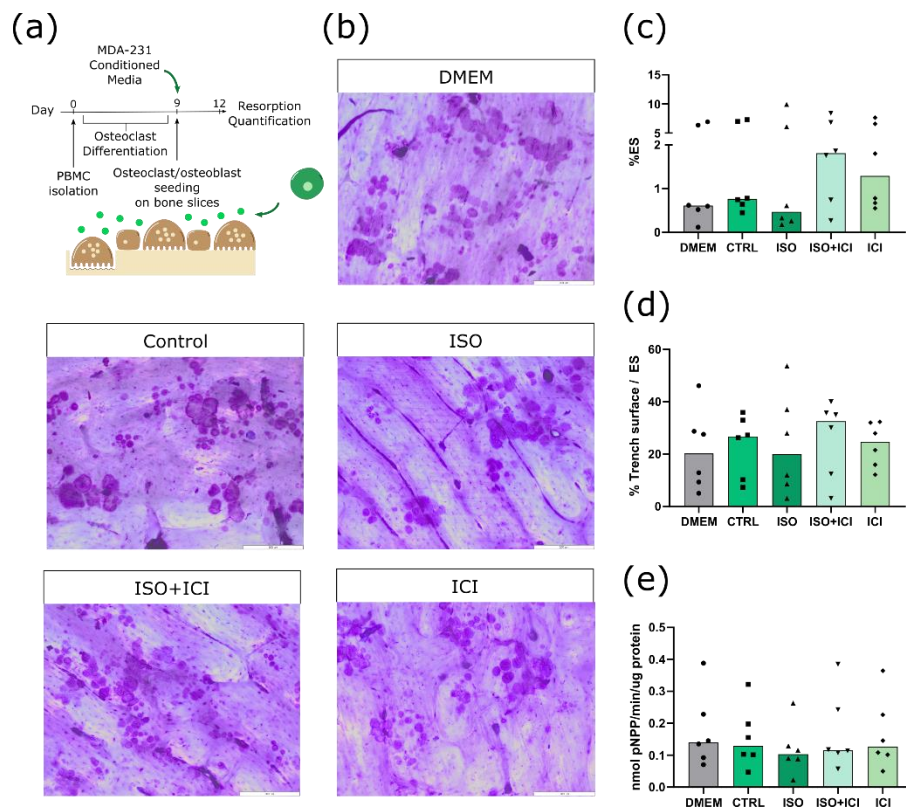


Figure 9. Effect of MDA-231 secretome on osteoclast/osteoblast co-culture. (a) Timeline of the resorption assay in a co-culture setting. Mature osteoclasts were seeded with osteoblasts and exposed to MDA-231 conditioned media for three days. (b) Representative micrographs of the surface of bone slices after three days of resorption in co-cultures. Scale bar - 200 μ m. (c) Estimated percentage of eroded surface, (d) trench percentage per total eroded surface and (e) TRAcP activity quantified at the end of the co-culture experiment. Data is expressed as median of individual data points from 6 independent experiments (Friedman's test followed by Dunn's multiple comparisons test, * $p \leq 0.05$).

3.2.3.4. Secretome of bone tropic MDA-1833 under β 2-AR activation does not affect human osteoclast differentiation and resorption activity

Bone is a highly innervated tissue and sympathetic neurons are found across the periosteum and around blood vessels in the bone marrow [47]. In addition, bone marrow resident cells were reported to express tyrosine hydroxylase (TH) and synthesize catecholamines [48, 49]. Therefore, in addition to the increased epinephrine levels in the plasma of metastatic BC patients, local production of catecholamines might also contribute to the development of metastatic foci during BC bone metastasis. It is then of

crucial importance to understand how the adrenergic signaling modulates the bone metastatic niche.

3.2.3.4.1. *Osteoclast monocultures*

During the course of extravasation and metastasis, BC cells acquire a set of characteristics that differ from the primary tumor. In order to ascertain whether bone tropic cells elicit different outcomes in osteoclast differentiation than its parental counterpart, pre-osteoclasts were exposed to β_2 -AR primed MDA-1833 secretome in a similar experimental layout as previously done with MDA-231 cells (Figure 5a). Contrarily to the effect of MDA-231 cells, secretome from ISO treated MDA-1833 cells did not affect the number of osteoclasts nor osteoclast area (Figure 5b,c,d).

Following the same reasoning as in MDA-231 secretome experiments, we proceeded to quantify mature osteoclast resorption activity under the effect of MDA-1833 secretome instead (Figure 5e). No differences were observed in the percentage of eroded surface when comparing the effect of ISO treated MDA-1833 secretome with respective controls (Figure 5f,g). However, ISO treated MDA-1833 secretome significantly blunted the ability of osteoclasts to resorb in trench mode in a β_2 -AR dependent fashion (Figure 5h). Nonetheless, this was not due to changes in osteoclastic TRAcP activity since no significant differences were found between conditions (Figure 5i).

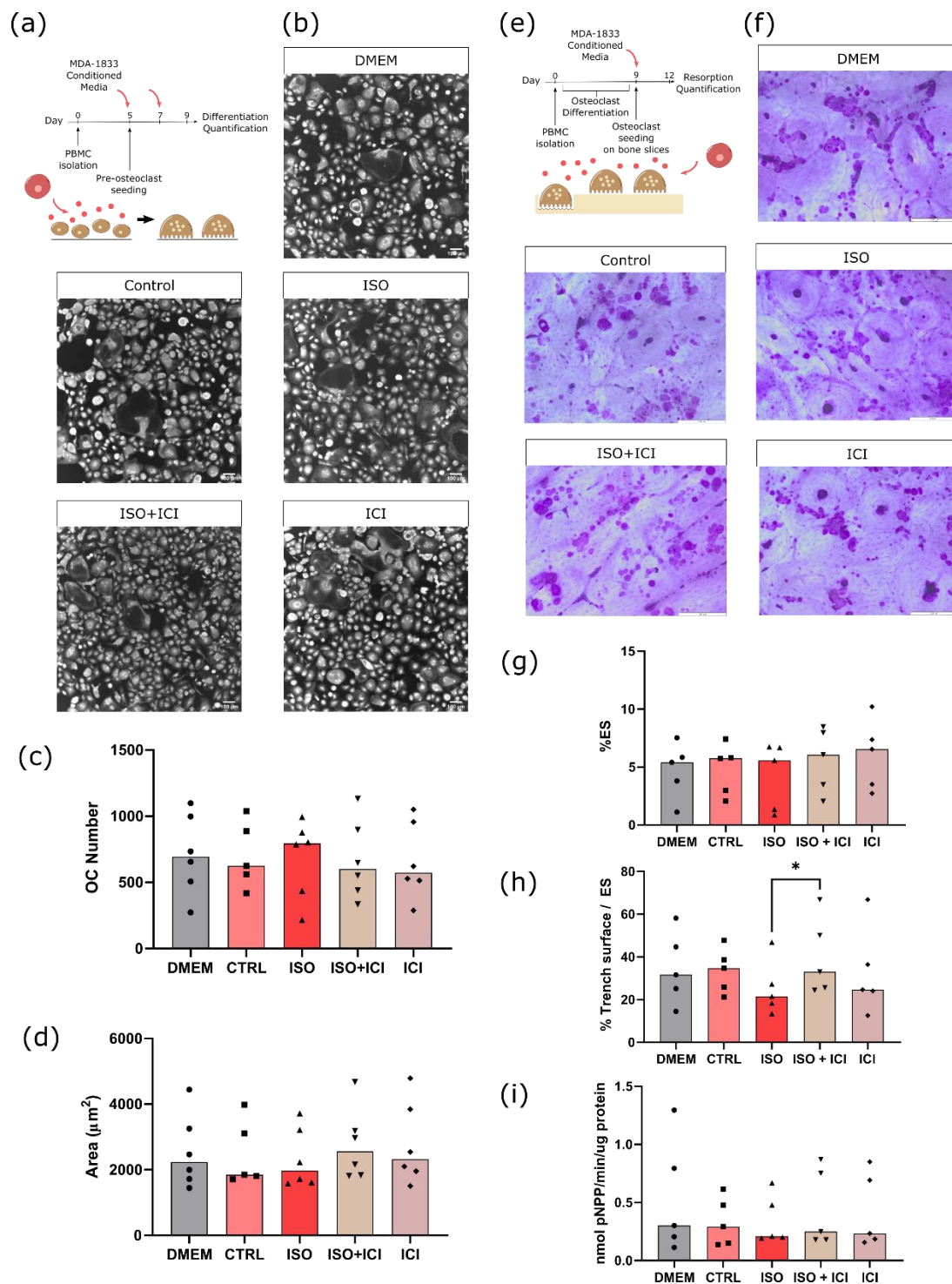


Figure 10. Effect of MDA-1833 conditioned medium on osteoclast differentiation and resorption activity. (a) Timeline of the osteoclast differentiation assay. Pre-osteoclasts are seeded after five days of culture and stimulated with MDA-1833 cell secretome for four more days, refreshing the media at day 7. (b) Representative micrographs of differentiated osteoclasts stained with HCS CellMask Deep Red Stain. Scale bar – 100 µm. (c) Osteoclast number and (d) area after four days of MDA-1833 secretome stimulation. Osteoclasts with three or more nuclei were included in the analysis. Data is

expressed as median of individual data points from 6 independent experiments (Kruskal-Wallis test). One data point from the CTRL condition was excluded due to a technical error. (e) Timeline of the resorption assay. Osteoclasts are differentiated for nine days and seeded on top of bone slices, followed by incubation with MDA-1833 cell secretome for another three days. (f) Representative micrographs of the surface of bone slices after three days of resorption. Scale bar - 200 μ m. (g) Estimated percentage of eroded surface, (h) trench percentage per total eroded surface and (i) TRAcP activity quantified at the end of the experiment. Data is expressed as median of individual data points from 5 independent experiments (Friedman's test followed by Dunn's multiple comparisons test, * $p \leq 0.05$).

3.2.3.4.2. *Osteoblast-osteoclast co-cultures*

Our findings show that the secretome of MDA-1833 under β_2 -AR activation did not significantly impact human osteoclast differentiation, although we could observe changes in trench resorption events. We then asked if RANKL producing osteoblasts would change the dynamic of the interaction between MDA-1833 conditioned medium and osteoclasts (Figure 6a). Similarly to osteoclast monocultures, conditioned medium from ISO treated MDA-1833 did not induce changes in osteoclast resorption activity in a osteoblast/osteoclast co-culture setting (Figure 6b,c). However, osteoblasts rescued the normal trench forming ability of osteoclasts since no changes in trench percentage were observed when ISO treated MDA-1833 secretome was used in a co-culture setting (Figure 6d). Furthermore, similarly to osteoclast monocultures, no significant differences in TRAcP activity were observed at the end of the experiment (Figure 6e).

In conclusion, secretome from MDA-1833 cells under β_2 -AR activity led to a decreased osteoclast aggressiveness evidenced by a reduction in trench resorption percentage but not in terms of total area of resorption events. This was only seen in osteoclast monocultures, since in presence of osteoblasts no differences were observed. Furthermore, MDA-1833 secretome did not affect osteoclast differentiation.

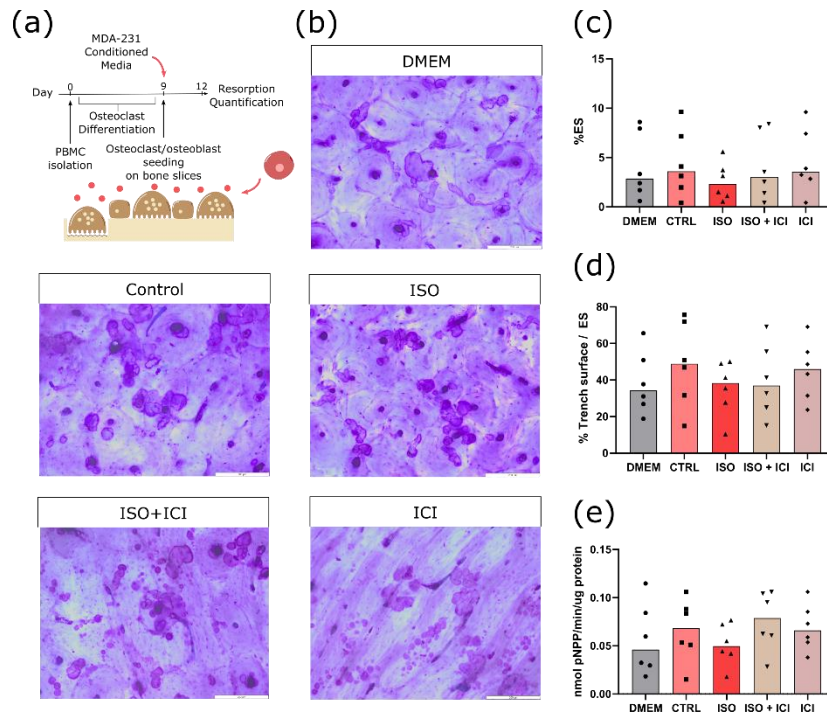


Figure 11. Effect of MDA-1833 secretome on osteoclast/osteoblast co-cultures. (a) Timeline of the resorption assay in a co-culture setting. Mature osteoclasts were seeded with osteoblasts and exposed to MDA-1833 conditioned media for three days. (b) Representative micrographs of the surface of bone slices after three days of resorption in co-cultures. Scale bar - 200 μ m. (c) Estimated percentage of eroded surface, (d) trench percentage per total eroded surface and (e) TRAcP activity quantified at the end of the co-culture experiment. Data is expressed as median of individual data points from 6 independent experiments (Friedman's test).

3.2.3.5. Bone tropic MDA-1833 and its parental counterpart MDA-231 express different levels of osteoclastogenic factors under β_2 -AR activation

Functional studies on osteoclast activity showed that, contrarily to the parental MDA-231 cells, bone tropic MDA-1833 cells do not impair osteoclast differentiation and activity. In order to understand what was driving these different outcomes, we first asked what were the main differences between both cell lines regarding protein expression under β_2 -AR activation. Proteomic screening of ISO treated MDA-1833 secretome was performed and compared to the secretome from ISO treated MDA-231 cell lines (Figure 7a,b). 69 proteins were significantly deregulated between ISO treated MDA-1833 and MDA-231 cell lines (31 upregulated and 38 downregulated proteins in ISO treated MDA-1833) (Figure 7c, Table S3). Of note, the proteins identified in proteomic analysis of ISO treated

MDA-231 cells STC-1 and CCN2 were also differentially expressed between ISO treated MDA-1833 and ISO treated MDA-231 secretome. In addition, insulin-like growth factor binding protein 7 (IGFBP7) and cystatin C (CST3), proteins previously described to inhibit osteoclastogenesis ^[50, 51], were downregulated in MDA-1833 samples. These results are consistent with the previous functional assays and emphasize the differential response to β_2 -AR signaling in the parental cell line MDA-231 and the bone tropic cell line MDA-1833. Furthermore, proteins that were differentially expressed in parental and bone tropic BC cell lines under β_2 -AR signaling were associated to biological processes such as platelet degranulation, extracellular structure organization and immune modulation (Figure 7d,e).

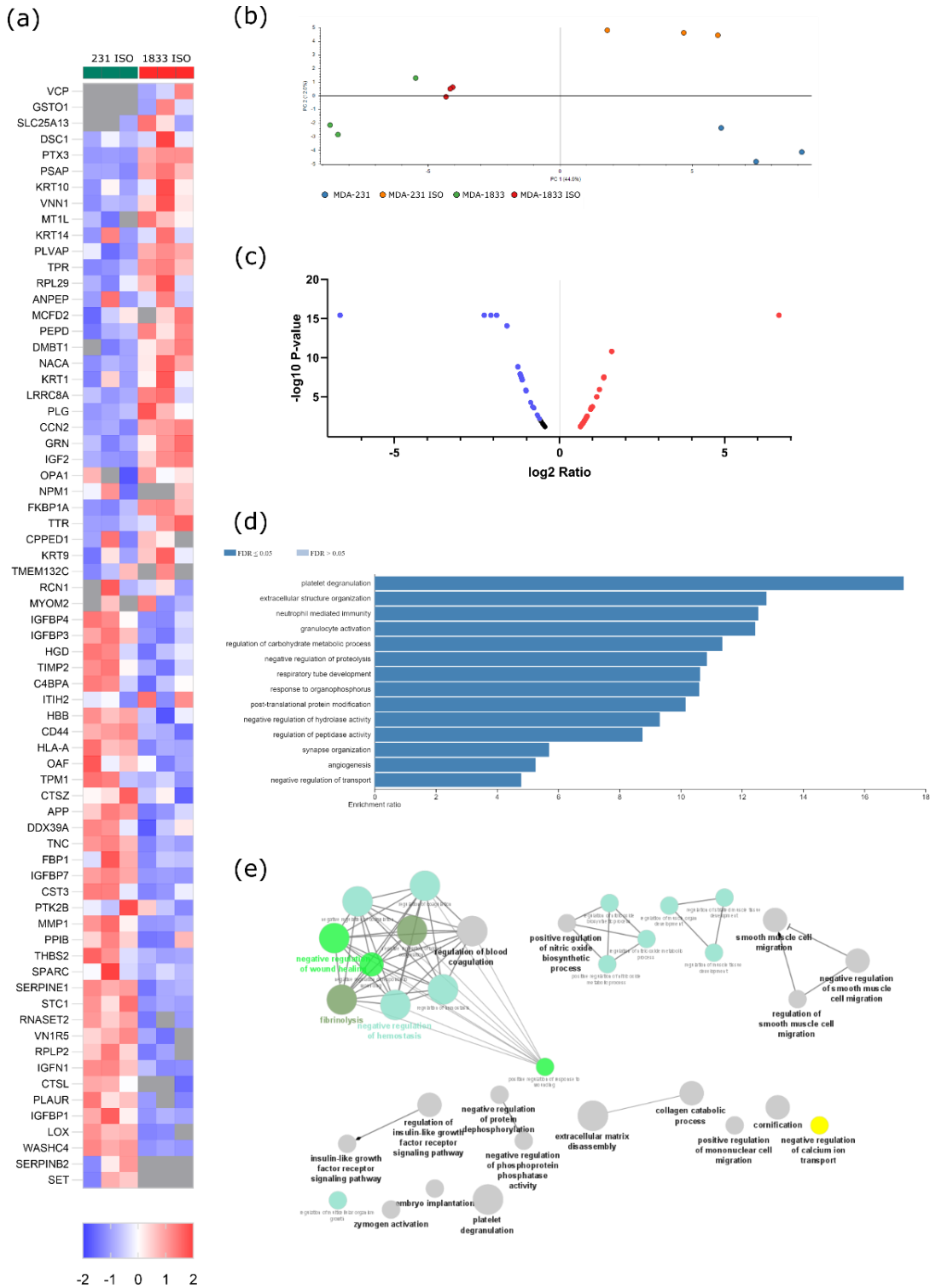


Figure 12. β_2 -AR signaling leads to different outcomes in parental MDA-231 or bone tropic MDA-1833 cells. (a) Heatmap depiction of significantly deregulated proteins found in conditioned medium from control or ISO treated MDA-231 and MDA -1833 cells (Student-t test, $p \leq 0.05$). The ratio of protein abundances was color coded as shown in the legend. Data from three independent samples is shown, one sample per column.

Gray cells represent proteins not detected in a particular sample. (b) PCA of deregulated proteins between MDA-231 and MDA-1833, both in control and ISO treated conditions. (c) Volcano plot distribution of significantly deregulated proteins in ISO treated MDA-1833 and ISO treated MDA-231 samples. The ratio between protein abundances between ISO MDA-1833 cells and ISO MDA-231 cells is plotted on the X axis, and p-value is plotted on the Y axis. Red dots represent proteins with a fold change ≤ 1.5 , while purple dots represent proteins with a fold change ≤ -1.5 . (d) Significantly enriched biological process terms in the group of deregulated proteins in ISO treated MDA-1833 and ISO treated MDA-231 cells. ORA was used and only processes with false discovery rate of ≤ 0.05 were shown. (e) Gene ontology biological processes network analysis of differentially expressed proteins in ISO treated MDA-1833 and ISO treated MDA-231 cells. Only networks with $p \leq 0.05$ were shown (Two sided hypergeometric test and Bonferoni step down correction).

3.2.4. Discussion

Metastatic dissemination of BC cells from the primary tumor to distant sites is the main cause of death of BC patients, being the bone the most common site of metastasis. Potential benefits of β 2-AR targeting were pointed out by several pre-clinical and epidemiological studies [6, 23, 52], but other epidemiological studies report no such benefits in larger patient cohorts [26-28]. Therefore, the effects of adrenergic signaling on BC are still controversial. In this study, using a combination of clinical data, proteomic screening and *in vitro* functional assays with human primary cells, we investigated the effect of sympathetic signaling in the crosstalk taking place between either parental or metastatic BC cells and bone cells.

Increased sympathetic tone in circulation is frequent in several types of cancers such as gastric and head and neck cancers [16, 17], and is also described in common surgical procedures during BC treatment [53]. Plasma catecholamine concentration was previously correlated with the occurrence of pain and depression symptoms in BC patients [54], and in turn depression was shown to promote prostate cancer metastasis [55]. Similarly, we observed augmented levels of epinephrine both in primary and advanced BC patients, pointing towards sympathetic modulation of BC during the course of the disease.

Some limitations apply to our clinical study. Age-specific differences between groups cannot be excluded since primary BC patients were significantly older than advanced BC patients and healthy donors. Furthermore, access to patient medication and co-

morbidities at the time of diagnosis and blood collection was limited, and obesity and diabetes as well as the intake of antihypertensive, analgesic or anxiolytic drugs could affect catecholamine synthesis or release into the circulation^[56-60]. These limitations could be addressed in a larger, randomized clinical trial with patients matched for comorbidities and treatment regimens.

The increased epinephrine content during BC establishment and progression that we observed highlight the need of a better understanding on the role of the SNS activity in BC progression and bone metastasis. In particular, β_2 -AR signaling was reported to be the major contributor for BC metastasis in *in vivo* models of chronic stress and SNS hyperactivity^[6, 61, 62]. Therefore, we focused on high β_2 -AR expressing parental MDA-231 and bone tropic MDA-1833 cells to further explore the β_2 -AR signaling pathway in a bone metastatic context.

We showed that the secretome of MDA-231 cells exhibits significant differences in terms of protein expression after activation of β_2 -AR signaling. In particular, STC-1 and Clu were upregulated in the MDA-231 secretome under sympathetic signaling. STC-1 is a known osteoclast inhibitor since transgenic mice expressing STC-1 under a muscle-specific promoter display increased cortical and trabecular bone thickness concomitant with a decreased osteoclast activity^[42]. Furthermore, STC-1 was shown to be directly involved in murine osteoclastogenesis suppression *in vitro*^[63]. Similarly, secreted Clu was shown to hamper osteoclastogenesis in murine osteoclast precursors^[43]. The upregulation of osteoclast inhibitors in MDA-231 secretome was consistent with the observed decrease in human osteoclast differentiation and bone matrix resorption activity in our model, in up to 6 independent osteoclast donors with blinded or unsupervised analysis. However, the crosstalk of osteoclast with human osteoblasts mitigated this effect. In contrast, paracrine signaling from metastatic MDA-1833 had no effect either on osteoclast monocultures or in co-culture with osteoblasts. Given that osteoclast differentiation and activity is tightly regulated by osteoblasts in the bone niche, our results suggest that sympathetic modulation of BC paracrine signaling does not affect osteoclast bone resorption activity and we would expect no differences of bone turnover in BC patients. Our findings are in agreement with a recent study by Chiou *et al*, where the authors demonstrate that injection of MDA-MB-231 secretome in immunocompromised mice led to increased bone formation in the pre-metastatic bone niche, with no changes in osteoclast activity^[5]. This altered bone matrix deposition could facilitate BC extravasation into the bone niche prior to metastatic foci establishment^[5]. However, we did not recapitulate the observations from previous studies that show modulation of bone resorption activity by BC cells, even before metastatic spread has occurred^[4, 64]. This might be an acceptable outcome in primary BC patients with no major

alteration in bone turnover, however it is paradoxical in stage IV metastatic BC patients that exhibit metastatic bone foci and extensive bone lesions. Moreover, previous studies indicate an exacerbation in bone destruction after β_2 -AR agonism, in immunosuppressed mice models of breast cancer bone metastasis as well as mice *in vivo* and *in vitro* models of pharmacological activation of β_2 -AR [6, 65-67]. Despite the fact that our findings are not aligned with these studies, species related differences in bone cell metabolism could explain the observed differences. It is widely accepted that BC secretome increase osteoclast differentiation and resorption in experiments using cells from mice [64, 68-71]. In contrast, the results obtained from experiments with human cells are not so homogeneous, with some studies reporting increases in osteoclastogenesis [68, 72] while others show decreased resorption activity [73]. Additional evidence of distinct outcomes in human and mouse cells arise from the observation that there is a significant increase in RANKL promoter activation in murine bone marrow stromal cells after exposure to paracrine signaling from BC cells (Figure S7). When assessing osteoclast activity in our model of human osteoblast/osteoclast co-cultures, no differences were observed in terms of matrix degradation after incubation with BC secretome. Furthermore, although sympathetic activation was reported to directly increase osteoclastogenesis in murine *in vitro* models [74, 75], no alterations in differentiation and resorption activity were apparent after daily activation of β_2 -AR in human osteoclasts/osteoblasts (Figure S8). Again, direct β_2 -AR stimulation in murine bone marrow stromal cells translated into increased RANKL promoter activation, while no differences were observed in human osteoblast RANKL production (Figure S9). To our knowledge, we are the first to describe the effect of BC paracrine signaling on human osteoclast activity under β_2 -AR agonism *in vitro*, and therefore species related differences should be accounted for when comparing with *in vivo* studies.

The bone metastatic niche is composed of multiple cell types that can contribute to the establishment of osteolytic bone metastasis [12]. We observed consistent and robust decrease of osteoclast differentiation and activity after incubation with conditioned medium from MDA-231 cells under β_2 -AR signaling. The inclusion of other cellular players such as cancer associated fibroblasts [76], endothelial cells [7] and a functional immune system [77] could change the dynamic of SNS activation in the bone metastatic niche. In addition, osteocytes account for the majority of osteoblast-lineage cells in bone and osteocyte-like cell lines were already described to increase osteolytic output in response to SNS activation [78]. Future studies should be conducted to analyze the contribution of other cell types in the dynamics of SNS modulation of BC bone metastasis. Furthermore, syngeneic *in vivo* BC models with immunocompetent mice could be used to address sympathetic modulation of the bone niche during metastasis,

in opposition to xenograft studies in nude mice that do not account for the contribution of immune cells.

The importance of these interactions is further highlighted by the anatomical proximity of sympathetic neurons and cells from the bone niche, which is expected to be translated into functional significance *in vivo*^[79]. However, norepinephrine is the main catecholamine released by sympathetic neuronal terminals, and although we show increased epinephrine concentration in the plasma of BC patients, no data is available on the local concentration of catecholamines at the bone niche. Since previous studies have shown that circulating epinephrine is dispensable for metastatic progression of BC *in vivo*^[80], it would be interesting to know how the local concentration of norepinephrine changes at the metastatic bone niche.

Proteomic screening identified multiple differentially expressed proteins between MDA-231 and MDA-1833 cells, similarly to what is described in other previous proteomic analysis studies^[81, 82]. In addition, β_2 -AR activation of osteoclast STC-1 upregulation and CCN2 downregulation were already described in parental MDA-231 cell lines stimulated with ISO^[83]. Interestingly, β_2 -AR signaling pathway activation leads to distinct outcomes in protein expression when comparing parental and bone tropic BC cell lines. Consistent with the downregulation of several proteins such as STC-1, IGFBP7 and CST3, MDA-1833 paracrine signaling did not decrease osteoclast differentiation and resorption activity of osteoclasts. These results are also coherent with previous reports that show that IGFBP7 expression was downregulated in human metastatic breast cancer tumors when compared to its matched primary tumors and were also implicated in decreased tumor growth *in vivo*^[84]. In addition, IGFBP7 was shown to impair murine osteoclastogenesis *in vitro* and *in vivo*^[50]. Furthermore, CST3 is a known inhibitor of osteoclastogenesis^[51] and its downregulation was previously correlated with BC aggressiveness and poor prognosis^[85]. These observations suggest that, under high sympathetic activity, the capacity of BC cell lines to modulate osteoclast activity is altered when they acquire metastatic traits, since bone tropic MDA-1833 paracrine signaling does not elicit osteoclast bone resorption impairment towards osteoclast bone resorption than parental MDA-231 cells in our model. Similar adaptations are found in brain metastatic cell lines, where BC cells become able to interact with their surrounding tissue that is inherently different from the primary tumor site^[86, 87]. Together with data from other studies that show an increased migratory capacity of metastatic BC cell lines after β_2 -AR agonism^[88], our observations point to distinct β_2 -AR downstream effectors in bone tropic cells that could putatively facilitate colonization of the bone microenvironment under high sympathetic input when compared to its parental cell line. Careful consideration must therefore be employed when designing therapeutic interventions, since we show that

both epinephrine concentration in the plasma of BC patients and BC cell response to β_2 -AR agonists changes during disease progression.

3.3. Comparison of the proteomic profile of primary and metastatic BC

At the primary site, BC cells are exposed to a multitude of biochemical and biophysical stimuli from neighboring cells and tissue ECM that trigger multiple signaling pathways, ultimately promoting proliferation, resistance to apoptosis, migration and escape from immune surveillance. Eventually, BC cells acquire a plethora of characteristic traits that allow them to egress from the primary tumor site into the circulatory system, from which they spread to distant sites of metastasis. Primary and metastatic BC are inherently different, but the complete picture on the protein expression changes that take place during metastatic trait acquisition is still missing.

In order to understand how the secretome of BC changes during metastasis, we compared the proteomic profile of primary MDA-231 and metastatic MDA-1833 BC cells, in control conditions without prior stimuli (Figure 8a). A total of 84 proteins were significantly deregulated when comparing the secretome of MDA-231 and MDA-1833 cell lines (36 upregulated and 48 downregulated proteins in the secretome of control MDA-1833 cells) (Figure 8b, Table S4). Furthermore, proteins differentially expressed in parental MDA-231 or bone tropic MDA-1833 cells were associated to biological processes such as platelet degranulation, post translational protein modification and immune modulation (Figure 8c,d).

Similarly to what was observed after ISO treatment, we observed increased levels of osteoclast inhibitors Clu, STC-1, IGFBP7 and CST3 in the secretome of control MDA-231 cells when compared to the secretome of MDA-1833 cells. In addition, Pentraxin 3 (PTX3) was significantly upregulated in metastatic MDA-1833 cells, which was already previously described to promote RANKL secretion in murine osteoblasts and subsequently promote osteoclastogenesis^[89]. Of note, LOX was exclusively produced in primary BC and was not detected in the secretome of metastatic MDA-1833. Primary tumor produced LOX was demonstrated to be crucial in the conditioning of the bone niche, facilitating pre-metastatic lesion formation and BC colonization of the bone^[4]. Interestingly, we show that BC cells stop expressing LOX after bone colonization, suggesting that LOX is primarily involved in the modulation of the bone metabolism at earlier stages of BC progression.

The upregulation of osteoclast inhibitors in primary MDA-231 cells would suggest that its secretome would be detrimental to osteoclast differentiation and resorption when compared to metastatic MDA-1833. However, osteoclast exposure to the secretome of MDA-231 and MDA-1833 in control conditions did not translate into altered osteoclast activity, either in mono-culture or in co-culture with osteoblasts (Figure 3-6). Our findings

suggest that the secretome from BC cells is not sufficient to exacerbate osteoclast activity, even in the presence of RANKL expressing osteoblasts. Further research on the contribution of other cellular players in the bone niche, as well as the role of BC direct cell-cell signaling, is required to better understand the establishment and exacerbation of the metastatic vicious cycle of bone degradation.

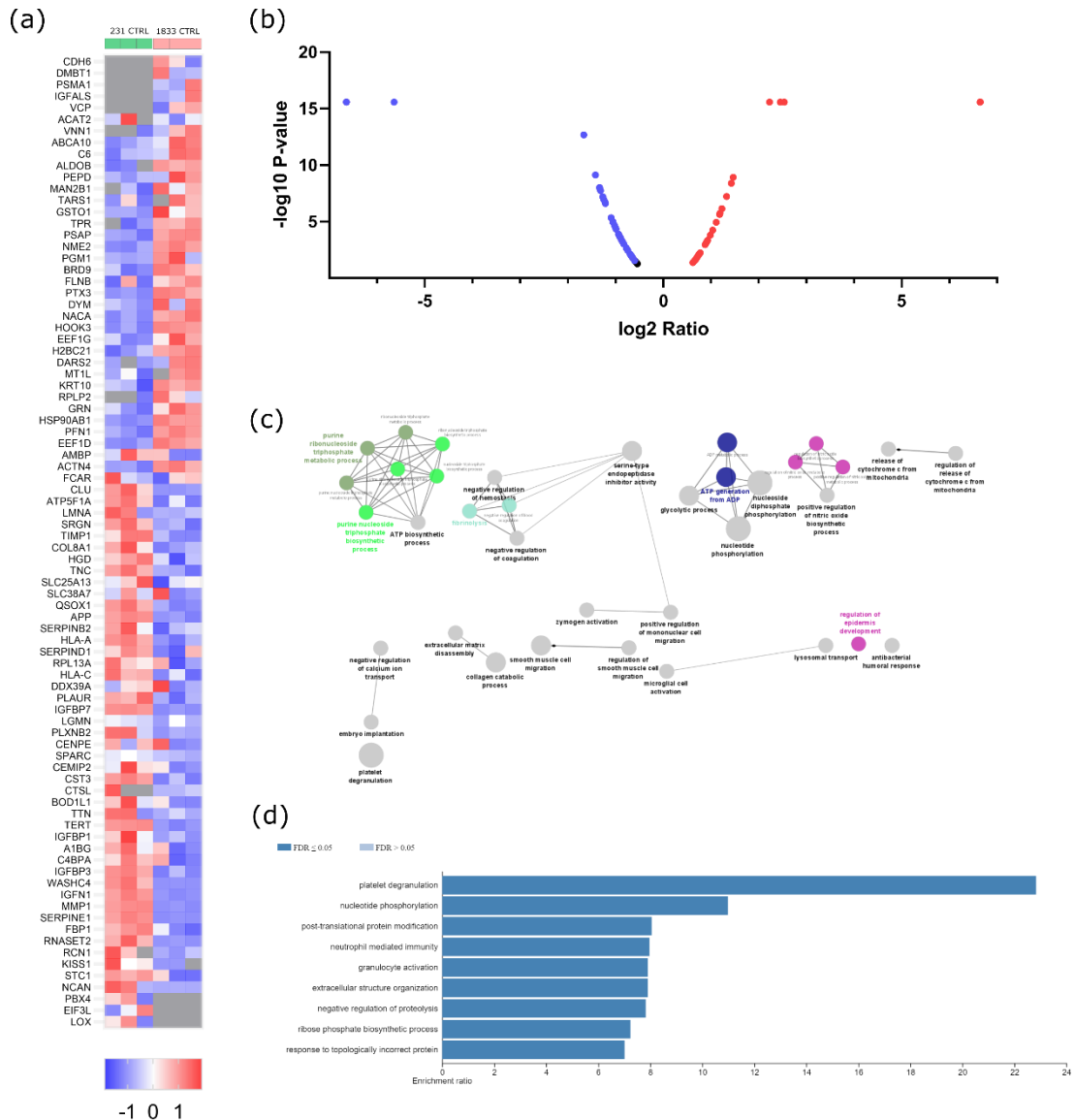


Figure 13. Metastatic trait acquisition leads to a differential proteomic profile. (a) Heatmap depiction of significantly deregulated proteins found in the secretome from control MDA-1833 and MDA-231 cells (Student-t test, $p \leq 0.05$). The ratio of protein abundances was color coded as shown in the legend. Data from three independent samples is shown, one sample per column. Gray cells represent proteins not detected in a particular sample. (b) Volcano plot distribution of significantly deregulated proteins in control MDA-1833 and MDA-231 samples. The ratio between protein abundances between MDA-1833 cells and MDA-231 cells is plotted on the X axis, and p-value is

plotted on the Y axis. Red dots represent proteins with a fold change ≤ 1.5 , while purple dots represent proteins with a fold change ≤ -1.5 . (c) Gene ontology biological processes network analysis of differentially expressed proteins in ISO treated MDA-1833 and ISO treated MDA-231 cells. Only networks with $p \leq 0.05$ were shown (Two sided hypergeometric test and Bonferoni step down correction).

(d) Significantly enriched biological process terms in the group of deregulated proteins in ISO treated MDA-1833 and ISO treated MDA-231 cells. ORA was used and only processes with false discovery rate of ≤ 0.05 were shown.

Supplementary Data

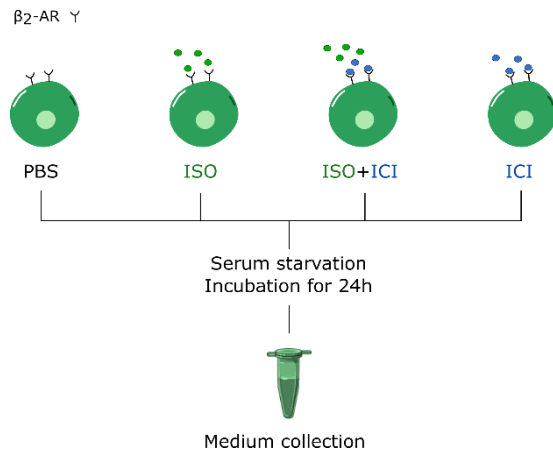


Figure S6. Conditioned medium collection from BC cell lines. β_2 -AR expressing cell lines were incubated with either PBS, 1 μ M ISO (Green dots), 1 μ M ISO + 1 μ M ICI or 1 μ M ICI (Blue dots). Incubation was performed in reduced serum conditions for 24h, after which medium was collected and centrifuged.

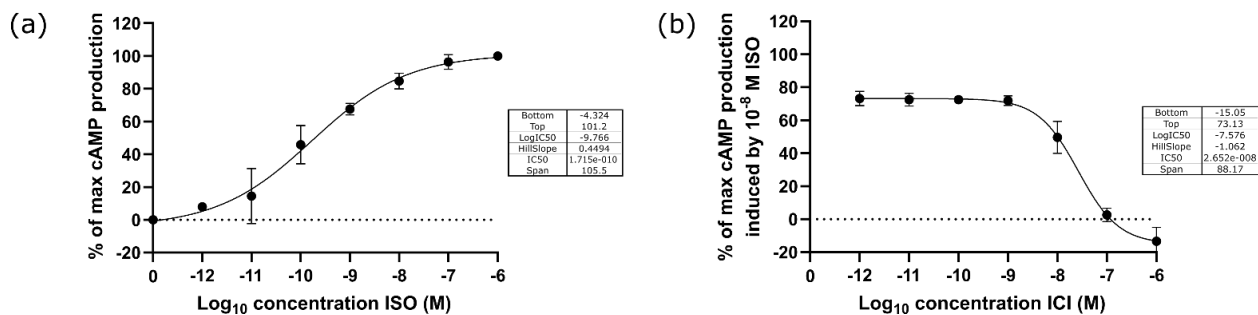


Figure S7. cAMP accumulation after ISO incubation in β_2 -AR expressing COS-7 cell lines. (a) ISO incubation leads to a dose-dependent accumulation of intracellular cAMP, peaking at a concentration of 10^{-6} M. (b) The addition of ICI before and simultaneously to ISO inhibits the accumulation of cAMP, completely abrogating cAMP accumulation at a concentration of 10^{-6} M.

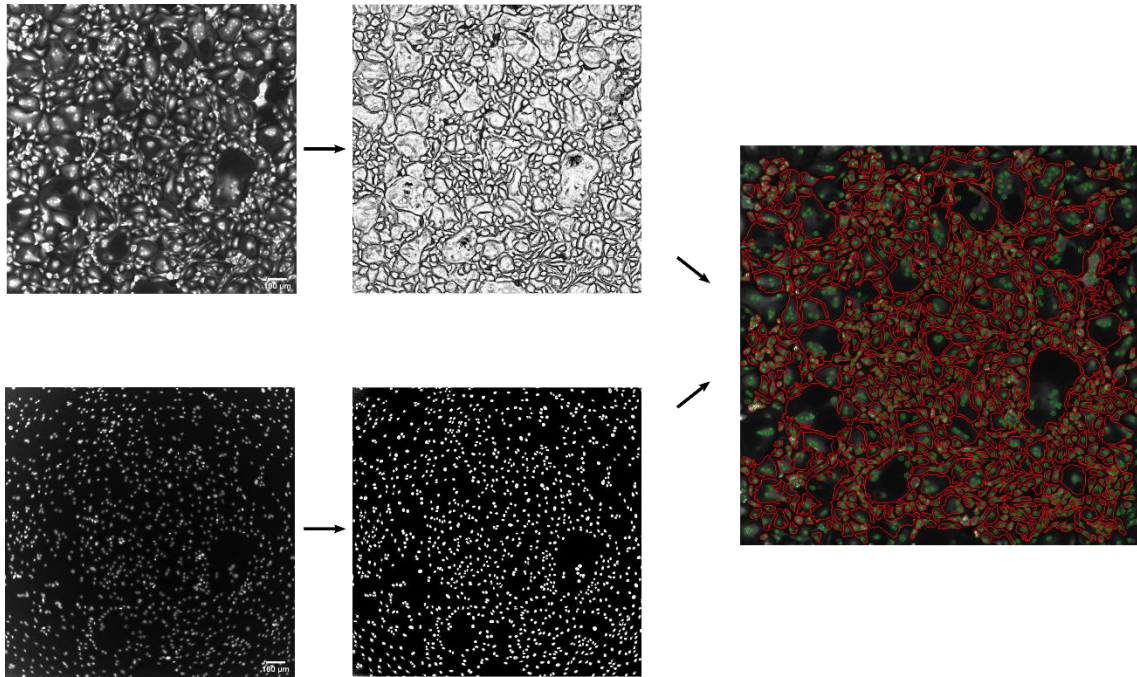


Figure S3. Automatic quantification of osteoclast differentiation. Raw images of HCS Cell Mask (top left) and DAPI (bottom left) are used to train the Ilastik toolkit. Automatic pixel classification is performed leading to the generation of probability masks either for the cell cytoplasm (top middle) or nuclei (bottom middle). Together with the raw images, the probability masks are loaded into a CellProfiler pipeline that automatically segments both the cytoplasm (right column, red) and the nuclei (right column, green) and generates excel files with the total number of osteoclasts and correspondent number of nuclei detected in the images.

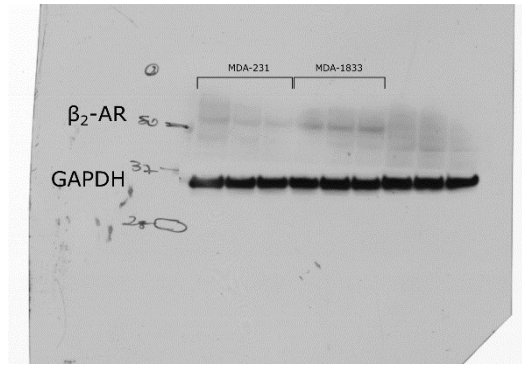


Figure S8. Uncropped Western Blot of of the expression of β_2 -AR on BC cell lines.

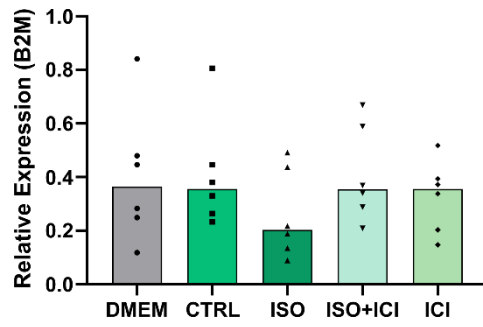


Figure S5. Osteoclast specific cathepsin K gene expression quantification. Pre-osteoclasts were treated with secretome of MDA-231 cells at day 5 of culture, and further cultured for another 4 days. The experiment was ended after fully differentiation of the osteoclasts at day 9, after which cells were lysed and mRNA was collected and purified. Data is expressed as median of individual data points from 6 independent experiments (Friedman's test).

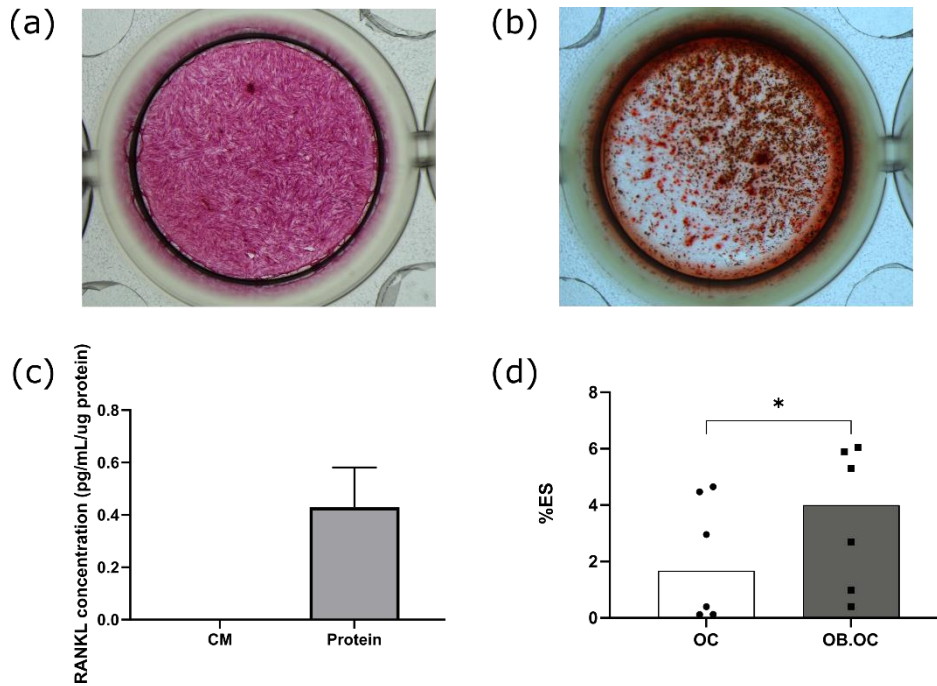


Figure S6. Cells obtained by trabecular bone outgrowth are from the osteoblast lineage. (a) After 7 days of culture, osteoblasts are positive for ALP. (b) After 14 days of culture, multiple calcium deposits are visible through alizarin red staining. Cells were cultured in 96-well plates, the whole well is shown. (c) RANKL quantification by ELISA. No RANKL was detected in the conditioned medium of osteoblasts, while most of it was detected in the cell lysates, suggesting that these cells express RANKL in the cell surface. Data from 2 independent experiments. (d) Comparison of osteoclast resorption activity between osteoclast monocultures and osteoblast/osteoclast co-cultures. Data is expressed as individual data points from 6 independent experiments (Friedman's test followed by Dunn's multiple comparisons test, $*p \leq 0.05$).

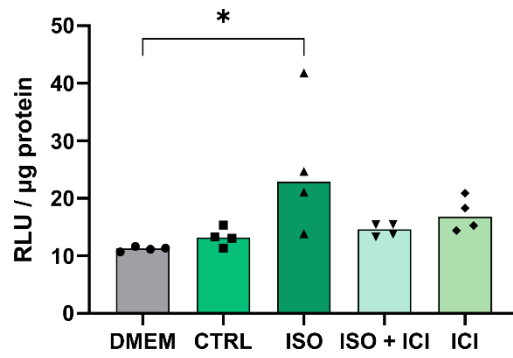


Figure S7. RANKL promotor activation in murine bone marrow stromal cells after incubation with MDA-231 conditioned medium. Bone marrow stromal cells express a luciferase reporter under RANKL promotor, and luminescence is quantified after incubation. Data is expressed as individual data points from 4 independent experiments (One Way ANOVA with Šidák's multiple comparison test, * $p \leq 0.05$).

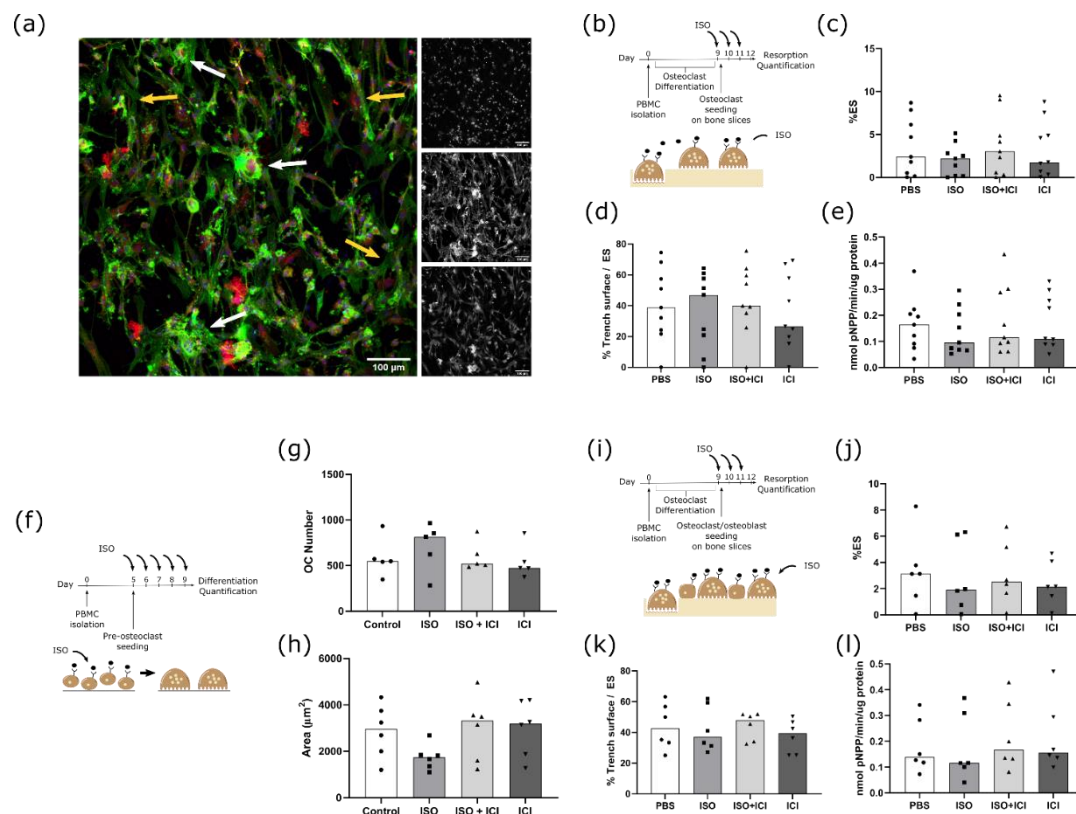


Figure S8. Direct effect of ISO on osteoclast differentiation and resorption activity. (a) Expression of β_2 -AR on osteoclasts (white arrows) and osteoblasts (yellow arrows). DAPI (blue), F-Actin (green) and β_2 -AR (red). Scale bar - 100 μm . Inset single channel images are shown on the right: DAPI (top), F-Actin (mid) and β_2 -AR (bottom). Inset scale bar – 100 μm . (b) Timeline of the resorption assay. Osteoclasts are differentiated for nine days and seeded on top of bone slices, followed by daily incubation with ISO for another three days. (c) Estimated percentage of eroded surface, (d) trench percentage per total eroded surface and (e) TRAcP activity quantified at the end of the experiment. Data is expressed as median of individual data points from 6 independent experiments (Friedman's test). (f) Timeline of the osteoclast differentiation assay. Pre-osteoclasts are seeded after five days of culture and stimulated daily with ISO for four more days, refreshing the media at day 7. (g) Osteoclast number and (h) area after four days of MDA-231 conditioned media stimulation. Osteoclasts with three or more nuclei were included in the analysis. Data is expressed as median of individual data points from 6 independent experiments (Friedman's test). (i) Timeline of the resorption assay in a co-culture setting. Mature osteoclasts were seeded with osteoblasts and stimulated daily with ISO for three days. (j) Estimated percentage of eroded surface, (k) trench percentage per total eroded surface and (l) TRAcP activity quantified at the end of the co-culture experiment. Data is expressed as median of individual data points from 6 independent experiments (Friedman's test).

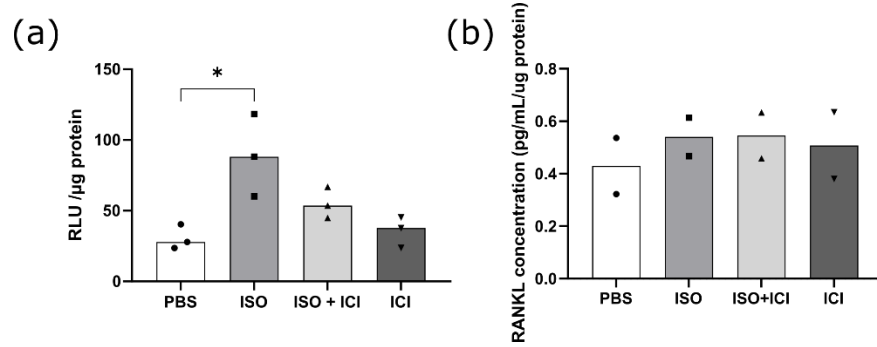


Figure S9. Direct effect of ISO on osteoblasts. (a) RANKL promotor activation in murine bone marrow stromal cells after incubation with MDA-231 conditioned medium. Bone marrow stromal cells express a luciferase reporter under RANKL promotor, and luminescence is quantified after incubation. Data is expressed as individual data points from 3 independent experiments (One Way ANOVA with Šidák's multiple comparison test, * $p \leq 0.05$). (b) Effect of ISO on the RANKL production in human osteoblasts, detected by ELISA. Data is expressed as individual data points from 2 independent experiments.

Table S1. Description of the cohort of BC patients.

	Median age (min-max)	Primary Tumor	Molecular Subtype	Menopausal Status	Distant metastasis Site at Diagnosis
Healthy Donors	58 (46-67)	N/A	N/A	N/A	N/A
Donor 1	62	N/A	N/A	N/A	N/A
Donor 2	58	N/A	N/A	N/A	N/A
Donor 3	57	N/A	N/A	N/A	N/A
Donor 4	48	N/A	N/A	N/A	N/A
Donor 5	62	N/A	N/A	N/A	N/A
Donor 6	46	N/A	N/A	N/A	N/A
Donor 7	56	N/A	N/A	N/A	N/A
Donor 8	65	N/A	N/A	N/A	N/A
Donor 9	56	N/A	N/A	N/A	N/A
Donor 10	51	N/A	N/A	N/A	N/A
Donor 11	64	N/A	N/A	N/A	N/A
Donor 12	57	N/A	N/A	N/A	N/A
Donor 13	55	N/A	N/A	N/A	N/A
Donor 14	62	N/A	N/A	N/A	N/A
Donor 15	67	N/A	N/A	N/A	N/A
Donor 16	60	N/A	N/A	N/A	N/A
Donor 17	55	N/A	N/A	N/A	N/A
Donor 18	63	N/A	N/A	N/A	N/A
Stage I BC patients	67 (45-73)	T1	Luminal-like		N/A
Patient 1	45	T1	Luminal B-like	Premenopausal	N/A
Patient 2	61	T1	Luminal B-like	Postmenopausal	N/A
Patient 3	66	T1	Luminal B-like	Postmenopausal	N/A
Patient 4	68	T1	Luminal A-like	Postmenopausal	N/A
Patient 5	71	T1	Luminal A-like	Postmenopausal	N/A
Patient 6	69	T1	Luminal B-like	Postmenopausal	N/A
Patient 7	68	T1	Luminal B-like	Postmenopausal	N/A
Patient 8	68	T1	Luminal B-like	Postmenopausal	N/A

Patient 9	67	T1	Luminal B-like	Postmenopausal	N/A
Patient 10	63	T1	Luminal B-like	Postmenopausal	N/A
Patient 11	61	T1	Luminal A-like	Postmenopausal	N/A
Patient 12	56	T1	Luminal A-like	Postmenopausal	N/A
Patient 13	68	T1	Luminal A-like	Postmenopausal	N/A
Patient 14	67	T1	Luminal A-like	Postmenopausal	N/A
Patient 15	57	T1	N/A	Postmenopausal	N/A
Patient 16	47	T1	Luminal A-like	Premenopausal	N/A
Patient 17	56	T1	N/A	Premenopausal	N/A
Patient 18	73	T1	N/A	Postmenopausal	N/A

Stage IV BC patients	53 (39-73)		Luminal-like		
Patient 1	59	T3	Luminal B-like	Postmenopausal	Bone
Patient 2	52	N/A	Luminal A-like	Postmenopausal	Bone
Patient 3	64	N/A	Luminal B-like	Postmenopausal	Lung, Bone, Brain
Patient 4	71	N/A	Luminal B-like	Postmenopausal	Bone, Liver, Lung
Patient 5	51	T2	Luminal B-like	N/A	Skin, Lung, Bone
Patient 6	57	T3	Luminal B-like	Premenopausal	Bone
Patient 7	53	N/A	Luminal B-like	Postmenopausal	Bone
Patient 8	51	N/A	Luminal B-like	Premenopausal	Bone

Patient 9	44	T3	Luminal A-like	Premenopa usal	Bone, Lung
Patient 10	56	T4	Luminal B-like	Postmenopa usal	Bone, Liver, Skin
Patient 11	58	T4	Luminal A-like	Postmenopa usal	Bone
Patient 12	41	T3	Luminal A-like	Premenopa usal	Bone
Patient 13	39	T2	Luminal A-like	Premenopa usal	Bone
Patient 14	70	T3	Luminal A-like	Postmenopa usal	Bone
Patient 15	47	T2	Luminal A-like	Premenopa usal	Bone, Liver
Patient 16	73	T4	Luminal A-like	Postmenopa usal	Bone, Liver
Patient 17	57	T2	HER2	Postmenopa usal	Bone, Lung
Patient 18	56	T4	HER2	Postmenopa usal	Bone, Liver, Brain

N/A – Not applicable/available

Table S2. Protein abundance ratio comparison between ISO treated MDA-231 and control MDA-231 samples

Gene Symbol	Abundance Ratio (ISOvsCTRL)	P value
<i>CDH6</i>	100	3,4E-16
<i>MCFD2</i>	100	3,4E-16
<i>IGFBP1</i>	2,976	3,4E-16
<i>ALDOB</i>	2,802	3,4E-16
<i>MAN2B1</i>	2,976	3,4E-16
<i>STC1</i>	2,652	3,4E-16
<i>PLAU</i>	2,568	3,4E-16
<i>ABCA10</i>	2,239	7,16E-12
<i>VNN1</i>	2,084	6,54E-10
<i>FABP1</i>	1,993	8,52E-09
<i>TARS1</i>	1,923	6,06E-08
<i>BRD9</i>	1,878	2,23E-07
<i>IGFBP4</i>	1,866	3E-07
<i>PTK2B</i>	1,754	4,9E-06
<i>WASHC4</i>	1,727	9,58E-06
<i>PRC1</i>	1,605	0,000169
<i>CLU</i>	1,596	0,000213
<i>SERPINB4</i>	1,566	0,000425
<i>CTSL</i>	1,508	0,001531
<i>TPR</i>	1,467	0,003897
<i>HOOK3</i>	1,466	0,00398
<i>DDX39A</i>	1,451	0,00539
<i>CTSD</i>	1,447	0,005945
<i>C6</i>	1,391	0,018738
<i>PLAUR</i>	1,382	0,02224
<i>H2BC21</i>	1,365	0,028902
<i>SRGN</i>	1,347	0,03991
<i>IGFBP7</i>	1,331	0,053154
<i>GSTO1</i>	0,01	3,4E-16
<i>PBX4</i>	0,01	3,4E-16
<i>NCAN</i>	0,035	3,4E-16
<i>CPPED1</i>	0,288	3,4E-16
<i>SLC25A13</i>	0,341	3,4E-16
<i>TTN</i>	0,386	3,4E-16
<i>DSC1</i>	0,404	6,42E-15
<i>KRT10</i>	0,52	5,62E-08
<i>KRT9</i>	0,534	2,23E-07
<i>LMNA</i>	0,56	1,95E-06
<i>SERPINE1</i>	0,588	1,76E-05

<i>IGFN1</i>	0,588	1,76E-05
<i>KRT1</i>	0,609	7,89E-05
<i>MMP1</i>	0,611	9,14E-05
<i>NPM1</i>	0,636	0,000337
<i>CENPE</i>	0,639	0,000404
<i>MAN2A1</i>	0,643	0,000495
<i>KISS1</i>	0,644	0,000527
<i>CCN2</i>	0,646	0,000604
<i>ANXA2</i>	0,654	0,000862
<i>ARHGDI1</i>	0,666	0,001608
<i>COL6A2</i>	0,677	0,002907
<i>FBP1</i>	0,679	0,003171
<i>VIM</i>	0,703	0,009364
<i>EIF5AL1</i>	0,708	0,011596
<i>KRT14</i>	0,718	0,016761
<i>ADH5</i>	0,723	0,020352
<i>ATP5F1A</i>	0,729	0,025211
<i>TERT</i>	0,731	0,02716
<i>ANPEP</i>	0,739	0,03368
<i>GOT1</i>	0,739	0,03429
<i>AKAP13</i>	0,741	0,035427
<i>HADHB</i>	0,741	0,03574
<i>COL9A1</i>	0,747	0,044673
<i>PLXNB2</i>	0,751	0,049436
<i>VPS45</i>	0,753	0,053683

Table S3. Protein abundance ratio comparison between ISO treated MDA-1833 and ISO treated MDA-231 samples

Gene Symbol	Abundance Ratio (1833 ISO vs 231 ISO)	P value
<i>VCP</i>	100	2,91E-16
<i>GSTO1</i>	100	2,91E-16
<i>SLC25A13</i>	2,985	1,19E-11
<i>DSC1</i>	2,539	2,23E-08
<i>PTX3</i>	2,526	2,72E-08
<i>PSAP</i>	2,314	8,84E-07
<i>KRT10</i>	2,31	9,32E-07
<i>VNN1</i>	2,184	7,5E-06
<i>MT1L</i>	1,995	0,000141
<i>KRT14</i>	1,971	0,000142
<i>PLVAP</i>	1,956	0,000171
<i>TPR</i>	1,956	0,000173
<i>RPL29</i>	1,939	0,000221
<i>ANPEP</i>	1,921	0,000294
<i>MCFD2</i>	1,782	0,002194
<i>PEPD</i>	1,777	0,002374
<i>DMBT1</i>	1,753	0,003348
<i>NACA</i>	1,733	0,004404
<i>KRT1</i>	1,733	0,004408
<i>LRRC8A</i>	1,693	0,007781
<i>PLG</i>	1,671	0,01031
<i>CCN2</i>	1,642	0,014896
<i>GRN</i>	1,64	0,015265
<i>IGF2</i>	1,627	0,017886
<i>OPA1</i>	1,624	0,018592
<i>NPM1</i>	1,601	0,024787
<i>FKBP1A</i>	1,593	0,027353
<i>TTR</i>	1,589	0,028658
<i>CPPED1</i>	1,563	0,038659
<i>KRT9</i>	1,551	0,045396
<i>TMEM132C</i>	1,548	0,04683
<i>RCN1</i>	0,737	0,050725
<i>MYOM2</i>	0,727	0,038623
<i>IGFBP4</i>	0,724	0,036342
<i>IGFBP3</i>	0,723	0,035024
<i>HGD</i>	0,72	0,032832
<i>TIMP2</i>	0,719	0,031821
<i>C4BPA</i>	0,719	0,03205
<i>ITIH2</i>	0,714	0,027865

<i>HBB</i>	0,714	0,028367
<i>CD44</i>	0,708	0,023916
<i>HLA-A</i>	0,701	0,019793
<i>OAF</i>	0,679	0,01009
<i>TPM1</i>	0,676	0,009081
<i>CTSZ</i>	0,665	0,006297
<i>APP</i>	0,659	0,005054
<i>DDX39A</i>	0,657	0,004593
<i>TNC</i>	0,637	0,002221
<i>FBP1</i>	0,627	0,00146
<i>IGFBP7</i>	0,585	0,000214
<i>CST3</i>	0,581	0,000174
<i>PTK2B</i>	0,58	0,00017
<i>MMP1</i>	0,568	0,000134
<i>PPIB</i>	0,546	3,84E-05
<i>THBS2</i>	0,545	3,74E-05
<i>SPARC</i>	0,496	1,29E-06
<i>SERPINE1</i>	0,493	1,06E-06
<i>STC1</i>	0,491	8,84E-07
<i>RNASET2</i>	0,457	5,2E-08
<i>VN1R5</i>	0,45	2,72E-08
<i>RPLP2</i>	0,442	1,37E-08
<i>IGFN1</i>	0,438	8,98E-09
<i>CTSL</i>	0,418	1,09E-09
<i>PLAUR</i>	0,332	6,37E-15
<i>IGFBP1</i>	0,267	2,91E-16
<i>LOX</i>	0,237	2,91E-16
<i>WASHC4</i>	0,206	2,91E-16
<i>SERPINB2</i>	0,01	2,91E-16
<i>SET</i>	0,01	2,91E-16

Table S4. Protein abundance ratio comparison between control MDA-1833 and MDA-231 samples

Gene Symbol	Abundance Ratio (1833 vs 231)	P value
<i>CDH6</i>	100	2,7E-16
<i>DMBT1</i>	100	2,7E-16
<i>PSMA1</i>	100	2,7E-16
<i>IGFALS</i>	100	2,7E-16
<i>VCP</i>	100	2,7E-16
<i>ACAT2</i>	5,794	2,7E-16
<i>VNN1</i>	5,478	2,7E-16
<i>ABCA10</i>	4,684	2,7E-16
<i>C6</i>	2,761	1,19E-09
<i>ALDOB</i>	2,757	1,27E-09
<i>PEPD</i>	2,684	4,09E-09
<i>MAN2B1</i>	2,512	5,9E-08
<i>TARS1</i>	2,345	7,16E-07
<i>GSTO1</i>	2,279	1,84E-06
<i>TPR</i>	2,266	2,25E-06
<i>PSAP</i>	2,158	1,15E-05
<i>NME2</i>	2,051	5,65E-05
<i>PGM1</i>	2,05	5,76E-05
<i>BRD9</i>	1,984	0,000154
<i>FLNB</i>	1,903	0,000459
<i>PTX3</i>	1,893	0,000531
<i>DYM</i>	1,862	0,00078
<i>NACA</i>	1,836	0,001091
<i>HOOK3</i>	1,709	0,00573
<i>EEF1G</i>	1,693	0,00704
<i>H2BC21</i>	1,669	0,009257
<i>DARS2</i>	1,669	0,009257
<i>MT1L</i>	1,637	0,013882
<i>KRT10</i>	1,613	0,018333
<i>RPLP2</i>	1,6	0,021696
<i>GRN</i>	1,597	0,022386
<i>HSP90AB1</i>	1,596	0,022529
<i>PFN1</i>	1,57	0,030082
<i>EEF1D</i>	1,563	0,032767
<i>AMBP</i>	1,538	0,041389
<i>ACTN4</i>	1,535	0,043018
<i>FCAR</i>	0,685	0,052105
<i>CLU</i>	0,682	0,047992
<i>ATP5F1A</i>	0,667	0,033275
<i>LMNA</i>	0,667	0,033393

<i>SRGN</i>	0,662	0,029209
<i>TIMP1</i>	0,66	0,028458
<i>COL8A1</i>	0,644	0,018012
<i>HGD</i>	0,643	0,017534
<i>TNC</i>	0,641	0,016351
<i>SLC25A13</i>	0,64	0,016089
<i>SLC38A7</i>	0,639	0,015616
<i>QSOX1</i>	0,636	0,014164
<i>APP</i>	0,633	0,012632
<i>SERPINB2</i>	0,629	0,011151
<i>HLA-A</i>	0,623	0,009257
<i>SERPIND1</i>	0,617	0,007521
<i>RPL13A</i>	0,615	0,007046
<i>HLA-C</i>	0,596	0,003474
<i>DDX39A</i>	0,583	0,002109
<i>PLAUR</i>	0,563	0,000948
<i>IGFBP7</i>	0,553	0,000609
<i>LGMN</i>	0,546	0,000455
<i>PLXNB2</i>	0,537	0,000275
<i>CENPE</i>	0,53	0,000205
<i>SPARC</i>	0,525	0,000154
<i>CEMIP2</i>	0,522	0,000135
<i>CST3</i>	0,521	0,00013
<i>CTSL</i>	0,503	4,57E-05
<i>BOD1L1</i>	0,499	3,44E-05
<i>TTN</i>	0,491	2,01E-05
<i>TERT</i>	0,489	1,86E-05
<i>IGFBP1</i>	0,482	1,16E-05
<i>A1BG</i>	0,481	1,04E-05
<i>C4BPA</i>	0,469	4,62E-06
<i>IGFBP3</i>	0,431	2,43E-07
<i>WASHC4</i>	0,428	1,78E-07
<i>IGFN1</i>	0,421	1,08E-07
<i>MMP1</i>	0,416	6,72E-08
<i>SERPINE1</i>	0,415	6,47E-08
<i>FBP1</i>	0,402	1,79E-08
<i>RNASET2</i>	0,398	1,2E-08
<i>RCN1</i>	0,396	9,91E-09
<i>KISS1</i>	0,373	7,57E-10
<i>STC1</i>	0,315	2,11E-13
<i>NCAN</i>	0,02	2,7E-16
<i>PBX4</i>	0,01	2,7E-16
<i>EIF3L</i>	0,01	2,7E-16

LOX	0,01	2,7E-16
-----	------	---------

Author Contributions: Conceptualization, F.C., D.S. and M.L.; methodology, F.C. and D.S.; software, F.C.; validation, F.C., D.S., S.T. and M.C.; formal analysis, F.C.; investigation, F.C., D.S., S.T., C.M., C.L., H.E., J.L. and M.C.; resources, M.R., C.J., M.L.; data curation, F.C. and D.S.; writing—original draft preparation, F.C.; writing—review and editing, F.C., D.S. and M.L.; visualization, F.C.; supervision, M.R., C.J. and M.L.; project administration, M.L.; funding acquisition, M.L. All authors have read and agreed to the published version of the manuscript.

Funding: This work was financed by FEDER—Fundo Europeu de Desenvolvimento Regional funds through the COMPETE 2020—Operacional Programme for Competitiveness and Internationalisation (POCI), Portugal 2020, and Portuguese funds through FCT/MCTES in the framework of the project “SproutOC” (POCI-01-0145-FEDER-030158, PTDC/MED-PAT/30158/2017). F.C. is a recipient of the Ph.D. fellowship SFRH/BD/128771/2017. M.C. is a recipient of the Ph.D. fellowship 2020.05177.BD. D.M.S. is a recipient of Post-Doc fellowship SFRH/BPD/115341/2016.

3.4. Chapter Conclusions

In summary, we present new data concerning the changes in circulating epinephrine that take place during BC and highlight the effect of β_2 -AR signaling on the crosstalk between BC cells and bone niche cells, osteoclasts and osteoblasts. Interestingly, although epinephrine levels in BC patients are maintained throughout disease progression, proteomic screening and functional studies identified distinct outcomes of β_2 -AR activation after BC metastasis. We show that, contrarily to what is expected, primary BC cells decrease osteoclast differentiation and resorption activity *in vitro* under β_2 -AR signaling activation. In opposition, secreted factors from β_2 -AR primed metastatic BC cells do not affect osteoclast differentiation and resorption in our model, suggesting that secreted factors from BC cells after β_2 -AR agonism are not involved in the local exacerbation of bone resorption activity. Future studies should focus on the study of cancer/osteoblast/osteoclast cell-cell direct interactions and the role of other cell types present in the bone marrow in the dynamics of SNS activation of the bone metastatic niche.

3.5. References

- [1] J. J. Yin, K. Selander, J. M. Chirgwin, M. Dallas, B. G. Grubbs, R. Wieser, J. Massagué, G. R. Mundy, T. A. Guise, (1999) TGF- β signaling blockade inhibits PTHrP secretion by breast cancer cells and bone metastases development, *The Journal of Clinical Investigation*, 103, 197-206
- [2] J. A. Sterling, B. O. Oyajobi, B. Grubbs, S. S. Padalecki, S. A. Munoz, A. Gupta, B. Story, M. Zhao, G. R. Mundy, (2006) The Hedgehog Signaling Molecule Gli2 Induces Parathyroid Hormone-Related Peptide Expression and Osteolysis in Metastatic Human Breast Cancer Cells, *Cancer Research*, 66, 7548-7553
- [3] T. A. Guise, J. J. Yin, S. D. Taylor, Y. Kumagai, M. Dallas, B. F. Boyce, T. Yoneda, G. R. Mundy, (1996) Evidence for a causal role of parathyroid hormone-related protein in the pathogenesis of human breast cancer-mediated osteolysis, *The Journal of Clinical Investigation*, 98, 1544-1549
- [4] T. R. Cox, R. M. H. Rumney, E. M. Schoof, L. Perryman, A. M. Høye, A. Agrawal, D. Bird, N. A. Latif, H. Forrest, H. R. Evans, I. D. Huggins, G. Lang, R. Linding, A. Gartland, J. T. Erler, (2015) The hypoxic cancer secretome induces pre-metastatic bone lesions through lysyl oxidase, *Nature*, 522, 106-110
- [5] A. E. Chiou, C. Liu, I. Moreno-Jiménez, T. Tang, W. Wagermaier, M. N. Dean, C. Fischbach, P. Fratzl, (2021) Breast cancer secreted factors perturb murine bone growth in regions prone to metastasis, *Science Advances*, 7, eabf2283
- [6] J. P. Campbell, M. R. Karolak, Y. Ma, D. S. Perrien, S. K. Masood-Campbell, N. L. Penner, S. A. Munoz, A. Zijlstra, X. Yang, J. A. Sterling, F. Elefteriou, (2012) Stimulation of Host Bone Marrow Stromal Cells by Sympathetic Nerves Promotes Breast Cancer Bone Metastasis in Mice, *PLOS Biology*, 10, e1001363
- [7] L. Clément-Demange, P. L. Mulcrone, T. Q. Tabarestani, J. A. Sterling, F. Elefteriou, (2018) β 2ARs stimulation in osteoblasts promotes breast cancer cell adhesion to bone marrow endothelial cells in an IL-1 β and selectin-dependent manner, *Journal of bone oncology*, 13, 1-10
- [8] P. L. Mulcrone, J. P. Campbell, L. Clément-Demange, A. L. Anbinder, A. R. Merkel, R. A. Brekken, J. A. Sterling, F. Elefteriou, (2017) Skeletal Colonization by Breast Cancer Cells Is Stimulated by an Osteoblast and β 2AR-Dependent Neo-Angiogenic Switch, *Journal of Bone and Mineral Research*, 32, 1442-1454
- [9] D. Verhoeven, C. Allemani, C. Kaufman, R. Mansel, S. Siesling, B. Anderson, (2019) Breast Cancer: global quality care optimizing care delivery with existing financial and personnel resources, *ESMO Open*, 4, e000861

- [10] A. Galvano, D. Scaturro, G. Badalamenti, L. Incorvaia, S. Rizzo, L. Castellana, S. Cusenza, S. Cutaia, D. Santini, F. Guadagni, M. Roselli, S. Gori, M. A. Latteri, V. Bazan, L. M. Giulia, A. Russo, (2019) Denosumab for bone health in prostate and breast cancer patients receiving endocrine therapy? A systematic review and a meta-analysis of randomized trials, *Journal of bone oncology*, 18, 100252
- [11] A. Soni, Z. Ren, O. Hameed, D. Chanda, C. J. Morgan, G. P. Siegal, S. Wei, (2015) Breast Cancer Subtypes Predispose the Site of Distant Metastases, *American Journal of Clinical Pathology*, 143, 471-478
- [12] K. N. Weilbaecher, T. A. Guise, L. K. McCauley, (2011) Cancer to bone: a fatal attraction, *Nature Reviews Cancer*, 11, 411-425
- [13] J. Fornetti, A. L. Welm, S. A. Stewart, (2018) Understanding the Bone in Cancer Metastasis, *Journal of Bone and Mineral Research*, 33, 2099-2113
- [14] F. Le Pape, G. Vargas, P. Clézardin, (2016) The role of osteoclasts in breast cancer bone metastasis, *Journal of bone oncology*, 5, 93-95
- [15] R. E. Coleman, P. I. Croucher, A. R. Padhani, P. Clézardin, E. Chow, M. Fallon, T. Guise, S. Colangeli, R. Capanna, L. Costa, (2020) Bone metastases, *Nature Reviews Disease Primers*, 6, 83
- [16] A. M. Mehedințeanu, V. Sfredel, P. O. Stovicek, M. Schenker, G. C. Târtea, O. Istrătoaie, A.-M. Ciurea, C. C. Vere, (2021) Assessment of Epinephrine and Norepinephrine in Gastric Carcinoma, *International Journal of Molecular Sciences*, 22, 2042
- [17] D. B. Bastos, B. A. M. Sarafim-Silva, M. L. M. M. Sundefeld, A. A. Ribeiro, J. D. P. Brandão, É. R. Biasoli, G. I. Miyahara, D. E. Casarini, D. G. Bernabé, (2018) Circulating catecholamines are associated with biobehavioral factors and anxiety symptoms in head and neck cancer patients, *PLOS ONE*, 13, e0202515
- [18] A. M. Decker, Y. Jung, F. C. Cackowski, K. Yumoto, J. Wang, R. S. Taichman, (2017) Sympathetic Signaling Reactivates Quiescent Disseminated Prostate Cancer Cells in the Bone Marrow, *Molecular Cancer Research*, 15, 1644-1655
- [19] Z. Huang, G. Li, Z. Zhang, R. Gu, W. Wang, X. Lai, Z.-K. Cui, F. Zeng, S. Xu, F. Deng, (2019) β 2AR-HIF-1 α -CXCL12 signaling of osteoblasts activated by isoproterenol promotes migration and invasion of prostate cancer cells, *BMC Cancer*, 19, 1142
- [20] F. Eleftheriou, (2018) Impact of the Autonomic Nervous System on the Skeleton, *Physiological Reviews*, 98, 1083-1112
- [21] F. Conceição, D. M. Sousa, J. Paredes, M. Lamghari, (2021) Sympathetic activity in breast cancer and metastasis: partners in crime, *Bone Research*, 9, 9
- [22] A. Kamiya, Y. Hayama, S. Kato, A. Shimomura, T. Shimomura, K. Irie, R. Kaneko, Y. Yanagawa, K. Kobayashi, T. Ochiya, (2019) Genetic manipulation of autonomic nerve

fiber innervation and activity and its effect on breast cancer progression, *Nature Neuroscience*, 22, 1289-1305

[23] D. G. Powe, M. J. Voss, K. S. Zänker, H. O. Habashy, A. R. Green, I. O. Ellis, F. Entschladen, (2010) Beta-Blocker Drug Therapy Reduces Secondary Cancer Formation in Breast Cancer and Improves Cancer Specific Survival, *Oncotarget*, 1,

[24] A. Melhem-Bertrandt, M. Chavez-MacGregor, X. Lei, E. N. Brown, R. T. Lee, F. Meric-Bernstam, A. K. Sood, S. D. Conzen, G. N. Hortobagyi, A.-M. Gonzalez-Angulo, (2011) Beta-Blocker Use Is Associated With Improved Relapse-Free Survival in Patients With Triple-Negative Breast Cancer, *Journal of Clinical Oncology*, 29, 2645-2652

[25] E. Botteri, E. Munzone, N. Rotmensz, C. Cipolla, V. De Giorgi, B. Santillo, A. Zanelotti, L. Adamoli, M. Colleoni, G. Viale, A. Goldhirsch, S. Gandini, (2013) Therapeutic effect of β -blockers in triple-negative breast cancer postmenopausal women, *Breast Cancer Research and Treatment*, 140, 567-575

[26] C. R. Cardwell, H. G. Coleman, L. J. Murray, F. Entschladen, D. G. Powe, (2014) Beta-blocker usage and breast cancer survival: a nested case-control study within a UK Clinical Practice Research Datalink cohort, *International Journal of Epidemiology*, 42, 1852-1861

[27] C. R. Cardwell, A. Pottegård, E. Vaes, H. Garmo, L. J. Murray, C. Brown, P. A. J. Vissers, M. O'Rourke, K. Visvanathan, D. Cronin-Fenton, H. De Schutter, M. Lambe, D. G. Powe, M. P. P. van Herk-Sukel, A. Gavin, S. Friis, L. Sharp, K. Bennett, (2016) Propranolol and survival from breast cancer: a pooled analysis of European breast cancer cohorts, *Breast Cancer Research*, 18, 119

[28] G. V. Sørensen, P. A. Ganz, S. W. Cole, L. A. Pedersen, H. T. Sørensen, D. P. Cronin-Fenton, J. P. Garne, P. M. Christiansen, T. L. Lash, T. P. Ahern, (2013) Use of β -Blockers, Angiotensin-Converting Enzyme Inhibitors, Angiotensin II Receptor Blockers, and Risk of Breast Cancer Recurrence: A Danish Nationwide Prospective Cohort Study, *Journal of Clinical Oncology*, 31, 2265-2272

[29] D. C. Pirapaharan, J. B. Olesen, T. L. Andersen, S. B. Christensen, P. Kjærsgaard-Andersen, J.-M. Delaisse, K. Søe, (2019) Catabolic activity of osteoblast lineage cells contributes to osteoclastic bone resorption in vitro, *Journal of Cell Science*, 132,

[30] K. Søe, J.-M. Delaissé, (2010) Glucocorticoids maintain human osteoclasts in the active mode of their resorption cycle, *Journal of Bone and Mineral Research*, 25, 2184-2192

[31] S. Berg, D. Kutra, T. Kroeger, C. N. Straehle, B. X. Kausler, C. Haubold, M. Schiegg, J. Ales, T. Beier, M. Rudy, K. Eren, J. I. Cervantes, B. Xu, F. Beuttenmueller, A. Wolny, C. Zhang, U. Koethe, F. A. Hamprecht, A. Kreshuk, (2019) ilastik: interactive machine learning for (bio)image analysis, *Nature Methods*, 16, 1226-1232

- [32] C. McQuin, A. Goodman, V. Chernyshev, L. Kamentsky, B. A. Cimini, K. W. Karhohs, M. Doan, L. Ding, S. M. Rafelski, D. Thirstrup, W. Wiegraebe, S. Singh, T. Becker, J. C. Caicedo, A. E. Carpenter, (2018) CellProfiler 3.0: Next-generation image processing for biology, *PLOS Biology*, 16, e2005970
- [33] J. Vanderoot, K. S e, D. M. H. Merrild, J.-M. Delaiss , G. H. van Lenthe, (2013) Glucocorticoid-Induced Changes in the Geometry of Osteoclast Resorption Cavities Affect Trabecular Bone Stiffness, *Calcified Tissue International*, 92, 240-250
- [34] D. M. H. Merrild, D. C. Pirapaharan, C. M. Andreasen, P. Kj rsgaard-Andersen, A. M. J. M ller, M. Ding, J.-M. Delaiss , K. S e, (2015) Pit- and trench-forming osteoclasts: a distinction that matters, *Bone Research*, 3, 15032
- [35] P. Boissy, T. L. Andersen, B. M. Abdallah, M. Kassem, T. Plesner, J.-M. Delaiss , (2005) Resveratrol Inhibits Myeloma Cell Growth, Prevents Osteoclast Formation, and Promotes Osteoblast Differentiation, *Cancer Research*, 65, 9943-9952
- [36] C. S. Hughes, S. Moggridge, T. M ller, P. H. Sorensen, G. B. Morin, J. Krijgsveld, (2019) Single-pot, solid-phase-enhanced sample preparation for proteomics experiments, *Nature Protocols*, 14, 68-85
- [37] H. Os rio, C. Silva, M. Ferreira, I. Gullo, V. M ximo, R. Barros, F. Mendon a, C. Oliveira, F. Carneiro, (2021) Proteomics Analysis of Gastric Cancer Patients with Diabetes Mellitus, *Journal of Clinical Medicine*, 10, 407
- [38] M. J. Curtis, S. Alexander, G. Cirino, J. R. Docherty, C. H. George, M. A. Giembycz, D. Hoyer, P. A. Insel, A. A. Izzo, Y. Ji, D. J. MacEwan, C. G. Sobey, S. C. Stanford, M. M. Teixeira, S. Wonnacott, A. Ahluwalia, (2018) Experimental design and analysis and their reporting II: updated and simplified guidance for authors and peer reviewers, *British Journal of Pharmacology*, 175, 987-993
- [39] P. Shannon, A. Markiel, O. Ozier, N. S. Baliga, J. T. Wang, D. Ramage, N. Amin, B. Schwikowski, T. Ideker, (2003) Cytoscape: A Software Environment for Integrated Models of Biomolecular Interaction Networks, *Genome Research*, 13, 2498-2504
- [40] Y. Liao, J. Wang, E. J. Jaehnig, Z. Shi, B. Zhang, (2019) WebGestalt 2019: gene set analysis toolkit with revamped UIs and APIs, *Nucleic Acids Research*, 47, W199-W205
- [41] Y. Kang, P. M. Siegel, W. Shu, M. Drobnjak, S. M. Kakonen, C. Cord n-Cardo, T. A. Guise, J. Massagu , (2003) A multigenic program mediating breast cancer metastasis to bone, *Cancer Cell*, 3, 537-549
- [42] E. H. Filvaroff, S. Guillet, C. Zlot, M. Bao, G. Ingle, H. Steinmetz, J. Hoeffel, S. Bunting, J. Ross, R. A. D. Carano, L. Powell-Braxton, G. F. Wagner, R. Eckert, M. E. Gerritsen, D. M. French, (2002) Stanniocalcin 1 Alters Muscle and Bone Structure and Function in Transgenic Mice, *Endocrinology*, 143, 3681-3690

- [43] B. Choi, S.-S. Kang, S.-W. Kang, B.-H. Min, E.-J. Lee, D.-H. Song, S.-M. Kim, Y. Song, S.-Y. Yoon, E.-J. Chang, (2014) Secretory clusterin inhibits osteoclastogenesis by attenuating M-CSF-dependent osteoclast precursor cell proliferation, *Biochemical and Biophysical Research Communications*, 450, 105-109
- [44] Y. Choi, J. H. Yoo, J.-H. Lee, Y. Lee, M.-K. Bae, Y.-D. Kim, H. J. Kim, (2020) Connective tissue growth factor (CTGF) regulates the fusion of osteoclast precursors by inhibiting Bcl6 in periodontitis, *International Journal of Medical Sciences*, 17, 647-656
- [45] S. Takahashi, S. V. Reddy, J. M. Chirgwin, R. Devlin, C. Haipek, J. Anderson, G. D. Roodman, (1994) Cloning and identification of annexin II as an autocrine/paracrine factor that increases osteoclast formation and bone resorption, *Journal of Biological Chemistry*, 269, 28696-28701
- [46] K. Sørensen, J.-M. Delaissé, (2017) Time-lapse reveals that osteoclasts can move across the bone surface while resorbing, *Journal of Cell Science*, 130, 2026-2035
- [47] M. Sayilekshmy, R. B. Hansen, J.-M. Delaissé, L. Rolighed, T. L. Andersen, A.-M. Heegaard, (2019) Innervation is higher above Bone Remodeling Surfaces and in Cortical Pores in Human Bone: Lessons from patients with primary hyperparathyroidism, *Scientific Reports*, 9, 5361
- [48] P. Vargovic, M. Laukova, J. Ukropec, G. Manz, R. Kvetnansky, (2016) Lipopolysaccharide induces catecholamine production in mesenteric adipose tissue of rats previously exposed to immobilization stress, *Stress*, 19, 439-447
- [49] P. Vargovic, J. Ukropec, M. Laukova, S. Cleary, B. Manz, K. Pacak, R. Kvetnansky, (2011) Adipocytes as a new source of catecholamine production, *FEBS Letters*, 585, 2279-2284
- [50] C. Ye, W. Hou, M. Chen, J. Lu, E. Chen, L. Tang, K. Hang, Q. Ding, Y. Li, W. Zhang, R. He, (2020) IGFBP7 acts as a negative regulator of RANKL-induced osteoclastogenesis and oestrogen deficiency-induced bone loss, *Cell Proliferation*, 53, e12752
- [51] M. Brage, A. Lie, M. Ransjö, F. Kasprzykowski, R. Kasprzykowska, M. Abrahamson, A. Grubb, U. H. Lerner, (2004) Osteoclastogenesis is decreased by cysteine proteinase inhibitors, *Bone*, 34, 412-424
- [52] J. G. Hiller, S. W. Cole, E. M. Crone, D. J. Byrne, D. M. Shackelford, J.-M. B. Pang, M. A. Henderson, S. S. Nightingale, K. M. Ho, P. S. Myles, S. Fox, B. Riedel, E. K. Sloan, (2020) Preoperative β -Blockade with Propranolol Reduces Biomarkers of Metastasis in Breast Cancer: A Phase II Randomized Trial, *Clinical Cancer Research*, 26, 1803-1811
- [53] M. F. Ramirez, D. Ai, M. Bauer, J.-N. Vauthey, V. Gottumukkala, S. Kee, D. Shon, M. Truty, H. M. Kuerer, A. Kurz, M. Hernandez, J. P. Cata, (2015) Innate immune function

after breast, lung, and colorectal cancer surgery, *Journal of Surgical Research*, 194, 185-193

[54] L. M. Thornton, B. L. Andersen, W. P. Blakely, (2010) The pain, depression, and fatigue symptom cluster in advanced breast cancer: Covariation with the hypothalamic–pituitary–adrenal axis and the sympathetic nervous system, *Health Psychology*, 29, 333-337

[55] Y. Cheng, X.-H. Gao, X.-J. Li, Q.-H. Cao, D.-D. Zhao, J.-R. Zhou, H.-X. Wu, Y. Wang, L.-J. You, H.-B. Yang, Y.-L. He, Y.-R. Li, J.-S. Bian, Q.-Y. Zhu, L. Birnbaumer, Y. Yang, (2018) Depression promotes prostate cancer invasion and metastasis via a sympathetic-cAMP-FAK signaling pathway, *Oncogene*, 37, 2953-2966

[56] G. Koch, L. Fransson, (1991) Acute Effects of Combined α/β -Adrenoceptor Blockade u Combined β -Receptor and Slow Channel Calcium Blockade in Ischemic Heart Disease Complicated by Hypertension: Hemodynamic and Adrenergic Responses, *American Journal of Hypertension*, 4, 709-713

[57] P. Roy-Byre, J. Fleishaker, C. Arnett, M. Dubach, J. Stewart, A. Radant, R. Veith, M. Graham, (1993) Effects of Acute and Chronic Alprazolam Treatment on Cerebral Blood Flow, Memory, Sedation, and Plasma Catecholamines, *Neuropsychopharmacology*, 8, 161-169

[58] C. L. Lowery, C. Elliott, A. Cooper, C. Hadden, R. N. Sonon, P. Azadi, D. K. Williams, J. D. Marsh, D. S. Woulfe, F. Kilic, (2017) Cigarette Smoking & Associated Alterations in Serotonin/Adrenalin Signaling Pathways of Platelets, *Journal of the American Heart Association*, 6, e005465

[59] L. Gilardini, G. Parati, A. Sartorio, G. Mazzilli, B. Pontiggia, C. Invitti, (2008) Sympathoadrenergic and metabolic factors are involved in ambulatory blood pressure rise in childhood obesity, *Journal of Human Hypertension*, 22, 75-82

[60] M. Nwokolo, S. A. Amiel, O. O'Daly, M. L. Byrne, B. M. Wilson, A. Pernet, S. M. Cordon, I. A. Macdonald, F. O. Zelaya, P. Choudhary, (2020) Hypoglycemic thalamic activation in type 1 diabetes is associated with preserved symptoms despite reduced epinephrine, *Journal of Cerebral Blood Flow & Metabolism*, 40, 787-798

[61] E. K. Sloan, S. J. Priceman, B. F. Cox, S. Yu, M. A. Pimentel, V. Tangkanangnukul, J. M. G. Arevalo, K. Morizono, B. D. W. Karanikolas, L. Wu, A. K. Sood, S. W. Cole, (2010) The Sympathetic Nervous System Induces a Metastatic Switch in Primary Breast Cancer, *Cancer Research*, 70, 7042-7052

[62] C. P. Le, C. J. Nowell, C. Kim-Fuchs, E. Botteri, J. G. Hiller, H. Ismail, M. A. Pimentel, M. G. Chai, T. Karnezis, N. Rotmensch, G. Renne, S. Gandini, C. W. Pouton, D. Ferrari, A. Möller, S. A. Stacker, E. K. Sloan, (2016) Chronic stress in mice remodels lymph vasculature to promote tumour cell dissemination, *Nature Communications*, 7, 10634

- [63] Y.-b. Niu, Y.-y. Yang, X. Xiao, Y. Sun, Y.-m. Zhou, Y.-h. Zhang, D. Dong, C.-r. Li, X.-l. Wu, Y.-h. Li, Q.-b. Mei, (2020) Quercetin prevents bone loss in hindlimb suspension mice via stanniocalcin 1-mediated inhibition of osteoclastogenesis, *Acta Pharmacologica Sinica*, 41, 1476-1486
- [64] X. Yuan, N. Qian, S. Ling, Y. Li, W. Sun, J. Li, R. Du, G. Zhong, C. Liu, G. Yu, D. Cao, Z. Liu, Y. Wang, Z. Qi, Y. Yao, F. Wang, J. Liu, S. Hao, X. Jin, Y. Zhao, J. Xue, D. Zhao, X. Gao, S. Liang, Y. Li, J. Song, S. Yu, Y. Li, (2021) Breast cancer exosomes contribute to pre-metastatic niche formation and promote bone metastasis of tumor cells, *Theranostics*, 11, 1429-1445
- [65] M. Nagao, T. N. Feinstein, Y. Ezura, T. Hayata, T. Notomi, Y. Saita, R. Hanyu, H. Hemmi, Y. Izu, S. Takeda, K. Wang, S. Rittling, T. Nakamoto, K. Kaneko, H. Kurosawa, G. Karsenty, D. T. Denhardt, J.-P. Vilardaga, M. Noda, (2011) Sympathetic control of bone mass regulated by osteopontin, *Proceedings of the National Academy of Sciences*, 108, 17767-17772
- [66] D. Kajimura, E. Hinoi, M. Ferron, A. Kode, K. J. Riley, B. Zhou, X. E. Guo, G. Karsenty, (2011) Genetic determination of the cellular basis of the sympathetic regulation of bone mass accrual, *Journal of Experimental Medicine*, 208, 841-851
- [67] M. Arai, T. Nagasawa, Y. Koshihara, S. Yamamoto, A. Togari, (2003) Effects of β -adrenergic agonists on bone-resorbing activity in human osteoclast-like cells, *Biochimica et Biophysica Acta (BBA) - Molecular Cell Research*, 1640, 137-142
- [68] Y. Guo, K. Tiedemann, J. A. Khalil, C. Russo, P. M. Siegel, S. V. Komarova, (2008) Osteoclast precursors acquire sensitivity to breast cancer derived factors early in differentiation, *Bone*, 43, 386-393
- [69] K. Aukes, C. Forsman, N. J. Brady, K. Astleford, N. Blixt, D. Sachdev, E. D. Jensen, K. C. Mansky, K. L. Schwertfeger, (2017) Breast cancer cell-derived fibroblast growth factors enhance osteoclast activity and contribute to the formation of metastatic lesions, *PLOS ONE*, 12, e0185736
- [70] S. Marino, R. T. Bishop, P. Mollat, A. I. Idris, (2018) Pharmacological Inhibition of the Skeletal IKK β Reduces Breast Cancer-Induced Osteolysis, *Calcified Tissue International*, 103, 206-216
- [71] H. Morgan, A. Tumber, P. A. Hill, (2004) Breast cancer cells induce osteoclast formation by stimulating host IL-11 production and downregulating granulocyte/macrophage colony-stimulating factor, *International Journal of Cancer*, 109, 653-660
- [72] Z. He, J. He, Z. Liu, J. Xu, S. F. Yi, H. Liu, J. Yang, (2014) MAPK11 in breast cancer cells enhances osteoclastogenesis and bone resorption, *Biochimie*, 106, 24-32

- [73] Y. S. Lau, L. Danks, S. G. Sun, S. Fox, A. Sabokbar, A. Harris, N. A. Athanasou, (2007) RANKL-dependent and RANKL-independent mechanisms of macrophage-osteoclast differentiation in breast cancer, *Breast Cancer Research and Treatment*, 105, 7-16
- [74] S. J. Aitken, E. Landao-Bassonga, S. H. Ralston, A. I. Idris, (2009) β -Adrenoreceptor ligands regulate osteoclast differentiation in vitro by direct and indirect mechanisms, *Archives of Biochemistry and Biophysics*, 482, 96-103
- [75] H. Kondo, S. Takeuchi, A. Togari, (2013) β -Adrenergic signaling stimulates osteoclastogenesis via reactive oxygen species, *American Journal of Physiology-Endocrinology and Metabolism*, 304, E507-E515
- [76] N. Mukaida, D. Zhang, S.-i. Sasaki, (2020) Emergence of Cancer-Associated Fibroblasts as an Indispensable Cellular Player in Bone Metastasis Process, *Cancers*, 12, 2896
- [77] J. Karavitis, L. M. Hix, Y. H. Shi, R. F. Schultz, K. Khazaie, M. Zhang, (2012) Regulation of COX2 Expression in Mouse Mammary Tumor Cells Controls Bone Metastasis and PGE2-Induction of Regulatory T Cell Migration, *PLOS ONE*, 7, e46342
- [78] Q. Yao, H. Liang, B. Huang, L. Xiang, T. Wang, Y. Xiong, B. Yang, Y. Guo, P. Gong, (2017) Beta-adrenergic signaling affect osteoclastogenesis via osteocytic MLO-Y4 cells' RANKL production, *Biochemical and Biophysical Research Communications*, 488, 634-640
- [79] M. R. Lorenz, J. M. Brazill, A. T. Beeve, I. Shen, E. L. Scheller, (2021) A Neuroskeletal Atlas: Spatial Mapping and Contextualization of Axon Subtypes Innervating the Long Bones of C3H and B6 Mice, *Journal of Bone and Mineral Research*, 36, 1012-1025
- [80] A. K. Walker, D. Martelli, A. I. Ziegler, G. W. Lambert, S. E. Phillips, S. J. Hill, R. M. McAllen, E. K. Sloan, (2019) Circulating epinephrine is not required for chronic stress to enhance metastasis, *Psychoneuroendocrinology*, 99, 191-195
- [81] L. Jin, Y. Zhang, H. Li, L. Yao, D. Fu, X. Yao, L. X. Xu, X. Hu, G. Hu, (2012) Differential secretome analysis reveals CST6 as a suppressor of breast cancer bone metastasis, *Cell Research*, 22, 1356-1373
- [82] J. A. Westbrook, S. L. Wood, D. A. Cairns, K. McMahon, R. Gahlaut, H. Thygesen, M. Shires, S. Roberts, H. Marshall, M. R. Oliva, M. J. Dunning, A. M. Hanby, P. J. Selby, V. Speirs, G. Mavria, R. E. Coleman, J. E. Brown, (2019) Identification and validation of DOCK4 as a potential biomarker for risk of bone metastasis development in patients with early breast cancer, *The Journal of Pathology*, 247, 381-391
- [83] M. Gruet, D. Cotton, C. Coveney, D. J. Boocock, S. Wagner, L. Komorowski, R. C. Rees, A. G. Pockley, A. C. Garner, J. D. Wallis, A. K. Miles, D. G. Powe, (2020) β 2-

Adrenergic Signalling Promotes Cell Migration by Upregulating Expression of the Metastasis-Associated Molecule LYPD3, *Biology*, 9, 39

[84] Y. Amemiya, W. Yang, T. Benatar, S. Nofech-Mozes, A. Yee, H. Kahn, C. Holloway, A. Seth, (2011) Insulin like growth factor binding protein-7 reduces growth of human breast cancer cells and xenografted tumors, *Breast Cancer Research and Treatment*, 126, 373-384

[85] J. Mori, C. Tanikawa, Y. Funouchi, P. H. Y. Lo, Y. Nakamura, K. Matsuda, (2016) Cystatin C as a p53-inducible apoptotic mediator that regulates cathepsin L activity, *Cancer Science*, 107, 298-306

[86] R. M. Burnett, K. E. Craven, P. Krishnamurthy, C. P. Goswami, S. Badve, P. Crooks, W. P. Mathews, P. Bhat-Nakshatri, H. Nakshatri, (2015) Organ-specific adaptive signaling pathway activation in metastatic breast cancer cells, *Oncotarget*, 6,

[87] Q. Zeng, I. P. Michael, P. Zhang, S. Saghafinia, G. Knott, W. Jiao, B. D. McCabe, J. A. Galván, H. P. C. Robinson, I. Zlobec, G. Ciriello, D. Hanahan, (2019) Synaptic proximity enables NMDAR signalling to promote brain metastasis, *Nature*, 573, 526-531

[88] C. K. Pon, J. R. Lane, E. K. Sloan, M. L. Halls, (2016) The β 2-adrenoceptor activates a positive cAMP-calcium feedforward loop to drive breast cancer cell invasion, *The FASEB Journal*, 30, 1144-1154

[89] E.-J. Lee, D.-H. Song, Y.-J. Kim, B. Choi, Y.-H. Chung, S.-M. Kim, J.-M. Koh, S.-Y. Yoon, Y. Song, S.-W. Kang, E.-J. Chang, (2014) PTX3 Stimulates Osteoclastogenesis by Increasing Osteoblast RANKL Production, *Journal of Cellular Physiology*, 229, 1744-1752

Chapter IV. Main Conclusions

4.1. Main Conclusions

In this thesis, we employed an organ-on-a-chip approach in order to dissect the crosstalk between the SNS and the BC bone metastatic niche. Organ-on-a-chip microfluidic models have emerged in recent years as versatile *in vitro* tools and have already been used to study BC cell extravasation and proliferation in bone mimicking substrates [1-3]. However, very few microfluidic models tackle the issue of bone innervation in the context of BC and, to our knowledge, none of them focused on the sympathetic control of BC bone metastasis.

We developed a new microfluidic model that is designed to compartmentalize distinct cellular types, i.e. sympathetic neurons, bone tropic BC cells and osteoclasts seeded on a relevant bone matrix, while facilitating the dynamic communication between compartments via secreted factors. We took advantage of 3D printing technology to produce molds for PDMS casting in a fast and cost-effective fashion, in alternative to standard photolithography procedures. This is crucial to allow the replication of our approach in other laboratories according to their specific research needs, since no prior access to expensive infrastructure or highly trained personnel is required.

Our metastasis-on-a-chip platform allowed the identification of new putative mechanisms of SNS control over BC cellular processes. We conclude that the dynamic communication between human sympathetic neurons, osteoclasts and BC cells favors a BC pro-inflammatory profile. Moreover, the use of the incorporated Quake valves to block the communication between neuronal and bone compartments showed that the direct crosstalk between osteoclasts and sympathetic neurons is dispensable for the observed increased levels of pro-inflammatory cytokines. With this work, we demonstrated that our platform could be applied in the dissection of signaling pathways involved in BC bone metastasis. In addition, by replacing and optimizing cellular or environmental components in our platform, we could potentially set the basis for additional fundamental and applied research in multiple physiological and pathological scenarios.

In addition to the conception of a new metastasis-on-a-chip model, we also sought to perform an in depth characterization of the sympathetic regulation of bone remodeling in a BC bone metastatic context. We wanted to clarify the relevance of circulating catecholamines in BC patients at distinct stages of disease progression and how are BC cellular processes affected by sympathetic input, with special emphasis on β_2 -AR signaling pathways. In addition, we investigated how the secretome from β_2 -AR primed primary or metastatic BC cells modulates osteoclastic bone degradation, replicating the interactions occurring at the BC bone metastatic niche.

We describe for the first time the profile of circulating Epi in early and advanced BC patients. We found that Epi levels are significantly increased in primary BC patients when compared to healthy donors and remain elevated throughout disease progression, pointing towards a relevant exacerbation of sympathetic signaling that could either directly modulate BC cells or other cellular players of the BC niche. Thus, these findings provide evidence for a dysregulation of Epi release that should warrant careful consideration on the treatment regimens of BC patients in a clinical setting.

Importantly, although the levels of circulating Epi are maintained across different stages of BC in the clinical setting, we observed distinct proteomic profiles in primary and metastatic BC cells after pharmacological activation of β_2 -AR *in vitro*. Consistently, exposure of human osteoclasts to the secretome of primary BC cells under β_2 -AR signaling translated into a robust decrease in osteoclast differentiation and bone degradation, in opposition to what was observed following osteoclast stimulation with the secretome of β_2 -AR primed metastatic BC cells. On the other hand, direct co-culture with human osteoblasts mitigated the deleterious effects of β_2 -AR primed primary BC secretome on osteoclast resorption activity. Since osteoblasts are major regulators of osteoclast activity *in vivo*, our findings challenge the theory that secreted factors from β_2 -AR primed BC cells are involved in the modulation of bone resorption. These observations have important implications for the design of future pre-clinical experiments and therapeutic strategies, since the increased circulating Epi levels throughout BC progression and the observed changes in the proteomic profile of metastatic BC cells did not translate into altered bone metabolism in our co-culture model. Nevertheless, our observations do not exclude the possible contribution of other cellular components of the bone metastatic niche, such as immune cells, fibroblasts, endothelial cells and osteocytes, that could promote the establishment of a metastatic vicious cycle of bone degradation under SNS activation.

Overall, this thesis provides new insights on the sympathetic modulation of BC in the context of bone metastasis. We demonstrated the relevance of circulating epinephrine levels throughout BC progression, since both primary and advanced BC patients exhibit exacerbated epinephrine levels when compared to healthy blood donors. Furthermore, using two distinct *in vitro* approaches, i.e. a novel metastasis-on-a-chip model and β_2 -AR pharmacological activation of BC, we show that sympathetic stimulus alters the protein expression of primary and metastatic BC. Nonetheless, these changes do not necessarily translate into altered bone resorption, which warrants further investigation on the consequences of sympathetic exacerbation in BC outcomes *in vivo* and in a clinical setting. Our metastasis-on-a-chip model could be used in the future to identify other soluble mediators such as extracellular vesicles or micro-RNAs that could be

involved in the crosstalk between BC and bone under sympathetic stimulus. Furthermore, clarifying whether the secretome of BC and osteoclasts affect NE release by neuronal cells would complement our findings in the future, using molecular biology techniques, image analysis tools or high throughput techniques such as RNA sequencing, both in general or at a single cell level. Ultimately, our model could potentially be used to study other bone tropic cancers such as prostate, lung and multiple myeloma that were already described to be affected by sympathetic stimuli ^[4-6], and thus improve our understanding of these interactions.

4.2. References

- [1] S. Bersini, J. S. Jeon, G. Dubini, C. Arrigoni, S. Chung, J. L. Charest, M. Moretti, R. D. Kamm, (2014) A microfluidic 3D in vitro model for specificity of breast cancer metastasis to bone, *Biomaterials*, 35, 2454-2461
- [2] J. S. Jeon, S. Bersini, M. Gilardi, G. Dubini, J. L. Charest, M. Moretti, R. D. Kamm, (2015) Human 3D vascularized organotypic microfluidic assays to study breast cancer cell extravasation, *Proceedings of the National Academy of Sciences*, 112, 214-219
- [3] X. Mei, K. Middleton, D. Shim, Q. Wan, L. Xu, Y.-H. V. Ma, D. Devadas, N. Walji, L. Wang, E. W. K. Young, L. You, (2019) Microfluidic platform for studying osteocyte mechanoregulation of breast cancer bone metastasis, *Integrative Biology*, 11, 119-129
- [4] S. Hassan, Y. Karpova, D. Baiz, D. Yancey, A. Pullikuth, A. Flores, T. Register, J. M. Cline, R. D'Agostino, Jr., N. Danial, S. R. Datta, G. Kulik, (2013) Behavioral stress accelerates prostate cancer development in mice, *The Journal of Clinical Investigation*, 123, 874-886
- [5] Y. Xia, Y. Wei, Z.-Y. Li, X.-Y. Cai, L.-L. Zhang, X.-R. Dong, S. Zhang, R.-G. Zhang, R. Meng, F. Zhu, G. Wu, (2019) Catecholamines contribute to the neovascularization of lung cancer via tumor-associated macrophages, *Brain. Behav. Immun.*, 81, 111-121
- [6] E. V. Yang, E. L. Donovan, D. M. Benson, R. Glaser, (2008) VEGF is differentially regulated in multiple myeloma-derived cell lines by norepinephrine, *Brain. Behav. Immun.*, 22, 318-323

Annex A



REVIEW ARTICLE OPEN

Sympathetic activity in breast cancer and metastasis: partners in crime

Francisco Conceição^{1,2,3}, Daniela M. Sousa^{1,2}, Joana Paredes^{1,4,5} and Meriem Lamghari^{1,2,3}

The vast majority of patients with advanced breast cancer present skeletal complications that severely compromise their quality of life. Breast cancer cells are characterized by a strong tropism to the bone niche. After engraftment and colonization of bone, breast cancer cells interact with native bone cells to hinder the normal bone remodeling process and establish an osteolytic “metastatic vicious cycle”. The sympathetic nervous system has emerged in recent years as an important modulator of breast cancer progression and metastasis, potentiating and accelerating the onset of the vicious cycle and leading to extensive bone degradation. Furthermore, sympathetic neurotransmitters and their cognate receptors have been shown to promote several hallmarks of breast cancer, such as proliferation, angiogenesis, immune escape, and invasion of the extracellular matrix. In this review, we assembled the current knowledge concerning the complex interactions that take place in the tumor microenvironment, with a special emphasis on sympathetic modulation of breast cancer cells and stromal cells. Notably, the differential action of epinephrine and norepinephrine, through either α - or β -adrenergic receptors, on breast cancer progression prompts careful consideration when designing new therapeutic options. In addition, the contribution of sympathetic innervation to the formation of bone metastatic foci is highlighted. In particular, we address the remarkable ability of adrenergic signaling to condition the native bone remodeling process and modulate the bone vasculature, driving breast cancer cell engraftment in the bone niche. Finally, clinical perspectives and developments on the use of β -adrenergic receptor inhibitors for breast cancer management and treatment are discussed.

Bone Research (2021)9:9

; <https://doi.org/10.1038/s41413-021-00137-1>

INTRODUCTION

Under physiological conditions, the sympathetic nervous system (SNS) is involved in the so-called “fight-or-flight” response to acute stress. Upon perceiving threats to internal homeostasis, the SNS acts on multiple molecular and cellular processes throughout the body that ensure a coordinated adaptive response to different stressors. Physical mobility is boosted through an increase in heart and respiratory rates, as well as through energy mobilization from adipose tissue and the liver^{1,2}. On the other hand, anabolic processes such as digestion, gastrointestinal motility and reproduction are hampered^{3,4}. Sympathetic signaling is mainly achieved through peripheral release of norepinephrine (NE) by sympathetic nerve terminals or systemic release of epinephrine (Epi) into the circulation by the adrenal glands. These catecholamines are the endogenous ligands of α/β adrenoreceptors (α -AR, β -AR), which exhibit widespread expression in a multitude of cell types and tissues^{5–8}. This family of receptors is composed of a total of nine G protein-coupled receptors (GPCRs): G_q -coupled α_{1A} , α_{1B} , and α_{1D} ARs; G_i -coupled α_{2A} , α_{2B} , and α_{2C} ARs; and finally, G_s -coupled β_1 , β_2 , and β_3 ARs.

Breast cancer is still a major socioeconomic issue and was the leading cause of cancer-specific death in women in 2018 (<https://gco.iarc.fr/today/home>). It is a highly heterogeneous disease that is usually characterized by estrogen receptor (ER), progesterone receptor (PR), and epidermal growth factor receptor

2 (HER2) status of the primary tumor. Advances in diagnostic and adjuvant therapies have increased the life expectancy of patients with breast cancer, but this condition remains incurable in later stages of disease progression⁹. Surgery and radiation therapy are the gold standards for the treatment of early-stage breast cancer, as are hormone therapy and the HER2-targeting antibody trastuzumab for HER2-positive cancers. Systemic administration of hormone therapy, targeted therapy, chemotherapy or a combination of these is usually the preferred treatment approach for late-stage metastatic breast cancer. However, the 5-year survival rate of women diagnosed with distant metastasis is 27% (<https://www.cancer.org/cancer/breast-cancer>). These treatments are still ineffective and commonly associated with toxic side effects; therefore, there is still a need for improved therapeutic options. A better understanding of the pathological processes through which breast cancer thrives in the host is of paramount importance to discovering new therapeutic targets.

In the past decade, the physiological mechanisms that govern the response to stress have emerged as potential therapeutic targets in breast cancer due to findings from several epidemiologic and preclinical studies^{10–12}. In particular, the action of NE and Epi on their cognate receptors has raised important considerations regarding their role in breast cancer progression, analogous to observations in other bone-tropic cancers such as prostate cancer^{13–17}. However, the adrenergic regulation of the multiple

¹ICS—Instituto de Investigação e Inovação em Saúde, Universidade do Porto, 4200-135 Porto, Portugal; ²INEB—Instituto Nacional de Engenharia Biomédica, Universidade do Porto, 4200-135 Porto, Portugal; ³CRAS—Instituto de Ciências Biomédicas Abel Salazar, Universidade do Porto, 4050-313 Porto, Portugal; ⁴IPATIMUP—Instituto de Patologia e Imunologia Molecular da Universidade do Porto, 4200-135 Porto, Portugal and ⁵FMUP—Faculdade de Medicina da Universidade do Porto, 4200-319 Porto, Portugal

Correspondence: Meriem Lamghari (lamghari@ineb.upp)

Received: 22 June 2020 Revised: 16 November 2020 Accepted: 20 November 2020

Published online: 05 February 2021

Cell line	Molecular subtype	AR(s) expressed	Reference
T47D	Luminal A (ER ⁺ , PR ⁺ , HER2 ⁻)	α _{2A} -AR, α _{2B} -AR, α _{2C} -AR	130
MCF7	Luminal A (ER ⁺ , PR ⁺ , HER2 ⁻)	α ₁ -AR, α _{2B} -AR, α _{2C} -AR, β ₁ -AR, β ₂ -AR	19, 50, 131, 132
ZR-75	Luminal A (ER ⁺ , PR ⁺ , HER2 ⁻)	β ₁ -AR, β ₂ -AR	131
BT474	Luminal B (ER ⁺ , PR ⁺ , HER2 ⁺)	β ₂ -AR	19
SKBR3	HER2 (ER ⁺ , PR ⁺ , HER2 ⁺)	β ₂ -AR	19
MDA-MB-453	HER2 (ER ⁺ , PR ⁺ , HER2 ⁺)	β ₂ -AR	131
MDA-MB-231	Basal (ER ⁻ , PR ⁻ , HER2 ⁻)	β ₂ -AR	11, 47, 132, 133
MDA-MB-468	Basal (ER ⁻ , PR ⁻ , HER2 ⁻)	β ₁ -AR, β ₂ -AR	131, 133
H5578T	Basal (ER ⁻ , PR ⁻ , HER2 ⁻)	α _{2A} -AR	132

cellular processes that drive breast cancer remains a matter of intense debate.

In this review, we discuss the current knowledge found in the literature concerning preclinical and clinical data on SNS modulation of breast cancer. Most patients with metastatic breast cancer present severe skeletal complications such as hypercalcemia, pain, and an increased incidence of fractures¹⁸. Therefore, insight into the sympathetic regulation of bone metastatic disease is also discussed in the following sections.

BREAST CANCER AND THE SNS: A COMPLEX PICTURE

Adrenoreceptors (ARs) have been reported to be expressed in a wide range of breast cancer cell lines (Table 1) as well as in tumor samples from patients with breast cancer^{19–21}. AR overexpression, particularly β₂-AR overexpression, was found to be correlated with poor prognosis of ER⁺ breast cancer patients in a recent study by Kurozumi et al.²¹, where immune biomarkers, such as the grades of tumor-infiltrating lymphocytes and programmed death ligand 1 expression, were shown to be significantly reduced in these patients. Another report by Liu et al.¹⁹ demonstrated that the β₂-AR level was correlated with lower disease-free survival and higher lymph node metastasis rates in a small cohort of HER2⁺ breast cancer patients. Both of these studies point to a putative role of β₂-AR in breast cancer pathology, but scrutinizing the mechanisms by which it promotes disease progression is still a complex exercise. In this section, we assemble the available data regarding the effect of multiple ARs on breast cancer, from primary tumor proliferation and survival to extracellular matrix (ECM) invasion and entry into the systemic circulation.

Proliferation and survival

Cancer cell proliferation and apoptosis inhibition are crucial hallmarks of cancer²². Adrenergic signaling has been implicated in several apoptosis pathways, and it has been previously suggested that endogenous catecholamines directly exert pro-survival effects on breast cancer cells^{23–25} (Figs. 1, 2). Epi was described as an antiapoptotic stimulus in human breast cancer cells in vitro, inactivating the proapoptotic protein BAD through phosphorylation in a PKA-dependent manner²⁴. Furthermore, another in vitro experiment by Reeder et al. showed that NE and Epi decrease the efficacy of commonly used drugs targeting proliferating cells, such as paclitaxel, since these catecholamines arrest MDA-MB-231 breast cancer cells in G1 phase, decelerating the cell cycle²⁵. These results are consistent with evidence from other in vitro studies showing that β₂-AR agonists inhibit triple-negative breast cancer cell proliferation and DNA synthesis^{23,26,27}. Strikingly, low concentrations of Epi increased MCF7 and MDA-MB-231 cell proliferation, while the β₂-AR agonist isoproterenol decreased the proliferation of both cell lines²⁷. These findings could be explained by the observation that Epi was shown to

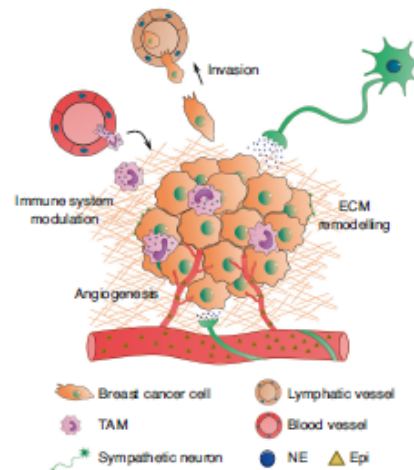


Fig. 1 Sympathetic control of breast cancer progression. NE released from sympathetic neurons closely associated with blood vessels, as well as Epi that diffuses from the circulation, modulate several important hallmarks of breast cancer such as survival, angiogenesis, immune surveillance escape, ECM remodeling and invasion. NE, norepinephrine; Epi, epinephrine; TAM, tumor-associated macrophage; ECM, extracellular matrix

differentially bind to distinct ARs depending on its concentration, with greater affinity for α₂-AR at nanomolar concentrations and shifting to β₂-AR binding at micromolar concentrations²³. Moreover, the increase in proliferation evoked by low concentrations of Epi was abrogated by the addition of the α₂-AR antagonist rauwolfscine²³. Exciting questions remain, such as the following: what is the impact of fluctuations in Epi or NE levels in the tumor microenvironment on breast cancer progression, and how can this knowledge be translated to a clinical setting? There is already recent in vivo evidence that sheds some light on the impact of circulating Epi on tumor growth; Walker and colleagues have shown that adrenal denervation and inhibition of Epi release do not impact disease progression²⁶.

Some observations from in vivo studies point to a negligible effect of β-ARs on primary tumor growth, since compared to vehicle control treatment, isoproterenol stimulation of orthotopic breast cancer tumors did not change primary tumor proliferation^{11,23,29,30}. It is unclear whether these results arose from the direct action of β₂-AR on tumor cell proliferation, inhibition of

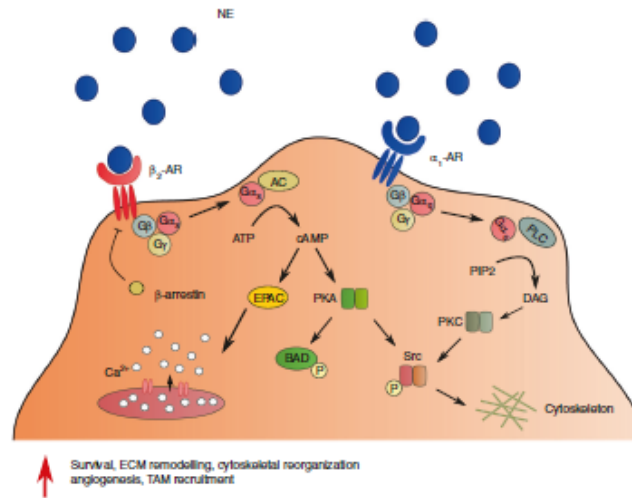


Fig. 2 Adrenergic receptor downstream signaling. β_2 -AR activation triggers several downstream signaling pathways, mediated by an increase in intracellular cAMP, leading to Ca^{2+} release, apoptosis inhibition through phosphorylation of BAD, and cytoskeletal rearrangement. β_2 -ARs are quickly desensitized by β -arrestins after ligand binding and signal transduction. Alternatively, α_1 -AR stimulation has also been described to promote invasive phenotypes through PKC-mediated signaling pathways. NE, norepinephrine; TAM, tumor-associated macrophage; ECM, extracellular matrix

tumor growth by other cell types in the stroma or even a combination of direct and indirect effects. Another study using human xenografts in immunocompromised mice reported increased ER⁺/PR⁺ breast cancer tumor growth after inoculation with the α_2 -AR agonist clonidine³¹. The increase in tumor growth was accompanied by a similar increase in the proliferation of tumor-associated fibroblasts, and thus, an indirect effect of α_2 -AR agonism through the tumor microenvironment cannot be ruled out³¹. It is also intriguing that Thaker et al. reported an increase in MDA-MB-231 tumor growth after chronic stress induction in an orthotopic breast cancer model³², contrasting with the studies previously discussed. Notably, pharmacological β -AR activation seems to inhibit primary tumor growth^{11,23}, while endogenous chronic stress either causes negligible effects or increases tumor growth^{29,30,32–34}. This observation raises important questions, such as whether compensatory mechanisms are exerted by other ARs in endogenous stress models, since Epi and NE can stimulate both α -ARs and β -ARs. In fact, α_2 -AR antagonists were shown to counteract the increase in tumor growth evoked by restraint stress³³. Lamkin and colleagues also showed that in the absence of chronic stress, α_2 -AR blockade recapitulated the tumor growth observed when the SNS was endogenously activated³⁵, adding another layer of complexity to the impact of SNS signaling on breast cancer. This effect probably arises because presynaptic α_2 -ARs in peripheral SNS neurons establish a negative feedback loop to control NE release from neuronal terminals³⁵. Thus, blockade of α_2 -ARs in the absence of chronic stress increases the release of NE in the tumor microenvironment, mirroring endogenous activation of the SNS.

Angiogenesis

As breast tumors proliferate and grow, the need for nutrients and oxygen rises concordantly. These needs are met by the sprouting of new blood vessels that give rise to a network of often aberrant vasculature in the tumor microenvironment³⁶. The SNS has emerged as an important player in neoangiogenesis, since it has

already been shown that sympathetic outflow can induce the secretion of proangiogenic factors, namely, vascular endothelial growth factor (VEGF), by breast cancer cells^{29,37–39}. In addition, direct cell–cell contact between breast cancer cells and endothelial cells leads to increased formation of capillary structures in vitro, a result markedly potentiated by the addition of NE³⁸. This effect was suggested to be mediated by the β_2 -AR/PKA/mTOR pathway and by upregulation of the Notch ligand Jagged-1, directly augmenting Notch signaling in endothelial cells³⁸. Interestingly, there seems to be a cell-specific response to β_2 -AR agonists in terms of VEGF expression that is not entirely due to differential β_2 -AR expression³⁷. β_2 -AR agonists were found to increase VEGF production in a brain-tropic variant of the MDA-MB-231 cell line in vitro but not in the parental cell line or in cells with low β_2 -AR expression, such as MCF7 cells³⁷. Distinct targets of downstream effectors of the β_2 -AR/PKA pathway in the different cell lines might explain the disparity in terms of angiogenic responses.

Other players have recently been suggested to be involved in the sympathetic regulation of tumor angiogenesis. Activation of peroxisome proliferator-activated receptor γ (PPAR γ) was shown to markedly decrease VEGF expression in 4T1 murine breast cancer cells in vitro, and NE was shown to inhibit PPAR γ expression in these cells⁴⁰. This inhibition was abrogated by the addition of ICI118551, pointing towards a β_2 -AR-mediated effect⁴⁰.

In addition to the in vitro data previously discussed, accumulating evidence from several in vivo studies indicates that chronic stress modulates neoangiogenesis and the lymphatic vasculature in breast cancer. Chronic restraint stress, as a model of endogenous SNS activation, was found to increase VEGFC secretion from MDA-MB-231 orthotopic tumors in immunocompromised mice, as well as from 66d4 tumors in immunocompetent mice, leading to increased tumor lymphatic vessel density²⁹. This effect was recapitulated or abrogated by isoproterenol or propranolol treatment, respectively, suggesting the existence of a β -AR-specific signaling pathway²⁹. Stress-induced production of

VEGF in 66cH primary breast tumors in mice and a consequent increase in vascularization were also described³⁰. The increased tumor vasculature was also suggested to be an additional route of cancer cell escape^{34,35} (Fig. 1), facilitating metastasis, as discussed in the following sections.

Immune system modulation

The crosstalk between the SNS and the immune system in the regulation of inflammation is already recognized. Dendritic cells and monocytes express both the α -AR and β -AR subtypes, and adrenergic activation in these cells leads to downregulation of tumor necrosis factor α (TNF- α), IL-1, and IL-6, resulting in the promotion of an immunosuppressive phenotype⁴⁰. The effect of the SNS on the different immune cell populations in the context of inflammation and hematopoiesis has already been previously reviewed⁴¹.

Among the many cellular components of the tumor microenvironment that are affected by SNS catecholamines, tumor-associated macrophages (TAMs) are crucial for cancer progression. SNS signaling prompts breast cancer cells to secrete proinflammatory cytokines, such as IL-6³⁷ and M-CSF³⁰, which can enhance the recruitment and infiltration of macrophages into the primary tumor (Fig. 1). On the other hand, β_2 -AR activation in macrophages increases the expression of cancer progression-promoting factors, such as transforming growth factor β (TGF- β), matrix metalloproteinase (MMP) 9, VEGF and cyclooxygenase-2 (COX2), *in vivo*³⁰. Macrophage expression of COX2 and consequent secretion of prostaglandin E2 (PGE2) further drives the production of VEGFC by cancer cells to induce lymphangiogenesis³⁹. In addition, in an orthotopic breast cancer model, peripheral sympathetic nerve ablation using 6-hydroxydopamine led to inhibition of TAM recruitment and to a decrease in tumor IL-6 levels⁴².

Upon chronic stress induction in syngeneic breast cancer mouse models, TAMs are mostly primed towards an immunosuppressive M2 phenotype: genes such as Arginase-1 and IL-10 are overexpressed, while M1 phenotype-characteristic genes are conversely downregulated^{30,43}. In addition, Bucsek et al. reported a significant decrease in tumor-infiltrating effector cytotoxic CD8⁺ T cells upon β -AR activation and concomitant 4T1 breast cancer tumor growth⁴⁴. Immunosuppressive CD4⁺ Treg cells and splenic myeloid-derived suppressor cells were also elevated in stressed mice⁴⁴.

Furthermore, and in agreement with the reports discussed above, Kamiya et al. elegantly illustrated the influence of tumor sympathetic innervation on immune checkpoint expression and cancer progression³⁴. With a viral vector-based tool, the authors were able to specifically denervate the tumor stroma without affecting surrounding tissues³⁴. The subsequent decrease in tumor NE content abrogated tumor growth and metastatic spread. Moreover, sympathetic denervation downregulated immune checkpoint molecules, such as programmed death 1 (PD-1), in β_2 -AR-expressing CD4⁺ and CD8⁺ tumor-infiltrating lymphocytes. The authors observed the same outcomes in chemically induced and spontaneous breast cancer models and reported correlations between the density of sympathetic fibers, PD-1 expression and tumor recurrence in a small cohort of human breast cancer patients³⁴.

These observations reinforce the hypothesis that SNS-driven immunosuppression and subsequent evasion of immune surveillance play an important role in breast cancer progression.

Extracellular matrix invasion

As the disease progresses, a cascade of cellular events triggers the ability of breast cancer cells to remodel and invade adjacent tissues, eventually escaping into the circulation through intravasation into blood or lymphatic vessels⁴⁵. Crosstalk between the tumor microenvironment and breast cancer cells is crucial for the acquisition of invasive features, and the SNS has been directly

linked to the process of epithelial-to-mesenchymal transition (EMT)⁴⁶.

Adrenergic signaling, namely, through β_2 -AR, has been shown to directly modulate several cellular processes in breast cancer cell lines. Isoproterenol stimulation led to increased invasive capacity of highly metastatic MDA-MB-231 cells *in vitro*, and this effect was β_2 -AR specific⁴⁶. Interestingly, overexpression of β_2 -AR in MCF7 cells resulted in increases in the number of invadopodia and the invasive capacity after incubation with isoproterenol⁴⁶.

The molecular mechanisms that govern this adrenergic response have begun to be elucidated in recent years. Stimulation of β_2 -AR *in vitro* causes the accumulation of intracellular cAMP through the G α_s /adenylyl cyclase pathway and consequent dephosphorylation of ERK1/2⁴⁷. This increase in cAMP activates PKA and exchange protein directly activated by cAMP, leading to increased mobilization of Ca²⁺ in a feedforward loop that ultimately drives cell invasion mechanisms⁴⁷ (Fig. 2). In other *in vitro* studies, β_2 -AR activation led to increased motility and invasiveness of MDA-MB-231 cells, partially through changes in actin remodeling and contractility and an increase in plasma membrane protrusions^{46,49}. Interestingly, the β -AR agonist isoproterenol reduced the number of focal adhesions while increasing the number of invadopodia, favoring motility in three-dimensional spaces but not on two-dimensional surfaces⁴⁸.

Although most of the available data in the literature are from experiments with β_2 -AR and MDA-MB-231 cells, other cell lines and ARs should not be overlooked. Dezong et al. reported that invasion and migration mediated by the proto-oncogenic tyrosine protein kinase Src were modulated by different ARs in the MDA-MB-231 and MCF7 cell lines *in vitro*, namely, β_2 -ARs and α_1 -ARs, respectively⁵⁰. Src was found to be targeted for phosphorylation via different signaling pathways, i.e., PKA in MDA-MB-231 cells and PKC in MCF7 cells⁵⁰. These data might explain the seemingly contradictory results observed in previous studies, where the migration capacity of MCF7 cells was described to be decreased upon stimulation with the β -AR agonist isoproterenol²⁷. The same study reported a decrease in MDA-MB-231 cell migration after isoproterenol stimulation²⁷, possibly because a parental MDA-MB-231 cell line was used instead of a highly metastatic variant of the MDA-MB-231 cell line⁴⁷⁻⁴⁹.

In addition to the direct effects of NE on breast cancer cells, stimulation of tumor stromal α_2 -AR was reported to promote breast cancer progression and invasion. Pharmacological activation of α_2 -AR but not α_1 -AR or β -AR increased the rate of metastasis in a syngeneic orthotopic breast cancer model⁵¹. These changes were correlated with altered collagen structure and were cancer cell independent, since the cell line used did not respond to NE *in vitro*⁵¹. However, no insight was provided on the stromal players targeted by α_2 -AR agonists that are involved in collagen remodeling.

As can be appreciated by the collective results of previous studies, the interplay between breast cancer and the SNS is extremely complex. Clearly, knowledge concerning the combination of α -AR and β -AR signaling on cancer progression, as well as on the distinct cellular players in the tumor microenvironment, is still scarce. Therefore, careful consideration should be exercised when designing experiments and therapeutic interventions.

BREAST CANCER METASTASIS AND THE BONE NICHE

After escaping into the vasculature, breast cancer cells disseminate and travel towards distant organs in a complex multistep process that has not yet been fully elucidated. Breast cancer exhibits specific tropism for organs such as the lung, brain, liver and bone, and there are indications that this tropism is associated with breast cancer receptor status⁵². Luminal A/B tumors are the most prevalent subtype in patients with breast cancer, and they mostly metastasize to bone^{53,54}. Luminal A/B bone metastases are

typically indolent in the first years of follow-up, and patients presenting only bone metastases have higher overall survival rates than patients presenting metastasis to other distant sites^{53,54}. However, ~70% of all late-stage breast cancer patients exhibit bone metastatic foci leading to severe complications such as hypercalcemia, pain and bone fractures^{52,55}. Metastatic foci are found mostly in long bones, ribs, the pelvis, and vertebrae, which contain abundant marrow and provide an immune context favorable for cancer cell survival; the bone marrow microenvironment is crucial for the maintenance of the hematopoietic stem cell niche⁵⁶. In addition, bone stromal cells secrete a combination of cytokines and growth factors that favor breast cancer cell homing, survival, and proliferation⁵⁷. Breast cancer cells establish close interactions with bone cells, namely, osteoclasts and osteoblast-lineage cells, and the SNS can potentiate this crosstalk.

The metastatic vicious cycle

The skeletal system plays a critical role in all stages of human development. The skeleton is responsible for locomotion; it is the preferential site for hematopoiesis, regulates mineral homeostasis and protects vital organs, such as the brain, heart and lungs. It is therefore crucial to maintain skeletal structural integrity and function throughout life. This maintenance is achieved mainly through a highly dynamic bone remodeling process, where the bone matrix is degraded and subsequently replaced by new mineralized bone in a coordinated fashion. Osteoclasts are specialized multinucleated cells of the hematopoietic lineage that are able to demineralize and resorb the bone matrix using a combination of secreted enzymes, such as cathepsin K (CatK)⁵⁸ and tartrate resistant acid phosphatase⁵⁹. During resorption, factors secreted from osteoclasts and byproducts of bone matrix degradation recruit precursors of bone-forming cells, coupling bone resorption and bone formation. These precursors of a mesenchymal lineage differentiate into mature osteoblasts, which are then responsible for the deposition of high amounts of ECM proteins and for their mineralization⁶⁰. Osteoblasts can then entomb themselves in the matrix that they produce and transform into osteocytes. These cells account for more than 90% of the cells present in cortical bone and have long extensions, creating an interconnecting network between osteocytes themselves and cells in the bone marrow⁶¹. Osteocytes are thought to have an endocrine⁶² and mechanosensitive role^{63,64} in bone, participating in complex adaptations to internal and external stimuli.

Breast cancer often leads to highly osteolytic bone metastases, where cancer cells exploit the normal bone remodeling process and shift the balance towards increased bone resorption. Parathyroid hormone-related protein (PTHrP), MMPs and PGE2 are some of the factors released by tumor cells that modulate the expression of receptor activator of NF- κ B ligand (RANKL) by osteoblasts, which is a master regulator of osteoclast differentiation^{65,66}. Increased RANKL production by osteoblasts and osteocytes in turn enhances osteoclast differentiation and activity, leading to extensive bone degradation. On the other hand, bone matrix-embedded factors released during resorption, such as TGF- β , insulin growth factor, and platelet-derived growth factor, further stimulate tumor growth and perpetuate a "vicious cycle" of bone destruction⁶⁷. Bisphosphonates and denosumab (an anti-RANKL human monoclonal antibody) are commonly used as adjuvant therapies for the treatment of metastatic bone disease to normalize the level of osteoclastic activity⁶⁸. However, although these treatments alleviate skeleton-related symptoms, new and more effective therapeutic targets are needed to suppress the establishment of the vicious cycle.

The SNS and bone metastatic disease

Bones are highly innervated organs, with a high density of sensory and sympathetic nerve fibers in the periosteum and along blood vessels in the bone marrow⁶⁹. A physical and functional

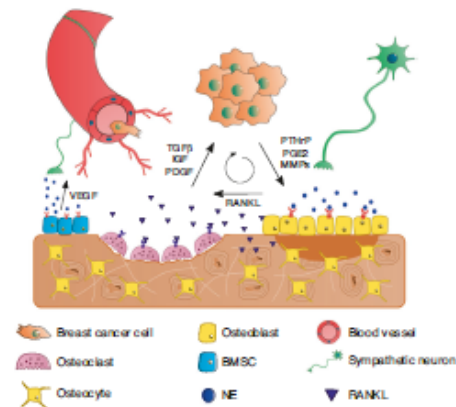


Fig. 3 The bone metastatic niche and the metastatic vicious cycle. Once engrafted in the bone, breast cancer cells secrete pro-osteoclastic factors such as PTHrP, PGE2, and MMPs, which induce the expression of RANKL by osteoblasts and osteocytes, promoting osteoclast differentiation and activity. In turn, factors released from the bone matrix enhance the growth of cancer cells, establishing a metastatic vicious cycle that leads to extensive bone degradation. NE, norepinephrine; BMSC, bone marrow stromal cell

association of nerve fibers and bone cells is to be expected⁷⁰, since the nerve fiber density is usually increased near surfaces with enhanced bone turnover⁷¹.

Although cells of osteoblast and osteoclast lineages have been reported to express α -AR mRNA, its relative expression compared to that of the β_2 -AR subtype is greatly reduced^{72–74}. β_2 -AR but not β_1 -AR or β_3 -AR is widely expressed in primary osteoclasts and osteoclastic cell lines^{75,76}, as well as in osteoblast lineage cells^{76–78}. β_2 -AR is fully functional in bone cells, since β_2 -AR agonism triggers an increase in intracellular cAMP in vitro⁷⁹. Interestingly, cells of the osteoblast lineage also express monoamine oxidase (MAO) α and MAO β ⁷⁹, as well as the NE transporter⁸⁰, and are thus able to take up and catabolize NE from the external milieu.

β_2 -AR activation in bone triggers osteoclastic differentiation, diminished bone formation and consequent bone loss (reviewed in⁸¹), mostly due to an increase in RANKL production by osteoblast lineage cells in vivo^{82,83} (Fig. 3). Similarly, β_2 -AR agonism was reported to increase RANKL production by the MLO-Y4 osteocytic cell line in vitro and consequently to induce the differentiation of the RAW264.7 osteoclastic cell line in coculture experiments⁸⁴. Although osteocytes have received increasing attention in recent years regarding their role in the modulation of breast cancer progression^{85–88}, data on the action of adrenergic signaling pathways on osteocytes in this context are still scarce. Osteocytes express β_2 -AR, and as they are the most common cell type in bone, the importance of their putative crosstalk with the SNS in breast cancer should not be overlooked. Regardless, SNS activation of osteoblast-lineage cells seems to further potentiate the establishment of a metastatic vicious cycle upon bone metastatic colonization of breast cancer.

Campbell and colleagues have made important contributions to this field of research. In a mouse model of bone metastasis established by intracardiac injection of bone-tropic MDA-MB-231 cells, the authors showed that adrenergic stimulation of the bone stroma potentiated the establishment of the metastatic vicious cycle¹¹. Chronic immobilization stress, as a model of endogenous sympathetic activity, was used to demonstrate that augmented catecholamine levels led to the formation of larger osteolytic lesions, an effect mediated by β_2 -AR¹¹. Moreover, isoproterenol

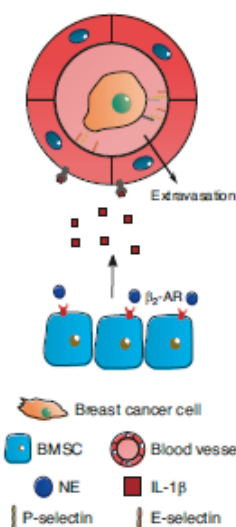


Fig. 4 Breast cancer cell extravasation into the bone niche. NE stimulation of stromal β₂-AR is associated with an increased release of VEGF and IL-1β, which leads to augmented angiogenesis and expression of P- and E-selectins in endothelial cells. The latter event promotes breast cancer cell extravasation from the circulation into the bone marrow

administration before injection of breast cancer cells increased the numbers of tumor foci and lesions in bone, suggesting that sympathetic triggering in the bone microenvironment facilitated breast cancer cell engraftment. The authors suggested that this effect was partially due to RANKL signaling and its chemotactic action on MDA-MB-231 cells¹¹.

In addition to augmented RANKL signaling, adrenergic stimuli promoted breast cancer extravasation and retention in the bone through modulation of the bone vasculature. Nude mice subjected to either chronic immobilization stress or isoproterenol administration showed increased VEGF-A expression by bone marrow stromal cells (BMSCs) and consequent angiogenesis, which resulted in the promotion of breast cancer cell colonization⁶⁰. Furthermore, incubation of BMSCs with isoproterenol led to the release of IL-1β, which in turn activated E/P-selectin expression in endothelial cells and enabled the adhesion and retention of breast cancer cells *in vitro*⁶⁰ (Fig. 4).

Interestingly, the interplay between the SNS and breast cancer in the bone metastatic niche is not unidirectional. Not only is the SNS capable of inducing breast cancer cell engraftment and proliferation through RANKL and VEGF-A signaling, but conversely, breast cancer may also be able to regulate AR dynamics in the bone niche. Breast cancer cell-secreted PTHrP is a well-known modulator of bone turnover in the metastatic niche (reviewed in⁹⁵). PTHrP binds to PTH receptor 1 (PTHr1) expressed in osteoblasts and upregulates RANKL expression to promote osteoclastogenesis, driving the vicious metastatic cycle⁹². Interestingly, PTHr1, β₂-AR, and their corresponding downstream pathways in osteoblastic cells seem to be intimately connected. Using germline β₂-AR knockout mice, Hanyu et al. demonstrated that β₂-AR expression is required for the osteoanabolic effect of PTH and that β₂-AR modulates the expression of PTHr1 target genes, such as RANKL, alkaline phosphatase, bone sialoprotein, and osteoprotegerin (a RANKL decoy receptor), in osteoblasts⁹³.

On the other hand, PTH was shown to directly downregulate β₂-AR expression in osteoblast-like MC3T3-E1 cells *in vitro*⁹⁴. This interdependency might be explained by common intracellular downstream effectors that are triggered by binding of their corresponding ligands. Both PTHr1 and β₂-AR are GPCRs that signal through the adenylyl cyclase/PKA axis and promote the phosphorylation of cAMP-response element binding protein to induce transcription of target genes⁹⁴. Furthermore, after ligand binding, both receptors are rapidly desensitized through pathways dependent on β-arrestin and β-adrenergic kinase^{195–97}, which can also act as protein scaffolds that subsequently lead to the activation of the mitogen-activated protein kinases ERK1/2 and several other effector molecules⁹⁸. However, while these interactions have been described to occur between PTHr1 and β₂-AR in the context of intermittent PTH treatment, it is still unknown whether breast cancer-secreted PTHrP can elicit the same response in the context of bone metastatic disease. Although PTHrP and PTH share the same receptor, there are several described noncanonical pathways for the action of PTHrP whose importance is still poorly understood⁹¹. Therefore, more data on the interplay between PTHrP and β₂-AR in breast cancer bone metastasis are urgently required, since this knowledge could change our understanding of the dynamics of β₂-AR expression in bone throughout the progression of this disease and facilitate the design of new, more effective therapeutic options.

BREAST CANCER AND BETA-BLOCKERS: A CLINICAL PERSPECTIVE

Although preclinical data are extremely valuable for understanding the many processes that control breast cancer progression and metastatic spread, it is crucial to translate the results into a clinical setting. In the past decade, increasing attention has been devoted to the effect of sympathetic activity on breast cancer patient survival and breast cancer recurrence¹⁰⁹. In this section, we will review the published epidemiologic and clinical data on the effect of several β-AR antagonists (henceforth called beta-blockers) on breast cancer and discuss the limitations associated with the interpretation of the reported results.

Epidemiologic studies have previously suggested that patients with cancer subjected to high levels of psychosocial stress usually have a poorer prognosis and survival than those not subjected to these conditions¹⁰⁹. SNS-targeting beta-blockers are thus potential therapeutic options for cancer and are already widely used in other pathological settings, such as the treatment of asthma and hypertension^{101,102}. The safety profile of these drugs is well described, and they are not associated with an increased incidence of breast cancer, as evidenced by previous epidemiologic studies^{103,104}.

A proof-of-principle study performed by Powe et al. analyzed the effect of beta-blocker prescription prior to breast cancer diagnosis on patient survival¹⁰. Reduced tumor recurrence and metastasis incidence and increased patient survival rates were reported in the beta-blocker-treated group, with no significant differences in tumor stage, tumor size, tumor grade or vascular invasion between the treated and placebo groups.

However, the population size in that study was relatively small, and no distinction between the type of beta-blockers used was included in the analysis¹⁰. Atenolol and bisoprolol are β₁-AR specific, while propranolol and timolol are nonspecific β_{1/2}-AR antagonists; therefore, the contributions of the different ARs to the reported results cannot be isolated. In fact, another population-based study by Barron et al. showed a beneficial effect of propranolol but not atenolol on breast cancer metastasis and patient survival¹⁰⁵. Interestingly, Melhem-Bertrand et al. reported a beneficial effect of the β₁-AR-targeting drugs metoprolol and atenolol on the recurrence of triple-negative breast cancer (TNBC) but not on ER-positive breast cancer, highlighting the importance

Table 2. Summary of epidemiologic studies regarding the influence of β -blockers on breast cancer outcomes

Treated group size/ total size	β -Blocker used (population size)	Improved patient survival (HR; CI)	Reduced tumor recurrence (HR; CI)	Reduced incidence of metastasis (HR; CI)	Reference
43/466	Atenolol (25) Propranolol (7) Bisoprolol (7) Timolol (4)	Yes (0.291; 0.119–0.715)	Yes (–)	Yes (0.430; 0.200–0.926)	10
595/4 738	Atenolol (525) Propranolol (70)	Yes (0.19; 0.06–0.60)	N.D.	Yes (–)	105
204/1 779	Atenolol (–) Metoprolol (–) Propranolol (–) Others (–)	No (0.76; 0.44–1.33)	No (0.86; 0.57–1.32)	N.D.	134
102/1 413	Metoprolol (43) Atenolol (38) Others (21)	No (0.64; 0.38–1.07)	Yes (0.52; 0.31–0.88)	N.D.	106
74/800	Carvedilol (11) Sotalol (3) Atenolol (27) Betaxolol (1) Bisoprolol (11) Metoprolol (8) Nebivolol (13)	Yes (0.42; 0.18–0.97)	Yes (0.52; 0.28–0.97)	Yes (0.32; 0.12–0.90)	108
3 660/18 733	Metoprolol (1 793) Atenolol (622) Propranolol (586) Others (659)	N.D.	No (1.3; 1.1–1.5)	N.D.	111
1 770/55 252	Propranolol (1 770)	No (0.94; 0.77–1.16)	N.D.	N.D.	99
1 443/5 754	Carvedilol (22) Sotalol (84) Atenolol (854) Bisoprolol (189) Metoprolol (45) Propranolol (249)	No (1.11; 0.94–1.32)	N.D.	N.D.	112
153/1 144	Bisoprolol (59) Metoprolol (48) Atenolol (28) Propranolol (13) Others (5)	No (1.05; 0.85–1.29)	Yes (0.81; 0.66–0.99)	N.D.	109
93/956	N.D.	Yes (0.48; 0.23–0.99)	No (0.93; 0.39–2.25)	Yes (0.40; 0.17–0.93)	29

HR hazard ratio, CI 95% confidence interval (lower limit–higher limit), N.D. no data

of breast cancer receptor status on the response to beta-blockers¹⁰⁶. Thus, it is still unclear which receptors are the main contributors to the reported beneficial effects of beta-blockers on breast cancer recurrence, and this topic is a matter of intense debate. However, we hypothesize that a broader acting beta-blocker, such as propranolol, could be even more beneficial than specific beta-blockers in managing breast cancer recurrence and metastasis.

Several studies have suggested that beta-blocker usage could be explored as an adjuvant therapy in breast cancer treatment^{10,29,106–109}. However, these studies have some limitations, such as a retrospective design, small population size, difficulties in the assessment of beta-blocker treatment duration and compliance, or a lack of access to data on comorbidities and other medications. Other retrospective studies reported no correlation

between beta-blocker usage and reduced breast cancer-specific mortality or recurrence^{99,110–112}, and thus, the benefits of these drugs remain controversial (for more details, refer to Table 2). Randomized clinical trials are warranted to assess the clinical relevance of beta-blockers for breast cancer treatment.

To our knowledge, the only results from phase II placebo-controlled clinical trials published to date address the effect of perioperative propranolol administration on several metastatic biomarkers in patients with early breast cancer. Zhou et al. reported decreased immunosuppression after the administration of propranolol compared to placebo controls during the perioperative period of breast cancer surgery¹¹³. Propranolol was also shown to block the proliferation of patient-derived regulatory T cells¹¹³. Shaashua¹¹⁴ and Halder¹¹⁵ reported a reduction in the expression of EMT-related genes in resected

primary tumors from patients simultaneously treated with propranolol and the COX-2 inhibitor etodolac. The resected tumors also showed reduced expression of prometastatic, antiapoptotic and proliferation markers; increased infiltration of B-cells; and a decreased population of TAMs. Propranolol- and etodolac-treated patients also presented reduced levels of the circulating inflammatory cytokines IFN γ and IL-6 and increased levels of NK cell activation during treatment¹¹⁴. Another randomized clinical trial by Hiller et al. showed similar results with the administration of propranolol for one week before surgical resection of the primary breast tumor¹¹⁶. In this study, compared to placebo-treated controls, patients treated with propranolol before surgery showed reduced EMT gene expression and increased dendritic cell infiltration and M1 macrophage polarization in the resected tumors. Interestingly, compared to clinically responsive patients, patients clinically nonresponsive to propranolol (i.e., without significant reductions in blood pressure and heart rate after beta blockade) showed decreased tumor EMT gene expression, although immune cell infiltration in the primary tumor was changed¹¹⁶. These clinical trials pointed to a possible beneficial effect of propranolol on reducing the metastatic potential of primary breast tumors. However, adequately powered clinical trials with a focus on overall survival and cancer recurrence are still needed before propranolol can be used for breast cancer treatment.

CONCLUSION AND FUTURE PERSPECTIVES

Despite the advances made in recent years, knowledge on the impact of endogenous stress on the complex interactions governing breast cancer disease progression is still incomplete. This review summarizes and combines the available data regarding SNS signaling in the orchestration of breast cancer.

To date, adrenergic signaling has been implicated in several steps of disease progression, promoting tumor growth, angiogenesis, immunosuppression and invasion (Fig. 1). While several *in vitro* studies and animal models have illustrated the intricate control exerted by the SNS over cancer cellular processes, the contributions of the different ARs expressed in the multiple cellular components of the tumor microenvironment remain puzzling. Furthermore, the inherent heterogeneity of breast cancer presents an additional challenge in modeling this disease. The distinctive AR expression patterns in breast cancer cell lines widely used in the various experimental models are certainly relevant, and more information on the adrenergic control of disease progression in different cell lines is urgently needed.

Modeling the various cellular and structural components of the cancer niche is still technically challenging. The use of immunodeficient mice is required for xenograft models, but the contribution of the immune system is not considered in these models. Thus, current *in vitro* and *in vivo* models do not completely recapitulate the complexity of the disease, but as new, more complicated models are developed, discerning the specific contributions of each cell type becomes increasingly difficult. Specific deletion of β_2 -AR in not only breast cancer cells²⁶ but also osteoblasts³⁰ and macrophages¹¹⁷ could be used as an important tool to elucidate the role of this receptor in various models of the disease, although no models of conditional β_2 -AR knockout specifically in osteodasts or osteocytes have been described to date. Furthermore, microfluidic systems have several advantages when compared to traditional *in vitro* models since they allow the compartmentalization of different cell types and the introduction of fluid flow, which can be physiologically relevant. Microfluidic platforms have already been developed for the study of breast cancer metastasis to bone^{118–121}, but modeling the SNS in these platforms is still challenging.

Metastatic tropism for bone is an evident feature of breast cancer, and bone is the most common site of metastasis in luminal

breast cancer patients⁵². Although adrenergic stimulation of the bone microenvironment is thought to increase osteolysis and potentiate the metastatic vicious cycle, the SNS-controlled interactions between breast cancer and bone cells remain mostly unexplored, apart from the contributions of Belderiou and his group^{11,89,90}. Although the use of luminal A breast cancer cell lines in bone metastasis models presents technical challenges due to the less invasive phenotype of these cell lines, it is crucial to understand the molecular changes that might be elicited by the SNS in these cells. Furthermore, since luminal A tumors are the most common subtype of breast tumors in patients, the use of luminal subtype breast cancer cells in *in vitro* and *in vivo* models of this disease is certainly more clinically relevant than the currently widespread use of aggressive TNBC cells.

Future developments in novel targeted therapeutic strategies, such as tumor-specific denervation via viral vectors³⁴, are exciting fields of research that will require input from various areas of expertise before becoming applicable in a clinical setting. It is still unclear whether this technique can be applied to locally and specifically denervate bone in preclinical studies. In addition, other denervation techniques, such as chemical sympathectomy by local delivery of guanethidine into the femoral bone marrow via an osmotic minipump, have been established¹²², which could help to clarify the role of sympathetic nerves in bone metastasis.

Finally, clinical observations on the usage of beta-blockers for the treatment of breast cancer suggest that interfering with SNS signaling could have beneficial effects on patients, particularly in the control of metastatic spread. However, systemic administration of beta-blockers can also have unforeseen consequences on the progression of breast cancer, and adequately powered clinical trials are needed before their therapeutic implementation. Targeted drug delivery systems could address the currently unmet clinical challenge of circumventing the disadvantages of systemic beta-blocker administration. The unique biochemical and biophysical characteristics of the bone microenvironment provide the means for targeted drug delivery to bone metastatic tumors. Bisphosphonates¹²³, acidic amino acid peptidic sequences¹²⁴, liposomes¹²⁵, organic¹²⁶, and inorganic¹²⁷ nanoparticles, chimeric peptides targeting CatK¹²⁸ and HER2-targeting nanoparticles¹²⁹ have been previously used to achieve bone metastasis-specific drug and gene delivery *in vivo*. Whether these strategies can be used to deliver SNS-targeting drugs specifically to the bone microenvironment and whether they can be translated into a clinical benefit remain to be elucidated.

Taken together, the data summarized in this review highlight the importance of SNS activation in breast cancer. In the next few years, exciting new developments are expected that would allow us to complement our understanding of the molecular cues that drive breast cancer progression.

ACKNOWLEDGEMENTS

This work was financed by FEDER—Fundo Europeu de Desenvolvimento Regional funds through the COMPETE 2020—Operational Programme for Competitiveness and Internationalisation (POCI), Portugal 2020, and Portuguese funds through FCT/MCTES in the framework of the project “SproutOC” (POCI-01-0145-FEDER-030158/PTDC/MED-PAT/30158/2017). F.C. is a recipient of the Ph.D. fellowship SFRH/BD/128771/2017. D.M.S. is a recipient of the postdoctoral fellowship SFRH/BPD/115341/2016.

ADDITIONAL INFORMATION

Competing interests: The authors declare no competing interests.


REFERENCES

- Lyons, C. E. et al. Optogenetic-induced sympathetic neuromodulation of brown adipose tissue thermogenesis. *FASEB J.* **34**, 2765–2773 (2020).

2. Cole, S. W., Nagaraja, A. S., Lutgendorf, S. K., Green, P. A. & Sood, A. K. Sympathetic nervous system regulation of the tumour microenvironment. *Nat. Rev. Cancer* **15**, 563–572 (2015).
3. Katayama, Y. et al. Signals from the sympathetic nervous system regulate hematopoietic stem. *Cell Egr. Bone Marrow Cell* **124**, 407–421 (2006).
4. Mani, B. K., Osborne-Lawrence, S., Vijayaraghavan, P., Hepler, C. & Zigman, J. M. β 1-Adrenergic receptor deficiency in ghrelin-expressing cells causes hypoglycemia in susceptible individuals. *J. Clin. Invest.* **126**, 3467–3478 (2016).
5. Anil, M., Nagasawa, T., Koshihara, Y., Yamamoto, S. & Togari, A. Effects of β -adrenergic agonists on bone-resorbing activity in human osteoclast-like cells. *Biochim. Biophys. Acta (BBA)—Mol. Cell Res.* **1640**, 137–142 (2003).
6. Huang, H. H., Brennan, T. C., Muir, M. M. & Mason, R. S. Functional α 1- and β 2-adrenergic receptors in human osteoblasts. *J. Cell Physiol.* **220**, 267–275 (2009).
7. Wu, L. et al. Bidirectional role of β 2-adrenergic receptor in autoimmune diseases. *Front. Pharmacol.* **9**, 1313 (2018).
8. Ali, D. C. et al. β -Adrenergic receptor, an essential target in cardiovascular diseases. *Heart Fail. Rev.* **25**, 343–354 (2020).
9. Galvano, A. et al. Denosumab for bone health in prostate and breast cancer patients receiving endocrine therapy? A systematic review and a meta-analysis of randomized trials. *J. Bone Oncol.* **18**, 100252 (2019).
10. Powe, D. G. et al. Beta-blocker drug therapy reduces secondary cancer formation in breast cancer and improves cancer specific survival. *Oncotarget* **1**, 628–638 (2010).
11. Campbell, J. P. et al. Stimulation of host bone marrow stromal cells by sympathetic nerves promotes breast cancer bone metastasis in mice. *PLoS Biol.* **10**, e1001369 (2012).
12. Obradović, M. M. S. et al. Glucocorticoids promote breast cancer metastasis. *Nature* **567**, 540–544 (2019).
13. Perron, L., Balaoui, I., Harel, F. & Maye, F. Antihypertensive drug use and the risk of prostate cancer (Canada). *Cancer Causes Control CCC* **15**, 535–541 (2004).
14. Hassan, S. et al. Behavioral stress accelerates prostate cancer development in mice. *J. Clin. Invest.* **123**, 874–886 (2013).
15. Magnon, C. et al. Autonomic nerve development contributes to prostate cancer progression. *Science* **341**, 1236361 (2013).
16. Dedier, A. M. et al. Sympathetic signaling reactivates quiescent disseminated prostate cancer cells in the bone marrow. *Mol. Cancer Res.* **15**, 1644–1655 (2017).
17. Coarf, C. et al. Influence of the neural microenvironment on prostate cancer. *Prostate* **78**, 128–139 (2018).
18. Jimenez-Andrade, J. M. et al. Bone cancer pain. *Ann. N. Y. Acad. Sci.* **1198**, 173–181 (2010).
19. Liu, D. et al. A Her2-let-7- β 2-AR circuit affects prognosis in patients with Her2-positive breast cancer. *BMC Cancer* **15**, 882 (2015).
20. Rivero, E. M. et al. Prognostic significance of α - and β 2-adrenoceptor gene expression in breast cancer patients. *Br. J. Clin. Pharmacol.* **85**, 2143–2154 (2019).
21. Kurozumi, S. et al. β 2-Adrenergic receptor expression is associated with biomarkers of tumor immunity and predicts poor prognosis in estrogen receptor-negative breast cancer. *Breast Cancer Res. Treat.* **177**, 603–610 (2019).
22. Hanahan, D., & Weinberg, Robert A. Hallmarks of cancer: the next generation. *Cell* **144**, 646–674 (2011).
23. Pérez Piñero, C., Bruzone, A., Sarappa, M., Castillo, L. & Lüthy, I. Involvement of α 2- and β 2-adrenoceptors on breast cancer cell proliferation and tumour growth regulation. *Br. J. Pharmacol.* **166**, 721–736 (2012).
24. Sastre, K. S. R. et al. Epinephrine protects cancer cells from apoptosis via activation of cAMP-dependent protein kinase and BAD phosphorylation. *J. Biol. Chem.* **282**, 14094–14100 (2007).
25. Reeder, A. et al. Stress hormones reduce the efficacy of paclitaxel in triple negative breast cancer through induction of DNA damage. *Br. J. Cancer* **112**, 1461–1470 (2015).
26. Słotkin, T. A. et al. β -adrenoceptor signaling and its control of cell replication in MDA-MB-231 human breast cancer cells. *Breast Cancer Res. Treat.* **60**, 153–166 (2000).
27. Gargiulo, L. et al. Differential α 2-adrenergic receptor expression defines the phenotype of non-tumorigenic and malignant human breast cell lines. *Oncotarget* **5**, 10058–10069 (2014).
28. Walker, A. K. et al. Circulating epinephrine is not required for chronic stress to enhance metastasis. *Psychoneuroendocrinology* **99**, 191–196 (2019).
29. Le, C. P. et al. Chronic stress in mice remodels lymph vasculature to promote tumour cell dissemination. *Nat. Commun.* **7**, 10634 (2016).
30. Sloan, E. K. et al. The sympathetic nervous system induces a metastatic switch in primary breast cancer. *Cancer Res.* **70**, 7042–7052 (2010).
31. Bruzone, A. et al. α 2-Adrenoceptors enhance cell proliferation and mammary tumor growth acting through both the stroma and the tumor cells. *Curr. Cancer Drug Targets* **11**, 763–774 (2011).
32. Thaler, P. H. et al. Chronic stress promotes tumor growth and angiogenesis in a mouse model of ovarian carcinoma. *Nat. Med.* **12**, 939–944 (2006).
33. Lamkin, D. M. et al. 2-Adrenergic blockade mimics the enhancing effect of chronic stress on breast cancer progression. *Psychoneuroendocrinology* **51**, 262–270 (2015).
34. Kamiya, A. et al. Genetic manipulation of autonomic nerve fiber innervation and activity and its effect on breast cancer progression. *Nat. Neurosci.* **22**, 1289–1305 (2019).
35. Hein, L., Altman, J. D. & Kobilla, B. K. Two functionally distinct α 2-adrenergic receptors regulate sympathetic neurotransmission. *Nature* **402**, 181–184 (1999).
36. Nagy, J. A., Chang, S.-H., Shih, S.-C., Dvorak, A. M. & Dvorak, H. F. Heterogeneity of the Tumor Vasculature. *Semin Thromb. Hemost.* **36**, 321–331 (2010).
37. Madden, K. S., Szpunar, M. J. & Brown, E. B. β -Adrenergic receptors (β -AR) regulate VEGF and IL-6 production by divergent pathways in high β -AR-expressing breast cancer cell lines. *Breast Cancer Res. Treat.* **130**, 747–758 (2011).
38. Chen, H. et al. Adrenergic signaling promotes angiogenesis through endothelial cell-tumor cell crosstalk. *Endocr. Relat. Cancer* **21**, 789–795 (2014).
39. Zhou, J. et al. Activation of β 2-adrenergic receptor promotes growth and angiogenesis in breast cancer by down-regulating PPAR γ . *Cancer Res. Treat.* **52**, 830–847 (2020).
40. Steinberg, E. M. Neural regulation of innate immunity: a coordinated non-specific host response to pathogens. *Nat. Rev. Immunol.* **6**, 318–328 (2006).
41. Hanoun, M., Maryanovich, M., Amal-Estapé, A. & Frinette, P. S. Neural regulation of hematopoiesis, inflammation, and cancer. *Neuron* **86**, 360–373 (2015).
42. Szpunar, M. J., Belcher, E. K., Dawes, R. P. & Madden, K. S. Sympathetic innervation, norepinephrine content, and norepinephrine turnover in orthotopic and spontaneous models of breast cancer. *Brain Behav. Immun.* **53**, 223–233 (2016).
43. Lamkin, D. M. et al. β -Adrenergic-stimulated macrophages: comprehensive localization in the M1-M2 spectrum. *Brain, Behav., Immun.* **57**, 338–346 (2016).
44. Busck, M. J. et al. β -adrenergic signaling in mice housed at standard temperatures suppresses an effector phenotype in CD8⁺ T cells and undermines checkpoint inhibitor therapy. *Cancer Res.* **77**, 5639–5651 (2017).
45. Bill, R. & Christofori, G. The relevance of BMT in breast cancer metastasis: correlation or causality? *FEBS Lett.* **589**, 1577–1587 (2015).
46. Chang, A. et al. β 2-Adrenoceptors on tumor cells play a critical role in stress-enhanced metastasis in a mouse model of breast cancer. *Brain Behav. Immun.* **57**, 106–115 (2016).
47. Pon, C. K., Lane, J. R., Sloan, E. K. & Hall, M. L. The β 2-adrenoceptor activates a positive cAMP-calcium feedforward loop to drive breast cancer cell invasion. *FASEB J.* **30**, 1144–1154 (2016).
48. Creed, S. J. et al. β 2-adrenoceptor signaling regulates invadopodia formation to enhance tumor cell invasion. *Breast Cancer Res.* **17**, 145 (2015).
49. Kim, T.-H. et al. Cancer cells become less deformable and more invasive with activation of β -adrenergic signaling. *J. Cell Sci.* **129**, 4563–4575 (2016).
50. Dezong, G., Zhongbing, M., Qinye, F. & Zhigang, Y. Carvedilol suppresses migration and invasion of malignant breast cells by inactivating Src involving cAMP/PKA and PKC δ signaling pathway. *J. Cancer Res. Ther.* **10**, 991–997 (2014).
51. Szpunar, M. J., Burke, K. A., Dawes, R. P., Brown, E. B. & Madden, K. S. The antidepressant desipramine and α 2-adrenergic receptor activation promote breast tumor progression in association with altered collagen structure. *Cancer Prev. Res.* **6**, 1262–1272 (2013).
52. Soni, A. et al. Breast cancer subtypes predispose the site of distant metastases. *Am. J. Clin. Pathol.* **143**, 471–478 (2015).
53. Ignatov, A., Eggemann, H., Burger, E. & Ignatov, T. Patterns of breast cancer relapse in accordance to biological subtype. *J. Cancer Res. Clin. Oncol.* **144**, 1347–1355 (2018).
54. Yang, H. et al. Impact of molecular subtypes on metastatic behavior and overall survival in patients with metastatic breast cancer: a single-center study combined with a large cohort study based on the surveillance, epidemiology and end results database. *Oncol Lett* **20**, 87 (2020).
55. Weilbaecher, K. N., Guise, T. A. & McCauley, L. K. Cancer to bone: a fatal attraction. *Nat. Rev. Cancer* **11**, 411–425 (2011).
56. Fomets, J., Weim, A. L. & Stewart, S. A. Understanding the bone in cancer metastasis. *J. Bone Miner. Res.* **33**, 2099–2113 (2018).
57. Kang, Y. Dissecting tumor-stromal interactions in breast cancer bone metastasis. *Endocrinol. Metab.* **31**, 206–212 (2016).
58. Drake, F. H. et al. Cathepsin K, but not cathepsin B, L, or S, is abundantly expressed in human osteoclasts. *J. Biol. Chem.* **271**, 12511–12516 (1996).
59. Hållén, J. M. et al. Tartrate-resistant acid phosphatase 5b: a novel serum marker of bone resorption. *J. Bone Miner. Res.* **15**, 1337–1345 (2000).
60. Ecarot-Charrier, B., Gioroux, F. H., van der Rest, M. & Pereira, G. Osteoblasts isolated from mouse calvaria initiate matrix mineralization in culture. *J. Cell Biol.* **96**, 639–643 (1983).
61. Kamioka, H., Honjo, T. & Takano-Yamamoto, T. A three-dimensional distribution of osteocyte processes revealed by the combination of confocal laser scanning microscopy and differential interference contrast microscopy. *Bone* **28**, 145–149 (2001).

62. Feng, J. Q. et al. Loss of DMP1 causes rickets and osteomalacia and identifies a role for osteocytes in mineral metabolism. *Nat. Genet.* **38**, 1310–1315 (2006).
63. Robling, A. G. et al. Mechanical stimulation of bone in vivo reduces osteocyte expression of *sost/sclerostin*. *J. Biol. Chem.* **283**, 5866–5875 (2008).
64. Kamei, M. A., Picconi, J. L., Lara-Castillo, N. & Johnson, M. L. Activation of β -catenin signaling in MLO-Y4 osteocytic cells versus 2T3 osteoblastic cells by fluid flow shear stress and PGE₂: Implications for the study of mechanosensation in bone. *Bone* **47**, 872–881 (2010).
65. Yin, J. J. et al. TGF- β signaling blockade inhibits PTHrP secretion by breast cancer cells and bone metastases development. *J. Clin. Invest.* **103**, 197–206 (1999).
66. Le Pape, F., Vargas, G. & Cézardin, P. The role of osteoclasts in breast cancer bone metastasis. *J. Bone Oncol.* **5**, 93–95 (2016).
67. Mundy, G. R. Metastasis to bone: causes, consequences and therapeutic opportunities. *Nat. Rev. Cancer* **2**, 584–593 (2002).
68. Rzaiz, K. et al. Randomized phase II trial of denosumab in patients with bone metastases from prostate cancer, breast cancer, or other neoplasms after intravenous bisphosphonates. *J. Clin. Oncol.* **27**, 1564–1571 (2009).
69. Charrier, S. R., Mitchell, S. A. T., Majuta, L. A. & Mantyh, P. W. The changing sensory and sympathetic innervation of the young, adult and aging mouse femur. *Neuroscience* **387**, 178–190 (2018).
70. Leitao, L. et al. Osteoblasts are inherently programmed to repel sensory innervation. *Bone Res.* **8**, 20 (2020).
71. Saylekshmy, M. et al. Innervation is higher above bone remodeling surfaces and in cortical pores in human bone: lessons from patients with primary hyperparathyroidism. *Sci. Rep.* **9**, 5361 (2019).
72. Fonseca, T. L. et al. Double disruption of $\alpha 2A$ and $\alpha 2C$ -adrenoceptors results in sympathetic hyperactivity and high bone-mass phenotype. *J. Bone Miner. Res.* **26**, 591–603 (2011).
73. Nishida, T. & Abe, K. $\alpha 1$ -Adrenergic receptor stimulation induces the expression of receptor activator of nuclear factor κB ligand gene via protein kinase C and extracellular signal-regulated kinase pathways in MC3T3-E1 osteoblast-like cells. *Arch. Oral Biol.* **52**, 778–785 (2007).
74. Himi, T., Tanaka, K. & Togari, A. $\alpha 1$ -adrenoceptor signaling in osteoblasts regulates *dnoc* genes and bone morphogenetic protein 4 expression through up-regulation of the transcriptional factor nuclear factor κB (NF κB)/E4 promoter-binding protein 4 (E4BP4). *J. Biol. Chem.* **289**, 17174–17183 (2014).
75. Kondo, H., Takeuchi, S. & Togari, A. β -Adrenergic signaling stimulates osteoclastogenesis via reactive oxygen species. *Am. J. Physiol. Endocrinol. Metab.* **304**, E507–E515 (2013).
76. Moore, R. E., Smith, C. K., Bailey, C. S., Voelkel, E. F. & Tashjian, A. H. Characterization of beta-adrenergic receptors on rat and human osteoblast-like cells and demonstration that beta-receptor agonists can stimulate bone resorption in organ culture. *Bone Miner.* **23**, 301–315 (1998).
77. Takada, S. et al. Leptin regulates bone formation via the sympathetic nervous system. *Cell* **111**, 305–317 (2002).
78. Togari, A. et al. Expression of mRNAs for neuropeptide receptors and β -adrenergic receptors in human osteoblasts and human osteogenic sarcoma cells. *Neurosci. Lett.* **233**, 125–128 (1997).
79. Aiken, S. J., Lando-Bassonga, E., Ralston, S. H. & Idris, A. I. $\beta 2$ -Adrenoceptor ligands regulate osteoclast differentiation in vitro by direct and indirect mechanisms. *Arch. Biochem. Biophys.* **482**, 96–103 (2009).
80. Ma, Y. et al. Extracellular norepinephrine clearance by the norepinephrine transporter is required for skeletal homeostasis. *J. Biol. Chem.* **288**, 30105–30113 (2013).
81. Behariou, F. Impact of the autonomic nervous system on the skeleton. *Physiol. Rev.* **98**, 1083–1112 (2018).
82. Behariou, F. et al. Leptin regulation of bone resorption by the sympathetic nervous system and CART. *Nature* **434**, 514–520 (2005).
83. Liang, H. et al. Selective $\beta 2$ -adrenoceptor signaling regulates osteoclastogenesis via modulating RANKL production and neuropeptides expression in osteocytic MLO-Y4 cells. *J. Cell. Biochem.* **120**, 7238–7247 (2019).
84. Yao, Q. et al. Beta-adrenergic signaling affect osteoclastogenesis via osteocytic MLO-Y4 cells' RANKL production. *Biochem. Biophys. Res. Commun.* **488**, 634–640 (2017).
85. Chen, A. et al. Attraction and compaction of migratory breast cancer cells by bone matrix proteins through tumor-osteocyte interactions. *Sci. Rep.* **8**, 5420 (2018).
86. Liu, S. et al. Osteocyte-driven downregulation of *snail* restrains effects of *Dlx2* inhibitors on mammary tumor cells. *Cancer Res.* **78**, 3865–3876 (2018).
87. Fan, Y. et al. Skeletal loading regulates breast cancer-associated osteolysis in a loading intensity-dependent fashion. *Bone Res.* **8**, 9 (2020).
88. Maroni, P. & Bendinelli, P. Bone, a secondary growth site of breast and prostate carcinomas: role of osteocytes. *Cancer* **12**, 1812 (2020).
89. Mulcrone, P. L. et al. Skeletal colonization by breast cancer cells is stimulated by an osteoblast and $\beta 2AR$ -dependent neo-angiogenic switch. *J. Bone Miner. Res.* **32**, 1440–1454 (2017).
90. Ckment-Damange, L., Mulcrone, P. L., Tabarean, T. Q., Sterling, J. A. & Elifantariou, F. $\beta 2ARs$ stimulation in osteoblasts promotes breast cancer cell adhesion to bone marrow endothelial cells in an $L-1\beta$ and selectin-dependent manner. *J. Bone Oncol.* **13**, 1–10 (2018).
91. Martin, T. J. & Johnson, R. W. Multiple actions of parathyroid hormone-related protein in breast cancer bone metastasis. *Br. J. Pharmacol.* 1–13 (2019). <https://doi.org/10.1111/bph.14709>. Online ahead of print.
92. Thomas, R. J. et al. Breast cancer cells interact with osteoblasts to support osteoclast formation. *Endocrinology* **140**, 4451–4458 (1999).
93. Hanyu, R. et al. Anabolic action of parathyroid hormone regulated by the $\beta 2$ -adrenergic receptor. *Proc. Natl Acad. Sci.* **109**, 7433–7438 (2012).
94. Moriya, S. et al. PTH regulates $\beta 2$ -adrenergic receptor expression in osteoblast-like MC3T3-E1 cells. *J. Cell. Biochem.* **116**, 142–148 (2015).
95. Bianchi, E. N. & Ferrar, S. L. β -arrestin2 regulates parathyroid hormone effects on a p38 MAPK and NF κB gene expression network in osteoblasts. *Bone* **45**, 716–725 (2009).
96. Spurney, R. F. Regulated expression of G protein-coupled receptor kinases (GRKs) and β -arrestins in osteoblasts. *Calcif. Tissue Int.* **73**, 153–160 (2003).
97. Fukuyama, S., Kong, G., Benovic, J. L. & Meurer, E. & J, A. H. T. β -adrenergic receptor kinase-1 acutely regulates PTH/PTHrP receptor signalling in human osteoblast-like cells. *Cell. Signal.* **9**, 469–474 (1997).
98. Gesty-Palmer, D. et al. Distinct β -arrestin- and G protein-dependent pathways for parathyroid hormone receptor-stimulated ERK1/2 Activation. *J. Biol. Chem.* **281**, 10856–10864 (2006).
99. Cardwell, C. R. et al. Propranolol and survival from breast cancer: a pooled analysis of European breast cancer cohorts. *Breast Cancer Res.* **18**, 119 (2016).
100. Chida, Y., Hamer, M., Wardle, J. & Steptoe, A. Do stress-related psychosocial factors contribute to cancer incidence and survival? *Nat. Clin. Pract. Oncol.* **5**, 466–475 (2008).
101. Lawrence, D. S., Sahay, J. N., Chatterjee, S. S. & Cruickshank, J. M. Asthma and beta-blockers. *Eur. J. Clin. Pharmacol.* **22**, 501–509 (1982).
102. Paterson, J. W. & Dollery, C. T. Effect of propranolol in mild hypertension. *Lancet* **288**, 1148–1150 (1966).
103. Fryzek, J. P. et al. A cohort study of antihypertensive medication use and breast cancer among Danish women. *Breast Cancer Res. Treat.* **97**, 231–236 (2006).
104. Li, C. L. et al. Relation between use of antihypertensive medications and risk of breast carcinoma among women ages 65–79 years. *Cancer* **98**, 1504–1513 (2003).
105. Barron, T. I., Connolly, R. M., Sharp, L., Bennett, K. & Visvanathan, K. Beta blockers and breast cancer mortality: a population-based study. *J. Clin. Oncol.* **29**, 2635–2644 (2011).
106. Melhem-Bertrandt, A. et al. Beta-blocker use is associated with improved relapse-free survival in patients with triple-negative breast cancer. *J. Clin. Oncol.* **29**, 2645–2652 (2011).
107. Montoya, A. et al. Use of non-selective β -blockers is associated with decreased tumor proliferative indices in early stage breast cancer. *Oncotarget* **8**, 6446–6460 (2016).
108. Botteri, E. et al. Therapeutic effect of β -blockers in triple-negative breast cancer postmenopausal women. *Breast Cancer Res. Treat.* **140**, 567–575 (2013).
109. Spera, G. et al. Beta blockers and improved progression-free survival in patients with advanced HER2 negative breast cancer: a retrospective analysis of the ROSE/TRIO-012 study. *Ann. Oncol.* **28**, 1836–1841 (2017).
110. Shah, S. M. et al. Does β -adrenoceptor blocker therapy improve cancer survival? Findings from a population-based retrospective cohort study. *Br. J. Clin. Pharmacol.* **72**, 157–161 (2011).
111. Sarasin, G. V. et al. Use of β -blockers, angiotensin-converting enzyme inhibitors, angiotensin II receptor blockers, and risk of breast cancer recurrence: a Danish nationwide prospective cohort study. *J. Clin. Oncol.* **31**, 2265–2272 (2013).
112. Cardwell, C. R., Coleman, H. G., Murray, L. J., Entschladen, F. & Powe, D. G. Beta-blocker usage and breast cancer survival: a nested case-control study within a UK Clinical Practice Research Datalink cohort. *Int. J. Epidemiol.* **42**, 1852–1861 (2014).
113. Zhou, L. et al. Propranolol attenuates surgical stress-induced elevation of the regulatory T cell response in patients undergoing radical mastectomy. *J. Immunol.* **196**, 3460–3469 (2016).
114. Shaath, L. et al. Perioperative COX-2 and β -adrenergic blockade improves metastatic biomarkers in breast cancer patients in a phase-II randomized trial. *Clin. Cancer Res.* **23**, 4651–4661 (2017).
115. Haldar, R. et al. Perioperative inhibition of β -adrenergic and COX2 signaling in a clinical trial in breast cancer patients improves tumor Ki-67 expression, serum cytokine levels, and PBMCs transcriptome. *Brah Behav. Immun.* **73**, 294–309 (2018).

116. Hillier, J. G. et al. Pre-operative β -blockade with propranolol reduces biomarkers of metastasis in breast cancer: a Phase II randomized trial. *Clin. Cancer Res.* **26**, 1803–1811 (2020).
117. Lechtenberg, K. J., Meyer, S. T., Doyle, J. B., Peterson, T. C. & Budwagner, M. S. Augmented β 2-adrenergic signaling dampens the neuroinflammatory response following ischemic stroke and increases stroke size. *J. Neuroinflammation* **16**, 112 (2019).
118. Mei, X. et al. Microfluidic platform for studying osteocyte mechanoregulation of breast cancer bone metastasis. *Integr. Biol.* **11**, 119–129 (2019).
119. Hao, S. et al. A Spontaneous 3D bone-on-a-chip for bone metastasis study of breast cancer cells. *Small* **14**, 1702787 (2018).
120. Bersht, S. et al. A microfluidic 3D in vitro model for specificity of breast cancer metastasis to bone. *Biomateriab* **35**, 2454–2461 (2014).
121. Jeon, J. S. et al. Human 3D vascularized organotypic microfluidic assays to study breast cancer cell extravasation. *Proc. Natl. Acad. Sci. USA* **112**, 214–219 (2015).
122. Dubový, P. et al. Local chemical sympathectomy of rat bone marrow and its effect on marrow cell composition. *Autonom. Neurosci: basic Clin.* **206**, 19–27 (2017).
123. Wu, H., Luo, Y., Xu, D., Ke, X. & Cui, T. Low molecular weight heparin modified bone targeting liposomes for orthotopic osteosarcoma and breast cancer bone metastatic tumors. *Int. J. Biol. Macromolecules* **164**, 2583–2597 (2020).
124. Jiang, B. et al. Dual-targeting delivery system for bone cancer: synthesis and preliminary biological evaluation. *Drug Deliv.* **19**, 317–326 (2012).
125. Zhang, G. et al. A delivery system targeting bone formation surfaces to facilitate RNAi-based anabolic therapy. *Nat. Med.* **18**, 307–314 (2012).
126. Salerno, M. et al. Bone-targeted doxorubicin-loaded nanoparticles as a tool for the treatment of skeletal metastases. *Curr. Cancer Drug Targets* **10**, 649–659 (2010).
127. Wang, C. et al. Tifolium-like platinum nanoparticle-mediated photothermal therapy inhibits tumor growth and osteolysis in a bone metastasis model. *Small* **11**, 2080–2086 (2015).
128. Wang, X. et al. Peptide decoration of nanovehicles to achieve active targeting and pathology-responsive cellular uptake for bone metastasis chemotherapy. *Biomater. Sci.* **2**, 961–971 (2014).
129. Kiewit, F. M. et al. Targeting of primary breast cancers and metastases in a transgenic mouse model using rationally designed multifunctional SPIONs. *ACS Nano* **6**, 2591–2601 (2012).
130. Castillo, L. F., Rivas, E. M., Goffin, V. & Lüthy, L. A. Alpha2-adrenoceptor agonists trigger prolactin signaling in breast cancer cells. *Cell. Signal.* **34**, 76–85 (2017).
131. Cakir, Y., Plummer, H. K., Ilthof, P. K. & Schuler, H. M. Beta-adrenergic and arachidonic acid-mediated growth regulation of human breast cancer cell lines. *Int. J. Oncol.* **21**, 153–157 (2002).
132. Vázquez, S. M. et al. Human breast cell lines exhibit functional α 2-adrenoceptors. *Cancer Chemother. Pharmacol.* **58**, 50–61 (2005).
133. Szalai, C. et al. Norepinephrine promotes the β 1-integrin-mediated adhesion of MDA-MB-231 cells to vascular endothelium by the induction of a GRC α release. *Mol. Cancer Res.* **10**, 197–207 (2012).
134. Ganz, P. A., Habel, L. A., Weltzien, E. K., Cain, B. J. & Cole, S. W. Examining the influence of beta blockers and ACE inhibitors on the risk for breast cancer recurrence: results from the IACE cohort. *Breast Cancer Res. Treat.* **129**, 549–556 (2011).

 **Open Access** This article is licensed under a Creative Commons Attribution 4.0 International License, which permits use, sharing, adaptation, distribution and reproduction in any medium or format, as long as you give appropriate credit to the original author(s) and the source, provide a link to the Creative Commons license, and indicate if changes were made. The images or other third party material in this article are included in the article's Creative Commons license, unless indicated otherwise in a credit line to the material. If material is not included in the article's Creative Commons license and your intended use is not permitted by statutory regulation or exceeds the permitted use, you will need to obtain permission directly from the copyright holder. To view a copy of this license, visit <http://creativecommons.org/licenses/by/4.0/>.

© The Author(s) 2021

Rights and permissions

Open Access This article is licensed under a Creative Commons Attribution 4.0 International License, which permits use, sharing, adaptation, distribution and reproduction in any medium or format, as long as you give appropriate credit to the original author(s) and the source, provide a link to the Creative Commons license, and indicate if changes were made. The images or other third party material in this article are included in the article's Creative Commons license, unless indicated otherwise in a credit line to the material. If material is not included in the article's Creative Commons license and your intended use is not permitted by statutory regulation or exceeds the permitted use, you will need to obtain permission directly from the copyright holder. To view a copy of this license, visit <http://creativecommons.org/licenses/by/4.0/>.

Annex B



A metastasis-on-a-chip approach to explore the sympathetic modulation of breast cancer bone metastasis



Francisco Conceição^{a,b,c}, Daniela M. Sousa^{a,b}, Joshua Loessberg-Zahl^f, Anke R. Vollertsen^g, Estrela Neto^{a,b}, Kent Sørensen^{h,1}, Joana Paredes^{a,d,e}, Anne Leferink^g, Meriem Lamghari^{a,b,c,*}

^a Instituto de Investigação e Inovação em Saúde (I3S), Universidade Do Porto, 4200-135, Porto, Portugal

^b INEB—Instituto Nacional de Engenharia Biomédica, Universidade Do Porto, 4200-135, Porto, Portugal

^c ICBAS—Instituto de Ciências Biomédicas Abel Salazar, Universidade Do Porto, 4050-313, Porto, Portugal

^d IPATMUP—Instituto de Patologia e Imunologia Molecular da Universidade Do Porto, 4200-135, Porto, Portugal

^e FMUP—Faculdade de Medicina da Universidade Do Porto, 4200-319, Porto, Portugal

^f BIOS Lab on a Chip Group, MESA+ Institute for Nanotechnology, Max Planck - University of Twente Center for Complex Fluid Dynamics, University of Twente, P.O. Box 217, 7500, AE Enschede, the Netherlands

^g Applied Stem Cell Technologies, TechMed Genos, University of Twente, PO Box 217, 7500, AE Enschede, the Netherlands

^h Clinical Cell Biology, Vejle Hospital/Lillebælt Hospital, Department of Regional Health Research, University of Southern Denmark, 7100, Vejle, Denmark

ARTICLE INFO

Keywords:

Metastasis-on-a-chip
Breast cancer
Bone metastasis
Sympathetic nervous system
Paincaine

ABSTRACT

Organ-on-a-chip models have emerged as a powerful tool to model cancer metastasis and to decipher specific crosstalk between cancer cells and relevant regulators of this particular niche. Recently, the sympathetic nervous system (SNS) was proposed as an important modulator of breast cancer bone metastasis. However, epidemiological studies concerning the benefits of the SNS targeting drugs on breast cancer survival and recurrence remain controversial. Thus, the role of SNS signaling over bone metastatic cancer cellular processes still requires further clarification. Herein, we present a novel humanized organ-on-a-chip model recapitulating neuro-breast cancer crosstalk in a bone metastatic context. We developed and validated an innovative three-dimensional printing based multi-compartment microfluidic platform, allowing both selective and dynamic multicellular paracrine signaling between sympathetic neurons, bone tropic breast cancer cells and osteoclasts. The selective multicellular crosstalk in combination with biochemical, microscopic and proteomic profiling show that synergistic paracrine signaling from sympathetic neurons and osteoclasts increase breast cancer aggressiveness demonstrated by augmented levels of pro-inflammatory cytokines (e.g. interleukin-6 and macrophage inflammatory protein 1α). Overall, this work introduced a novel and versatile platform that could potentially be used to unravel new mechanisms involved in intracellular communication at the bone metastatic niche.

1. Introduction

Breast cancer bone metastasis is an complex process that encompasses cell extravasation from the circulatory system into the bone, engraftment on a suitable niche, escape from dormancy, proliferation and uncoupling of the bone remodeling to fuel tumor growth [1]. Bone is the most common site of metastasis in breast cancer. Within the bone, breast cancer cells over-activate bone resorbing osteoclasts and shift the physiological balance in bone remodeling towards increased bone

destruction. This leads to severe skeletal complications, such as bone pain, hypercalcemia and bone fractures [1]. The elucidation of the cellular and molecular mechanisms by which breast cancer cells engraft and proliferate in the bone niche is, therefore, of crucial importance to improve the available therapeutic options. However, several barriers still hamper the study of the metastatic bone niche. In vivo models, which are able to recapitulate the complexity of the human disease, are limited and of difficult execution, whereas the dissection of specific signaling pathways involved in bone metastasis progression is extremely complex.

Abbreviations: PDMS, polydimethylsiloxane; SNS, Sympathetic Nervous System; NE, norepinephrine; TH, tyrosine hydroxylase; MCP-1, monocyte chemoattractant protein 1; IL-6, interleukin 6; MIP-1α, macrophage inflammatory protein 1α; IL, interleukin.

* Corresponding author. Instituto de Investigação e Inovação em Saúde (I3S), Universidade Do Porto, 4200-135, Porto, Portugal.

E-mail address: lamghari@ineb.up.pt (M. Lamghari).

¹ Present address: Clinical Cell Biology, Pathology Research Unit, Department of Clinical Research, University of Southern Denmark, 5230 Odense, Denmark.

<https://doi.org/10.1016/j.mtbio.2022.100219>

Received 14 December 2021; Received in revised form 10 February 2022; Accepted 12 February 2022

Available online 14 February 2022

2590-0064/© 2022 Published by Elsevier Ltd. This is an open access article under the CC BY-NC-ND license (<http://creativecommons.org/licenses/by-nc-nd/4.0/>).

Furthermore, high mortality rates and pain associated with the *in vivo* modelling of this specific disease inherently raises ethical constraints that limit the use of animal models. On the other hand, classical *in vitro* models are simplistic and do not replicate the native features of the bone microenvironment.

Microfluidic tools have emerged in the past decade as an alternative to conventional *in vitro* and *in vivo* models, since these combine three dimensional (3D) matrices with human cells while allowing a fine control over spatial and temporal parameters of culture [2]. In addition, fluidic connection of different cell compartments as well as the control of flow and shear facilitates more physiologically relevant modelling [3]. Microfluidic platforms have in the past been already used as models for bone cancer processes including: i) selective tropism of myeloma and breast cancer cells towards bone cells [2,4]; ii) extravasation of breast cancer cells from circulation into extracellular matrix (ECM) structures based on collagen or fibrin [5–8]; iii) colorectal, myeloma and breast cancer cell engraftment and proliferation in mineralized matrices [9–12]; iv) cancer drug screening and toxicity assessment [3,13]. Thus, microfluidic technology can tackle constraints associated to standard *in vitro* tools in the study of the crosstalk occurring during breast cancer bone metastasis, and thus improve our knowledge on the signaling pathways governing the metastatic process.

Despite the numerous advantages of metastasis-on-a-chip *in vitro* tools, the typical photolithography processes used in their fabrication require expensive infrastructure and highly skilled personnel. 3D printing is becoming a viable alternative for microfluidic fabrication since it combines accessibility of standard benchtop 3D printers and a high degree of design freedom which is not trivial to achieve via photolithography [14]. Furthermore, advances in printer technology have improved surface roughness of 3D printed template molds, to the point that the resulting prototypes become compatible with plasma sealing procedures [15]. 3D printing is also suited for valve fabrication, which allows the control of flow resistance and diffusion through the different fluidic compartments [16].

The sympathetic nervous system (SNS) was brought to light as a potential therapeutic target for the treatment of breast cancer due to several findings in pre-clinical and epidemiologic studies [17–19], which correlated sympathetic hyperactivity and poor patient prognosis. However, the beneficial effect of SNS targeting drugs on the treatment of breast cancer remains controversial, since other reports failed to replicate such correlations [20,21]. It is well established that the SNS acts on multiple cellular targets throughout the body, mainly via the release of norepinephrine (NE) by sympathetic nerve endings and through systemic release of epinephrine into circulation. Functional studies demonstrated that the sympathetic stimulus is able to increase breast cancer circulating tumor cell retention and extravasation to the bone [22]. Nonetheless, dissection of sympathetic signaling in the context of human breast cancer bone metastasis was not yet reported and the mechanisms governing breast cancer cell response to sympathetic input within the bone microenvironment are still poorly understood.

As stated above, microfluidic tools offer multiple advantages regarding standard *in vitro* models such as compartmentalization and fine tuning of culture parameters. We have previously established models of neuronal/non-neuronal cellular communication in compartmentalized microfluidic devices to address sensory innervation in the bone microenvironment [23,24]. However, to date there are no microfluidic models described for the study of sympathetic stimuli on the breast cancer bone metastatic niche.

In this study, we have designed and prototyped a new 3D printing based metastasis-on-a-chip platform to reproduce the effect of sympathetic activation on the dynamic crosstalk that occurs between breast cancer cells and bone cells in a fully humanized model. Our platform combines three different human cell types: 1) a bone tropic breast cancer cell variant, 2) sympathetic neurons and 3) human peripheral blood derived osteoclasts seeded on top of a bone matrix. The microfluidic platform was specially designed to physically separate the cells into

different compartments to facilitate the identification of secreted factors involved in intercellular communication while preventing direct cell-cell interactions. Furthermore, inclusion of fluidic flow between different compartments allow a unidirectional communication from one compartment to the remaining ones. Our metastasis-on-a-chip platform is based on static diffusion in order to facilitate bidirectional communication between each compartment. Additionally, our platform also allows the manipulation of communication between the different compartments through the use of incorporated pressure actuating valves. We were able to successfully optimize the culture of each cell type and demonstrated that the dynamic interaction between neurons, breast cancer cells and osteoclasts translates into an increased pro-inflammatory phenotype. In addition, manipulation of the communication between compartments allowed us to show that direct neuronal stimulation of osteoclasts is not required to observe inflammatory cytokine upregulation. Based on these results, we believe that our versatile platform can be a potential tool for fundamental research on multiple research topics. The use of widely accessible 3D printing technology further highlights the adaptability of our metastasis-on-a-chip platform.

2. Materials and methods

2.1. Fabrication and assembly of the metastasis-on-a-chip platform

Each microfluidic component was made out of poly-dimethylsiloxane (PDMS, Sylgard 184, Dow Corning) using specially designed 3D printed molds. Molds were designed using SolidWorks (Dassault Systemes) and 3D printed in a Form 3 printer (Formlabs) with a Grey V4 resin (Formlabs). These molds were post-processed by two rounds of immersion in isopropanol for 15 min to remove uncured resin, followed by air-drying and a heat treatment of 3 h at 60 °C. PDMS was then cast into the mold with a 10:1 (w/w) ratio of base and curing agent and thermally cured for 1 h 30 min at 60 °C. Each PDMS slab was separated from the mold and cleaned with residue-free tape until plasma treatment.

The microfluidic platform was designed for single use and is composed of three different structural parts bonded together: a top slab containing patterned cell compartments and diffusion channels, a bottom slab containing valve structures and a simple membrane in between. Top slabs have three equidistant compartments 6 mm in diameter for cell culturing (each with two medium inlets) which are interconnected through 4.5 mm long semi-circular channels 300 µm wide and 150 µm high. The bone and cancer compartment are 1.2 mm deep to accommodate the bone slice (400 µm thick) and the spheroid, while the Neuronal compartment is 600 µm deep.

PDMS membranes were produced by spin coating 1.6 mL PDMS at a 10:1 (w/w) ratio of base and curing agent on top of a perfluorodecyltrichlorosilane coated silicon wafer (10 cm diameter) with an initial spinning step at 500 rpm for 15 s and 100 rpm/s acceleration, followed by a second step at 1500 rpm for 75 s and 1000 rpm/s acceleration. The membranes were then thermally cured for 1 h 30 min at 60 °C.

Metastasis-on-a-chip platform assembly was achieved by covalent bonding of the different components. The membrane and cell compartment slab were first covalently bound together through oxygen plasma treatment for 1 min on a Zepto Plasma Cleaner (Diener Electronic). The membrane was then cut along the contour of the PDMS slab using a scalpel and lifted from the silicon wafer. Medium inlets and pressure inlets were then punched out of the bonded membrane and the cell compartment slab using a 1 mm biopsy puncher (Kai Medical). The resulting structures were then bonded to the valve structure slab by oxygen plasma treatment as described previously. Right after treatment and before bonding, bovine bone slices (boneslices.com, Denmark) were placed in the bone cell compartment. Both slabs were then bonded together. Each microfluidic unit was sterilized with 70% ethanol, washed thrice with phosphate buffered saline (PBS) and equilibrated in complete medium. Neuronal compartments were incubated in a solution of 5 µg/

mL laminin (Sigma-Aldrich) in DMEM/F12 medium (Gibco) with 10% FBS and 1% penicillin/streptomycin (Pen/Strep, Gibco) (DMEM/F12 complete medium) for 2 h at 37 °C. Compartments were washed twice with DMEM/F12 complete medium and kept at 37 °C until cell seeding.

2.2. Osteoclast isolation

Human CD14⁺ monocytes were isolated from buffy coats of healthy female blood donors as previously described [25]. Briefly, Peripheral Blood Mononuclear Cells (PBMCs) were separated using gradient centrifugation in Ficoll-Paque Plus (GE Healthcare). PBMCs were then resuspended in 0.5% Biotin-free Bovine Serum Albumin (BSA, Sigma-Aldrich) and 2 mM EDTA in PBS, incubated in BD IMag™ anti-human CD14 magnetic particles (BD-Biosciences) and magnetically separated according to manufacturer's instructions. CD14⁺ cells were seeded in T75 flasks in α -MEM (Gibco) supplemented with 10% FBS, 1% Pen/Strep and 25 ng/mL of recombinant human macrophage colony stimulating factor (rhM-CSF, R&D Systems) at 5% CO₂ at 37 °C in a humidified incubator for 2 days. Cells were then differentiated into mature osteoclasts by supplementing the medium with 25 ng/mL M-CSF and receptor activator of NF- κ B ligand (RANKL, R&D Systems) for further 7 days of culture, changing medium twice.

2.3. Breast cancer cell spheroids

MDA-MB-231-BoM 1833 human breast carcinoma cell line (MDA-1833 henceforth), a bone tropic variant of the MDA-MB-231 cell line, was obtained from Dr. J. Massagué (Memorial Sloan-Kettering Cancer Center, New York). MDA-1833 cells were expanded in DMEM High Glucose (Gibco) with 10% FBS and 1% Pen/Strep (DMEM complete medium) at 37 °C and 5% CO₂ in a humidified incubator, changing medium twice a week until reaching 80% confluence. Cells were then trypsinized (0.25% w/v trypsin, 0.1% w/v glucose and 0.05% EDTA in PBS, Life Technologies), seeded at a density of 10 000 cells per well on round bottom ultra-low adhesion 96-well plates (Corning) and incubated for 4 days in DMEM complete medium with 2.5% Matrigel Basement Membrane Matrix (Corning) to induce formation of cell spheroids.

2.4. Neuronal-like cell differentiation

SH-SY5Y (ATCC) cells were used as a model of human sympathetic neurons since these cells were previously reported to be able to produce NE [26]. SH-SY5Y cells were expanded in DMEM/F12 Complete medium at 37 °C and 5% CO₂ in a humidified incubator, changing medium twice a week until reaching 80% confluence. Cells were then trypsinized and 20 000 cells were seeded in the laminin coated neuronal compartments and incubated at 37 °C overnight. Differentiation was induced by Opti-MEM medium (Gibco) supplemented with 0.5% FBS, 1% Pen/Strep and 0.1 μ M Retinoic Acid over the course of one week, changing medium every day.

2.5. Metastasis-on-a-chip cell seeding

Microfluidic experiments were set up during the course of 10 days. In order to isolate compartments before cell seeding and ensure full physical separation of the different cell types, compartments were sealed off by closing the valves with a pressure of 600 mbar using a FlowEZ2000 mbar pressure controller module (Fluigent). SH-SY5Y cells were seeded on the neuronal compartment as previously described and differentiated for 7 days with the valves open. At day 7, medium from the bone compartment was changed for α -MEM supplemented with 0.5% FBS, 1% Pen/Strep and 25 ng/mL rhM-CSF (Osteoclast Medium) and the medium from the cancer compartment was changed for DMEM High Glucose supplemented with 0.5% FBS and 1% Pen/Strep. Differentiated osteoclasts were then detached with Accutase (Gibco) for 10 min at 37 °C, centrifuged and seeded on the bone slice at a density of 75 000 cells in Osteoclast Medium, being left to adhere for 4 h. MDA-1833 individual cell

spheroids were transferred to the cancer compartment, one spheroid per microfluidic device, and the platform was incubated at 37 °C for 3 days to allow bone resorption to occur. When required, valves were closed with a pressure of 600 mbar throughout the experiment. The bone compartment was supplemented with fresh 50 ng/mL rhM-CSF and rh-RANKL daily. After 3 days, experiments were ended and conditioned medium was collected from each compartment while keeping the valves closed. In addition, one replicate from each condition was used for immunocytochemistry: medium was removed and the compartments were washed with PBS twice before immunocytochemistry.

2.6. Immunocytochemistry

Cells in the microfluidic platform were fixed in 4% paraformaldehyde for 10 min at RT followed by 3 steps of washing with PBS and blockage of unspecific staining in a blocking solution of 5% FBS, 5% Horse Serum (Invitrogen) and 0.25% Triton X-100 (Sigma-Aldrich) in PBS for 1 h at 37 °C. Samples were then incubated with primary antibodies overnight at 4 °C (mouse anti- β III Tubulin 1:2000 [Promega]; rabbit anti-TH 1:100 [Merck]; mouse anti-CATK 1:100 [Santa Cruz Biotechnology]; rabbit anti-CD49f [Sigma-Aldrich]). After incubation, samples were washed thrice with PBS and labeled with secondary antibodies accordingly (Invitrogen, 1:1000 dilution) together with Flash Phalloidin™ (Biolegend) for actin staining, for 1 h at RT. Finally, cells were washed thrice with PBS and counterstained with DAPI (1:1000 dilution), washed again to remove excess DAPI and kept at 4 °C until imaging. Images were acquired in a Leica SP5 confocal microscope at a resolution of 1024 \times 1024 pixels and z-step of 5 μ m. Brightness was adjusted for better visualization and z-projections as well as artificial cell coloring were performed using ImageJ.

2.7. Flow cytometry

MDA-1833 cell spheroids were removed from the metastasis-on-a-chip platform and dissociated with Accutase at 37 °C for 20 min in a microtube, pipetting up and down every 5 min. At least 10 spheroids were pooled for each condition in one independent experiment. A commercial kit for Annexin V-APC staining (BD Pharmingen) was used according to manufacturer's instructions, but only using 1 μ L of Annexin V and 3 μ L Propidium Iodide. Immunostaining was performed in 1X Binding Buffer and quantified using a FACS CANTO II (BD Immunocytometry Systems) and FlowJo™ software (BD).

2.8. Enzyme-linked immunosorbent assays (ELISA)

Conditioned medium was collected from each compartment by closing the respective valves and aspirating the medium. Conditioned medium was centrifuged at 4 °C at 400 g for 5 min to remove cellular debris, transferred to a new microtube and frozen at -80 °C until quantification. NE was quantified by ELISA (Abnova) from conditioned medium collected and pooled from SH-SY5Y monoculture controls from three independent experiments. Quantification was performed according to manufacturer's indications, but 300 μ L of conditioned medium was used in each replicate and a 1 ng/mL standard was added so that our samples would fit in the calibration curve. Protein levels of each sample were quantified using the DC Protein Assay (Bio-Rad) according to the manufacturer's instructions and were used to normalize differences between conditions.

The levels of interleukin 11 (IL-11) was quantified by ELISA (R&D Systems) from breast cancer and bone compartments of the metastasis-on-a-chip platform according to manufacturer's indications. Medium was diluted 10x before quantification to fit the calibration curve and samples were normalized using the total protein levels as mentioned above.

The levels of interleukin 6 (IL-6) and macrophage inflammatory protein 1 α (MIP-1 α) were similarly quantified by ELISA (Sigma-Aldrich)

from the breast cancer compartments of the microfluidics (unless otherwise stated) according to manufacturer's instructions. Medium was diluted 90x before quantification to fit the calibration curve and samples were normalized using the total protein levels.

2.9. Quantification of bone resorption

Osteoclast resorption events were stained with toluidine blue (Sigma-Aldrich). The entire bone surface was analysed using a G50 100 graticule (Pysy Optics) installed on the ocular of an BH-2 optical microscope (Olympus) as previously described [27]. The total number of events present throughout the bone surface were counted using the graticule as a frame (using a total of 16–17 graticules per bone slice). Individual resorption events were divided in two resorption types, pits and trenches. Pits are single, circular excavations with well-defined edges while trenches are elongated and continuous grooves with a length/width ratio equal or greater than two [28]. The percentage of trenches per total events was used to compare individual experiments independently of eroded surface variations. Samples were blinded before eroded surface quantification by one researcher.

2.10. Proteomic analysis

Conditioned medium from four MDA-1833 spheroids cultured either on the metastasis-on-a-chip platform or in 96 well-plates was pooled and centrifuged at 300 g for 5 min to pellet cellular debris. Conditioned media was then transferred to micro tubes and protein concentration was measured as described above. 50 µg of protein from each condition was processed using the solid-phase-enhanced-sample-preparation (SP3) protocol, as previously described [29], followed by enzymatic digestion overnight with trypsin/LysC (2 µg) at 37 °C and 1000 rpm.

Protein identification was carried out by nano Liquid Chromatography coupled with Mass Spectrometry (LC-MS/MS) and data was analysed with Proteome Discoverer software (Thermo Scientific) as described by Osrio et al. [30]. The ratio between the protein abundances in the conditioned medium from microfluidic and well plates was used to compare between both conditions.

2.11. Protein array

After tri-culture in the microfluidic platform, cancer compartment conditioned medium from three independent experiments was pooled and screened for proteins involved in bone metabolism using the G-Series Human Bone Metabolism Array 1000 (RayBiotech) according to manufacturer's instructions. Briefly, the arrays were blocked for 30 min and incubated with 100 µL of sample overnight at 4 °C, followed by incubation with biotinylated antibody cocktail for 4 h at room temperature. The slides were then incubated with Cy3 conjugated streptavidin for 1 h in the dark at room temperature. After washing steps, droplets were removed using a compressed argon stream. Slides were sent to the supplier to be imaged (Tebu-Bio). Array data was analysed using the Spot-xel® software (Version 2.2.2, SICASYS Software GmbH) and the GAL file supplied by the manufacturer. After alignment with the GAL file, data was extracted using the original image without changes in intensity values. Quantification of the intensity values was performed by Flex-Spot Detection method and with noise filtering and local background correction method. Extracted intensity values were then analysed using the Excel analysis tool supplied by the manufacturer. After intra-assay normalization, intensity values were normalized for protein content, values for the culture medium alone were subtracted to each sample and fold-changes relative to controls were calculated.

2.12. Statistics

All experiments were performed at least three times. One-way ANOVA test followed by Holm-Sidk's multiple comparison test was

used to assess statistical significance between conditions. When two conditions were being compared, nonparametric Mann-Whitney tests were used. Differences between groups were considered significant when *p < 0.05, **p < 0.01, ***p < 0.001. Data analysis was performed using GraphPad Prism software v.9.1.0 for Windows (GraphPad Software).

3. Results

3.1. Bone metastasis-on-a-chip design

The aim of this study was to establish a model that would allow us to clarify how breast cancer cells respond to sympathetic stimuli in a bone metastatic context, specifically focusing on the contribution of cell-secreted factors. In order to achieve this, the versatility of microfluidic platforms was appealing, since these would allow study of complex interactions between cancer cells and other significant cell components in the metastatic process, in a fully humanized system. Instead of using standard photolithography for the production of microfluidic devices, we took advantage of 3D printing to be able to quickly prototype our molds in a cost-effective fashion, while maintaining an adequate resolution (smallest feature of the mold is 150 µm while the minimum laser spot size of the 3D printer is 85 µm).

Our microfluidic chip was designed to compartmentalize three different cell types with no direct cell-cell contact but still allow diffusion dependent chemical communication between compartments (Fig. 1a and b). Importantly, we are able to dictate the direction of communication between compartments by using Quake valves incorporated in the metastasis-on-a-chip design. This microfluidic chip is composed of three different structural parts bonded together: a top slab containing patterned cell compartments and diffusion channels, a bottom slab containing valve structures and a simple membrane in between (Fig. 1c).

The ability to close the diffusion channels is an important feature both for cell seeding and to explore indirect routes of communication between different compartments. With that in mind, valve structures 500 µm wide and 1 mm long were included in the center of the diffusion channels to block the communication between compartments when desired (Fig. 1d). Three Quake valves were included on our microfluidic platform, one on each diffusion channel. Pressure applied on each valve channel will push the flexible 40 µm thick PDMS membrane located between the main PDMS slabs, closing the diffusion channels (Fig. 1e and f). To test the valves, the diffusion channels were filled with Toluidine Blue dye and a pressure of 600 mbar was applied to the valve channel. Micrographs of the valve section show that there was no dye in the diffusion channel when the valves were in a closed state (Fig. 1f, right) while dye was observed in the diffusion channel when the valves were in an open state (Fig. 1f, left). Similarly, 5 kDa fluorescent-labelled Dextran was not able to diffuse through a closed valve, further validating their functionality (Fig. S1). Furthermore, no diffusion was observed from one compartment to the other when all the valves were closed after three days of incubation, which was a relevant timeframe for our cell culture setup (Fig. S1). The closure of the valves was reversible (Supplementary movie 1) and the valves maintained their function over 20 cycles of opening and closure without rupturing (data not shown).

As already mentioned, current in vitro models fail to replicate the three-dimensional features of in vivo bone, which has profound biological and biomechanical implications in osteoclast biology. To circumvent that limitation, mineralized bone ECM preserving the structural and biological cues of in vivo bone were included in our model. Furthermore, to hamper the migration of osteoclasts and breast cancer cells from each respective compartment, a spatial offset between the bone and cancer compartment floor and the diffusion channels was incorporated in the design (Fig. 1d, right panel). This was not the case for the neuronal compartment to allow neuronal cells to elongate their axonal extensions into the diffusion channels and maximize the dissemination of neuronal factors to the other compartments.

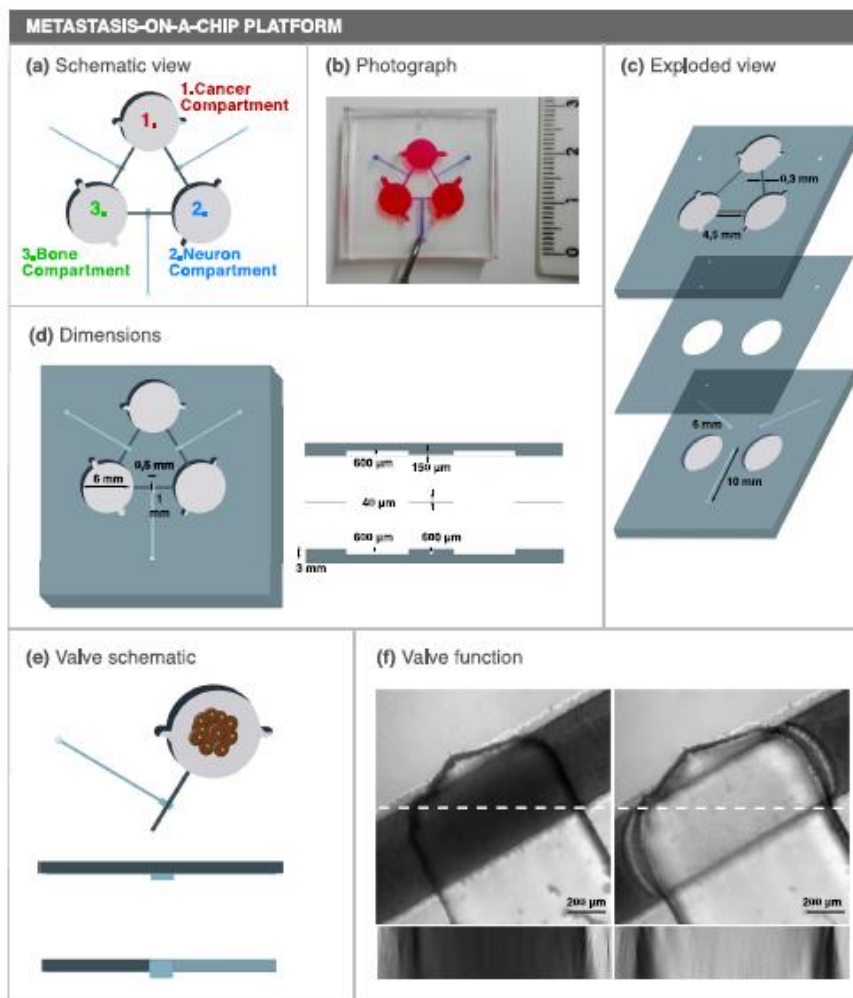


Fig. 1. Concept and design of a novel microfluidic platform with three interconnected culture chambers. (a) Schematic representation of the microfluidic platform and (b) photograph of an assembled microfluidic colored with food dyes. (c) Exploded view of the three components of the microfluidic platform. (d) Top (left) and side (right) view of the microfluidic platform. (e) Schematic view of a functioning valve. When pressure is applied in the valve channel, the flexible PDMS membrane occludes the diffusion channel, blocking the communication between compartments. (f) Valve segment z projection of an open valve (left) or closed valve (right) after applying a 600 mbar pressure on the valve channel. The microfluidic compartments were filled with toluidine blue dye and a 250 μm stack was obtained on a confocal microscope. An XZ orthogonal view is also shown below each respective image (corresponding to the dashed line). Scale bar 200 μm .

3.2. Cancer compartment: 3D culture and proteomic analysis

To form bone metastasis, disseminated breast cancer cells acquire a specific set of characteristics that are distinct from the primary tumor [31]. Accordingly, bone tropic breast cancer cell (MDA-1833) spheroids were used as a model of breast cancer cells that are more prone to establish metastasis in the bone, which have been previously characterized [31] and are shown to be biologically relevant for the study of bone metastasis. In addition, breast cancer spheroids are commonly used to replicate the 3D features of *in vivo* tumors [32].

Spheroids were introduced in the cancer compartment and cultured for 3 days inside the platform (Fig. 2a). First, cell morphology was assessed by F-actin staining of MDA-1833 spheroids inside the microfluidic compartment (Fig. 2b). In addition, integrin $\alpha 6$ (CD49f) was previously reported to be expressed in triple negative breast cancer cells [33] and, concordantly, positive staining for CD49f in the surface of MDA-1833 cells was observed (Fig. 2c). Therefore, surface marker expression was maintained inside our platform.

After morphological characterization of the bone tropic cells, the apoptotic profile of spheroids cultured inside the microfluidic was

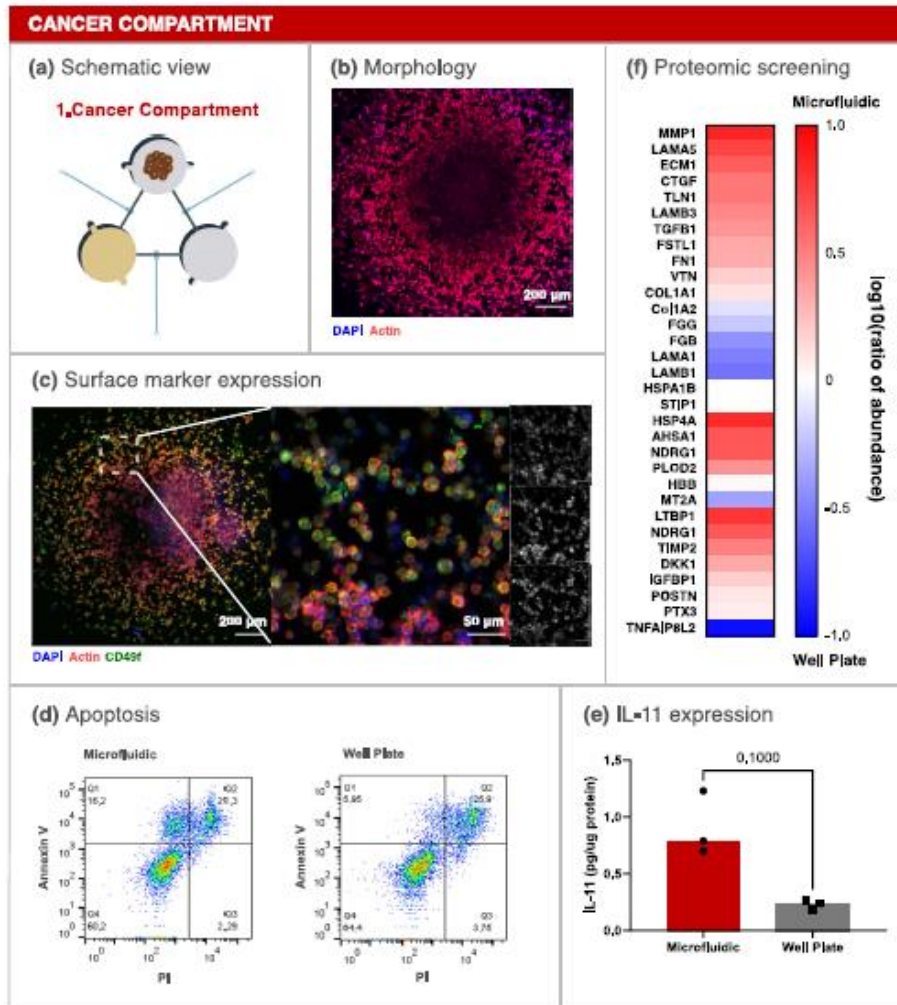


Fig. 2. Breast Cancer compartment optimization. (a) Schematic representation of the breast cancer compartment (b) Micrograph of a MDA-1833 cell spheroid cultured for 3 days on the microfluidic platform. Blue - DAPI. Red - F-actin. Scale bar - 200 μ m. (c) Expression of CD49f on MDA-1833 cells. DAPI (blue), F-Actin (red) and CD49f (green). Scale bar - 200 μ m. Inset single channel images are shown on the right DAPI (blue, top), F-Actin (red, mid) and CD49f (green, bottom). Inset scale bar - 50 μ m. (d) Annexin V quantification by flow cytometry of breast cancer spheroids cultured inside the microfluidic platform (left) or in standard well plates (right). Ten spheroids were pooled together for the analysis. (e) IL-11 quantification in conditioned media from MDA-1833 spheroids cultured in the microfluidic platform or in well plates. Data is expressed as median of individual data points from 3 independent experiments and was normalized to the total protein content (Mann-Whitney test, $p = 0.1000$). (f) Proteomic screening of the conditioned media from MDA-1833 spheroids cultured in the microfluidic or in standard well plates. Data is represented as the logarithm of base 10 of the ratio between the abundance of each secreted protein within the microfluidic and well plate.

compared to spheroids grown in standard 96-well plates. No differences regarding spheroid size were observed (Fig. S2) and Annexin V staining showed that cell apoptosis was similar between conditions (Fig. 2d). We then investigated whether the environment in the microfluidic platform evoked changes in the conditioned medium of MDA-1833 cells. Breast cancer cells express a plethora of pro-inflammatory factors, of which interleukin (IL) 11 was previously implicated in breast cancer progression and bone metastasis [34]. IL-11 was therefore quantified and we observed a clear trend towards increased IL-11 levels inside the

microfluidic compartment when compared to MDA-1833 cultured in standard 96-well plates (Fig. 2e). Thus, we further hypothesized that our microfluidic platform could recapitulate a more aggressive breast cancer phenotype. To confirm this, the conditioned medium from MDA-1833 spheroids cultured inside the microfluidic platform and in normal 96-well plates was collected and screened for the presence of proteins relevant for our model. The level of several matrix-associated proteins was increased in the conditioned medium from MDA-1833 spheroids cultured in our metastasis-on-a-chip platform, namely connective tissue

growth factor (CTGF) and matrix metalloproteinase 1 (MMP1), which were already described to promote breast cancer progression in the bone niche (Fig. 2f) [31,35–37]. Additionally, multiple proteins previously reported to be involved in bone metabolism were shown to be more abundant when MDA-1833 spheroids were cultured inside the microfluidic platform when compared to 96-well plates, such as latent transforming growth factor- β (TGF- β) binding protein 1 (LTBP1) and Dickkopf-1 (DKK1) (Fig. 2f).

3.3. Sympathetic neuronal compartment: cell differentiation and catecholamine release

Sources for human sympathetic neurons for in vitro culture are scarce. Sympathetic neurons were previously obtained from human Pluripotent Stem Cells (hPSCs), however protocols for differentiation are inefficient and of difficult execution [38]. Nonetheless, neuroblastoma cell lines have been reported to produce NE [39], which is the main sympathetic neurotransmitter. In order to model the sympathetic nervous system contribution to bone metastasis, SH-SY5Y neuron-like cells were included in the microfluidic platform (Fig. 3a). The neuronal compartment was coated with laminin and SH-SY5Y cells were allowed to differentiate for 7 days under retinoic acid stimulation, after which they presented long axonal extensions (Fig. 3b). Tyrosine hydroxylase (TH) is the rate limiting enzyme in the NE synthesis cascade and commonly expressed in sympathetic neurons. TH expression was verified in SH-SY5Y cells cultured in the microfluidic platform, confirming that SH-SY5Y cells maintain a sympathetic phenotype when cultured in our metastasis-on-a-chip platform (Fig. 3c). Since NE secretion would be the main contributor to our metastatic model, NE was subsequently quantified in the conditioned medium of the neuronal compartment (Fig. 3d).

NE was detected in a nanomolar concentration range, a concentration sufficient for adrenergic receptor stimulation [40]. No significant differences were observed between SH-SY5Y cells cultured in the microfluidic platform and the 96-well plate regarding NE production, validating the assumption that sympathetic input is maintained in our platform.

3.4. Bone compartment: bone resorbing osteoclasts on mineralized ECM

Breast cancer is usually of osteolytic nature, leading to extensive bone degradation. Osteoclasts, multinucleated cells that are able to resorb the bone, are therefore crucial players in the establishment of metastatic bone lesions. In fact, proteins released from the bone matrix during resorption as well as other osteoclast-secreted factors are able to modulate breast cancer cell behavior and also neuron activation in the bone microenvironment [41,42]. Aiming to replicate these interactions, mature human osteoclasts were cultured on top of bone slices inside the microfluidic platform for three days, refreshing RANKL and M-CSF daily to ensure ample access to these cytokines (Fig. 4a). Characteristic features of mature osteoclasts were observed, namely large cytoplasm area, actin ring formation and osteoclast marker cathepsin K expression (Fig. 4b and c). Of note, different morphologies were observed in various osteoclasts, namely circular actin rings (Fig. 4b) or crescent-shaped actin rings (Fig. 4c), which reflect the direction of resorption and are characteristic of different resorption modalities [28,43]. Osteoclasts are inherently capable of resorbing the bone while being static or while moving across the surface of the bone, generating resorption pits or trenches, respectively (Fig. 4d, e, Fig. S3). Accordingly, resorption pits and trenches were visible on the surface of the bone slices, demonstrating that osteoclasts were not only morphologically differentiated but also fully functional (Fig. 4d).

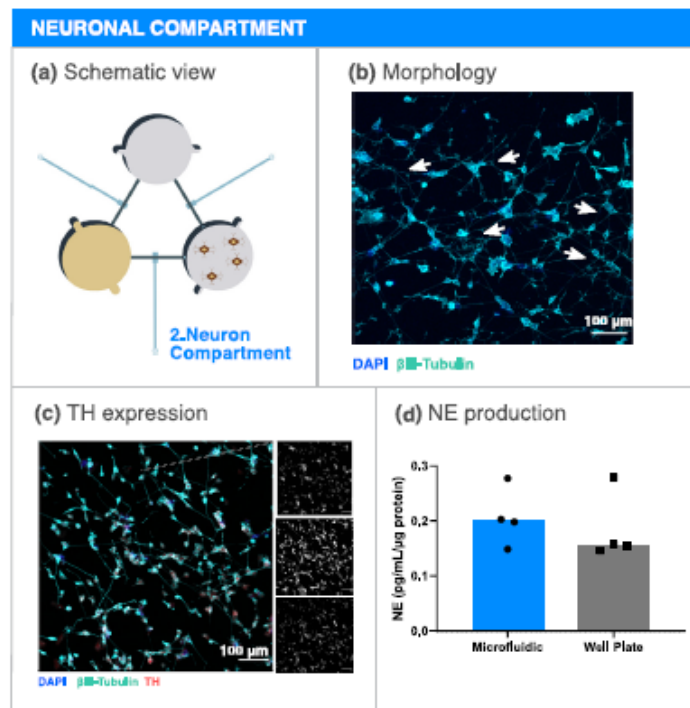


Fig. 3. Neuron-like cell compartment optimization. (a) Schematic representation of the neuron-like cell compartment. (b) Micrograph of SH-SY5Y cells cultured for 7 days inside the microfluidic compartment. Several neuronal extensions are highlighted in white arrows. Blue - DAPI; Cyan - β III Tubulin. Scale bar 100 μ m. (c) Expression of the sympathetic marker TH in SH-SY5Y cultured in the microfluidic platform. Single channel images are showed on the right. Blue (Top) - DAPI; Cyan (Mid) - β III Tubulin; Red (Bottom) - TH. Scale bar - 100 μ m. (d) NE concentration quantification in SH-SY5Y conditioned medium from the microfluidic platform or in well plates. Data is expressed as median of individual data points from 4 independent experiments and was normalized to the total protein content (Mann-Whitney test, non-significant).

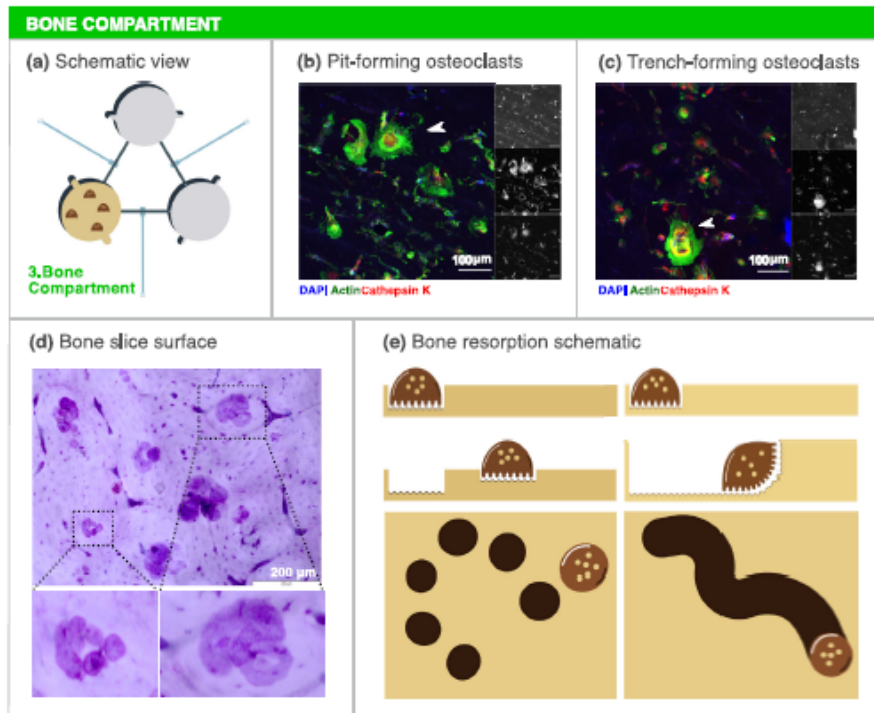


Fig. 4. Bone compartment optimization. (a) Schematic representation of the bone compartment. (b) Micrograph of mature, multinucleated osteoclasts on the surface of the bone slice. The white arrowhead shows an osteoclast with a circular actin ring, characteristic of resorption pit formation. (c) Mature osteoclasts on top of a bone slice. The white arrowhead shows an osteoclast with a crescent-shaped actin ring, characteristic of a resorption trench formation. Single channel images are shown on the right. Blue (Top) - DAPI; Green (Mid) - Actin; Red (Bottom) - Cathepsin K. Scale bar - 100 μ m. (d) Toluidine blue staining of the surface of the bone slice after three days of culture. Several resorption events are seen throughout the bone slice. In the left inset resorption pits are visible while in the right inset an example of a trench is shown. Scale bar - 200 μ m. (e) Schematic representation of osteoclast resorption activity. Osteoclasts are capable of stationary resorption (left) or resorption while moving through the bone surface (right), leading to the formation of resorption pits or trenches respectively.

3.5. Non-selective crosstalk: opening communication between breast cancer-neuron-osteoclast

After individual characterization of each compartment, MDA-1833 cells, SH-SY5Y cells and osteoclasts were cultured simultaneously in the microfluidic platform (Fig. 5a). To that end, SH-SY5Y were first seeded and differentiated with retinoic acid for 7 days, followed by osteoclast and MDA-1833 seeding in their respective compartments (Fig. 5b). Cells were further cultured for 3 days, refreshing RANKL and M-CSF daily in the bone compartment until the end of the experiment. Cell morphology of each cell type was confirmed by immunocytochemistry in the end of the experiment (Fig. 5c). This was an important validation step since we were able to show that similar morphology and differentiation status were achieved when all cells were cultured simultaneously, even though each compartment encompassed different culture media that were mixed by diffusion during the course of the experiment.

As stated above, the aim of this platform was to investigate how breast cancer cells would respond to sympathetic stimuli under osteoclast crosstalk, by focusing our study on breast cancer secreted factors. Since proteins described to modulate the bone microenvironment were detected in the conditioned media of MDA-1833 cells in the previous optimization step, we decided to restrict our search by using a bone metabolism protein array. Conditioned medium was extracted from the

breast cancer compartment in the end of each experiment and screened for proteins that could be relevant for our model, e.g. IL-6 and monocyte chemoattractant protein 1 (MCP-1). After normalization for total protein content, the relative expression of each protein in the breast cancer compartment was determined (Fig. 5d). Of note, when breast cancer cells were co-cultured with osteoclasts, increased levels of IL-6, IL-8, MCP-1 and macrophage inflammatory protein 1 α (MIP-1 α) were observed in the breast cancer compartment, which point to an effect of osteoclasts on MDA-1833 secretome. Interestingly, the pro-inflammatory setting was further exacerbated when SH-SY5Y cells were added to the model, where the levels of IL-6 and MIP-1 α were further augmented (Fig. 5d). Indeed, sympathetic stimulus has been described to increase IL-6 levels in MDA-231 breast cancer cells with high β -adrenergic receptor (β -AR) expression [44] and both MDA-1833 and human osteoclasts express several ARs, being therefore responsive to sympathetic stimuli (Fig. S4). Based on these results, MIP-1 α and IL-6 were then selected as potential candidate targets of sympathetic signaling in breast cancer and proceeded to validate the array by quantifying the expression of these cytokines by ELISA. Again, we observed a significant increase in MIP-1 α in the cancer compartment when all cell types were cultured together with the valves in an open state (Fig. 5e). Importantly, the levels of MIP-1 α detected in the cancer compartment, when MDA-1833 cells were co-cultured with either osteoclasts or neurons, did not differ from MDA-1833

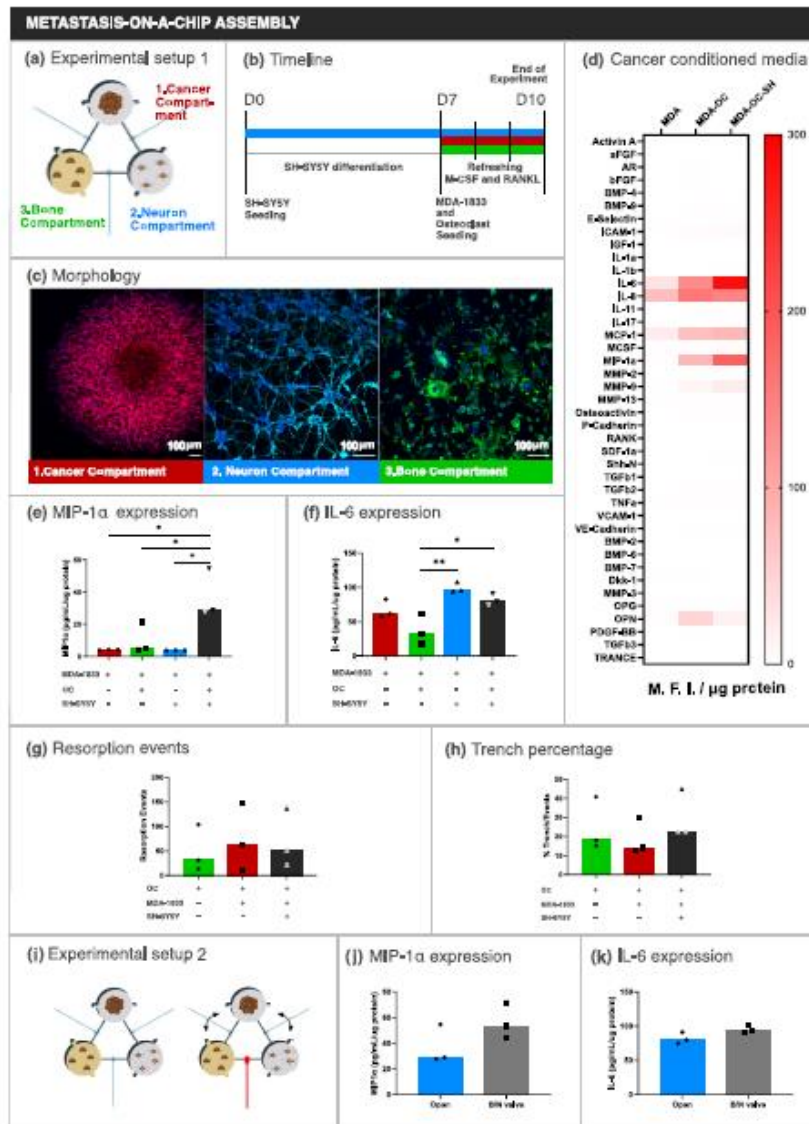


Fig. 5. Tri-culture assembly on the microfluidic platform. (a) Schematic representation of the assembled microfluidic platform. (b) Timeline of the experiment. (c) Representative micrographs of (1) the cancer compartment, (2) the neuron compartment and (3) the bone compartment. Scale bar – 100 μm . (d) Bone metabolism array data of conditioned medium from the cancer compartment. Data is represented as Mean Fluorescence Intensity and normalized by total protein content. (e, f) Quantification of MIP1 α and IL-6 concentration in conditioned media from the breast cancer compartment by ELISA. Data is expressed as median of individual data points from 3 independent experiments and was normalized to the total protein content (One-way ANOVA test, * $p < 0.05$, ** $p < 0.01$). (g) Quantification of resorption event number and (h) percentage of trench number relative to total number of events. Data is expressed as median of individual data points from 3 independent experiments (One-way ANOVA test, non-significant). (i) Schematic representation of the experimental setting. Closing the valve between the neuronal and bone compartment forces communication to be preferentially through the cancer compartment. (j) Quantification of MIP1 α and (k) IL-6 concentration in conditioned media from the breast cancer compartment by ELISA. Data is expressed as median of individual data points from 3 independent experiments and was normalized to the total protein content (Mann-Whitney test, non-significant).

monoculture. These results highlight the potential of our microfluidic platform to capture the synergistic effect of multiple cell crosstalk and the importance of a dynamic interaction between the three cell types. On the other hand, IL-6 levels were significantly increased in the tri-culture condition when compared to MDA-1833 and osteoclast co-culture controls but were similar to MDA-1833 monoculture controls (Fig. 5f). The increase in IL-6 appears to be due to neuronal inputs, since the addition of SH-SY5Y cells sharply increased IL-6 production as could be seen in MDA-11833 and neuron co-culture controls. MDA-1833 cells are the main source of IL-6 since only residual IL-6 was detected in neuronal or osteoclast mono-culture controls (Fig. 5g).

Despite the augmented levels of MIP-1 α and IL-6 pro-inflammatory mediators in the cancer compartment, these did not affect overall osteoclast resorption activity nor resorption mode in the bone compartment (Fig. 5g and h).

Taken together, our results demonstrate the importance of the dynamic communication between the different players in the metastatic niche and the ability of our microfluidic platform to capture these complex interactions.

3.6. Selective crosstalk closing communication between neurons and osteoclasts

Intercellular communication on the microfluidic platform is dynamic, where each different cell type is able to shape the response of the other cells over the course of the experiment. The inclusion of valves in our platform adds an extra layer of complexity, allowing the manipulation of the communication by stopping the flow between two specific compartments. The observed increase in pro-inflammatory factors in our model supported by other previous reports have shown that direct sympathetic stimulus increases breast cancer aggressiveness [44]. Thus, we hypothesized that the blockage of communication between the neuron and bone compartment would not affect the production of pro-inflammatory cytokines in our model. Taking advantage of the Quake valves incorporated in our metastasis-on-a-chip model, we assembled the tri-culture while keeping the valve between neuron and bone compartments closed, in order to assess the impact of different communication routes on the production of IL-6 and MIP-1 α in the cancer compartment (Fig. 5i). As hypothesized, closing the valve between neuronal and bone compartment did not change the levels of MIP-1 α nor IL-6 (Fig. 5 j, k). These results suggest that direct communication between SH-SY5Y cells and osteoclasts is not required for the observed levels of IL-6 and MIP-1 α levels in the breast cancer compartment, since limiting communication between neuron and osteoclasts did not change the levels of these cytokines secreted by breast cancer cells.

4. Discussion

The crosstalk between the multiple components of the breast cancer bone metastatic niche is inherently complex. Although *in vitro* models provide a simplistic view of these intricate interactions, microfluidic systems can be used as versatile tools that are able to recapitulate important hallmarks of disease progression. Our work describes a new metastasis-on-a-chip platform designed to dissect the interplay between different cellular players within the breast cancer bone metastatic niche. This microfluidic platform retains a high degree of complexity by allowing the culture of at least three different human cell types simultaneously, namely bone tropic breast cancer cells, neurons and osteoclasts. Moreover, the physical separation of the cellular components enables a dynamic crosstalk between the different cell types exclusively through secreted factors, which will result in a cleaner readout interpretation, since direct cell-cell interactions do not occur in our model.

The majority of the microfluidic platforms used in the literature are produced using soft lithography processes that, although allowing a high degree of spatial resolution, also require costly facilities and highly qualified personnel. Using affordable consumer grade 3D printers, we

were able to produce resin molds with adequate resolution and a smooth surface compatible with plasma cleaning bonding processes. Furthermore, the combination of features of different heights in the same mold facilitates rapid prototyping and can be translated into a design freedom that is not feasible in standard photolithography. For the first time, we describe a research tool that integrates human bone tropic breast cancer, neuron cells and osteoclasts in a single PDMS platform manufactured from 3D printed molds. We believe that this methodology could be employed in other research settings, since we used widely accessible 3D printers and computer aided design tools that do not require specialized training. Our platform was designed for the analysis of secreted factors involved in the crosstalk taking place at the bone metastatic niche, but compartment dimensions, channel length and cellular types could be prototyped and adapted to fit the needs of different biological questions.

Bone tropic MDA-1833 breast cancer cell spheroids were chosen to mimic a breast cancer bone metastatic niche. Cell spheroids are widely used to model tumor niche interactions and present advantages regarding metabolic gradients, apoptosis and drug resistance profiles when compared to standard monolayer culture techniques [45,46]. MDA-1833 cell spheroids were successfully introduced in the microfluidic platform and presented similar size and apoptosis levels as spheroids grown in normal 96 well plates. However, the environmental features inherent of the microfluidic compartment, such as lower access to nutrients and oxygen, seem to have an impact in MDA-1833 protein expression. Normalized IL-11 levels were shown to be increased in the metastasis-on-a-chip platform when compared to 96-well plates, coherent with a more pro-inflammatory and osteolytic phenotype. In addition, MDA-1833 cells were first described by Kang et al. and are reported to express a myriad of other osteolytic factors [31]. Of note, we showed that LTBP1 is more abundant in the conditioned medium of MDA-1833 cells cultured in the microfluidic platform when compared to normal 96-well plates. Osteoclasts are capable of cleaving LTBP1, which is subsequently involved in the release of TGF- β from the bone matrix during bone resorption [47] and will then fuel tumor growth in the bone niche. Furthermore, we showed that proteins from the matrisome [48], such as MMP1 and CTGF, were also increased in our microfluidic platform, consistent with an increased breast cancer aggressive behavior.

Since solid tumors are often of hypoxic nature due to limited or aberrant oxygen supply, hypoxia has profound implications in breast cancer progression and it has been already implicated in the establishment of bone metastasis [49]. Accordingly, the topographic features of our microfluidic platform imply a lower medium volume in the cell compartments and consequently a lower access to oxygen and nutrients environment when compared with a standard well plate. Hypoxia is described to promote the expression of CTGF in MDA-MB-231 cells [50], which might explain the observed increase in CTGF secretion.

Although we have focused on bone tropic breast cancer secreted peptides in our study, our microfluidic platform can be potentially used to analyze other secreted factors such as cancer-derived exosomes. Exosomes are extracellular vesicles that can deliver proteins, lipids and microRNAs to modulate cellular communication and have already been implicated in breast cancer bone metastasis and osteoclast differentiation [51]. In the future, this novel system can be potentially used to evaluate how sympathetic neuronal activation alters the secretion of exosomes by bone tropic breast cancer cells.

In order to study breast cancer associated bone pain, the crosstalk between sensorial neurons and breast cancer cells with microfluidic platforms has been previously modelled [52]. However, to our knowledge, no previous attempts have been made to model sympathetic neuron - breast cancer cellular interactions in a bone metastatic context using microfluidic technology. The culture of murine sympathetic ganglia in microfluidic platforms was established to study cardiomyocyte stimulation, but human sources of sympathetic neurons are limited. Retinoic acid differentiated SH-SY5Y cells have been previously used as models of sympathetic neurons [39], since these cells are capable of expressing the sympathetic marker TH and produce NE. In our model, we were able to

successfully cultivate NE-secreting human sympathetic neurons, which was fundamental to achieve our final goal.

Previous microfluidic models, where murine osteoclasts derived from RAW264.7 cells were co-cultured with osteocytes to unravel the effect of mechanostimulation on the crosstalk between these cellular players, have been also already described [53]. However, as far as we are aware, our work is the first to describe the culture of human osteoclasts in a microfluidic platform. One of the advantages of our proposed model is the addition of bone slices to the bone compartment. Bone slices retain important topographic and biochemical cues that are crucial for osteoclastic resorption activity, allowing for resorption activity readouts that were not yet previously seen in microfluidic devices. Importantly, in addition to the total extent of osteoclast resorption activity, it is possible to distinguish different resorption modalities in the surface of the bone slices. Variations in the trench content relative to the total number of events could be indicative of differences in collagenolysis versus demineralization rates and cathepsin K activity [54]. In addition, trench resorption is faster and favors bone fragility, and is associated with more aggressive bone degradation [25].

After optimization steps, microfluidic assembly of all three cell types allowed a unique glance at the intercellular crosstalk that occurs at the bone metastatic niche. In our metastasis-on-a-chip platform, we showed that bone tropic breast cancer cells received synergistic inputs from neurons and osteoclasts that resulted in increased levels of pro-inflammatory cytokines. Interestingly, IL-6 and MIP-1 α were already implicated in the progression of breast cancer bone metastasis and osteoclastogenesis [55,56]. Furthermore, our results are consistent with previous studies where sympathetic stimulus increases IL-6 production in breast cancer [44] and melanoma cell lines *in vitro* [57]. On the other hand, osteoclast secreted factors or proteins released from the bone matrix during resorption were also described to promote breast cancer growth [58,59]. As could be seen in MIP-1 α secretion levels, we showed that dynamic communication, contrarily to standard conditioned medium approaches, is of vital importance to recapitulate interactions that could take place at the bone metastatic microenvironment.

One of the main features of our platform is the inclusion of valves in each of the interconnecting channels. These valves were designed based on the Quake valve architecture, where pressure applied to a flexible membrane allows the closure of a fluidic channel [60]. Quake valves were previously used in both photolithography [61] and 3D printing applications [16] and are a valuable tool for fluidic control. In this microfluidic platform, Quake valves serve two main purposes: 1) we were able to constrain each different cell in its respective compartment during cell seeding and 2) we could alter the diffusion pattern and directionality of the stimuli from one compartment to another. We demonstrated that by closing the communication between bone and neuron compartments, cytokine levels secreted by breast cancer cells did not change significantly, pointing towards a negligible effect of direct neuron-osteoclast communication on the changes observed in the cancer compartment. Although epinephrine was reported to increase differentiation of human osteoclast-like cells, the direct effect of NE on human osteoclast activity is still unknown [62]. Future effort should be directed towards understanding what are the osteoclast/neuron derived factors that promote a breast cancer pro-inflammatory phenotype.

Our model presents some limitations in its current form. First, we included sympathetic neurons and osteoclasts but the bone metastatic niche is extremely complex and composed of multiple cellular players [1]. We could potentially use our microfluidic platform to study how resident macrophages and lymphocytes, osteocytes, hematopoietic stem cells, fibroblasts and endothelial cells could also contribute to the establishment and progress of the metastatic disease. For instance, future improvements to this microfluidic model would include the addition of immune cells to the cancer compartment. Since macrophages are responsive to NE [63], it would be interesting to assess how they impact breast cancer bone metastasis under sympathetic stimulus. In addition, under sympathetic stimulation, osteoblast derived vascular endothelial

growth factor (VEGF) and IL-1 β was able to modulate endothelial cells to facilitate breast cancer cell extravasation from circulation into the bone marrow niche, both *in vitro* and *in vivo* [18,22]. A different platform design would be required to include endothelial cells, though, to allow hydrogel seeding, fluidic flow and self-assembly of blood vessels.

Second, several studies have shown that breast cancer cells induce osteolysis via osteoblast-lineage cells and not by direct osteoclast stimulation [64,65]. Parathyroid hormone-related protein (PTHrP) is described to be secreted by breast cancer cells and to promote the production of RANKL by osteoblasts, subsequently resulting in osteoclast activation [65]. Furthermore, the secretome from MDA-MB-231 cells was recently described to modulate osteoblast mediated bone matrix deposition *in vivo* [66]. On the other hand, osteoblasts were observed in close contact with prostate and breast cancer cells in clinical bone metastasis biopsies, suggesting that not only secreted factors but also direct cell-cell contact between osteoblasts and cancer cells could be important for osteoclastogenesis and bone degradation [67]. The addition of primary human osteoblasts in the cancer compartment, mimicking the interactions that take place between tumor cells and cancer associated fibroblasts, could be an interesting upgrade to the microfluidic model in order to fully recapitulate the bone resorption promoting capacity of breast cancer cells.

Third, the potential of our platform to investigate the effect of different cancer cell lines on the bone niche could be further explored. We focused on metastatic MDA-1833 breast cancer cells to mimic the local colonization of bone, nevertheless it would be interesting to assess how the parental cell line MDA-MB-231 react to osteoclast secreted factors under sympathetic activation. Furthermore, differences in the role of distinct molecular subtypes of breast cancer on the bone niche, such as luminal-like or epidermal growth factor receptor 2 (HER2) enriched breast cancer cell lines, could be investigated in future studies. Finally, prostate cancer, lung cancer and multiple myeloma also display bone tropism [59], and thus studying the effect of sympathetic stimuli on prostate/lung or multiple myeloma bone metastatic niche would demonstrate the translational potential of our model.

5. Conclusion

In summary, we have developed a new model of sympathetic regulation of breast cancer in a bone metastatic context through the integration of breast cancer cells, osteoclasts and sympathetic neuron-like SH-SY5Y cells on the same microfluidic platform. Our model displays several advantages compared to other breast cancer metastatic models: 1) manufacture is cheap and accessible without the need for specialized staff and equipment; 2) integrates a full humanized system with bone tropic breast cancer cells; 3) contains a bone matrix with intact biomechanical and biochemical cues leading to relevant bone resorption readouts; 4) includes three quake valves that allow compartment isolation during cell seeding and modulation of diffusion directionality. We successfully characterized the culture of different cell types on our platform, which led to the identification of inflammatory mediators that could be involved in the breast cancer response to sympathetic stimuli in the context of bone metastasis.

Collectively, our findings could set the basis for additional exploration of the mechanisms that govern sympathetic modulation of breast cancer bone metastasis. Further insights on the cancer-bone-neuron crosstalk could be gained by manipulating the microenvironment of each compartment by the addition of different cell players, the use of specific signaling pathway inhibitors or by including breast cancer knock-out variants. In the future, our metastasis-on-a-chip platform could also potentially be applied for drug screening assays and incorporate patient-derived tumor samples or osteoclasts for improved translational relevance. Importantly, this work presented a new platform that could be used as basis for fundamental research on various physiological and pathological settings, with the possibility of changing the different cell types to cater the needs of individual research questions.

Credit author statement

Francisco Conceição: Conceptualization, Methodology, Validation, Formal Analysis, Investigation, Writing - Original Draft, Visualization. **Daniela M. Sousa:** Investigation, Writing - Review & Editing. **Joshua Loessberg-Zahl:** Methodology, Writing - Review & Editing. **Anke R. Vollertsen:** Methodology, Writing - Review & Editing. **Estrela Neto:** Investigation, Writing - Review & Editing. **Kent Sæ:** Supervision, Writing - Review & Editing. **Joana Paredes:** Supervision, Writing - Review & Editing. **Anne Leferink:** Resources, Supervision, Conceptualization, Writing - Review & Editing. **Meriem Lamghari:** Supervision, Project Administration, Funding Acquisition, Writing - Review & Editing.

Data availability

The data that support the findings of this study is available from the corresponding authors upon reasonable request.

Declaration of competing interest

The authors declare that they have no known competing financial interests or personal relationships that could have appeared to influence the work reported in this paper.

Acknowledgements

The authors would like to acknowledge Inez Duursma for the first generation design of the three compartment microfluidic chip and Hugo Osório and the I3S Scientific Platform Proteomics for the help with the proteomic screening of cancer conditioned medium. The authors also thank Pedro Sousa and Anabela Nunes from the I3S Communication Unit for their help in illustration design. The authors acknowledge the support of the I3S Scientific Platform Bioimaging, member of the national infrastructure PPBI - Portuguese Platform of Bioimaging (PPBI-POCI-01-0145-FEDER-0221.22), for confocal imaging acquisition. This work was financed by FEDER—Fundo Europeu de Desenvolvimento Regional funds through the COMPETE 2020—Operational Programme for Competitiveness and Internationalisation (POCI), Portugal 2020, and Portuguese funds through FCT/MCTES in the framework of the project “SproutOC” (POCI-01-0145-FEDER-030158, PTDC/MED-PAT/30158/2017). F.C. is a recipient of the Ph.D. fellowship SFRH/BD/128771/2017. D.M.S. is a recipient of Post-Doc fellowship SFRH/BPD/115341/2016. J.L. and A.R.V. were funded under the VESCEL ERC Advanced Grant to A. van der Berg (grant no. 669768).

Appendix A. Supplementary data

Supplementary data to this article can be found online at <https://doi.org/10.1016/j.mtbio.2022.100219>.

References

- K.N. Weilbaecher, T.A. Guise, L.K. McCauley, Cancer to bone: a fatal attraction, *Nat. Rev. Cancer* 11 (2011) 411–425.
- J. Kong, Y. Luo, D. Jin, F. An, W. Zhang, L. Liu, J. Li, S. Fang, X. Li, X. Yang, B. Hu, T. Liu, A novel microfluidic model can mimic organ-specific metastasis of circulating tumor cells, *Oncotarget* 7 (2016) 78421–78432.
- A. Chramiec, D. Telis, K. Yeager, A. Marturano-Kruik, J. Pak, T. Chen, L. Hao, M. Wang, R. Lock, D.N. Tavalat, M.B. Lee, J. Kim, K. Ronald-Bouchard, G. Vunjak-Novakovic, Integrated human organ-on-a-chip model for predictive studies of anti-tumor drug efficacy and cardiac safety, *Lab Chip* 20 (2020) 4357–4372.
- J. Almeida, S.K. George, S. Herberg, M. Devansetty, C.D. Porada, A. Skardal, G. Almeida-Porada, Deconstructed microfluidic bone marrow on-a-chip to study normal and malignant hematopoietic cell-niche interactions, *Small* 15 (2019) 1902971.
- S. Bersini, J.S. Jeon, G. Dubini, C. Arrigoni, S. Chung, J.L. Charest, M. Moretti, R.D. Kamm, A microfluidic 3D in vitro model for specificity of breast cancer metastasis to bone, *Biomaterials* 35 (2014) 2454–2461.
- J.S. Jeon, S. Bersini, M. Gilardi, G. Dubini, J.L. Charest, M. Moretti, R.D. Kamm, Human 3D vascularized organotypic microfluidic assays to study breast cancer cell extravasation, *Proc. Natl. Acad. Sci. Unit. States Am.* 112 (2015) 214–219.
- L.L. Buchd, B.P. Casavant, P.A. Young, K.W. Ellicott, H.S. Basu, D.J. Beebe, A microfluidic coculture and multiphoton FAD analysis assay provides insight into the influence of the bone microenvironment on prostate cancer cells, *Integrative Biology* 6 (2014) 627–635.
- X. Mei, K. Middleton, D. Shin, Q. Wan, L. Xu, Y.-H.V. Ma, D. Devadas, N. Walji, L. Wang, F.W.K. Young, L. You, Microfluidic platform for studying osteocyte mechanoregulation of breast cancer bone metastasis, *Integrative Biology* 11 (2019) 119–129.
- J. Ahn, J. Lim, N. Jusoh, J. Lee, T.-F. Paik, Y. Kim, J. Kim, N.J. Jeon, 3D microfluidic bone tumor microenvironment comprised of hydroxyapatite/fibrin composite, *Front. Bioeng. Biotechnol.* 7 (2019).
- S. Hao, L. Ha, G. Cheng, Y. Wan, Y. Xia, D.M. Sosnoski, A.M. Mastro, S.-Y. Zheng, A spontaneous 3D bone-on-a-chip for bone metastasis study of breast cancer cells, *Small* 14 (2018) 1702967.
- A. Marturano-Kruik, M.M. Nava, K. Yeager, A. Chramiec, L. Hao, S. Robinson, E. Guo, M.T. Raimondi, G. Vunjak-Novakovic, Human bone perivascular niche-on-a-chip for studying metastatic colonization, *Proc. Natl. Acad. Sci. Unit. States Am.* 115 (2018) 1256–1261.
- W. Zhang, W.Y. Lee, D.S. Siegel, P. Tolia, J. Zilberberg, Patient-specific 3D microfluidic tissue model for multiple myeloma, *Tissue Eng. C Methods* 20 (2013) 663–670.
- D.B. Chou, V. Faganias, Y. Milton, R. David, P. Pop-Damkov, D. Ferguson, A. MacDonald, G. Vargis Böllikbaşı, C.E. Joyce, L.S. Moreira Teixeira, A. Rech, A. Jiang, F. Gilamar, S. Jalli-Firooznezhad, B.A. Rufong, J.R. O’Sullivan, C.F. Ng, Y. Choe, S. Marquez, K.C. Myers, O.K. Weinberg, R.P. Hasegawa, R. Novak, O. Levy, R. Prandi-Basu, C.D. Novina, A. Shimamura, L. Ewart, D.E. Ingber, On-chip recapitulation of clinical bone marrow toxicities and patient-specific pathophysiology, *Nature Biomedical Engineering* 4 (2020) 394–406.
- P.J. Kilton, M.H. Rosnes, V. Sans, V. Dragovic, I. Gronin, Configurable 3D-printed microfluidic and microfluidic ‘lab on a chip’ reactionware devices, *Lab Chip* 12 (2012) 3267–3271.
- G. Coninas, A. Suska, D. Filippini, Low cost lab-on-a-chip prototyping with a consumer grade 3D printer, *Lab Chip* 14 (2014) 2978–2982.
- Y.-S. Lee, N. Bhattacharjee, A. Fokh, 3D-printed Quake-style microvalves and micropumps, *Lab Chip* 18 (2018) 1207–1214.
- J.P. Campbell, M.R. Kaslik, Y. Ma, D.S. Pezaris, S.K. Masood-Campbell, N.L. Penner, S.A. Munoz, A. Zijlstra, X. Yang, J.A. Sterling, F. Eleftherou, Stimulation of host bone marrow stromal cells by sympathetic nerves promotes breast cancer bone metastasis in mice, *PLoS Biol.* 10 (2012) e1001363.
- L. Clément-Demaings, P.I. Mulcross, T.Q. Tabatabaie, J.A. Steding, F. Eleftherou, β 2AR stimulation in osteoblasts promotes breast cancer cell adhesion to bone marrow endothelial cells in an IL-1 β and selectin-dependent manner, *Journal of Bone Oncology* 13 (2018) 1–10.
- D.G. Powe, M.J. Vos, K.S. Zanker, H.O. Habely, A.P. Green, I.O. Ellis, F. Eleftherou, Beta-Blocker drug therapy reduces secondary cancer formation in breast cancer and improves cancer specific survival, *Oncotarget* 1 (2010).
- C.R. Cardwell, A. Forrester, E. Vos, H. Gamo, L.J. Murray, C. Brown, P.A.J. Vissers, M. O’Rourke, K. Vasanathan, D. Conlin-Renton, H. De Schutter, M. Lambie, D.G. Powe, M.P. van Herk-Sukel, A. Gavin, S. Fris, L. Sharp, K. Bennett, Prognosis and survival from breast cancer: a pooled analysis of European breast cancer cohort, *Breast Cancer Res.* 18 (2016) 119.
- C.R. Cardwell, H.G. Coleman, L.J. Murray, F. Eleftherou, D.G. Powe, Beta-blocker usage and breast cancer survival: a nested case-control study within a UK Clinical Practice Research Datalink cohort, *Int. J. Epidemiol.* 42 (2014) 1852–1861.
- P.I. Mulcross, J.P. Campbell, L. Clément-Demaings, A.L. Ashinder, A.R. Morkid, R.A. Brekken, J.A. Sterling, F. Eleftherou, Skeletal colonization by breast cancer cells is stimulated by an osteoblast and β 2 α -dependent neo-angiogenic switch, *J. Bone Miner. Res.* 32 (2017) 1442–1454.
- E. Neto, C.J. Alves, D.M. Sousa, I.S. Alencastre, A.H. Lourenço, L. Leitão, H.R. Ryu, N.L. Jeon, R. Fernandes, P. Aguiar, R.D. Almeida, M. Lamghari, Sensory neurons and osteoblasts: close partners in a microfluidic platform, *Integrative Biology* 6 (2014) 586–595.
- L. Leitão, E. Neto, F. Conceição, A. Moutão, M. Couto, C.J. Alves, D.M. Sousa, M. Lamghari, Osteoblasts are inherently programmed to sepd sensory innervation, *Bone Research* 8 (2020) 20.
- K. Spa, J.-M. Delaisot, Glucocorticoids maintain human osteoclasts in the active mode of their resorption cycle, *J. Bone Miner. Res.* 25 (2010) 2184–2192.
- J.M. May, Z.-c. Qi, M.E. Meredith, Mechanisms of ascorbic acid stimulation of norepinephrine synthesis in neuronal cells, *Biochem. Biophys. Res. Commun.* 426 (2012) 148–152.
- J. Vanderoort, K. Spa, D.M.H. Meerlid, J.-M. Delaisot, G.H. van Lenthe, Glucocorticoid-induced changes in the geometry of osteoclast resorption cavities affect trabecular bone stiffness, *Calcif. Tissue Int.* 92 (2013) 240–250.
- D.M. Meerlid, D.C. Pirapaharan, C.M. Anderson, P. Kjærgaard-Andersen, A.M. Møller, M. Ding, J.-M. Delaisot, K. Spa, Pit- and trench-forming osteoclasts: a distinction that matters, *15032-15032, Bone research* 3 (2015).
- C.S. Hughes, S. Moggridge, T. Miller, P.H. Sorensen, G.R. Modin, I. Krijgsveld, Single-pot, solid-phase-enhanced sample preparation for proteomics experiments, *Nat. Protoc.* 14 (2019) 68–85.
- H. Osório, C. Silva, M. Ferreira, I. Gullo, V. Máximo, R. Barros, F. Mendonça, C. Oliveira, F. Carneiro, Proteomics analysis of gastric cancer patients with diabetes mellitus, *J. Clin. Med.* 10 (2021) 407.

- [31] Y. Kang, P.M. Siegel, W. Shu, M. Drobnjak, S.M. Kaloupek, C. Cordon-Cardo, T.A. Guise, J. Masugue, A multigenic program mediating breast cancer metastasis to bone, *Cancer Cell* 3 (2003) 537–549.
- [32] T. Ishiguro, H. Ohata, A. Sato, K. Yamawaki, T. Enomoto, K. Okamoto, Tumor-derived spheroids: relevance to cancer stem cells and clinical applications, *Cancer Sci.* 108 (2017) 283–289.
- [33] D.L. Brooks, L.P. Schwab, R. Krut'ina, D.N. Parke, A. Sethuraman, D. Hoogewijs, A. Schög, I. Gorwald, M. Fan, R.H. Wenger, T.N. Sengroves, ITGA6 is directly regulated by hypoxia-inducible factors and enriches for cancer stem cell activity and invasion in metastatic breast cancer models, *Mol. Cancer* 15 (2016) 26.
- [34] W.-I. Cai, W.-D. Huang, B. Li, T.-R. Chen, Z.-X. Li, C.-L. Zhao, H.-Y. Li, Y.-M. Wu, W.-J. Yan, J.-R. Xiao, microRNA-124 inhibits bone metastasis of breast cancer by repressing Interleukin-11, *Mol. Cancer* 17 (2018) 9.
- [35] L.J. van 't Veer, H. Dai, M.J. van de Vijver, Y.D. He, A.A.M. Hart, M. Mao, H.L. Petroni, K. van der Kooy, M.J. Martin, A.T. Witteveen, G.J. Schreiber, R.M. Kerkhoven, C. Roberts, P.S. Linsley, R. Bernardi, S.H. Friend, Gene expression profiling predicts clinical outcome of breast cancer, *Nature* 415 (2002) 530–536.
- [36] B. Kim, H. Yin, S. Jung, A. Moon, D.-Y. Noh, Z.H. Lee, H.J. Kim, H.-H. Kim, A CTGF/RUNX2-RANKL Axis in breast and prostate cancer cells promotes tumor progression in bone, *J. Bone Miner. Res.* 35 (2020) 155–166.
- [37] N. Okuyama, A. Matsumine, R. Konug, H. Wakabayashi, A. Uchida, Matrix metalloproteinase-1 is a crucial bone metastasis factor in a human breast cancer-derived highly invasive cell line, *Oncol. Rep.* 20 (2008) 1497–1504.
- [38] N. Zedler, F. Farahi, N.C. Dubois, N. Saurat, F. Lafaille, L. Saug, B. Zimmer, J. Tchui, M.A. Söllman, G. Lee, J.-I. Casanova, L. Stader, Capturing the biology of disease severity in a PSC-based model of familial dysautonomia, *Nat. Med.* 22 (2016) 1421–1427.
- [39] J. Kowalevich, D. Langford, Considerations for the use of SH-SY5Y neuroblastoma cells in neurobiology, *Methods Mol. Biol.* 1078 (2013) 9–21.
- [40] C. Pérez Pínez, A. Bruzone, M. Sarappa, L. Castillo, I. Lirio, Involvement of $\alpha 2$ - and $\beta 2$ -adrenoceptors on breast cancer cell proliferation and tumour growth regulation, *Br. J. Pharmacol.* 166 (2012) 721–736.
- [41] F. Le Pape, G. Vargis, P. Gézardín, The role of osteoclasts in breast cancer bone metastasis, *J. Bone Oncol.* 5 (2016) 93–95.
- [42] A.S. Andfesson, C.R. Donnelly, R.R. Ji, Reciprocal interactions between osteoclasts and nociceptive sensory neurons in bone cancer pain, *Pain Rep* 6 (2021) e867.
- [43] K. Sae, J.-M. Delaite, Time-lapse reveals that osteoclasts can move across the bone surface while resorbing, *J. Cell Sci.* 130 (2017) 2026–2035.
- [44] K.S. Madden, M.J. Sepuniar, E.B. Brown, β -Adrenergic receptors (β -AR) regulate VEGF and IL-6 production by divergent pathways in high β -AR-expressing breast cancer cell lines, *Breast Cancer Res. Treat.* 130 (2011) 747–758.
- [45] Y. Imamura, T. Mukohara, Y. Shimoda, Y. Taniguchi, N. Chayaban, M. Toyoda, N. Kiyota, S. Takao, S. Kono, T. Nakamura, H. Minami, Comparison of 2D- and 3D-culture models as drug-testing platforms in breast cancer, *Oncol. Rep.* 33 (2015) 1837–1843.
- [46] X. Jiang, L. Ren, P. Tebon, C. Wang, X. Zhou, M. Qu, J. Zhu, H. Ling, S. Zhang, Y. Xue, Q. Wu, P. Bandaru, J. Lee, H.-J. Kim, S. Ahadian, N. Alhamakhi, M.R. Dokme, J. Wu, Z. Gu, W. Sun, A. Khademhosseini, Cancer-on-a-Chip for modeling immune checkpoint inhibitor and tumor interactions, *Small* 17 (2021) 2004282.
- [47] S.L. Dallas, J.L. Rosser, G.R. Mundy, L.F. Bonewald, Proteolysis of latent transforming growth factor- β (TGF- β)-binding protein-1 by osteoclasts: a cellular mechanism for release of TGF- β from bone matrix, *J. Biol. Chem.* 277 (2002) 21352–21360.
- [48] R.O. Hynes, A. Naba, Overview of the matrisome—an inventory of extracellular matrix constituents and functions, *Cold Spring Harbor Perspect. Biol.* 4 (2012).
- [49] T. Hiraga, S. Kinzaka-Kondoh, K. Hirota, M. Hiraoka, T. Yoneda, Hypoxia and hypoxia-inducible factor-1 expression enhance osteolytic bone metastases of breast cancer, *Cancer Res.* 67 (2007) 4157–4163.
- [50] D.F. Higgins, M.P. Biju, Y. Akai, A. Wu, R.S. Johnson, V.H. Haase, Hypoxic induction of Ctgf is directly mediated by Hif-1, *Am. J. Physiol. Ren. Physiol.* 287 (2004) F1223–F1232.
- [51] X. Yuan, N. Qian, S. Ling, Y. Li, W. Sun, J. Li, R. Du, G. Zhong, C. Liu, G. Yu, D. Cao, Z. Liu, Y. Wang, Z. Qi, Y. Yao, F. Wang, J. Liu, S. Hao, X. Jin, Y. Zhao, J. Xue, D. Zhao, X. Guo, S. Liang, Y. Li, J. Song, S. Yu, Y. Li, Breast cancer exosomes contribute to pre-metastatic niche formation and promote bone metastasis of tumor cells, *Theranostics* 11 (2021) 1429–1445.
- [52] T. Okui, M. Hira, S. Ryumon, K. Ono, Y. Kunitada, S. Baragi, A. Sasaki, G.D. Roodman, F.A. White, T. Yoneda, The HMGB1/RAGE axis induces bone pain associated with colonization of 4T1 mouse breast cancer in bone, *Journal of Bone Oncology* 25 (2021) 100330.
- [53] K. Madsfara, S. Al-Dujaili, X. Mei, A. Günther, L. You, Microfluidic co-culture platform for investigating osteocyst-osteoclast signalling during fluid shear stress mechanostimulation, *J. Biomech.* 59 (2017) 35–42.
- [54] K. See, D.M.H. Meeseld, J.-M. Delaite, Steering the osteoclast through the demineralization-collagenolysis balance, *Bone* 56 (2013) 191–198.
- [55] H. Wakabayashi, T. Hamaguchi, N. Nagao, S. Kato, T. Iino, T. Nakamura, A. Sudo, Interleukin-6 receptor inhibitor suppresses bone metastases in a breast cancer cell line, *Breast Cancer* 25 (2018) 566–574.
- [56] K.L. Weber, M. Doucet, A. Shauer, N. Hsu, D. Huang, J. Fogel, S.L. Kominsky, MIP-15 activates NFATc1 and enhances osteoclastogenesis: involvement of both PI3K and NFB signaling, *PLoS One* 7 (2012), e40799.
- [57] E.V. Yang, S.-J. Kim, E.L. Donovan, M. Chen, A.C. Gross, J.L. Webster-Markton, S.H. Barsky, R. Glaser, Norepinephrine upregulates VEGF, IL-8, and IL-6 expression in human melanoma tumor cell lines: implications for stress-related enhancement of tumor progression, *Brain Behav. Immun.* 23 (2009) 267–275.
- [58] J.J. Yin, K. Selander, J.M. Chirgwin, M. Dallas, R.G. Grubbs, R. Wieser, J. Masague, G.R. Mundy, T.A. Guise, TGF- β signaling blockade inhibits PTHrP secretion by breast cancer cells and bone metastases development, *J. Clin. Invest.* 103 (1999) 197–206.
- [59] R.E. Coleman, P.I. Croucher, A.R. Padhani, P. Clisardin, E. Chow, M. Fallon, T. Guise, S. Colanelli, R. Capanna, L. Costa, Bone metastases, *Nat. Rev. Dis. Prim.* 6 (2020) 83.
- [60] M.A. Unger, H.P. Chou, T. Thomsen, A. Scherer, S.R. Quake, Monolithic microfabricated valves and pumps by multilayer soft lithography, *Science* 288 (2000) 113–116.
- [61] R. Li, X. Zhang, X. Lv, L. Geng, Y. Li, K. Qiu, Y. Deng, Microvalve controlled multi-functional microfluidic chip for dual-cell co-culture, *Anal. Biochem.* 539 (2017) 48–53.
- [62] M. Arai, T. Nagasawa, Y. Koshihara, S. Yamanoto, A. Togari, Effects of β -adrenergic agonists on bone-resorbing activity in human osteoclast-like cells, *Biochim. Biophys. Acta Mol. Cell Res.* 1640 (2003) 137–142.
- [63] F.K. Sloan, S.J. Paccaman, B.F. Cox, S. Yu, M.A. Pimentel, V. Tangkavanakul, J.M.G. Azevaló, K. Morimoto, B.D.W. Kannikolas, L. Wu, A.K. Sood, S.W. Cole, The sympathetic nervous system induces a metastatic switch in primary breast cancer, *Cancer Res.* 70 (2010) 7042–7052.
- [64] L. Zheng, K. Zhu, H. Jiao, Z. Zhao, L. Zhang, M. Liu, W. Deng, D. Chen, Z. Yao, G. Xiao, PTHrP expression in human MDA-MB-231 breast cancer cells is critical for tumor growth and survival and osteoblast inhibition, *Int. J. Biol. Sci.* 9 (2013) 830–841.
- [65] R.J. Thomas, T.A. Guise, J.J. Yin, J. Elliott, N.J. Horwood, T.J. Martin, M.T. Gillespie, Breast cancer cells interact with osteoblasts to support osteoclast formation, *Endocrinology* 140 (1999) 4451–4458.
- [66] A.E. Chou, C. Liu, I. Moreno-Jiménez, T. Tang, W. Wägermaier, M.N. Dean, C. Fischbach, P. Razi, Breast cancer-secreted factors perturb murine bone growth in regions prone to metastasis, *Sci. Adv.* 7 (2021) eab2283.
- [67] A. Sulejmanovic, T. Takahashi, H. Sano, H. Ogawa, S. Yano, H. Kasayama, K. Inami, H. Uehara, Enhancement of osteoclastogenic activity in osteolytic prostate cancer cells by physical contact with osteoblasts, *Br. J. Cancer* 104 (2011) 505–513.



A metastasis-on-a-chip approach to explore the sympathetic modulation of breast cancer bone metastasis

Francisco Conceição ^{a, b, c}, Daniela M. Sousa ^{a, b}, Joshua Loessberg-Zahl ^f, Anke R. Vollertsen ^g, Estrela Neto ^{a, b}, Kent Sørensen ^{h, 1}, Joana Paredes ^{a, d, e}, Anne Leferink ^g, Meriem Lamghari ^{a, b, c} ✉

[Show more](#) ▾

+ [Add to Mendeley](#) [Share](#) [Cite](#)

<https://doi.org/10.1016/j.mtbio.2022.100219>

[Get rights and content](#)

Under a Creative Commons [license](#)

● [Open access](#)